ISBN 978-82-471-2014-9 (printed ver.)
ISBN 978-82-471-2015-6 (electronic ver.)
ISSN 1503-8181

Doctoral theses at NTNU, 2010:30

Guro Grøneng

Stability Analyses of the Åknes Rock Slope, Western Norway

Guro Grøneng
Doctoral Thesis

NTNU
Norwegian University of
Science and Technology

Doctoral theses at NTNU, 2010:30

NTNU
Norwegian University of
Science and Technology
Thesis for the degree of
philosophiae doctor
Faculty of Engineering Science and Technology
Department of Geology and Mineral Resources Engineering

NTNU
Norwegian University of
Science and Technology

Guro Grøneng

Stability Analyses of the Åknes Rock Slope, Western Norway

Thesis for the degree of philosophiae doctor

Trondheim, February 2010

Norwegian University of
Science and Technology
Faculty of Engineering Science and Technology
Department of Geology and Mineral Resources Engineering

NTNU
Norwegian University of
Science and Technology

NTNU
Norwegian University of Science and Technology

Thesis for the degree of philosophiae doctor

Faculty of Engineering Science and Technology
Department of Geology and Mineral Resources Engineering

ISBN 978-82-471-2014-9 (printed ver.)
ISBN 978-82-471-2015-6 (electronic ver.)
ISSN 1503-8181

Doctoral Theses at NTNU, 2010:30

Printed by Tapir Uttrykk

Abstract

In the alpine topography of western Norway rockslides constitute a potential danger for generation of tsunamis in the fjords. The Åknes rockslide area was first brought to the public's attention in 1964, when local people claimed that the back scarp, located 700-900 m a.s.l. was widening. Bolts were installed on both sides of the back scarp and manual measurement of the distance across was started in 1986. A comprehensive monitoring program with several types of movement measurements is in operation in the rockslope area today, funded by the Norwegian Natural Disaster Fund since 2004. Due to the potential hazard for a tsunami generated as a result of a large scale rockslope failure, the rockslide monitoring project is one of the most comprehensive in the world at present.

Among the most important issues in rockslope stability analysis are potential failure geometry, shear strength of the sliding plane(s) and groundwater conditions. In a large complex rockslide such as the Åknes sliding area, considerable uncertainties are related to these factors.

Failure geometry at Åknes has been evaluated based on a combination of geophysical and geotechnical datasets and an interactive 3D geovisualization model for visual analysis. Geometric modelling and volume estimation of the sliding area has been carried out for three different scenarios: Scenario A with a basal sliding surface located 40-55 m below the surface (estimated area and volume 510,000 m^2 and 20×10^6 m^3, respectively); Scenario B with a basal sliding surface located 105-115 m below the surface (estimated area and volume 575,000 m^2 and 43×10^6 m^3, respectively), and Scenario C with a basal sliding surface located 150-190 m below the surface (estimated area and volume 742,000 m^2 and 85×10^6 m^3, respectively). Of these, Scenario B has been concluded to represent the most likely basal sliding plane location and hence the most realistic area- and volume estimates.

Potential sliding planes in a rock slope generally consist of geological layers or strata which possess smaller shear strength than the surrounding rock mass. Shear strength

estimation of sliding planes is always a key factor for reliable rock slope stability analysis. At Åknes, the sliding plane is complex, consisting of a combination of:

(a) Unfilled joints (rock-to-rock contacts)
(b) Filled joints (gouge material)
(c) Bridges of intact rock

The shear strengths of components (a)−(c) span a great range, and before any kind of stability analysis can be carried out, a realistic quantification of the resultant shear strength of the combined sliding plane has to be made. A methodology for estimating this resultant shear strength has been developed, resulting in a possible range of shear strengths depending on the amount of unfilled joints, filled joints and bridges of intact rock in addition to the normal stress (σ_n) acting on the sliding plane. Based on field observations, drill core logging and back analysis, estimation of most likely composition of the sliding plane at Åknes has resulted in an amount of 25-35% failure along gouge filled joints, 1-3% intact rock failure and 62-74% failure along unfilled foliation joints.

Detailed data on displacements and meteorology are available based on extensive monitoring of the slope since 2004. Analysis of the meteorological effects on displacements in the back scarp of the Åknes rockslide has shown that the displacements are mainly related to variations in groundwater level in the upper part of the slope. The groundwater level is in turn affected by the seasonal meteorological variations. The largest net expansions of the back scarp are recorded in spring, when the groundwater is fed by melting water from snow in the catchment area in addition to rainfall. In winter, when the ground is frozen and covered with a 1-3 m thick snow cover, no significant displacement is recorded. Indications of reduced meteorological influence on the displacements with time have been found for the analysed period (November 2004 - August 2008) as most of the displacement events in the back scarp have been recorded in the first half of the period (September 2004−August 2006).

Stability of the slope has been evaluated using 2D and 3D numerical modelling based on $Phase^2$ and $FLAC^{3d}$, respectively. This analysis has incorporated data from geometry analysis and shear strength analysis for the sliding plane(s), as well as data from field and laboratory work and groundwater analysis. Analyses based on $Phase^2$ show that a shear strength according to a composition of 35% failure along gouge filled joints, 1% intact rock failure and 64% failure along unfilled foliation joints results in a critical stability with a Strength Reduction Factor (SRF) of 0.96, while an alternative composition of 35% failure along gouge filled joints, 3% intact rock failure and 62% failure along unfilled foliation joints results in a SRF of 1.1.

Longterm stability of the slope has been evaluated based on the Burger-Creep Viscoplastic (c-visc) material model in $FLAC^{3D}$. The analysis has shown that a set of parameters believed to represent the present situation (a composite sliding layer with 3% failure of intact rock, 35% failure along gouge filled joints and 62% failure along unfilled joints and a fractured rockmass above the sliding layer with M-C parameters corresponding to GSI 62; "good surface conditions") results in stabilisation of the displacements within the 100 years modeled. However, due to gradual reduction in the shear strength parameters over time, the toe according to the analysis becomes unstable and the surface displacements increase within the same time span with a set of parameters representing a possible future scenario (a composite sliding layer with 1% intact rock, 35% gouge and 64% unfilled joints and a fractured rockmass corresponding to GSI 37; "fair surface conditions"). Although exact timing of failure is not possible based on the modelling carried out in this thesis, this analysis is believed to represent valuable basis for further analysis which may be carried out as more knowledge regarding the geometry and composition of the sliding plane(s) and the groundwater conditions in the sliding area become available.

Acknowledgments

First I would like to thank my supervisor Professor Bjørn Nilsen. He has been very helpful giving advice, support and guidance. I greatly appreciate his readiness to answer questions in addition to being a well-organised supervisor.

My friend Arne Jenssen introduced me to *MATLAB*, has been tremendously helpful and has shown great endurance when it comes to teaching me programming on his spare time.

I would also like to mention the women finishing their PhD theses within the area of geology/engineering geology while my PhD thesis was in progress; namely Guri Venvik Ganerød, Kristin Hilde Holmøy and Inger-Lise Solberg. They have all been a source for motivation and professional discussions, in addition to being supportive throughout the PhD period. I've genuinely enjoyed getting to know them professionally as well as personally.

I feel gratitude towards all my PhD colleagues at the Department of Geology and Mineral Resources Engineering for the great atmosphere and friendship. Thanks to them, every single day in the office has had enjoyable moments.

Finally, I would like to thank my personal friend Olav Aune for the excellent friendship, for being encouraging, patient and always ready to support, around the clock, during these years. You always believed I could finish.

This thesis has been financed by the International Centre for Geohazards (ICG) and by teaching assistance at the Norwegian University of Science and Technology, NTNU. The National Fund for Natural Damage Assistance, Møre and Romsdal county and the Åknes/Tafjord project have also contributed to this work.

Trondheim, Norway, October 2009

Note on contributions

Paper I: Shear strength estimation for Åknes sliding area in western Norway

Authors: Guro Grøneng, Bjørn Nilsen and Rolf Sandven

The candidate wrote this paper and carried out the field work and laboratory analyses for rock. Bjørn Nilsen suggested the methodology presented in the paper and gave input to the field work and manuscript. Rolf Sandven contributed to the geotechnical analyses of soil and interpretation of results.

The paper was published in International Journal of Rock Mechanics and Mining Sciences (2009), Vol. 46, pages 479-488, doi:10.1016/j.ijrmms.2008.10.006.

Paper II: Geovisualization, geometric modelling and volume estimation of the Åknes rockslide, western Norway

Authors: Trond Nordvik, Guro Grøneng, Guri Venvik Ganerød, Bjørn Nilsen, Chris Harding and Lars H. Blikra

Development of the geovisualization model was a collaboration between Nordvik, Ganerød and the candidate. However, all implementations were carried out by the first author. Input to the model, geoscientific interpretations and evaluations were carried out by the candidate and Guri Venvik Ganerød. The writing of this paper was a joint effort among the three first authors.

The paper was published in Bulletin of Engineering Geology and the Environment (2009), Vol. 68, pages 245-256, doi:10.1007/s10064-009-0198-x.

Paper III: Meteorological effects on seasonal displacements of the Åknes rockslide, western Norway

Authors: Guro Grøneng, Hanne H. Christiansen, Bjørn Nilsen and Lars H. Blikra

The candidate wrote this paper and carried out the analyses. Hanne H. Christiansen gave input to the analyses and wrote parts of the description dealing with meteorology

in addition to reviewing the manuscript. Bjørn Nilsen contributed to the discussion and reviewed the manuscript. Lars H. Blikra reviewed the manuscript.

The paper was submitted to Landslides (May 2009).

Paper IV: Time-dependent behavior of the Åknes rockslide area in western Norway

Authors: Guro Grøneng, Ming Lu, Bjørn Nilsen and Arne K. Jenssen

The candidate wrote this paper and carried out the numerical modelling. Ming Lu gave input to the modelling and interpretation of the results. Bjørn Nilsen gave input to the modelling and reviewed the manuscript. Arne K. Jenssen developed a function which generates coordinates for bricks in $FLAC^{3D}$ based on coordinate files for the topography and sliding layer and played an important role in $MATLAB$-programming which was used to generate inputfiles to $FLAC^{3D}$.

The paper was submitted to Engineering Geology (September 2009).

UNDER BERGFALLET

Du bur under bergfall.
Og du veit det.
Men du sår din åker
og trør trygt ditt tun
og lèt dine born leika
og legg deg som inkje var.

Det hender,
når du stør deg på ljåen
ein sumarkveld,
at augo sviv som snarast
yver bergsida
der dei segjer
sprekken
skal vera, og det hender
du vert liggjande vaken
og lyda etter
steinsprang
ei natt.

Og kjem raset,
kjem det ikkje uventa.
Men du tek til å rydja
den grøne boti
under berget
um du då har livet.

Olav H. Hauge (1951)

Contents

1 Introduction

1.1 Background

The term "*geohazards*" can be defined as: "a geological state that represents or has the potential to develop further into a situation leading to damage or uncontrolled risk" according to Norwegian Geotechnical Institute's website. The term thus covers a very wide field. Large scale rockslides represent a serious geohazard in Norway, mainly due to tsunamis following the rockslides causing destruction and loss of lives. During the last 100 years, 174 people have lost their lives in three rockslide events in western Norway.

This thesis is prepared within the International Center for Geohazards (ICG), which is a "Center of Excellence" appointed by The Research Council of Norway from 2003. ICG is established by 5 partners; The Norwegian Geotechnical Institute (NGI) as the host institution, Geological Survey of Norway (NGU), NORSAR, The University of Oslo (UiO) and The Norwegian University of Science and Technology (NTNU). The activity of the center is at present organized in nine projects where staff members of the partner institutions and MSc-/PhD students from UiO and NTNU do research together:

Project P2 Risk assessment for geohazards
Project P3 Seismic hazard, risk and loss
Project P4 Stability of rock slopes
Project P5 Geomechanical modelling
Project P6 Offshore geohazards
Project P7 Slope instability assessment and hazard zonation
Project P9 Slide dynamics and mechanics of disintegration
Project P10 Tsunamis
Project P12 Monitoring, remote sensing and early warning systems

As can be seen from the projects involved, ICG research cover areas like landslides, clay slides, slides in marine sediments, rockslides, earthquakes, tsunamis and related topics such as risk assessment, hazard zonation, monitoring and early warning systems. This thesis is a part of Project P4; Stability of rock slopes, and further focus will hence be on

rock slope stability.

Historical rockslides in Norway documented in a geohazard database at the NGU show that three counties with high, steep topographic relief of fjords and valleys are in particular exposed to rockslides; Sogn & Fjordane, Møre & Romsdal and Troms (Blikra et al., 2006). Initial site inspections thus were carried out at Nordnesfjellet (Troms county), Åknes, Børa and Tafjord (all in Møre & Romsdal county) and Aurland (Sogn & Fjordane county) which are rockslide sites described in Braathen et al. (2004). However, the Åknes sliding area was chosen as an unique study area, mainly due to an allocation from the National Fund for Natural Damage Assistance from 2004. The funding initiated establishment of the Åknes/Tafjord project in the municipality of Stranda, and monitoring data from the Åknes rockslide has been made available for this study through this project and NGU.

A high frequency of rockslides is generally identified in the county of Møre & Romsdal by geological mapping on land and in fjords (Figure 1). Almost 200 individual events have been mapped, with distinct concentrations in the inner fjord areas (Blikra et al., 2006). The Storfjorden area where the Åknes sliding area is situated is defined as a "high susceptibility zone" based on a spatial distribution and temporal pattern of events (Blikra et al., 2005). A total of 59 individual events larger than 0.5×10^6 m^3 are mapped in this area (Longva et al., 2009; Blikra et al., 2005).

Some of the catastrophes in the counties of Møre & Romsdal and Sogn & Fjordane are documented in Furseth (2006) and Bjerrum and Jørstad (1968), including Skafjellet in 1731, Tjelle in 1756, Loen (Ramnefjell) in 1905 and 1936 and Tafjord (Heggura) in 1934 (Table 1 and Figure 2). The Tafjord (Heggura) rockslide in 1934 destroyed the villages of Tafjord and Fjørå, Figure 3(a) and 3(b) shows the village Fjørå before and after the slide, respectively. The rockslide generated a tsunami of 12-14 m here and claimed 17 casualties (Furseth, 2006).

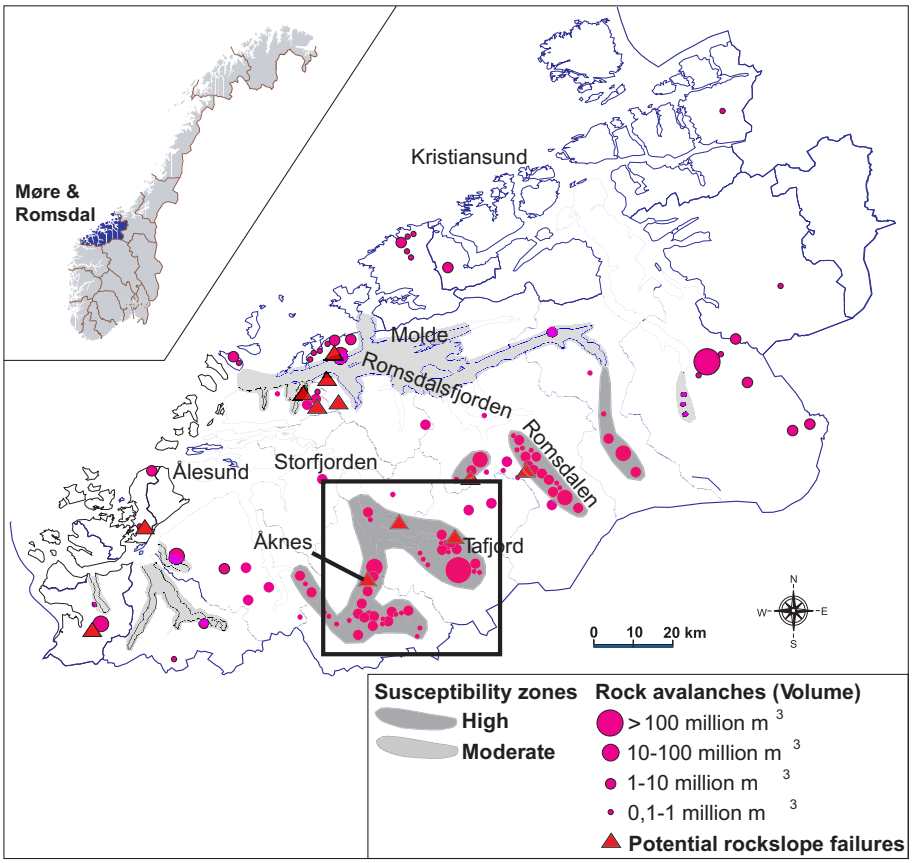

Figure 1: Susceptibility map based on geological mapping, field investigations, georadar profiling, refraction seismic profiling and excavations on land and in fjords (Blikra et al., 2006).

Rockslide	Year	Volume [m^3]	H$_{tsunami}$ [m]	Casualties
Skafjellet	1731	$> 0.1 \times 10^6$	30	17
Tjelle	1756	15×10^6	50	32
Loen	1905	0.4×10^6	40	61
Tafjord	1934	1.5×10^6	17	40
Loen	1936	1×10^6	74	74

Table 1: Selected historical documented rockslides in the counties of Møre & Romsdal and Sogn & Fjordane. H$_{tsunami}$ refers to maximum recorded height of tsunamis in historical documents.

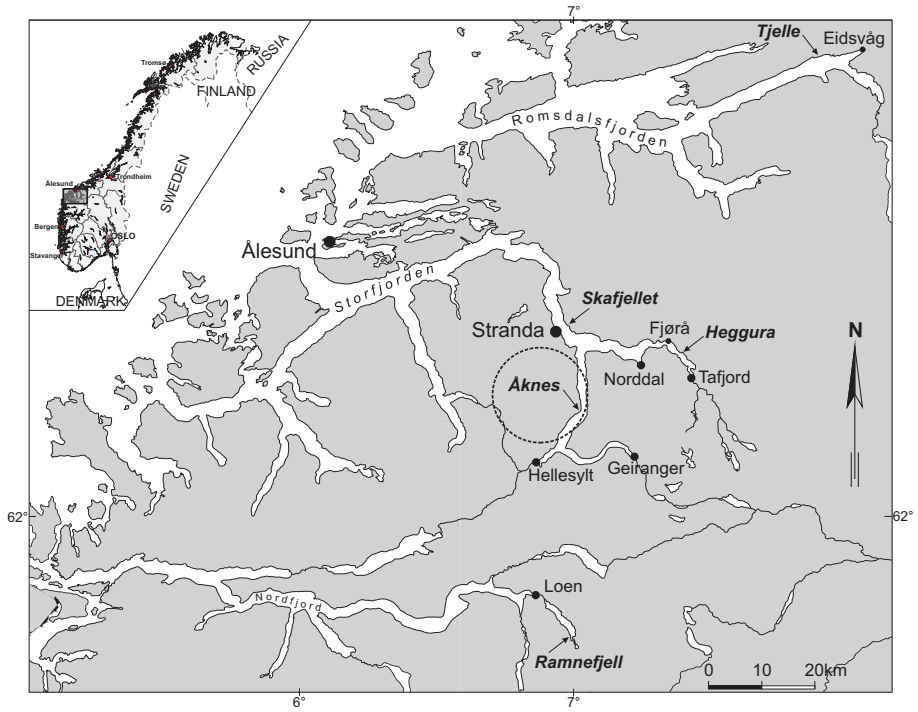

Figure 2: The Åknes rock slope, the town of Stranda and historical rockslide locations discussed.

Tsunami modelling indicates that several settlements along the Storfjorden will be endangered as a result of a large scale rock slope failure at Åknes (Eidsvig and Harbitz, 2005), among them the people living at the nearby communities Geiranger and Hellesylt located by the fjord, and the town of Stranda, 15 km away from Åknes (Figure 2). In addition, the large amount of tourists visiting the area during the summer months are potentially affected as the Geirangerfjord is one of Norway's most visited tourist attractions (listed on the UNESCO's World heritage list).

(a) (b)

Figure 3: a) The village Fjøråå before the rockslide at Tafjord (Heggura) in 1934 b) The village after the slide. Photos from Furseth (2006).

1.2 Åknes rockslide area

The unstable slope at Åknes is oriented in NE-SW direction along the W-side of the Storfjorden and was brought to the public's attention in 1964, by local people claiming that the back scarp was widening (Sandersen et al., 1996). Signs of instability at the Åknes rockslide area have been evidenced by occurrence of three smaller rockslides, all along the western boundary of the area, the most recent in 1960, with an estimated volume of approximately 100,000 m^3 (Kveldsvik et al., 2008, 2006). Monitoring of the back scarp started in 1986 by the installation of two pair of bolts for manual reading of the distance across the back scarp, and today, the rockslide monitoring project at Åknes is one of the largest in the world.

Several master thesis and project assignments have been prepared related to Åknes sliding area within Project P4, which this thesis has benefited from, including collection of geological data (Ragvin, 2005; Holsbrekken, 2006), numerical studies of the slope (Ragvin, 2006), analysis of the the correlation between displacement and precipitation (Holsbrekken, 2007), analysis of borehole geophysical data (Aardal, 2006, 2007) and possible effects of drainage (Moen, 2007, 2008). In addition, one PhD thesis has been prepared on static and dynamic stability analyses of the slope (Kveldsvik, 2008).

1.2.1 Description

Using the generally accepted landslide terminology of Petley (1978) and Cruden and Varnes (1996), the main scarp is located approximately 700-900 m a.s.l., extending 800 m in E-W direction (Figure 4(a)). The main scarp is progressively developing toward the east, where it at present ends with an opening of 0.5-1 m (Figure 4(b)). In the western part, the opening is in the order of 2-3 m (Figure 4(c)). At the western end of the scarp, a relieved graben structure with an estimated volume of 300,000-400,000 m^3 has developed (Figure 4(d)). The western flank is defined by a steeply dipping NNW-SSE strike slip fault which is a dominant feature in the area, while indications of a NNE-SSW trending fault with a gentle dip to the northwest might define the eastern flank of the area (Ganerød et al., 2008). The toe is not defined, however, field mapping has revealed a line of springs located at approximately 75-100 m a.s.l. (Frei et al., 2008), indicating a possible lower boundary of the unstable area. Morphological compression features which are mapped in field (Blikra, 2008), may also indicate a toe at this elevation.

Geophysical surveys by the use of 2D resistivity, refraction seismic and ground penetrating radar (GPR) have been carried out in order to map the subsurface (Ganerød et al., 2008; Rønning et al., 2006). The surveys have indicated several scenarios for the basal surface of rupture, and an undulating basal sliding surface located at 105-115 m has been proposed as the most likely scenario in Nordvik et al. (2009).

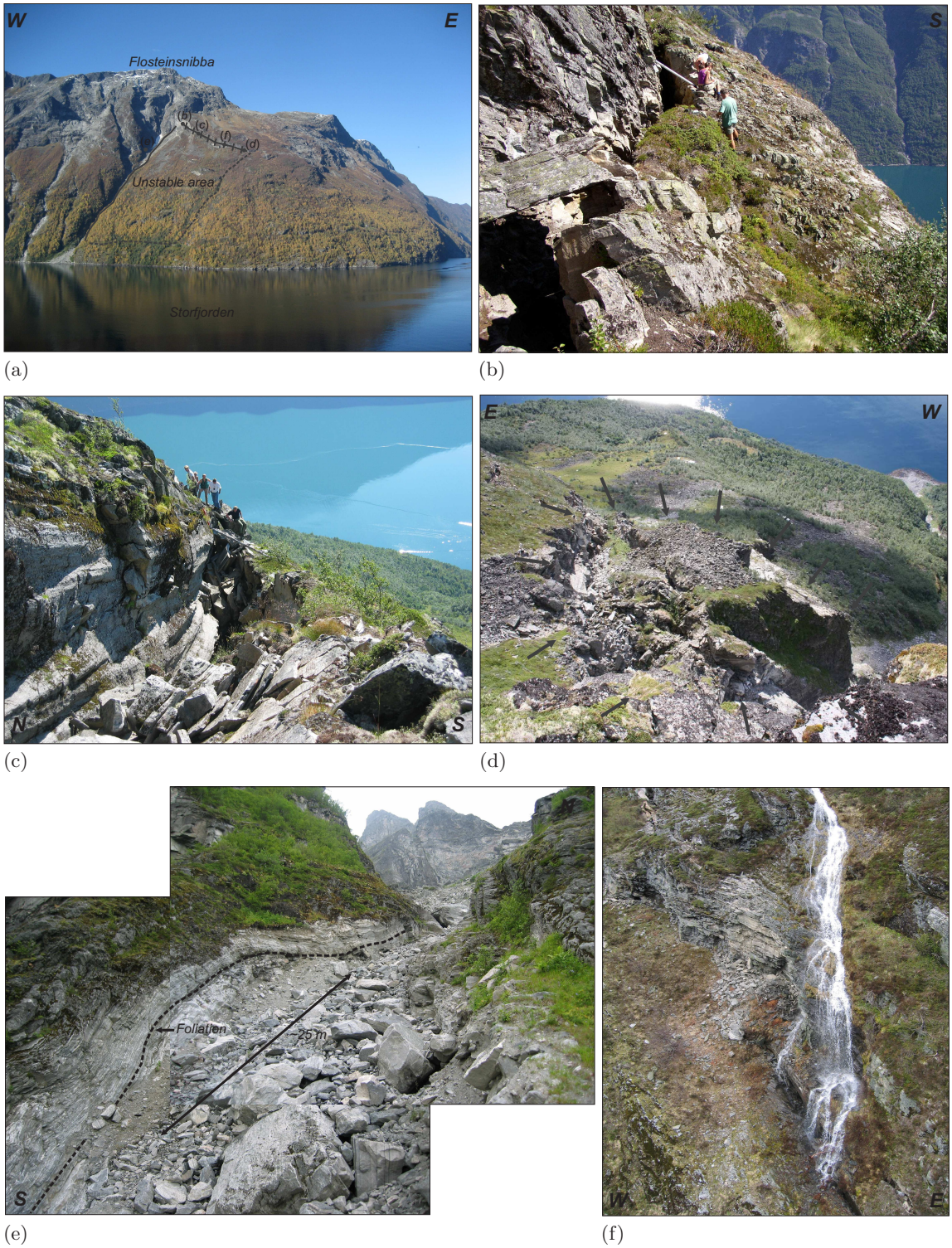

(a) (b)

(c) (d)

(e) (f)

Figure 4: a) Åknes rockslide area, with photo locations b) Back scarp opening in the eastern part (0.5-1 m) c) Back scarp opening in the western part (2-3 m) d) Relieved graben structure located in the western end of the back scarp e) Foliation in the area f) Water infiltrating the back scarp in spring.

1.2.2 Geology

The Åknes rockslide is located in the Western Gneiss Region. The bedrock of the area is dominated by gneisses of Proterozoic age, which was altered and reworked during the Caledonian orogeny (Tveten et al., 1988). The gneisses have a magmatic origin and are described in the geological map sheet as undifferentiated gneisses that are locally migmatitic in composition, varying from quartz-dioritic to granitic. On the basis of logs from seven boreholes at the three drilling sites in the slope (Figure 5), three types of gneiss; quartz-dioritic, granitic and gneisses rich in biotite have been identified (Ganerød et al., 2007).

Geological conditions believed to contribute to slope instability and potential failure at the Åknes rockslide area are: 1) a steep slope angle averaging approximately 35° and 2) foliation oriented parallel to the slope, dipping steeply S-SE along the main scarp ((Ganerød et al., 2008; Braathen et al., 2004)).

1.2.3 Hydrological conditions

The groundwater level is measured by piezometers which were installed in the upper and middle borehole in November 2006. From November 2006 to August 2008, the groundwater levels fluctuated between -42.5 and -46.5 m below the surface in the middle borehole, and between -51 and -60 m in the upper borehole. Groundwater levels recorded in the boreholes fluctuated simultaneously in this period, indicating a shared groundwater regime in this area. The fluctuations were however, largest in the upper borehole, reflecting the close location to the back scarp, which is believed to constitute a major feature for infiltration of water to the sliding area. This is evidenced by high groundwater tables when precipitation is high in autumn and spring when a combination of melting water (Figure 4(f)) and precipitation infiltrates the back scarp (Grøneng et al., 2009).

1.2.4 Displacement

Displacement in the sliding area is monitored at the surface by several instruments which can be divided into manually and continuously displacement measurements (Figure 5):

Manually recording instruments

- Bolts in the back scarp from 1986 (a total of seven sets of bolts)
- GPS- and reflector points throughout the area since 2004 (a total of 18 GPS points and 19 reflector points)
- Bolts for tape extensometer reading in selected joints from 2005 (a total of 14 sets of bolts)

Continuously recording instruments

- Extensometers in the back scarp from 1993 (a total of five extensometers today)
- Ground-based radar scanning of the slope from the opposite side of the fjord (1-3 month campaigns since 2005)
- GPS-antennas since 2007 (a total of eight GPS-antennas)
- Ground-based radar with reflector points since 2009 (a total of nine reflector points)
- Totalstation with prisms since 2007 (a total of 21 prisms)
- Laser recordings for monitoring of a local graben structure since 2005 (a total of two lasers)

In addition, five crackmeters/tiltmeters is being installed at the moment in selected joints throughout the area. In general, the displacements in the back scarp show a steady widening over the last 18 years, on the average in the order of 18-25 mm/year (Kveldsvik et al., 2006). According to manual measurement campaigns of GPS/reflector points operative since 2004, the unstable slope can be divided into four areas based on the direction of movement and velocity (based on measurements in the period October 2004−August 2007):

Area I SW individually moving graben structure defined by GPS8 and laser/reflectors L1/R1 and L2/R2 with average annual displacement in the order of 70-145 mm/year

Area II S-SW moving area defined by GPS6-8, R4-8, R14-18 with average annual displacement in the order of 70 mm/year

Area III SE moving area defined by GPS9, GPS13, R9, R12-13 and R19 with average annual displacement in the order of 20 mm/year

Area IV Inconsistently moving area defined by GPS10-12, GPS14-18, R9-R11

The lower part of the slope is moving inconsistently due to unfavorable position of the GPS points in terms of satellite signal reception, vegetation and meteorological factors influencing the measurements (Nordvik and Nyrnes, 2009; Ganerød et al., 2008).

In addition to the monitoring of surface displacements, two boreholes (upper and middle borehole) are equipped with a Differential Monitoring System (DMS) since 2006. The monitoring interval of the columns was -32 to -82 m in upper borehole and -16.5 to -66.5 m in the middle borehole. Until July 2007, the data indicates a relative displacement around -51 m to -52 m in the upper borehole, corresponding to a maximum of 1 cm/year and at -34 m in the middle borehole, corresponding to approximately 1 cm/year (Kveldsvik, 2008). However, the length of the DMS-columns limits the measurement interval in the boreholes, which allows for preliminary conclusions related to the displacement at depth at present. The instrumentation was moved to lower parts autumn of 2007, and this will allow documentation of potential movement in lager depths.

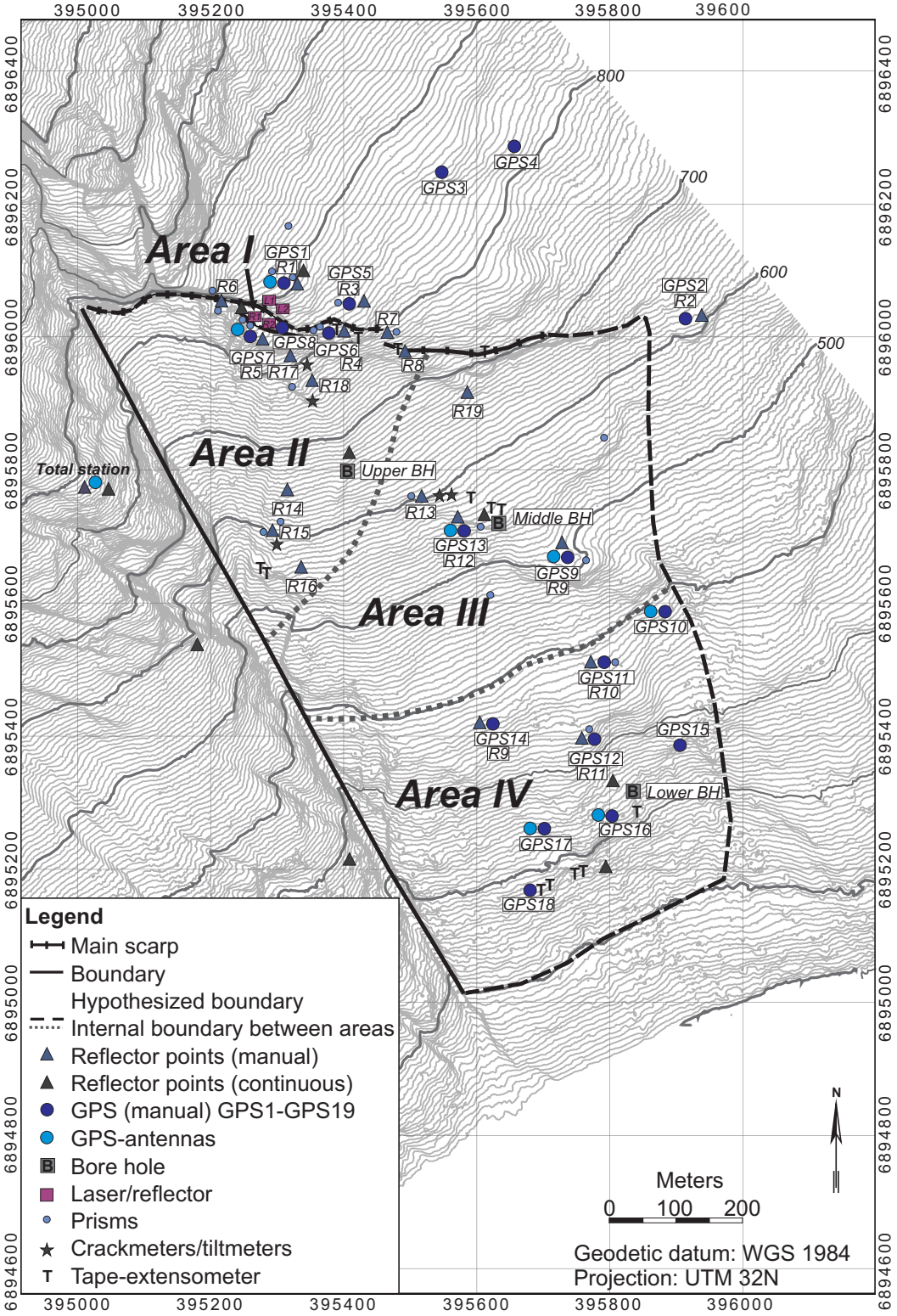

Figure 5: Instruments for measurement of the displacement at Åknes. Localisation of extensometers and bolts in the back scarp are not included (see Grøneng, Christiansen, Nilsen & Blikra (2009) for placement).

1.3 Objective

The objective of this thesis is to contribute to improvement of knowledge of the stability at the Åknes sliding area, by studying in detail some important factors for slope stability. The results are believed to increase the understanding of the following factors controlling the slope stability at Åknes:

- The extent and geometry of the sliding area, including volume estimations
- The composition and shear strength of the sliding plane(s)
- The influence of groundwater and meteorology on the stability
- The time dependent deformation of the area, including predictions for future stability

1.4 Organisation of thesis

The thesis is divided into sections as described in the following:

Section 2 and 3: Theoretical basis and Methodology
Relevant theory related to rock slope stability and methods used are presented.

Section 4: Comments on main papers
The main papers prepared for publication are briefly discussed in sections 4.1-4.4. A total of four main papers are prepared, all dealing with different factors controlling the stability at Åknes.

Section 5: Discussion and Main conclusions
A joint discussion of the papers is presented and the main conclusions of the thesis are drawn.

Main Papers
The main papers I-IV are included in full length.

Appendices

Appendices in this thesis includes the following:

Appendix A Additional paper (Paper V)

Appendix B Front cover of reports I-II

Appendix C Total list of publications during PhD

In addition to the four main papers, contributions have been made to one paper dealing with the geology at Åknes (Ganerød et al., 2008), and one report for the Norwegian Geological Survey documenting the corelogging of 1,050 m of cores from a total of seven boreholes at Åknes (Ganerød et al., 2007). One report has also been prepared for Dept. of Geology and Mineral Resources Engineering at NTNU on determination of input parameters for Barton-Bandis joint shear strength formulation (Grøneng and Nilsen, 2009).

2 Theoretical basis

2.1 Stability of large scale rock slopes

Analysis of the stability of a large scale rock slope represents a challenge due to the geological complexity and large volume of unstable mass normally involved ($> 0.1 \times 10^6$ m^3). Some of the early work on this topic with relation to slopes in hard unweathered rock in Norway were carried out by Bjerrum and Jørstad (1968) and Terzaghi (1963). In most cases, several factors influence the stability and rate of movement of a rock slope, such as:

- Slope topography
- Orientation of discontinuity planes and foliation
- Shear strength of discontinuities and intact rock
- Groundwater pressure
- In situ stress conditions
- Seismic activity
- Freezing/thawing effects

The relative importance of each of these factors may vary considerably, however, in most cases the orientation and characteristics of discontinuity planes and groundwater conditions are the most important factors (Wyllie and Mah, 2004; Nilsen and Palmstrøm, 2000; Hoek and Bray, 1981).

The discontinuities define the potential sliding plane(s), while the shear strength of the discontinuities represents the resistance against failure. Groundwater may affect the stability of a slope in several ways:

- By reducing the normal stress; groundwater pressure will reduce the normal stress acting on the sliding plane(s) and by this reduce the friction along the sliding plane(s).
- By acting as a driving force; the groundwater may act directly as a driving force in tension joints.

- By reducing the internal friction; the groundwater may reduce the internal friction, i.e. the strength of joint filling material and possibly also cause swelling of gouge material.
- Due to expansion by freezing; water expands by approximately 10% when freezing, which may cause considerably displacements and forces reducing the stability.
- By causing erosion; in weak rock, flowing water may cause washout and erosion reducing the stability.

Many authors, such as Wyllie and Mah (2004), Wieczorek (1996) and Coates (1990), have discussed the relation between groundwater and slope stability in general terms. Shear strength reduction of filled discontinuities in rock is dependent on the thickness of the clay filling as discussed by Barton (1974). For large scale rockslides, processes working at depth are the most important factor and such failures can be caused by several factors. A study of four large historical rockslides in Norway (Loen 1905 and 1936, Tafjord in 1934 and Modalen in 1953) concluded that failures may have occurred as result of reduction in shear strength due to increase in water pressure or by reduction in joint roughness due to mechanical or chemical disintegration (Sandersen et al., 1996). Increase in the water pressure could in turn be related to meteorological factors such as rainfall intensity, rate of snowmelt, temperature, air humidity, wind velocity, solar radiation and snow depth.

Conceptually, rock slope failure can be seen as the progressive accumulation of events with time that act to degrade the equilibrium state of the slope, with each event bringing the slope closer to failure (Eberhardt et al., 2001). Each event could be related to different groundwater-related triggering types, such as heavy rainfall/snowmelt or freeze-thaw cycle which progressively reduces the effective strength or cohesion of the rock mass until a triggering episode which eventually leads to slope failure. Internationally, the relation between large scale rockslides and these triggering events has been widely discussed in the literature. The most well known case is the 1963 disastrous Vaiont rock slope failure in northern Italy (slide volume of 270×10^6 m^3), which occurred as a consequence of the construction of a 265 m high arch dam. The importance of rising and lowering of the

reservoir level, precipitation and decrease of sliding resistance of the rock materials has been discussed by Hendron and Patton (1985), M*ü*ller (1968), Kenney (1967) and M*ü*ller (1964) amongst others. Additional international case studies where groundwater has been discussed in relation to slope stability include for instance the 1991 Randa rock slope failure in Switzerland, where heavy snowmelt has been discussed as one of several triggering mechanisms (Eberhardt et al., 2001), the 1987 Val Pola rock avalanche in Italy (slide volume of 40×10^6 m^3) where heavy rainfall preceded the failure (Govi (2002) and references therein), the 1907 Frank slide in Canada (slide volume of 30×10^6 m^3) where freezing and melting of snow in rock joints have been mentioned as a triggering factor (Cruden and Martin (2007) and references therein) and the 1806 Goldau slide in Switzerland (slide volume of 20×10^6 m^3) where the effect of heavy rainstorms has been discussed (Terzaghi and Voight (1979) and references therein).

2.2 Failure mechanisms

The mechanical behaviour of deep-seated landslides such as the one at Åknes is complicated to fully understand due to the depth of the basal shear surface and associated problems with localizing and accessing the zone of deformation. Several models of failure mechanisms have been proposed in the literature, one of them by Stead et al. (2004) who for the most complex case describes a failure mechanism involving deep-seated multi-block failure with internal shearing in combination with brittle-ductile deformation for complex deep-seated rockslides (Figure 6). Petley and Allison (1997) simulated the stress-srain environment at the bottom of a deep-seated landslide and found that some materials (mudrocks) showed a combination of ductile and brittle deformation inducing long periods of creep followed by sudden failure, supporting this failure mechanism. Petley (1996) has also argued such a failure mechanism for the 1963 Vaiont slide, where the shear zone deformed as a result of mechanisms that were initially ductile (development of micro-cracks in the clay layers withing the landslide), but which transitioned to a brittle state as strain accumulated. The final failure was triggered by development of a discrete shear plane as

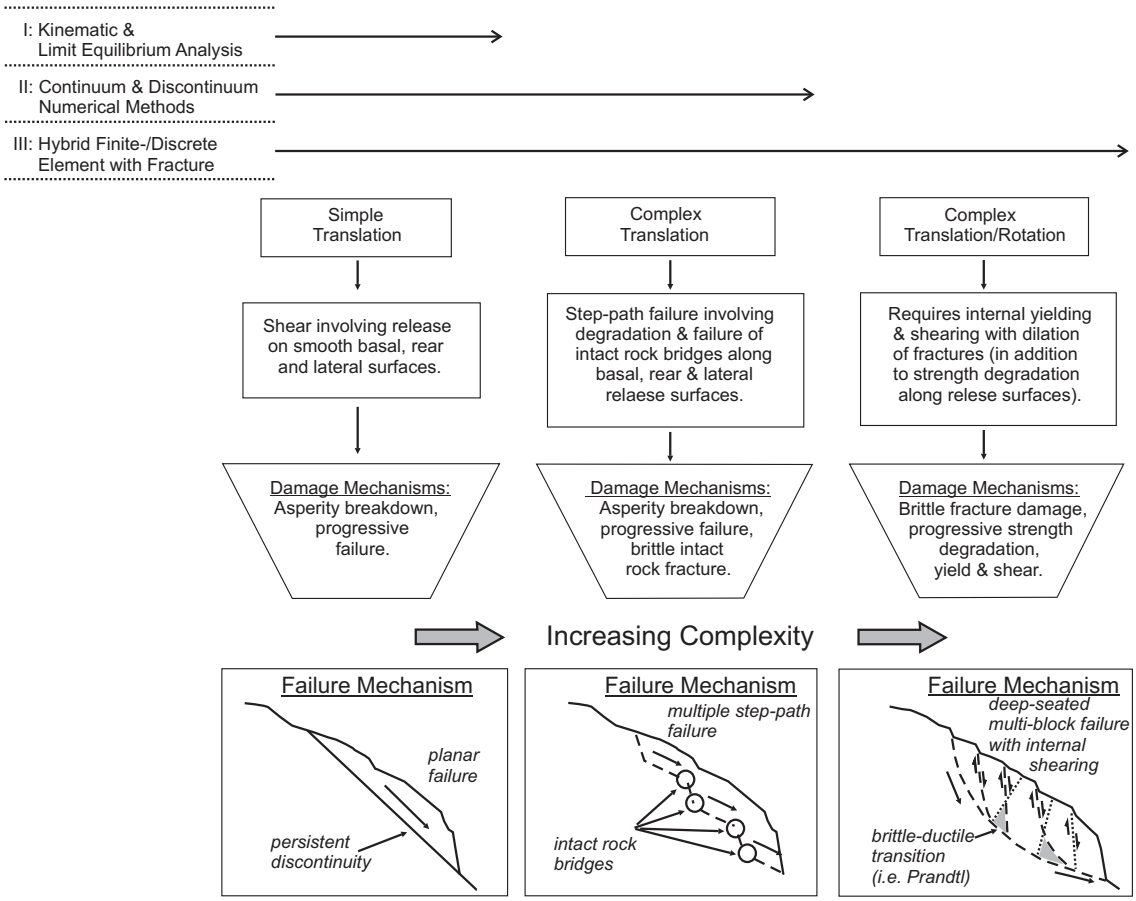

Figure 6: Three levels of stability analysis and related failure mechanisms (Stead et al., 2004).

a result of the merging of the micro-cracks.

In addition to failure models, several classification systems of failure mechanisms of rock slides have been proposed in the literature. Table 2 suggested by Hungr and Evans (2004) is an example of a classification based on the rock structure and the mechanical properties of the rock mass and includes examples of internationally well-documented rockslides. In light of this classification, the Åknes slide is an unconstrained, compound rock slide in strong rock (as described in Ganerød et al. (2008)), similar to the Vaiont slide.

Structural control	No	Systematic structural control					
Dominant mechanism	systematic	Sliding				Toppling	
Kinematics	structural	Translational	Compound			Flexural	Block
Constraint	control	Unconstrained	Constrained				
			At toe	At scarp			
Mechanism Type	A Rock slump B Rock collapse	C Block slide Wedge slide	D Structurally defined compound slide	E Block slide with toe breakout	F Compound slide	G Flexural topple	H Block topple
Typical behaviour in weak rock	Slow, rotational movement (Plateau d'Assy)	Catastrophic (Mt. Granier)	-	Slow (Downie Slide)	Slow (Liard Plateau)	Slow (La Clapiere)	-
Typical behaviour in strong rock	Catastrophic collapse, steep slopes, (Elm)	Catastrophic, limited pre-failure deformation (Goldau)	Catastrophic, large pre-failure deformation (Vaiont)	Catastrophic, (Madison)	-	- (Mystery Creek)	Catastrophic

Table 2: Classification of failure mechanisms of large rock slides (after Hungr and Evans (2004)).

2.3 Time-dependent behaviour of deep seated landslides

Deep-seated landslides and large-scale rock avalanches are two types of mass movements which display different movement rates, the former normally with very slow or extremely slow rates of movement (very slow and extremely slow are defined as <1.6 m/year and <60 mm/year respectively, according to Cruden and Varnes (1996)), while the latter display rapid or extremely rapid downslope movement (defined as >5 m/sec). According to Oyagi et al. (1994), the ultimate failure of a slope has often been "prepared" by a long period of extremely slow "creep" type movement. Deep-seated landslides which at present are moving slowly, hence may represent the initial stage of slope movements which might lead to accelerated deformations and finally large-scale rock avalanches (Oyagi et al., 1994). Time-dependent behavior of deep seated landslides has been discussed in the literature since the 1960's (Dramis and Sorriso-Valvo, 1994), and various terms are used for these phenomena. Some of them are listed in Table 3.

Ter-Stepanian (1966) identified different types of depth creep in rock slopes, including

Term	Reference
Depth creep	Ter-Stepanian (1966)
Deep-seated creep	Nemčock (1972)
Deep-seated continuous creep	Hutchinson (1968)
Sackung	Zischinsky (1966), Savage and Varnes (1987)
Flow	Petley (1978)
Mass rock creep (MRC)	Radbruch-Hall (1978), Chigira (1992)
Deep-seated gravitational slope deformations (DGSD)	Dramis and Sorriso-Valvo (1994)

Table 3: Classification of deep-seated slope movements.

planar depth creep in stratified rocks. This is for situations when the slope is oriented parallel to the bedding planes and the geological structure represents alternation of strong and weak strata (Figure 7(b)), which is also the case at Åknes (the geology of Åknes is presented in Ganerød et al. (2008)).

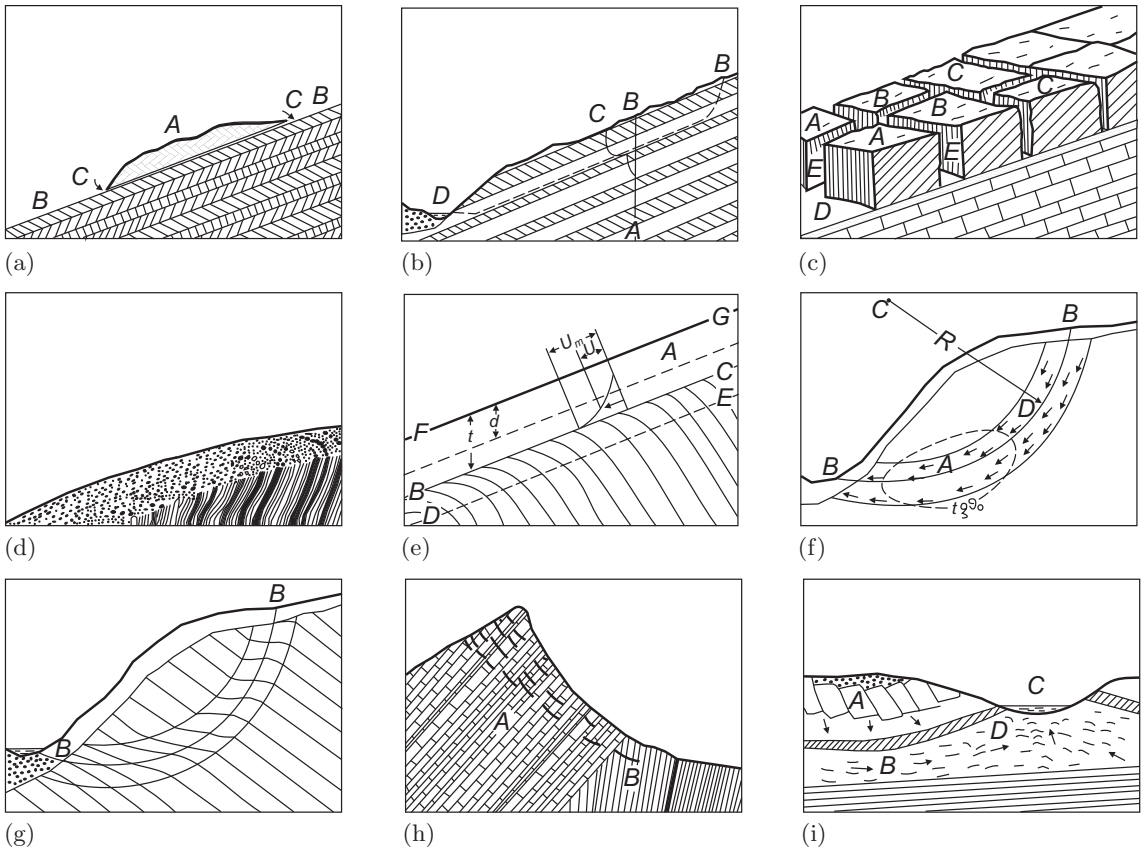

Figure 7: Creep mechanisms in rock masses after Ter-Stepanian (1966) a) Slab creep b) Consequent creep c) Block creep d) Outcrop creep or solifluction e) Terminal creep f) Asequent creep g) S-like creep h) Insequent creep i) Compensating creep.

The term deep-seated gravitational slope deformations (DGSD) is widely used today, and according to Dramis and Sorriso-Valvo (1994), DGSD can be described as a group of mass movement phenomena characterized by the following:

- The deforming mass may or may not be bounded by a continuous yielding surface; however, the continuity of such surface is not indispensable to explain the surficial deformations.
- The volume of masses involved is of the order of several hundred thousands of cubic meters or more, the thickness is several tens of meters or more.
- Scale factors, as discussed by Goguel (1978), may influence the mechanical proper-

ties of the rock and, consequently, the deformation mechanism.

- The total displacement is small in comparison to the magnitude of the mass.

2.3.1 Time-dependent behavior of rock material

In rock mechanics, the idealized form of a creep curve can be divided into three separate "regions" as shown in Figure 8, where the creep strain may be represented by (Jaeger and Cook, 1968):

$$\epsilon = \epsilon_e + \epsilon_1(t) + Vt + \epsilon_3(t) \tag{1}$$

where ϵ_e is the instantaneous elastic strain, $\epsilon_1(t)$ is the transient creep, Vt is the steady-state creep, and $\epsilon_3(t)$ the accelerating creep.

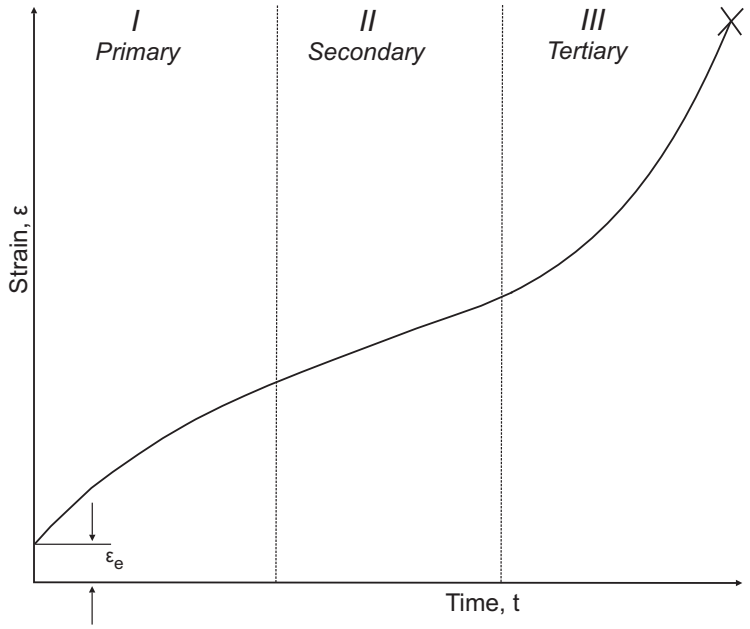

Figure 8: Idealized creep behavior for rock materials and cohesive soils (modified from Jaeger and Cook (1968)).

The three "regions" may be described as follows:

I : The strain-time curve is concave downwards, creep in this region is called primary or transient.

II : The strain-time curve has approximately constant slope, creep in this region is secondary or steady-state creep.

III : The strain-time curve is accelerating, creep in this region is tertiary and leads rapidly to failure.

According to Pomeroy (1978), the creep mechanisms for rocks can be explained based on stress concentrations that must occur in non-homogenous materials when loaded. Natural materials contain voids and cracks which if stressed will grow. The stress concentrations may decrease as a consequence of cracks propagating, merging or by running into a pore.

One approach adopted to study the creep of geological materials is the rheological approach, where idealized models (viscoelastic, viscoplastic, elasto-viscoplastic, Burgers, nonlinear visco-plastic, etc.) are fitted to experimental behavior of specific materials by means of numerical constants (Crosta and Agliardi, 2003). In this thesis, numerical modelling by the use of rheological models has been carried out in Paper V (Grøneng et al., 2009), and therefore a short description of the basic rheological models is given in the next section.

Slope creep is due to modifications in slope geometry, material properties and geomechanical features of discontinuities (Crosta and Agliardi, 2003). The idealized form of the creep curve may also apply to a creeping rockslope, as demonstrated by the sudden increase in the deformation rate before complete failure as discussed for the Ruinon rock slide (Crosta and Agliardi, 2003) and the Vaiont landslide (Kilburn and Petley, 2003; Pomeroy, 1978), both in Italy.

2.3.2 Rheological models

Rheological models offer a mathematical description of the fundamental behaviour for creep. The models are built up as combinations of linear elasticity and viscosity, and may be represented by simple mechanical models. The basic models are the Maxwell and Kelvin rheological models which form Burger model when combined in series. The Maxwell and Kelvin models consist of combinations of the linear elastic Hookean and the perfectly viscous Newtonian substance, which are the two basic models in rheology (see Figure 9).

Burger's model gives the simplest representation of a material which shows an instantanous strain, transient creep and steady state creep (Figure 9e). If the stress is released after some time, displacements will be permanent. In view of the general creep curve in Figure 8, the Burger's model is the simplest model that can be used to trace strain up to the onset of tertiary creep. The deformability constants have the following physical meaning:

G_2 is the elastic shear modulus

G_1 controls the amount of delayed elasticity

η_2 describes the rate of viscous flow

η_1 determines the rate of delayed elasticity

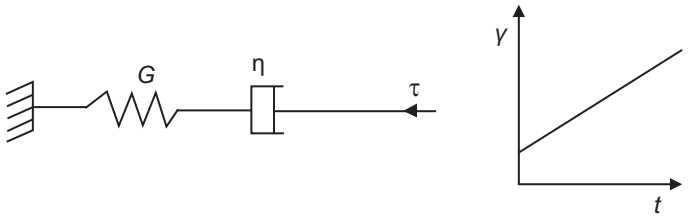

(a) Maxwell body (Two-constant liquid)

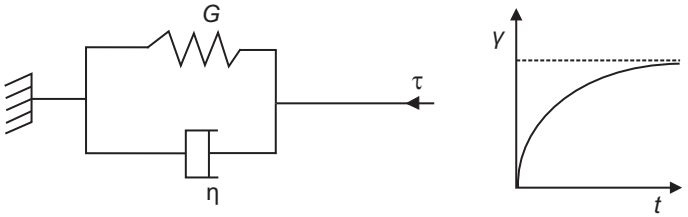

(b) Kelvin body (Two-constant solid)

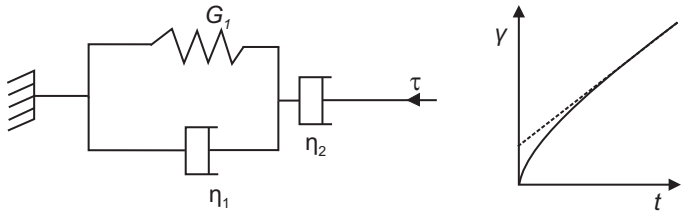

(c) Generalized Maxwell body (Three-constant liquid)

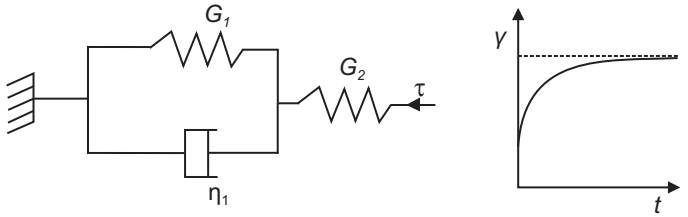

(d) Three constant solid

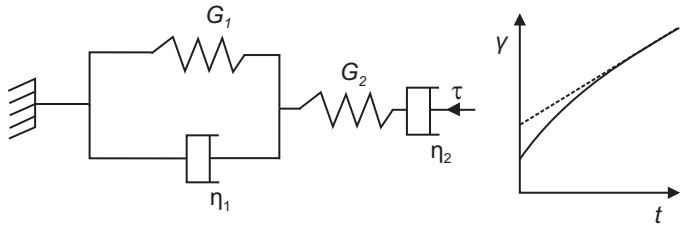

(e) Burgers body (Four-constant liquid)

Figure 9: Basic rheological models (from Goodman (1980)).

3 Methodology

3.1 Field work

Extensive field work with main focus on geological mapping has been carried out by the author during the summers of 2004, 2005 and 2006. Outcrops throughout the area were described in detail, including measurements of strike/dip, registration of joint frequency and -continuity, joint roughness (JRC), Schmidt hammer rebound values, Q-values and Geological Strength Index (GSI) values. Samples of rock and gouge were collected in order to carry out laboratory analysis. The field work has also included follow-up and core logging of four of the seven boreholes at three drilling sites in the area (summer of 2005). Fracture frequency, Rock Quality Designation (RQD), joint material and core loss were registered together with a general description of the cores. The cores were also later logged at the Geological Survey of Norway, where orientation of joints and foliation and lithological logging were included. The logging resulted in an internal report (Ganerød et al., 2007).

In addition, displacement measurements have been carried out by the use of tape extensometer, which was used to measure the distance across selected joints throughout the area based on two annual measurement campaigns from 2005 to 2008 (Kveldsvik and Grøneng, 2007).

3.2 Laboratory testing

Laboratory testing of rock and soil has been carried out by the author at the NTNU/SINTEF Engineering Geology and Rock Mechanics Laboratories and at the NTNU Geotechnical Laboratory. Triaxial testing of rock and soil was performed as described in Paper I (Grøneng et al., 2009) and basic friction angle for cores was determined and described in Grøneng and Nilsen (2009).

In addition, the SINTEF Rock Mechanics Laboratory has tested cores obtained by coredrilling at Åknes for several standard parameters which have been used in this thesis. These tests have included deformability of rock (Young's modulus, E_i), Poisson's ratio

(ν), Uniaxial Compressive Strength (UCS), tensile strength by Brazilian test (σ_t), sound velocity (v) and density (ρ). Description of the testing methods and results are given in Ganerød et al. (2007).

3.3 Numerical modelling

Numerical modelling is a more recent development in slope stability analysis than the more traditional limit equilibrium method. Several numerical methods are offered (see Figure 10) and characteristics, applications and limitations of the methods used in slope stability analysis are described and discussed for instance in Eberhardt (2006), Wyllie and Mah (2004) and Coggan et al. (1998). Two modelling tools have been used in this thesis work; $Phase^2$ developed by *Rocscience* and $FLAC^{3D}$ developed by *Itasca*. The choice of modelling tools is based on the desire to perform parameter studies ($Phase^2$) and to model time-dependent characteristics with a three-dimensional model ($FLAC^{3D}$). Both programs are based on continuous differential models, however $Phase^2$ is based on Finite Element Method (FEM) whereas $FLAC^{3D}$ is based on Finite Difference Method (FDM).

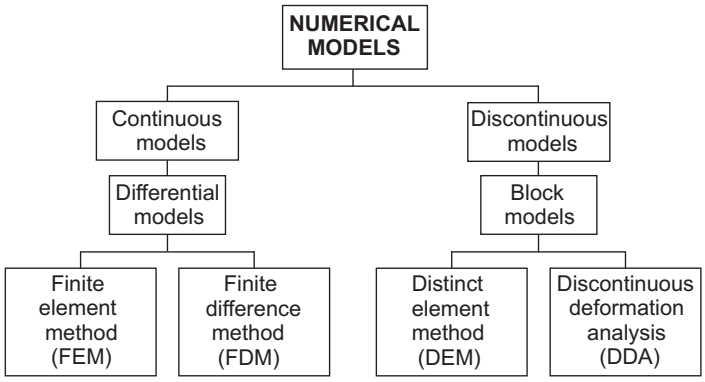

Figure 10: Numerical methods used in slope stability analysis.

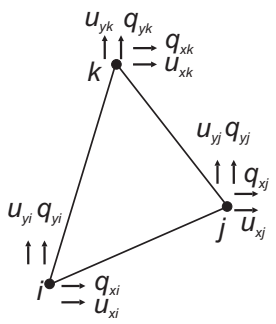

Figure 11: Triangular finite element with induced nodal displacements and forces (u_{xi}, q_{xi}, u_{yi}, q_{yi}, etc.) (Brady and Brown, 2005).

FEM divides the body into smaller "elements" of various shapes (e.g. triangles and rectangles for 2D-modelling) held together at the "nodes" (vertices or mid-edge of the elements). A representative 2D-element is shown in Figure 11, with the points i, j, k defining the nodes. Displacements within the element are related to the displacements at the nodes through so-called shape functions. Stresses are calculated at one or more points inside each of the elements. Transmission of internal forces between the edges of adjacent elements are represented by interactions at the nodes of the elements.

In 2D-modelling based on the specific FDM used in $FLAC$, the body is divided into a finite difference mesh consisting of quadrilateral elements. Inside the program, each element is subdivided into two overlayed sets of constant-strain triangular elements, as shown in Figure 12. The four elements are termed a, b, c and d. The deviatoric stress components of each triangle are maintained independently, requiring sixteen stress components to be stored for each quadrilateral ($4\times\sigma_{xx}, \sigma_{yy}, \sigma_{zz}, \sigma_{xy}$). The force vector exerted on each node is taken to be mean of the two force vectors exerted by the two overlaid quadrilaterals. $FLAC$ is advantageous for large deformations due to the fact that if one pair of triangles becomes badly distorted, the corresponding quadrilateral is not used; nodal forces from the other quadrilateral are used instead. Stresses and strains are calculated for each of the four triangles and averaged to give the stress and strain for that element.

The finite element method and the finite difference method both produce a set of algebraic equations to solve, however, the main difference between them is how they are solved. The FDM in $FLAC$ uses an "explicit" time marching method to solve the algebraic equations, while matrix-oriented solution schemes are more common in FEM. In the explicit calculation method (illustrated in Figure 13), the equations of motion are solved to derive new velocities and displacements from stresses and forces. Strain rates

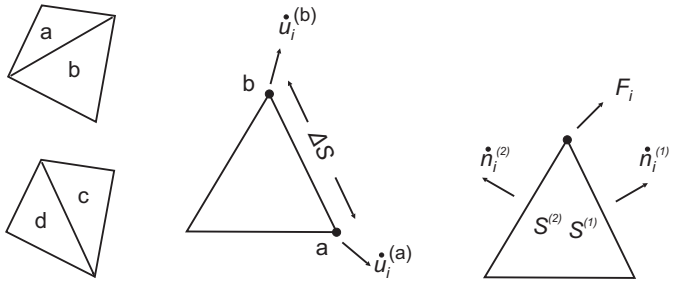

Figure 12: (a) Overlaid quadrilateral elements used in $FLAC$ (b) Typical triangular element with velocity vectors (c) Nodal force vector (from $Itasca$ (2002)).

are then derived from velocities and new stresses from strain rates. The calculations are carried out over one timestep, during which velocities are assumed to be constant. This requires that the timestep is smaller than the time it takes for information to pass from one element to another.

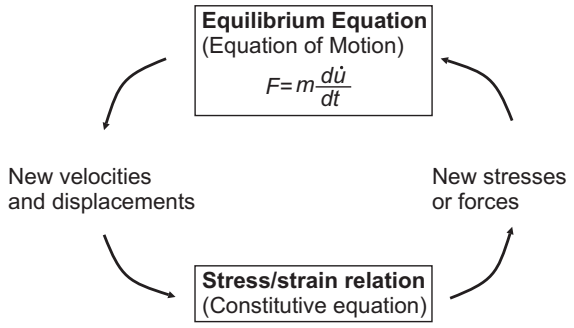

Figure 13: Explicit time marching calculation cycle (from $Itasca$ (2002)).

In the FEM, an implicit method is often used for solving the equations, in which every element communicates with every other element during one solution step and several iterations are necessary before compatibility and equilibrium are obtained. More detailed descriptions of FEM and FDM is given by Brady and Brown (2005) (FEM and FDM), $Itasca$ (2002) (FDM), Pande et al. (1990) (FEM) and others.

3.3.1 $Phase^2$

$Phase^2$ is a 2D elasto-plastic finite element stress analysis program for underground or surface excavations in rock or soil. The program can be used for a wide range of engineering purposes, including support design, finite element slope stability analysis and groundwater seepage analysis. A wide range of material models are offered in $Phase^2$, version 6, as shown in Figure 14. Detailed descriptions of program applications and material models are given in the program manual (*Rocscience*, 2005).

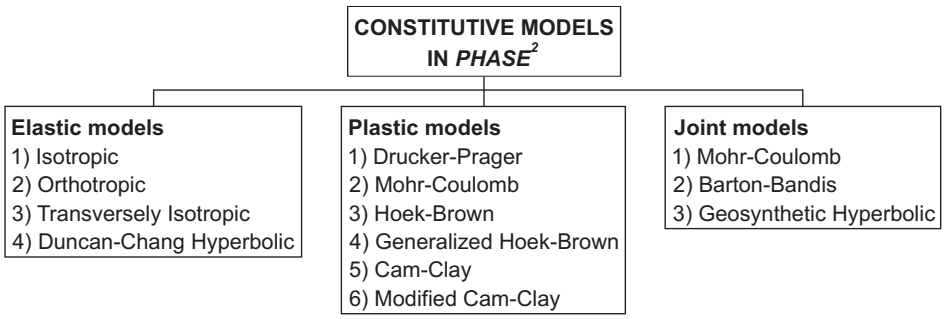

Figure 14: Constitutive models available in $Phase^2$ (*Rocscience*, 2005).

One of the major features of $Phase^2$, version 6, is finite element slope stability analysis using the Shear Strength Reduction (SSR) method. This option can be used with either Mohr-Coulomb or Hoek-Brown strength parameters. The factor of safety, F, in FEM slope stability analysis is defined as for traditional limit-equilibrium analysis (Duncan, 1996):

$$F = \frac{Shear\ strength\ of\ material\ (rock\ or\ soil)}{Shear\ strength\ required\ for\ equilibrium} \tag{2}$$

The Shear Strength Reduction (SSR) method is widely used to determine the factor of safety of a slope based on FEM. The method reduces the shear strength of slope materials until the situation becomes unstable. Failure is defined as the point when when the finite element model does not converge to a solution, because equilibrium cannot be maintained. The critical factor at which failure occurs is taken to be the factor of safety.

3.3.2 $FLAC^{3D}$

$FLAC^{3D}$ is a 3D explicit finite-difference method (FDM) program for engineering mechanics computation. The three-dimensional program simulates the behavior of structures consisting of soil, rock or other materials that undergo plastic flow when their yield limits are reached. $FLAC^{3D}$, version 3.0, offers twelve constitutive models in addition to eight creep material models as shown in Figure 15.

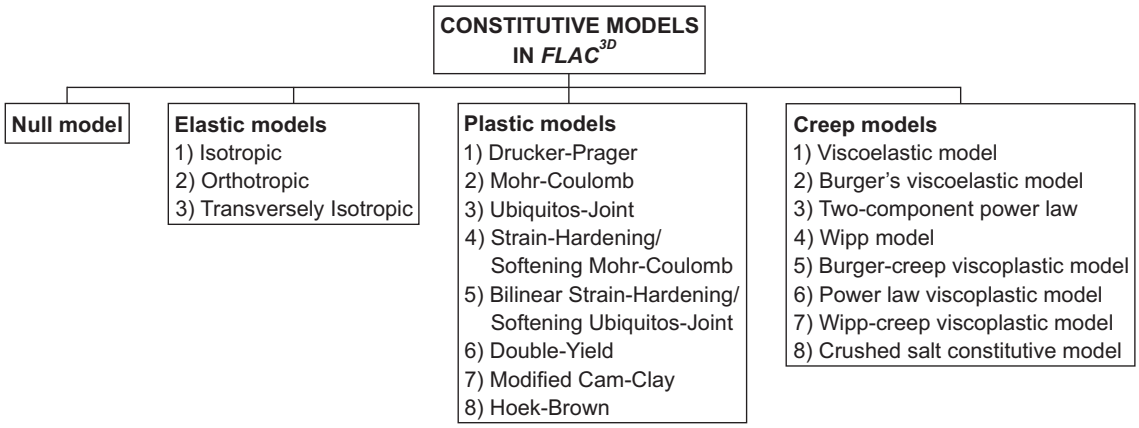

Figure 15: Constitutive models available in $FLAC^{3D}$ (*Itasca*, 2002).

Further details regarding the program applications and material models are given in the program manual (*Itasca*, 2002).

4 Comments on main papers

The main papers based on this PhD research are numbered I-IV and included in full length after this introductory part of the thesis. Brief comments on the papers and the main conclusions based on each paper are given in the following.

4.1 Paper I: Shear Strength Estimation for Åknes Sliding Area in Western Norway

Sliding planes in rock masses have lower shear strengths than the surroundings and are particularly susceptable to sliding displacement. There are different types of sliding surfaces, and for Åknes, it is believed that the zone of deformation is highly complex and consists of a combination of the following:

(a) Unfilled joints (rock-to-rock contacts). These are believed to represent foliation in the gneiss, and possibly also exfoliation.
(b) Filled joints containing gouge of 1-5 cm thickness.
(c) Bridges of intact rock.

Shear strengths (τ) of (a) to (c) cover a great range, and a methodology for how these can be combined to form a resultant shear strength of the overall sliding zone has been developed in this paper. The method also represents an alternative to the commonly used method of back-calculation, where the shear strength is found based on assuming a safety factor equal to one for failed slope.

The basic methodology in this paper is illustrated by Figure 16. As can be seen, the method results in the resultant active friction angle ($\phi_{a,res}$), depending on the relative percentage of materials present in the sliding plane and the acting normal stress, $\sigma_{n,acting}$.

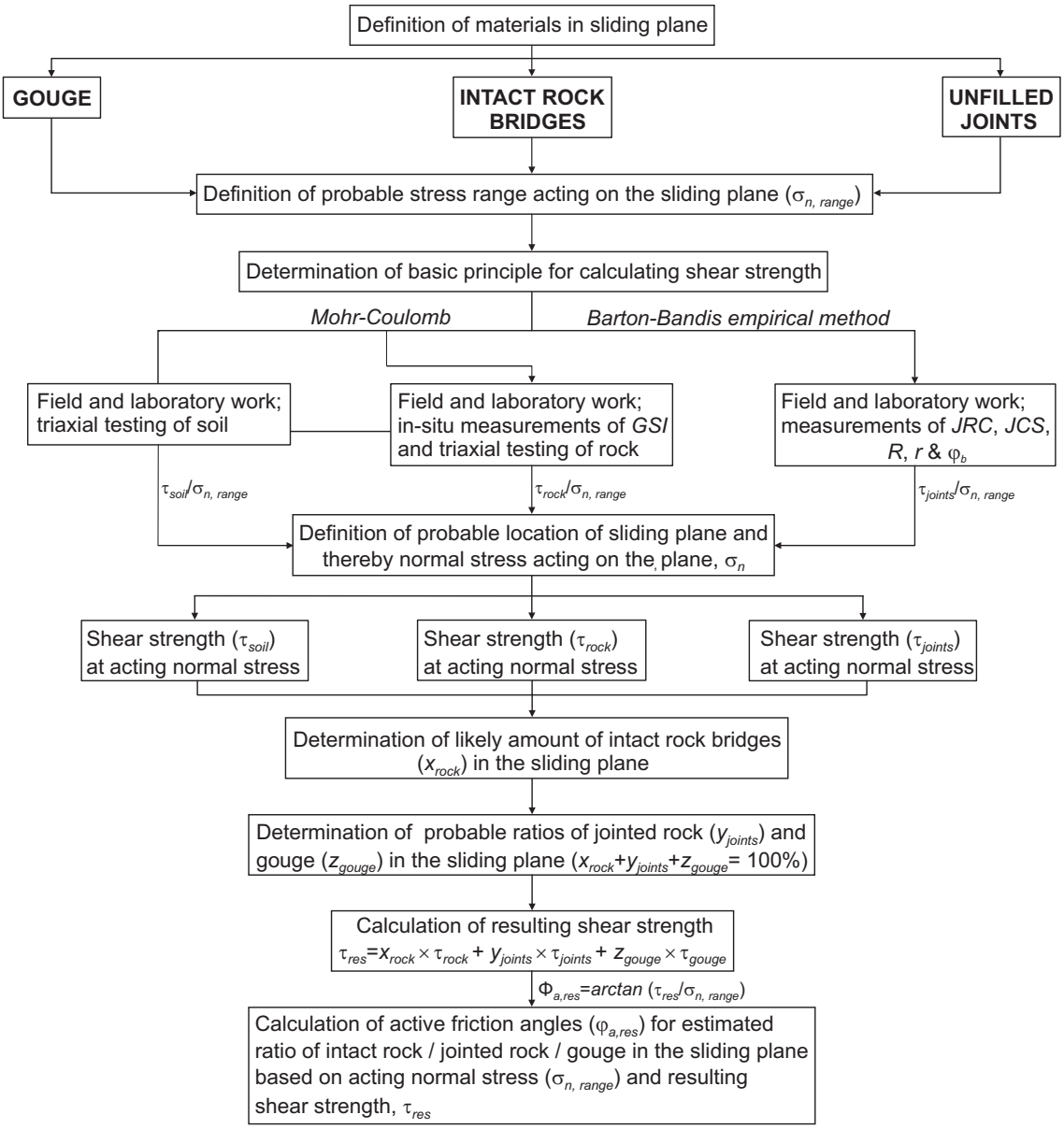

Figure 16: Flowchart illustrating methodology for defining resultant shear strength parameters (resultant active friction angle, ($\phi_{a,res}$), cohesion (c_{res}) and friction angle (ϕ_{res})) of complex sliding plane.

The normal stress acting on the sliding plane has been calculated for two scenarios, with sliding planes located 25 and 60 m below the surface, respectively, resulting in a normal stress range of 0.5-1.3 MPa. Based on the methodology in Figure 16, the ranges of resulting shear stress (τ_{res}) were determined to be 0.5-0.75 MPa and 1.05-1.3 MPa for sliding planes located 25 and 60 m below the surface, respectively, and alternative compositions of the sliding plane of 1-3% intact rock, 25-35% gouge and 62-74% rock-to-rock contacts. These assumed compositions of the sliding plane were based on a combination of field observations and drill core logging. Active friction angles calculated for the relevant normal stress range and for the same assumed composition of the sliding plane were in the range 37-47° for 1% intact rock failure and 43-57° for 3% intact rock failure.
The methodology is used to calculate resultant cohesion (c_{res}) and resultant friction angle (ϕ_{res}) based on the active friction angle ($\phi_{a,res}$) in Figure 16, which is used in numerical modelling presented in Section 5.1 and Paper IV (Grøneng et al., 2009).

4.2 Paper II: Geovisualization, Geometric Modelling and Volume Estimation of the Åknes Rockslide, Western Norway

This paper describes an interactive 3D software application (3D model) which integrates geophysical, geological and engineering geological data collected from the Åknes rockslide site during extensive field work in the summers of 2004-2007. Detailed geological mapping, geophysical investigations and drilling of seven boreholes at three locations has generated a vast amount of geological data. The 3D model is based on OpenSceneGraph (OSG) which is a freely available high level library for development of 3D graphics applications. The use of the interactive 3D model has enabled the determination of three scenarios for the geometry of the rock slide and resulted in estimations of the geometric extent and volume of potential rock slope failure for each scenario. Figure 17 illustrates the type of data used as a basis for determining the three scenarios.

The geophysical investigations included in the geovisualization model are seven 2D resistivity profiles (five slope parallel profiles with E-W strike, and two down-slope profiles

with N-S strike, totalling about 10,000 m) and seven GPR (georadar) profiles (four slope parallel profiles with E-W strike, one profile with NE-SW strike, and two down-slope profiles with N-S strike, totalling about 5,300 m). Data from corelogging of seven boreholes at three different sites in the rockslide area (three vertical holes to 150 m depth, one inclined hole by 60° to 150 m depth and three vertical holes down to 200 m depth) were also included in the 3D model as well as detailed photographs of the cores. Borehole investigation data in the 3D-model included parameters as shown in Figure 17 (logging of one borehole at each drilling site). Details on the geological and geophysical data included in the 3D model are discussed by Ganerød et al. (2008).

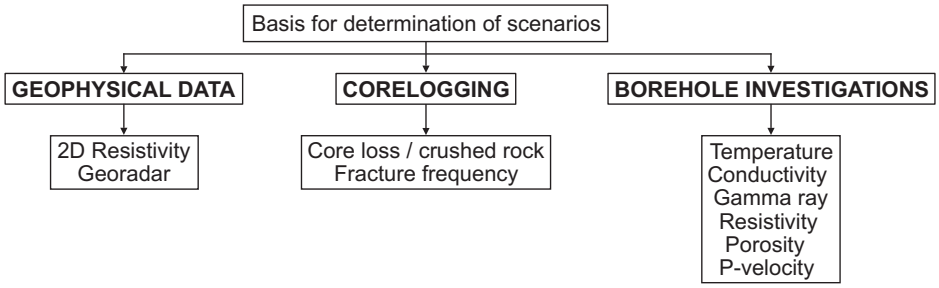

Figure 17: Flowchart illustrating type of data used in the interactive 3D-model for determination of three different scenarios for location of the basal sliding surface at Åknes.

The three scenarios for location of the basal sliding plane were:

Scenario A An undulating basal sliding plane located 40-55 m below the surface, resulting in a horisontal area of 510,000 m^2 and volume of 20×10^6 m^3.

Scenario B An undulating basal sliding plane located 105-115 m below the surface, resulting in a horisontal area of 575,000 m^2 and volume of 43×10^6 m^3.

Scenario C Basal sliding plane located 150-190 m below the surface, resulting in a horisontal area of 742,000 m^2 and volume of 85×10^6 m^3.

Scenario B was concluded to be the most likely scenario while Scenario C was selected as "worst case scenario" in this paper.

4.3 Paper III: Meteorological Effects on Seasonal Rock Displacements of the Åknes Rockslide, Western Norway

In this paper, the effects of the meteorology and groundwater on the relative stability of the upper part of the slope were investigated. Results have been analysed for the period November 2004−August 2008 from continuous displacement recordings by five extensometers installed across the back scarp and two laser beams monitoring the displacement of an individually moving graben structure located in the western end of the back scarp.

Surveillance by extensometers across the back scarp started as early as August 1993 by installation of three extensometers (Ext. 1, Ext. 2 and Ext. 3a). In August 2004, two additional extensometers were installed (Ext. 4 and Ext. 5), in addition to changing the direction of Ext. 3a (termed Ext. 3b after the new measuring direction). Recordings from the extensometers thus are available for a 14-year period, as shown in Figure 18. However, the records due to technical problems are not complete. For instance, measurements from the five-year period from August 1998 to September 2003 are subjected to a high degree of noise, due to an error in the daily reading routine. The extensometers have also been periodically out of order, as evidenced by the more than two-year period from June 1996 to September 1998, the four-month period from February 2002 to June 2002 and the nearly two-year period from January 2003 to November 2004. During these periods, no deformation data has been registered. Due to lightning, which destroyed the data transmission from the extensometers, data are also lacking for the period mid February to July 2008. Ext. 4 and 5 have limited recordings due to damage by snow avalanches; Ext. 4 has no recordings after July 2005 and Ext. 5 was operative only for a period of about one year (November 2004−November 2005). Concerning periods with continuous recordings, the total measuring period of 14 years thus can be divided into three periods:

1) August 1993−July 1996
2) September 1998−September 2003
3) November 2004−August 2008

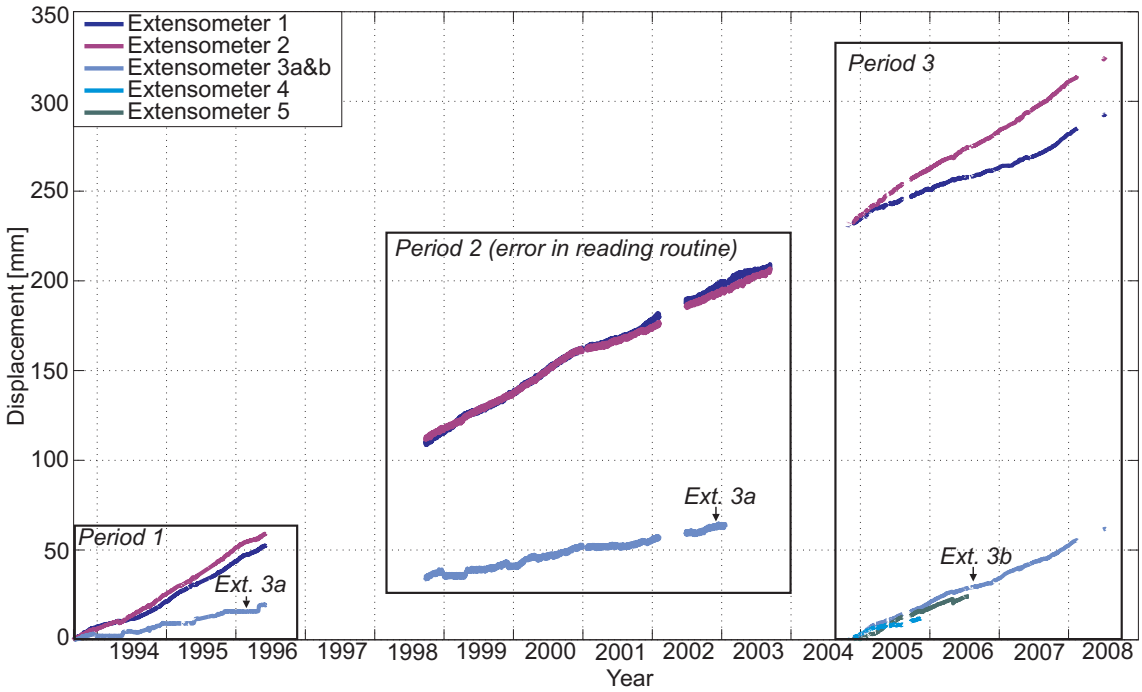

Figure 18: Extensometer records from the back scarp since August 1993.

In order to analyse the displacements in relation to the meteorology, it was decided to focus on period 3) as data from a meteorological station at the Åknes site was available from November 2004. Also, data from monitoring of groundwater levels in upper and middle borehole were available from November 2006 and laser data from monitoring of the graben structure in the westernmost part of the back scarp was available from December 2005. Period 1) is previously analysed with respect to meteorology by Larsen (1999) and Sandersen et al. (1996) while period 2) is not relevant for detailed day-to-day analysis due to the error in reading routine during this period.

A total of twelve "events", where expansion or contraction of the back scarp has been recorded by more than one extensometer, have been analysed in detail with respect to meteorology and groundwater levels (where available). The paper concludes that the relative stability of the upper area at Åknes is highly affected by the groundwater level. Large fluctuations in groundwater levels in spring and early summer (due to varying feeding of the groundwater from snowmelt in addition to precipitation), causes the largest net

expansion of the back scarp. Stable groundwater levels in summer and early autumn result in no significant displacement events in the back scarp while reductions in temperatures to below 0°C in autumn and early winter cause reduction of the distance (interrupted by air temperature increases to above 0°C due to the marine climate in the western part of Norway causing expansion). In late winter the temperatures are stable below the freezing point and the ground is covered with a 1-3 m thick snow cover, resulting in no significant displacement. The results in this paper also show that a majority of events from the extensometer records (10 out of a total of 12) were recorded in the first half of the analysed period (September 2004−August 2006), indicating less significant meteorological effects on the displacements in the back scarp in the last half of the period (September 2006−August 2008).

4.4 Paper IV: Time-dependent behavior of the Åknes Rockslide Area in Western Norway

In this paper, an analysis of time-dependent deformation of the Åknes slope is carried out based on numerical modelling. The Burger-Creep Viscoplastic (cvisc) material model in $FLAC^{3D}$ was chosen for analysis since this model represents creep behavior up to onset of tertiary creep. Geometry of the sliding plane was based on coordinates of the basal sliding surface with the most likely geometry in the 3D geovisualization model presented in Paper III (Nordvik et al., 2009). Considerable effort was related to the generation of a rockslope model in $FLAC^{3D}$. A methodology for reading coordinate files from airborne laser scanning of the slope (representing the topography) and coordinates representing the sliding surface from the geovisualization model (described in Paper II) and subsequently generating the input file necessary for a model generation in $FLAC^{3D}$ was developed based on $MATLAB$ (MathWorks, 2006) as shown in Figure 19. Based on the input file generated by the methodology presented in Figure 19, the modelling has been carried out as presented in Figure 20. The modelling was carried out for two alternative sets of parameters, one set believed to be representative of the present situation, and one believed to represent

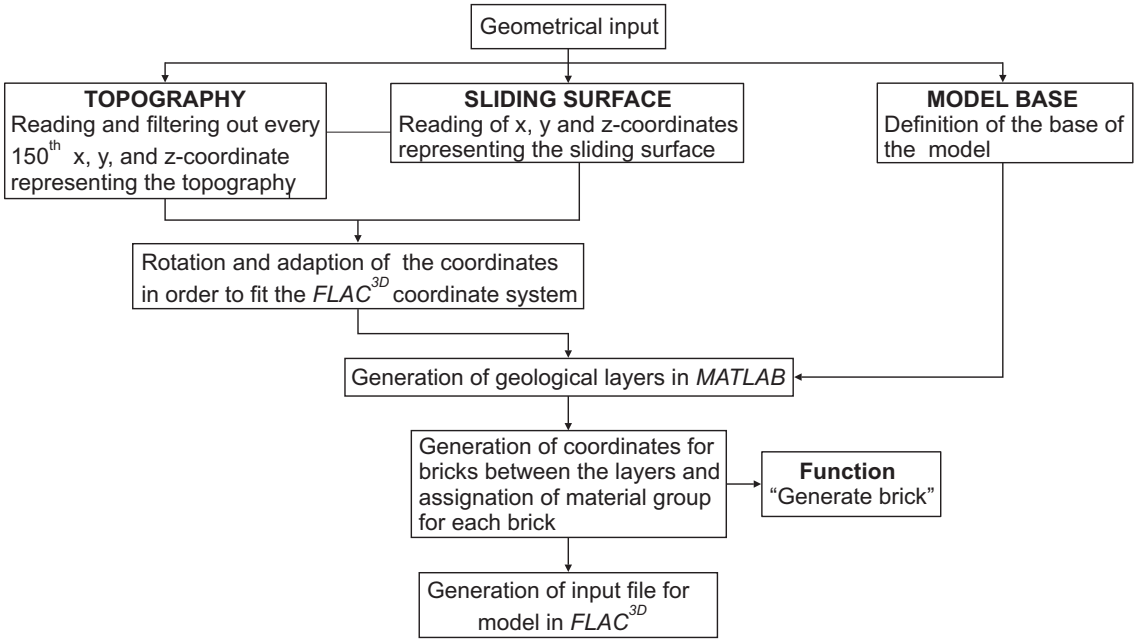

Figure 19: Methodology for reading coordinate files and generating input file in $MATLAB$ for model in $FLAC^{3D}$.

a realistic future scenario. Parameters for the first case were determined by estimating a composition of the sliding layer according to the methodology presented in Paper I, with Mohr-Coulomb parameters representing 3% failure of intact rock bridges, 62% failure along unfilled joints and 35% failure along gouge-filled joints. Creep parameters for the cvisc material model were determined by calibrating the model to an average displacement rate of 26 mm/year in the central area of the model (corresponding to monitoring data from GPS/reflector points). Mohr-Coulomb parameters for the unstable rock mass above the sliding layer were determined by laboratory testing of various types of gneiss in the area (discussed under "Laboratory testing" in section 3.2). Scaling of the parameters to in-situ condition was carried out based on *RocLab* (Rocscience, 2002) and an average measured GSI-value 62 (presented in Paper I), reflecting "good surface conditions" according to the GSI rating system. The rock mass below the sliding layer was modeled as an elastic material in order to force the focus on the sliding layer and the rock mass above it. The model was fixed at the base while the potential unstable rock mass above the sliding zone

as well as the sliding zone itself were free to move down-slope, except for the toe. As the toe does not daylight in field, the lower boundary of the model was fixed in the horizontal direction. Several scenarios were modeled in search of a future scenario which resulting in an unstable lower boundary in the model. For the sliding layer, an estimation of 1% failure of intact rock bridges, 65% failure along unfilled joints and 35% failure along gouge-filled joints was used to determine Mohr-Coluomb parameters. Creep parameters for the cvisc material model and elastic parameters for the rock mass below the sliding layer were kept constant. Mohr-Coulomb parameters for the unstable mass above the sliding layer were determined by scaling the parameters from laboratory testing with a GSI 37, representing "fair surface conditions". The latter alternative parameters resulted in an unstable toe and increased displacements throughout the 100 year period, indicating critical shear strength parameters.

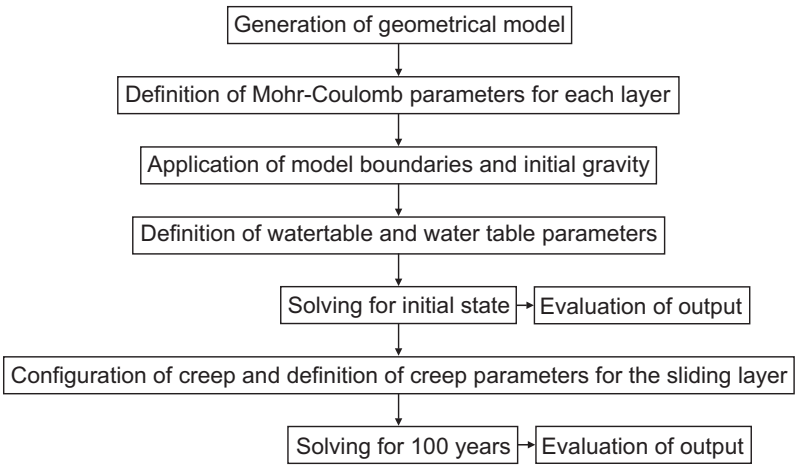

Figure 20: Methodology for creep modelling in $FLAC^{3D}$.

5 Discussion and conclusions

5.1 Discussion

The thesis covers a study of several factors important for slope stability at the Åknes sliding area, as well as stability analysis based on numerical modelling. As each of the main papers has an individual discussion, and important aspects have also been discussed has been presented in Sections 4.1−4.4, an overall discussion is presented here. The methodology for slope stability analyses typically consists of three steps: (1) Definition of potential failure geometry, (2) Definition of parameters influencing on stability, most importantly the shear strength of the sliding plane(s) and groundwater conditions and (3) Analysis/calculation of safety factor or risk of failure by limit equilibrium methods or numerical modelling. The papers prepared for this thesis are in principle related to the steps as shown in Figure 21.

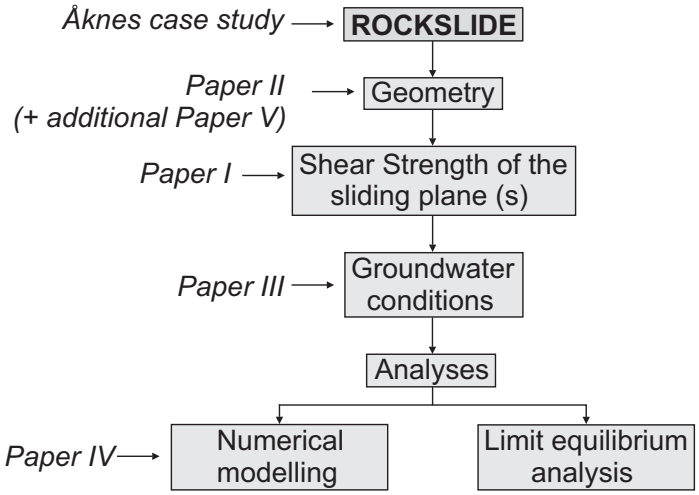

Figure 21: Flowchart illustrating the methodology for slope stability analyses and the relation between the papers.

The thesis thus deals with all the different steps of stability analysis, all essential for the success of estimating the stability of large scale rockslides. A challenge has been to process the increasing amount of datasets and new knowledge which have become available in the Åknes project during the progress of the thesis. A methodology for estimation of resultant shear strength of a complex sliding plane is presented in Paper I (Grøneng et al., 2009), and resultant shear strengths are estimated for two scenarios; basal sliding surfaces located 25 and 60 m below the surface, respectively. The groundwater table in this analysis is assumed to be located at the depth of the lower sliding surface (60 m below the surface) in this analysis. However, as more geological/geotechnical data and sophisticated geovisualization became available, the location of the basal sliding surface is adjusted in Paper II (Nordvik et al., 2009) to a geometry where it is undulating and located 105-115 m below the surface. Analyses of meteorology and groundwater in Paper III (Grøneng et al., 2009) show that the groundwater level fluctuated between -42.5 and -46.5 m below the surface in the middle borehole, and between -51 and -60 m in the upper borehole during the period analysed (December 2006−August 2008), indicating a shared groundwater regime in the upper area. In order to carry out a verification of the methodology for shear strength estimation presented in Paper I, with the most likely geometry presented in Paper II (scenario B) and groundwater analysis in Paper III, modelling has been carried out based on $Phase^2$ (*Rocscience*, 2005) and the Shear Strength Reduction (SSR) analysis. A sliding plane located at an average depth of 110 m below the central part of the sliding surface has been modeled according to the findings in Paper II, and alternatives of 1, 3 and 5% intact rock bridges in the basal sliding plane have been studied. The parameters are hence calculated based on a normal stress of $\sigma_n = 1.8$ MPa, representing an average groundwater table located 60 m above the basal sliding plane (σ_n=γ_{rock}×h×cosα_{slope}-γ_w×h_w). The groundwater levels have been estimated to correspond to average groundwater levels in the upper and middle boreholes (-56 and -44 m, respectively), according to findings in Paper III. In the lower borehole, the groundwater level was measured throughout July 2008, and an average groundwater level of -42 m has been used in the lower area. Based on the occurrence of springs mapped in the field at an

elevation of 75-100 m a.s.l. (mentioned in Paper II), the groundwater level is assumed to daylight at the same elevation as the assumed toe. A likely amount of intact rock bridges in the sliding plane is assumed to be in the order of 1-3% in Paper I, while the likely amount of gouge is assumed to be in the order of 25-35%. Based on this, three scenarios have been modeled, with 1, 3 and 5% intact rock, respectively. The amount of gouge is set to 35% in all scenarios, hence, the percentages of unfilled joints are 64%, 62% and 60%, respectively (see Table 5). A model has been generated in $Phase^2$ as shown in Figure

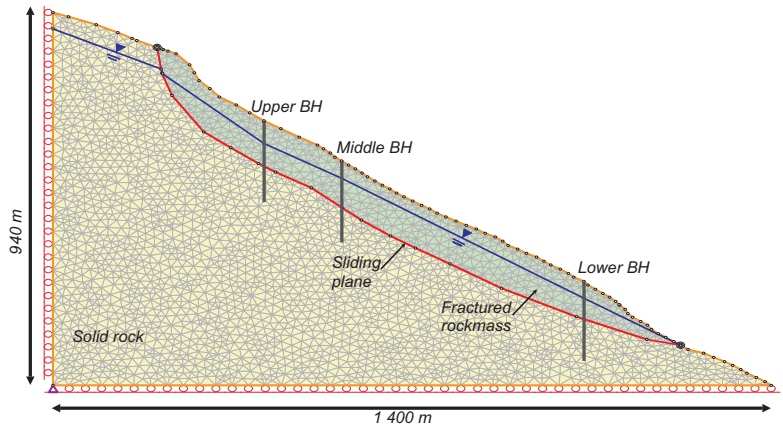

Figure 22: Model in $Phase^2$ with a sliding plane located at an average depth of 110 m below the surface.

22 with three layers; solid rock, a sliding plane (modeled as a continuous joint of 25 cm width) and fractured rock mass above the sliding plane. Calculations are performed based on body force only. As discussed in Paper I, assumptions have been made of how the open characters of the back scarp and other discontinuities affect the stress conditions.

The solid rock is modeled as an elastic material, forcing the focus away from this part of the model, while the fractured rock mass is modeled as a plastic material. Residual values for c and ϕ is set equal to the initial values, 15 MPa and 48°, respectively. The input parameters for the respective layers are based on laboratory testing of rock cores (Ganerød et al., 2007) and shown in Table 4. The parameters for the joint are calculated based on the methodology presented in Paper I (c_{res} and ϕ_{res}), and estimation of Joint

Stiffness is carried out as described in $Phase^2$ manual (*Rocscience*, 2005):

$$k_n = \frac{E_i \, E_m}{L(E_i - E_m)} \tag{3}$$

$$k_s = \frac{G_i \, G_m}{L(G_i - G_m)} \tag{4}$$

where

E_m and G_m = rock mass modulus and rock mass shear modulus

E_i and G_i = intact rock modulus and intact rock shear modulus

k_n and k_s = joint normal stiffness and joint shear stiffness

L = mean joint spacing

As can be seen from Table 5, the resultant cohesion and friction angle (c_{res} and ϕ_{res}) for the sliding plane vary according to the percentage of intact rock. E_{rm} is obtained from *RocLab* by scaling the GSI-value to fit the friction angle, ϕ_{res}. The table also shows the Strength Reduction Factors (SRF) as obtained from SSR-analyses in $Phase^2$.

	Laboratory testing			Input in *RocLab*		Parameters from *RocLab*			
Layer	UCS [MPa]	E_i [GPa]	ν	GSI	m_i	c [MPa]	ϕ[°]	σ_t [MPa]	E_m [GPa]
Solid rock	144	38.7	0.13	85	25	15	48	1.1	34.1
Fractured rock	144	38.7	0.13	62	25	11.5	43	0.3	21.9

Table 4: Input parameters and parameters obtained from *RocLab*.

Rock bridges [%]	Gouge [%]	Joints [%]	$\phi_{a,res}$ [°]	c_{res} [MPa]	ϕ_{res} [°]	ν	E_{rm} [MPa]	SRF
1	35	64	39	0.23	32.5	0.3	2 609	0.96
3	35	62	45	0.46	32.8	0.3	2 775	1.1
5	35	60	50	0.7	33.1	0.3	2 955	1.23

Table 5: Parameters for a joint (width=25 cm) 110 m below the surface (σ_n = 1.8 MPa) and resulting SRF values based on $Phase^2$.

According to the results, parameters of 1% rock bridges (c_{res}=0.23 MPa and ϕ_{res}=32.5°) result in a Strength Reduction Factor (SRF) smaller than 1.0, reflecting an unstable situation, while estimations based on 3 and 5% rock bridges result in $SRF > 1$. Yielding shown in Figures 23(a)-(c) indicates that a sliding plane with 3% intact rock, 62% unfilled joints and 35% gouge (c_{res}=0.47 MPa and ϕ_{res}=32.7°) results in a realistic SRF-value. Although the SRF is in this case above the critical value of 1, this is not characterised as a stable situation. For instance, in rockslope stability analyses carried out for open pit mines, the short-term and long-term factors of safety of 1.3 and 1.5, respectively, are regarded to be the minimum acceptable value in Hoek and Bray (1981). In Wyllie and Mah (2004), a range of 1.2-1.4 is given as acceptable factors of safety for slope designs in mining situations. The effect of yielding along the sliding plane is distinct in all cases although largest with 1% intact rock. Based on the modelling carried out here, failure of 2-3% intact rock bridges is believed to be realistic for the situation at Åknes at present.

Several simplifications have however been made in $Phase^2$. For instance, the model is a continuous FEM-model, while in reality, joint systems are believed to control the displacements of the sliding area. Further, the sliding plane is modeled as a continuous joint of 25 cm width at the base of the sliding rock mass. In reality, the sliding is believed to be complex and takes place along several sliding planes. Also, the groundwater is modeled at an average level in three boreholes, while the groundwater regime in the area is believed to be more complex.

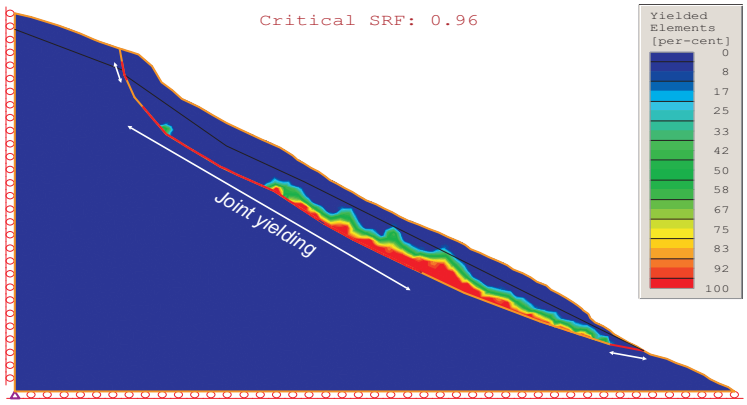

(a)

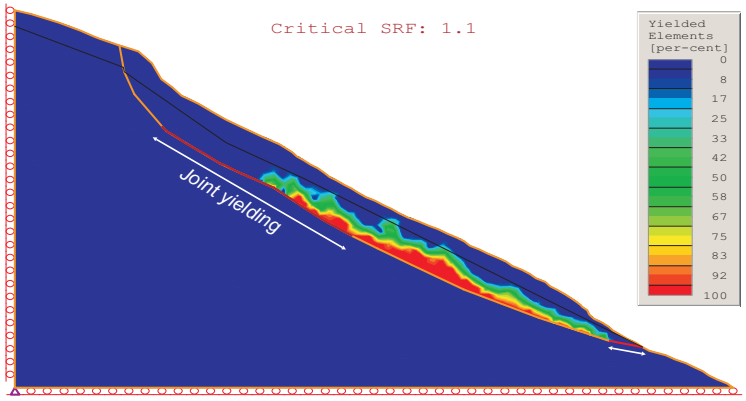

(b)

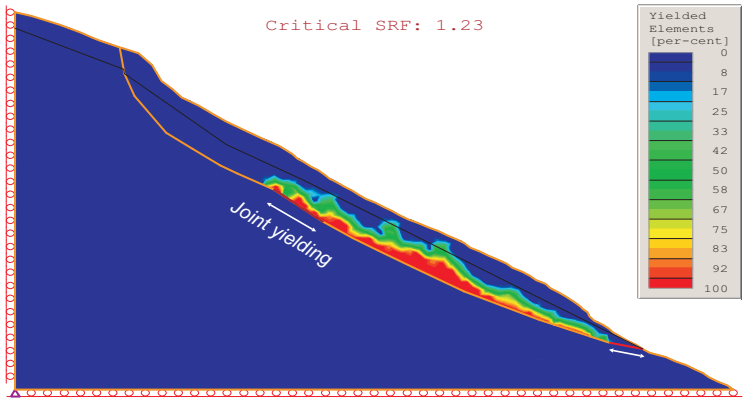

(c)

Figure 23: Yielding with Mohr Coulomb parameters based on a) 1% failure of intact rock, 64% failure along unfilled joints and 35% failure along gouge filled joints b) 3% failure of intact rock, 62% failure along unfilled joints and 35% failure along gouge filled joints c) 5% failure of intact rock, 60% failure along unfilled joints and 35% failure along gouge filled joints.

The longterm stability of the slope has been been modeled based on $FLAC^{3D}$, as presented in Paper IV (Grøneng et al., 2009). Two sets of parameters have been used, the first set believed to be representative of the present situation at Åknes, and the second set believed to represent a future situation. The first case results in a retardation of the displacements of the slope, while the second set results in increased displacements and an unstable toe. Figure 24 is an illustration of a possible development for the Åknes case, based on analyses in this thesis: a gradual decrease of the shear strength for the sliding plane as well as for the unstable mass located above from the assumed present situation (sliding plane with 3% intact rock bridges, 35% failure along gouge filled joints and 62% failure along unfilled joints and an unstable rock mass above with a GSI value 62) to a future unstable scanerio (sliding plane with 1% intact rock bridges, 35% failure along gouge filled joints and 64% failure along unfilled joints and an unstable rock mass above with a GSI value 37).

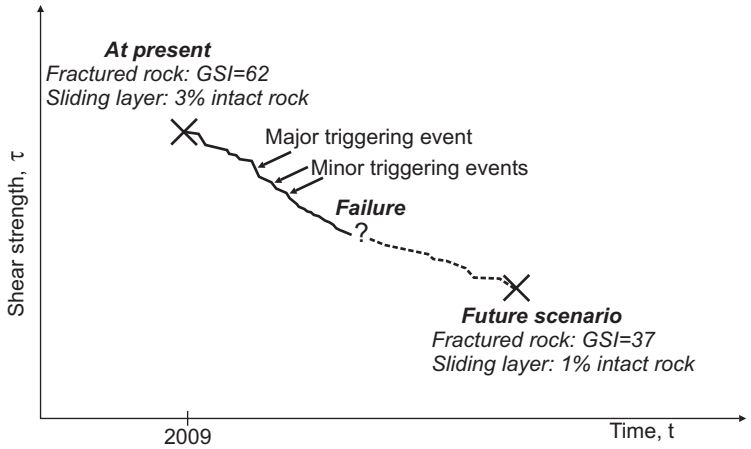

Figure 24: Illustration of how a gradual decrease in shear strength from the situation at present at Åknes might lead to slope failure, based on analyses in this thesis.

Major and minor triggering events most likely are represented by fluctuations in groundwater levels (as discussed in Paper III) and seismic activity, as discussed by Kveldsvik et al. (2009). Unfortunately, it is hardly possible to determine the time of failure by the modelling carried out in this thesis. Still, it contributes to a better understanding of

the factors controlling the stability at Åknes, and also defines a methodology for better evaluating shear strength parameters for a composite sliding plane, as well as estimating critical shear strength values for the unstable rock mass.

5.2 Main conclusions

Based on the analysis in this thesis, the following main conclusions can be drawn regarding the slope stability at Åknes and relating factors:

- A resultant shear strength may be estimated based on a methodology evaluating the composition of a basal sliding plane and combining shear strengths of various materials. The method requires calculation of the normal stress acting on the sliding plane. Based on field observations and drill core logging, estimation of most likely composition of the sliding plane at Åknes is 25-35% failure along gouge filled joints, 1-3% intact rock failure and 62-74% failure along unfilled foliation joints.

- Incorporating geotechnical and geophysical data into an interactive 3D geovisualization model greatly enhances the analysis of probable geometries of an unstable rockslope. At Åknes, the most likely geometry of the basal sliding surface is believed to be an undulating sliding surface located 105-115 m below the surface, resulting in area- and volume estimates for the unstable rock mass in the order of 575,000 m^2 and 43×10^6 m^3, respectively.

- Analysis of the meteorology and groundwater measured in upper and middle borehole at Åknes in the period November 2006−August 2008 indicates that the groundwater level at Åknes is highly related to the amount of water infiltrating the back scarp. The greatest fluctuations in groundwater levels are found in spring, with temperatures fluctuating around the freezing point in combination with snowmelt, leading to large variations in discharge of meltwater into the back scarp in addition to infiltration by precipitation. The lowest groundwater level is found during winter, when the temperatures are below freezing point and no water is discharged into the back scarp. Analysis of data from upper and middle boreholes suggests a shared groundwater regime in this part of the slope.

- Analysis of the displacement recorded by five extensometers in the period September 2004−August 2008 shows that the largest net expansions of the back scarp are

recorded in springtime (mid March through May) and early summer (June), mainly due to large increases in the groundwater level as result of snowmelt. In summer and early autumn (mid June through September), the groundwater level is stable and no significant displacement events are recorded in the back scarp. In autumn and early winter (October to mid January), decreases in air temperature to below 0°C causes reduction in the distance across the back scarp, but due to the marine climate, this is often interrupted by air temperature increases to above 0°C causing expansion. In late winter (mid January to mid March) no significant displacement is recorded, due to stable frozen conditions and the presence of a permanent snow cover.

- Measurements of the distance across the back scarp at Åknes in September 2004−August 2008 shows that the back scarp was more active in the first half (September 2004−August 2006) than in the second half of the period (September 2006−August 2008), indicating less significant meteorological effect on the displacements in the back scarp after September 2006.

- Numerical modelling based on $Phase^2$ indicates that composition of the basal sliding plane at Åknes with 3% failure of intact rock, 62% failure along unfilled joint and 35% failure along gouge filled joints results in a Strength Reduction Factor (SRF) of 1.1, while an alterantive composition of 1% failure of intact rock, 64% failure along unfilled joint and 35% failure along gouge filled joints results in a SRF of 0.96. This indicates that the sliding plane today most likely consists of between 1% and 3% intact rock.

- Analysis of the long term stability at Åknes based on the Burger-Creep Viscoplastic material model available in $FLAC^{3D}$ shows that a set of parameters representing the present situation (a composite sliding layer with 3% failure of intact rock, 35% failure along gouge filled joints and 62% failure along unfilled joints and a fractured rock mass above the sliding layer with M-C parameters representing a GSI of 62 "good surface conditions") results in retardation of the displacements within a 100

year period. However, due to gradual reduction in the shear strength parameters over time, a set of parameters believed to represent a future scenario (a composite sliding layer with 1% failure of intact rock, 35% failure along gouge filled joints and 64% failure along unfilled joints and a fractured rock mass above the sliding layer with M-C parameters according to a GSI of 37 "fair surface conditions") results in an unstable toe and increased surface displacements.

- Reduction in the joint roughness along the sliding plane due to mechanical and/or chemical disintegration in addition to major and minor triggering events such as large fluctuations in groundwater level and seismic activity will contribute to a gradual decrease in shear strength of the sliding plane(s) as well as the unstable rock mass above. The exact time of failure at Åknes is, however, hardly possible to predict by the modelling carried out in this thesis.

References

Aardal, I. B. (2006). Geophysical borehole data from Åknes. Project work at Norwegian University of Science and Technology (NTNU), Dept. of Geology and Mineral Resources Engineering.

Aardal, I. B. (2007). Åknes skredområde - analyse av korrelasjonar mellom borholsgeofysikk og bruddfrekvens frå kjernelogging. Master's thesis, Norwegian University of Science and Technology (NTNU), Dept. of Geology and Mineral Resources Engineering. In Norwegian.

Barton, N. (1974). A review of the shear strength of filled discontinuities in rock. Technical Report 105, Norwegian Geotechnical Institute (NGI).

Bjerrum, I. and F. A. Jørstad (1968). Stability of natural rock slopes in Norway. Technical Report 79, Norwegian Geotechnical Institute (NGI).

Blikra, L. H. (2008). The Åknes rockslide; monitoring, threshold values and early-warning. In Z. Chen, J. Zhang, Z. Li, F. Wu, and K. Ho (Eds.), *Proceedings of 10th international symposium on landslides and engineered slopes, China*, pp. 1089–1094. Taylor and Francis Group.

Blikra, L. H., O. Longva, A. Braathen, E. Anda, J. F. Dehls, and K. Stalsberg (2006). Rock slope failures in Norwegian fjord areas: examples, spatial distribution and temporal pattern. In S. G. Evans, G. S. Mugnozza, A. Strom, and R. L. Hermanns (Eds.), *Landslides from Massive Rock Slope Failure*, Series IV: Earth and Environmental Sciences, NATO Science Series, Vol. 49, pp. 475–496. Springer.

Blikra, L. H., O. Longva, C. Harbitz, and F. Løvholt (2005). Quantification of rock-avalanche and tsunami hazard in Storfjorden, western Norway. In K. Senneset, K. Flaate, and J. Larsen (Eds.), *Landslides and Avalanches: ICFL 2005 Norway*, pp. 57–63. Taylor and Francis Group.

Braathen, A., L. H. Blikra, S. S. Berg, and F. Karlsen (2004). Rock-slope failures in Norway; type, geometry, deformation mechanisms and stability. *Norwegian Journal of Geology 84*, 67–88.

Brady, B. H. G. and E. T. Brown (2005). *Rock Mechanics for Underground Mining* (3^{rd} ed.). Springer.

Chigira, M. (1992). Long-term gravitational deformation of rocks by mass rock creep. *Engineering Geology 32*, 157–184.

Coates, D. R. (1990). *Groundwater Geomorphology*, Chapter The relation of subsurface water to downslope movement and failure, pp. 51–76. Geological Society of America. Special Paper 252.

Coggan, J. S., D. Stead, and J. Eyre (1998). Evaluation of techniques for quarry slope stability assessment. Technical Report Sect. B: Appl. Earth Sci. 107, Trans. Inst. Min. Metall. B139-B147.

Crosta, G. B. and F. Agliardi (2003). Failure forecast for large rock slides by surface displacement measurements. *Canadian Geotechnical Journal 40*, 176–191.

Cruden, D. and D. J. Varnes (1996). *Landslides: Investigation and Mitigation*, Chapter Landslide types and processes, pp. 36–75. Transportation Research Board Special Report 247, National Academy Press.

Cruden, D. M. and C. D. Martin (2007). Before the Frank slide. *Canadian Geotechnical Journal 44*, 765–780.

Dramis, F. and M. Sorriso-Valvo (1994). Deep-seated gravitational slope deformations, related landslides and tectonics. *Engineering Geology 38*, 231–243.

Duncan, J. M. (1996). State of the art: Limit equilibrium and finite-element analysis of slopes. *Journal of Geotechnical Engineering 122*(7), 577–596.

Eberhardt, E. (2006). From cause to effect: using numerical modelling to understand rock slope instability mechanisms. In S. G. Evans, G. S. Mugnozza, A. Strom, and R. L. Hermanns (Eds.), *Landslides from Massive Rock Slope Failure*, Series IV: Earth and Environmental Sciences, NATO Science Series, Vol. 49, pp. 85–101. Springer.

Eberhardt, E., H. Willenberg, S. Loew, and H. Maurer (2001). Active rockslides in Switzerland - understanding mechanisms and processes. In E. K. H. K. M. Kühne, H. H. Einstein and R. Pöttler (Eds.), *UEF International Conference on Landslides - Causes, Impacts and Countermeasures, Davos, Switzerland*, pp. 25–34. Verlag Glückauf GmbH.

Eidsvig, U. and C. Harbitz (2005). Innledende numeriske analyser av flodbølger som følge av mulige skred fra Åkneset. Technical Report 20031100-2, Norwegian Geotechnical Institute (NGI). In Norwegian.

Frei, C. H., S. Loew, and F. Leuenberger-West (2008). First results of a large-scale multitracer test within an unstable rockslide area (Åknes, Norway). Geophysical Research Abstracts, Vol. 10, EGU2008- A-08930. SRef-ID: 1607-7962/gra/EGU2008-A-08930.

Furseth, A. (2006). *Skredulykker i Norge*. Tun Forlag AS. In Norwegian.

Ganerød, G. V., G. Grøneng, I. B. Aardal, and V. Kveldsvik (2007). Core logging of seven boreholes from Åknes, Stranda municipality, Møre and Romsdal county. Technical Report 2007.020, Norwegian Geological Survey (NGU).

Ganerød, G. V., G. Grøneng, J. S. Rønning, E. Dalsegg, H. Elvebakk, J. F. Tønnesen, V. Kveldsvik, T. Eiken, L. H. Blikra, and A. Braathen (2008). Geological model of the Åknes rockslide, western Norway. *Engineering Geology 102*, 1–18.

Goguel, J. (1978). *Rockslides and Avalanches, Developments in Geotechnical Engineering*, Chapter Scale-dependent rockslide mechanisms, with emphasis on the role of pore fluid vaporisation, pp. 693–706. Elsevier.

Goodman, R. E. (1980). *Introduction to Rock Mechanics*. John Wiley & Sons Inc.

Govi, M. (2002). *Catastrophic Landslides: Effects, Occurrence and Mechanisms*, Volume Reviews in Engineering Geology, Volume XV, Chapter Val Pola rock avalanche of July 28, 1987, in Valtellina (Central Italian Alps, pp. 71–89. The Geological Society of America.

Grøneng, G., H. H. Christiansen, B. Nilsen, and L. H. Blikra (2009). Meteorological effects on seasonal displacements of the Åknes rockslide, western Norway. Submitted to: Landslides, May 2009.

Grøneng, G., M. Lu, B. Nilsen, and A. K. Jenssen (2009). Time-dependent behavior of the Åknes rockslide area in western Norway. Submitted to: Engineering Geology, September 2009.

Grøneng, G. and B. Nilsen (2009). Procedure for determining input parameters for Barton-Bandis joint shear strength formulation. Technical Report 38, Norwegian University of Science and Technology (NTNU), Dept. of Geology and Mineral Resources Engineering.

Grøneng, G., B. Nilsen, and R. Sandven (2009). Shear strength estimation for Åknes sliding area in western Norway. *International Journal of Rock Mechanics and Mining Sciences 46*, 479–488.

Hendron, A. J. and F. D. Patton (1985). The Vaiont slide: A geotechnical analysis based on new geologic observations of the failure surface. Technical Report GJ-85-5, Department of the Army, U.S. Army Corps of Engineers, Washington.

Hoek, E. and J. Bray (1981). *Rock Slope Engineering* (Revised 3^{rd} editon ed.). SPON Press Taylor and Francis Group.

Holsbrekken, E. (2006). Åknes: Collection of climatic-, precipitation- and deformation data. Project assignment at Norwegian University of Science and Technology (NTNU), Dept. of Geology and Mineral Resources Engineering.

Holsbrekken, E. (2007). Åknes landslide area - analysis of correlation between displacement and climate/precipitation. Master's thesis, Norwegian University of Science and Technology (NTNU), Dept. of Geology and Mineral Resources Engineering.

Hungr, O. and S. G. Evans (2004). The occurrence and classification of massive rock slope failure. *Felsbau 2*, 16–23.

Hutchinson, J. N. (1968). *The Encyclopedia of Geomorphology*, Volume III, Chapter Mass Movement, pp. 688–695. Reinhold Book Corporation.

Itasca (2002). $FLAC^{3D}$ *User manual* (2.10 ed.). Itasca Consulting Group, Minnesota, USA.

Jaeger, J. C. and N. G. W. Cook (1968). *Time-dependent effects* (2nd ed.). John Wiley & Sons Inc.

Kenney, T. C. (1967). Stability of the vaiont-valley slope. *Felsmechanik und Ingenieurgeologie v/1*, 10–16.

Kilburn, C. R. J. and D. N. Petley (2003). Forecasting giant, catastrophic slope collapse: lessons from Vajont, Northern Italy. *Geomorphology 54*, 21–32.

Kveldsvik, V. (2008). *Static and dynamic stability analyses of the 800 m high Åknes rock slope, western Norway.* Ph. D. thesis, Norwegian University of Science and Technology (NTNU), Dept. of Geology and Mineral Resources Engineering. 2008:128.

Kveldsvik, V., T. Eiken, G. V. Ganerød, G. Grøneng, and N. Ragvin (2006). Evaluation of movement data and ground conditions for the Åknes rock slide. In *Stability of rock slopes in open pit mining and civil engineering situations, Cape Town*, pp. 279–300. The South African Institute of Mining and Metallurgy.

Kveldsvik, V. and G. Grøneng (2007). Åkerneset: Tape-extensometermålinger første gangs avlesning. Technical note at Norwegian Geotechnical Institute (NGI). Project: 20051018 Åknes/Tafjord-prosjektet, revision 3. In Norwegian.

Kveldsvik, V., A. M. Kaynia, F. Nadim, R. Bhasin, B. Nilsen, and H. H. Einstein (2009). Dynamic analysis of the 800 m high Åknes rock slope using UDEC. *International Journal of Rock Mechanics and Mining Sciences 46*, 686–698.

Kveldsvik, V., B. Nilsen, H. H. Einstein, and F. Nadim (2008). Alternative approaches for analyses of a 100,000 m^3 rock slide based on Barton-Bandis shear strength criterion. *Landslides 5*, 161–176.

Larsen, J. O. (1999). Tension cracks and landslides in steep hard rock mountains in the norwegian fjord districts. In *Proceedings of the Second International Conference on Landslides, Slope Stability & Safety of Infra-structures*, pp. 193–200.

Longva, O., L. H. Blikra, and J. F. Dehls (2009). Rock avalanches - distribution and frequencies in the inner part of Storfjorden, møre og Romsdal County, Norway. Technical Report 2009:002, Geological Survey of Norway.

MathWorks, T. (2006). *MATLAB-the Language of Technical Computing* (7.1 ed.). The MathWorks Inc, Massachusetts.

Müller, L. (1964). The rock slide in the Vajont valley. *Felsmechanik und Ingenieurgeologie 1*, 148–212.

Müller, L. (1968). New considerations on the Vajont slide. *Felsmechanik und Ingenieurgeologie 6*, 1–91.

Moen, B. (2007). Åknes - vurdering av mulighet for drenering og andre stabiliserende tiltak. Project work at Norwegian University of Science and Technology (NTNU), Dept. of Geology and Mineral Resources Engineering.

Moen, B. (2008). Åknes skredområde - analyse av mulig effekt av dreneringstiltak. Master's thesis, Norwegian University of Science and Technology (NTNU), Dept. of Geology and Mineral Resources Engineering. In Norwegian.

Nemčock, A. (1972). Gravitational slope deformation in high mountains. In *24th IGC, Montreal*, pp. 132–141. Section 13.

Nilsen, B. and A. Palmstrøm (2000). *Engineering Geology and Rock Engineering*. Norwegian Group of Rock Mechanics.

Nordvik, T., G. Grøneng, G. V. Ganerød, B. Nilsen, C. Harding, and L. H. Blikra (2009). Geovisualization, geometric modelling and volume estimation of the Åknes rockslide, western Norway. *Bulletin of Engineering Geology and the Environment 68*(2), 245–256.

Nordvik, T. and E. Nyrnes (2009). Statistical analysis of surface displacements an example from the Åknes rockslide, western Norway. *Natural Hazards and Earth System Sciences 9*(3), 713–724.

Oyagi, N., M. Sorriso-Valvo, and B. Voight (1994). Introduction to the special issue of the symposium on deep-seated landslides and large-scale rock avalanches. *Engineering Geology 38*, 187–188.

Pande, G. N., G. Beer, and J. R. Williams (1990). *Numerical Methods in Rock Mechanics*. John Wiley & Sons Ltd.

Petley, D. (1978). *Slope Movement Types and Processes*. TRB National Research Council.

Petley, D. (1996). *Advances in Hillslope Processes*, Volume 2, Chapter The Mechanics and Landforms of Deep-Seated Landslides, pp. 823–834. John Wiley & Sons Ltd.

Petley, D. N. and R. J. Allison (1997). The mechanics of deep-seated landslides. *Earth Surface Processes and Landforms 22*, 747–758.

Pomeroy, C. D. (Ed.) (1978). *Creep of Engineering Materials*. The Institution of Mechanical Engineers.

Radbruch-Hall, D. H. (1978). *Rockslides and Avalanches 1, Natural Phenomena*, Volume 1, Chapter Gravitational creep of rock masses on slopes, pp. 607–657. Elsevier.

Ragvin, S. N. (2005). Geological data from Åknes landslide area. Project work at Norwegian University of Science and Technology (NTNU), Dept. of Geology and Mineral Resources Engineering.

Ragvin, S. N. (2006). Åknes landslide area - numerical modelling with *Plaxis*. Master's thesis, Norwegian University of Science and Technology (NTNU), Dept. of Geology and Mineral Resources Engineering.

Rocscience (2002). *Rocscience, RocLab* (1.010 ed.). Rocscience Inc, Toronto.

Rocscience (2005). *Phase*^{2} *User manual* (6.001 ed.). Rockscience Inc., Toronto, Canada.

Rønning, J. S., E. Dalsegg, H. Elvebakk, G. V. Gnerød, and J. F. Tønnesen (2006). Geofysiske målinger Åknes og Tafjord, Stranda og Nordal kommune, Møre og Romsdal. Technical Report 2006.002, Geological Survey of Norway (NGU). In Norwegian.

Sandersen, F., S. Bakkehøi, E. Hestnes, and K. Lied (1996). The influence of meteorological factors on the initiation of debris flows, rockfalls, rockslides and rockmass stability. In K. Senneset (Ed.), *Landslides*, pp. 97–114. Balkema.

Savage, W. Z. and D. J. Varnes (1987). Mechanics of gravitational spreading of steep-sided ridges ('sackung'). *Bulletin of the International Association of Engineering Geology 35*, 31–36.

Stead, D., E. Eberhardt, and J. S. Coggan (2004). Developments in the characterization of complex rock slope deformation and failure using numerical techniques. *Engineering Geology 83*, 217–235.

Ter-Stepanian, G. I. (1966). Types of depth creep of slopes in rock masses. In *1*st *Congr. Int. Soc. Rock Mech., Lisbon*, Volume II, pp. 157–160.

Terzaghi, K. (1963). Stability of steep slopes on hard unweathered rock. Technical Report 50, Norwegian Geotechnical Institute (NGI).

Terzaghi, R. and B. Voight (1979). *Rockslides and Avalanches, Developments in Geotechnical Engineering*, Chapter Karl Terzaghi on rockslides: the perspective of a half-century, pp. 111–133. Elsevier.

Tveten, E., O. Lutro, and T. Thorsnes (1988). Bergrunnskart Ålesund. 1:250 000. Geological map. In Norwegian.

Wieczorek, G. F. (1996). *Landslides: Investigation and Mitigation*, Chapter Landslide triggering mechanisms, pp. 76–87. Transportation Research Board Special Report 247, National Academy Press.

Wyllie, D. C. and C. W. Mah (2004). *Rock Slope Engineering, Civil and Mining* (4^{th} ed.). SPON Press Taylor and Francis Group.

Zischinsky, U. (1966). On the deformation of high slopes. In *1^{st} Congr. Int. Soc. Rock Mech., Lisbon*, Volume 2, pp. 179–185.

Main papers

Paper I

Shear strength estimation for Åknes sliding area in western Norway

Authors: Guro Grøneng, Bjørn Nilsen and Rolf Sandven

The paper was published in International Journal of Rock Mechanics and Mining Sciences (2009), Vol. 46, pages 479-488, doi:10.1016/j.ijrmms.2008.10.006.

International Journal of Rock Mechanics & Mining Sciences 46 (2009) 479–488

Contents lists available at ScienceDirect

International Journal of Rock Mechanics & Mining Sciences

journal homepage: www.elsevier.com/locate/ijrmms

Shear strength estimation for Åknes sliding area in western Norway

Guro Grøneng [a,*], Bjørn Nilsen [a], Rolf Sandven [b,1]

[a] Department of Geology and Mineral Resources Engineering/International Centre for Geohazards (ICG), Norwegian University of Science and Technology (NTNU), Trondheim, Norway

[b] Department of Civil and Transportation Engineering, Norwegian University of Science and Technology (NTNU), Geotechnical Division, Trondheim, Norway

ARTICLE INFO

Article history:
Received 12 March 2008
Received in revised form
27 October 2008
Accepted 31 October 2008
Available online 20 December 2008

Keywords:
Rockslide
Sliding plane
Shear strength
Triaxial tests
Barton–Bandis empirical method

ABSTRACT

This paper deals with the unstable rock-slope at Åknes sliding area, located in the county of Møre and Romsdal in western part of Norway. The sliding body has a complex geometry with several sliding planes at different levels, involving unfilled joints, gouge material/brecciated material as well as bridges of intact rock. Stability of the rock slope strongly depends on the shear strength of the sliding plane(s) and this paper discusses the shear strength of the materials present, ranging between the strength of intact rock and crushed, clay containing gouge material. Estimation of the in situ shear strength at the Åknes sliding area is discussed on the basis of triaxial test results and the Barton–Bandis empirical method. Triaxial tests have been carried out on samples of gouge material from a potential sliding plane and intact rock specimens, while the empirical method has been applied for rock joints in the area. Comparison and correlation with experimental results found in literature have also been made. The resultant shear strength range for the zone of sliding has been found to be in the range of 0.5–1.3 MPa, depending on the normal stress and the composition of the sliding zone.

1. Introduction

Potential sliding planes in a rock slope are generally caused by geological layers or strata which, compared to the surroundings, possess smaller shear strength and are thus exposed for sliding displacement. Shear strength estimation of sliding planes is a key factor for reliable rock slope stability analysis. In large scale rock slopes, the sliding plane in most cases is not uniform, but rather complex, consisting of a combination of the following:

(a) unfilled joints (rock-to-rock contacts),
(b) filled joints (gouge material) and
(c) bridges of intact rock.

One well-known case where such complex sliding plane was believed to exist was in Vaiont, for which numerous studies have been conducted related to the character of the 1963-slide. Whether interbeds of clay were present along the failure surface has been discussed amongst other by Brolili [1], Müller [2,3] and Kenney [4], but the report from Hendron and Patton [5] seems to conclude that multiple layers of clay with 50–80% clay, commonly 1–2 cm thick, were present along most of the sliding surface. Although the presence of a substantial number of rock-to-rock contacts as well as shearing across bedding planes were acknowledged by Hendron and Patton, the shear strength along the base of the slide was assumed to be related to the residual strength of the clay in the analyses of the failure.

The shear strengths of components (a)–(c) represent a great span, and before any kind of stability analysis can be done, a realistic quantification of the resultant shear strength of the combined sliding plane has to be made. The methodology for estimating this resultant shear strength, which is rarely discussed in literature, is the main subject of this paper. The Åknes sliding area in western Norway is used as case. Based on reliable quantification of resultant shear strength, numerical analysis of the rock slope will be carried out. Discussion of such analysis are, however, beyond the scope of this paper.

At the Åknes rock slide area, field investigations indicate a landslide with complex geometry. The results from an extensive investigation program operating at Åknes since 2004 will be used as a basis for analysis. In the following, the Åknes case will be described, and a methodology for estimation of the resultant shear strength of the Åknes case will be presented.

2. The Åknes rockslide area

The Åknes sliding area is oriented in NW–SE direction along the W-side of Storfjorden in Møre and Romsdal County in western Norway (Fig. 1). The area draws considerable attention in Norway

* Corresponding author. Tel.: +47 7359 4807; fax: +47 7359 4814.
E-mail addresses: guro.groneng@ntnu.no (G. Grøneng), bjorn.nilsen@ntnu.no (B. Nilsen), rolf.sandven@multiconsult.no (R. Sandven).
[1] Present address: Multiconsult AS, 7486 Trondheim, Norway.

1365-1609/$ - see front matter Crown Copyright © 2008 Published by Elsevier Ltd. All rights reserved.
doi:10.1016/j.ijrmms.2008.10.006

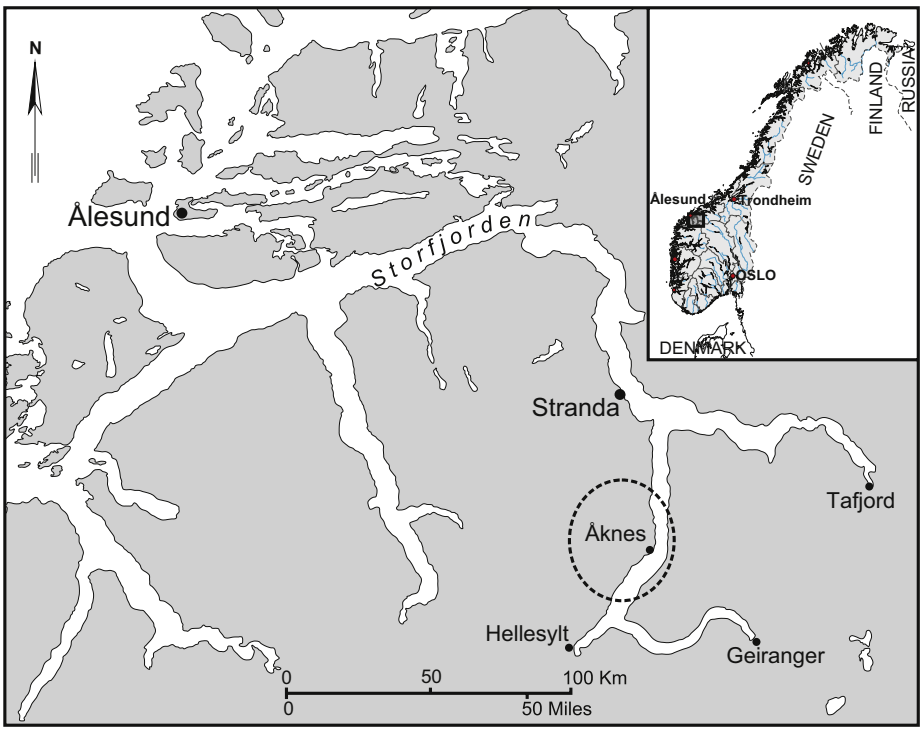

Fig. 1. Location of the Åknes sliding area.

due to the hazard of a tsunami which could be generated as a result of a large scale rock slope failure. Tsunami modelling indicates that several villages along the adjacent fjord Storfjorden will be endangered [6] as well as thousands of tourists who visit the fjords in the summer months. Documentation of historical rockslides has shown that stability problems have occurred on several occasions in western Norway, where the ice has eroded deep valleys and fjords in metamorphic rock during the glacial periods [7]. Geological mapping on land and in fjords in the County has identified a high frequency of rock-slope failures since the last glaciation, 10 000 years ago [8]. In Storfjorden, mapping by swath bathymetry has revealed at least 59 rock-slope failures larger than 0.5 million m^3, illustrating the potential hazard due to rock avalanches [9].

The Åknes rockslide area is situated in the slope below the mountain Flosteinsnibba with an average slope angle of approximately 35°, and was brought to the public's attention in 1964 by local people claiming that the tension crack associated to the back scarp was widening [10]. The area and volume of the potential unstable rock mass are estimated to be 780 000 m^2 and 30–40 million m^3, respectively [11]. The western boundary is defined by a steeply dipping, NNW–SSE striking strike slip fault while the eastern boundary is defined by a gently NW dipping, NNE–SSW trending fault [12] (Fig. 2). The upper boundary of the unstable area is represented by a distinct, more or less continuous tension crack with approximate length 800 m (Fig. 3).

Annual downhill movement in the order of 1–4 cm has been monitored at the back scarp since 1986 [10,13,14], and photogrammetric studies of displacement rates since 1961 indicate an average displacement in the order of 6 cm/year [14], indicating that the slope is deforming at a more or less constant rate. Signs of instability have been evidenced by occurrence of three smaller rockslides in the slope, all along the western boundary. The most recent (1960) had an estimated volume of approximately 100 000 m^3 [14].

The bedrock in the area is predominantly gneiss, Proterozoic in age, and metamorphosed during the Caledonian mountain building phase. The gneisses are magmatic in origin, classified as undifferentiated quartz-dioritic to granitic, locally with migmatitic composition [15]. Petrographic logging of the rock cores recovered from three drilling sites in the slope (Fig. 2) has identified three types of gneiss varying from quartz-dioritic to granitic as well as gneisses rich in biotite [12]. The gneisses rich in biotite have an overall, south to southeast steeply dipping foliation.

3. The sliding zone at Åknes

The geometry and overall properties of the sliding planes are the most critical input parameters for a rock slope stability analysis. The slope is partially covered with scree material which restricts mapping of cracks and joints to sparse outcrops in the area. However, on the basis of geological mapping, geophysical surveys and drilling of boreholes, the internal structure has been interpreted. The exact configuration and position of the sliding plane are not yet finally defined, but one alternative believed to be realistic is shown in Fig. 4.

Seismic surveys have indicated that the basal detachment horizon has an undulating form and is located at 25–60 m below the surface [12]. Geological conditions believed to contribute to slope instability and potential failure at the Åknes rockslide area are believed to be the steep slope angle averaging approximately 35° and foliation oriented parallel to the slope [11,12,14,16].

The foliation in the area can be studied in some detail in the west wall of the crevasse which represents the western boundary of the area. The characteristic style of the foliation can clearly be seen in Fig. 5 (location P1). Interpretation of the seismic surveys shows a possible sliding plane daylighting at approximately 150 m a.s.l. A potential evidence for this is a rock overhang, 50 m long (location P2), at an elevation of approximately 175 m a.s.l. (Fig. 6).

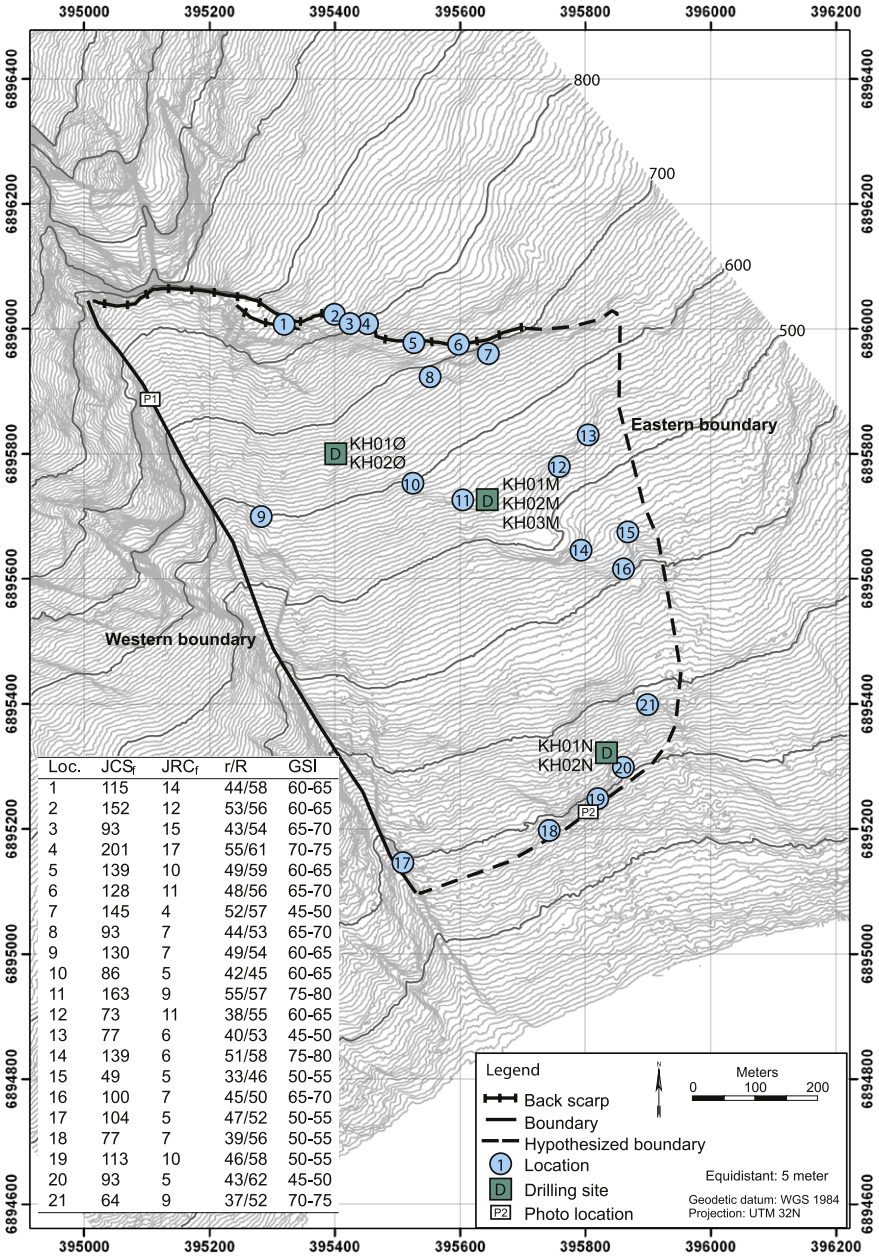

Loc.	JCS_r	JRC_f	r/R	GSI
1	115	14	44/58	60-65
2	152	12	53/56	60-65
3	93	15	43/54	65-70
4	201	17	55/61	70-75
5	139	10	49/59	60-65
6	128	11	48/56	65-70
7	145	4	52/57	45-50
8	93	7	44/53	65-70
9	130	7	49/54	60-65
10	86	5	42/45	60-65
11	163	9	55/57	75-80
12	73	11	38/55	60-65
13	77	6	40/53	45-50
14	139	6	51/58	75-80
15	49	5	33/46	50-55
16	100	7	45/50	65-70
17	104	5	47/52	50-55
18	77	7	39/56	50-55
19	113	10	46/58	50-55
20	93	5	43/62	45-50
21	64	9	37/52	70-75

Fig. 2. Topographic map showing boundaries for the unstable area at Åknes, measurement locations, drilling sites and photo locations.

On the basis of logs from seven boreholes at the three drilling sites, it is evident that the rock mass is heterogeneous and contains a considerable number of discontinuities [17]. Six of the boreholes are vertical, three of them are drilled down to a depth of 200 m. Generally, the rock is heavily fractured down to 70 m (average fracture frequency 10 fractures/m). In this depth interval, crushed rock, breccia and gouge are common; typical thicknesses are up to 30–40 cm for crushed rock and breccia, and up to 5 cm for gouge. The theory of a complex sliding zone is supported by the absence of a distinct sliding plane in the logs.

The objective of this study is to discuss a methodology for reliable estimation of the resultant shear strength of the sliding zone. Estimates of internal friction angle (ϕ) and cohesion (c) for the gouge and rock material based on triaxial testing as well as estimates for the various parameters of the Barton–Bandis empirical method for unfilled joints thus will be made.

4. Shear strength of gouge material

4.1. Description of the gouge material

The gouge material was sampled from a weakness plane located at the potential toe of the Åknes slide, approximately 180 m a.s.l. The plane daylights inside a cave, at the base of an overhanging cliff, and is 1–3 cm thick. Although the amount of accessible material was limited, three samples were successfully collected from this plane. The grain size distribution of the samples have been analyzed (Fig. 7), indicating that the clay content varies from 9% to 19%. Semi-quantitative mineralogical composition based on X-ray diffraction analysis is presented in Table 1. Swelling mineral (smectite) was detected in one of the samples but was not possible to determine quantitatively. Swelling tests conducted on four samples from the area show a

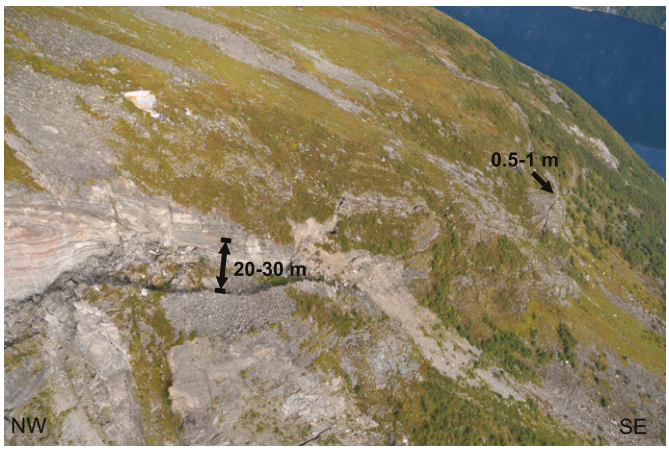

Fig. 3. Extensometer no. 5 in the back scarp towards the eastern boundary of the sliding area.

free swelling of 89–103%, indicating an inactive gouge material according to classification by the Norwegian Group of Rock Mechanics [18].

Consolidation of the gouge material is assumed to correspond with the actual overburden at the site of sample collection ($\sigma_v = \gamma_{rock} \times h$), which gives a maximum vertical stress of 300 kPa. Previous shear displacement most likely has taken place, since the gouge material probably is formed by a shearing process which has caused crushing of mica-rich layers in the gneissic rock. The shear strength is assumed to be at the residual value and cohesion is assumed to be 0 due to the destruction of cohesive bonds.

4.2. Triaxial testing procedure

Triaxial testing of gouge was performed at the NTNU Geotechnical Laboratory according to procedures recommended by the International Society of Soil Mechanics and Geotechnical

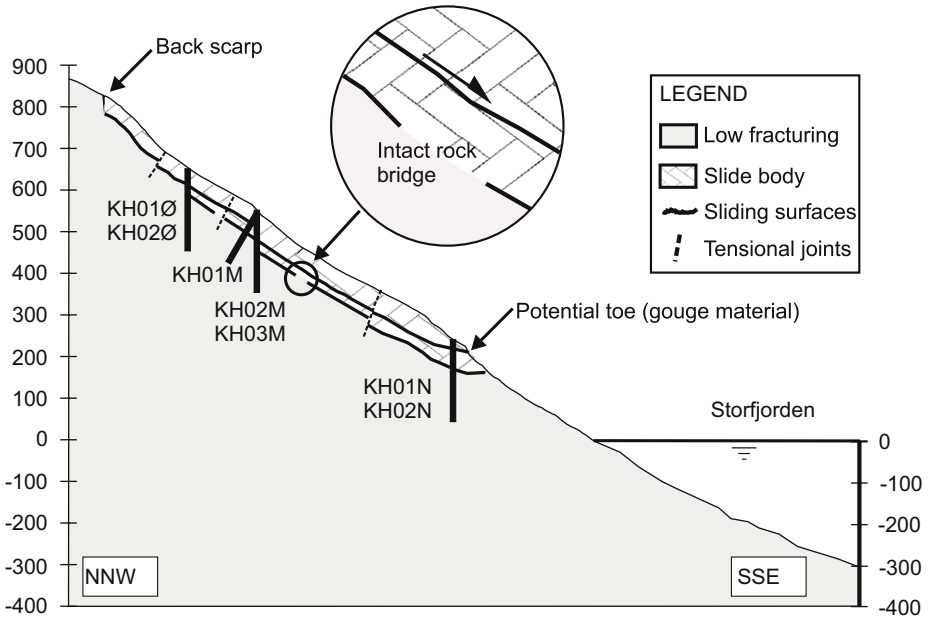

Fig. 4. Cross section representing configuration of sliding zone for the Åknes slide.

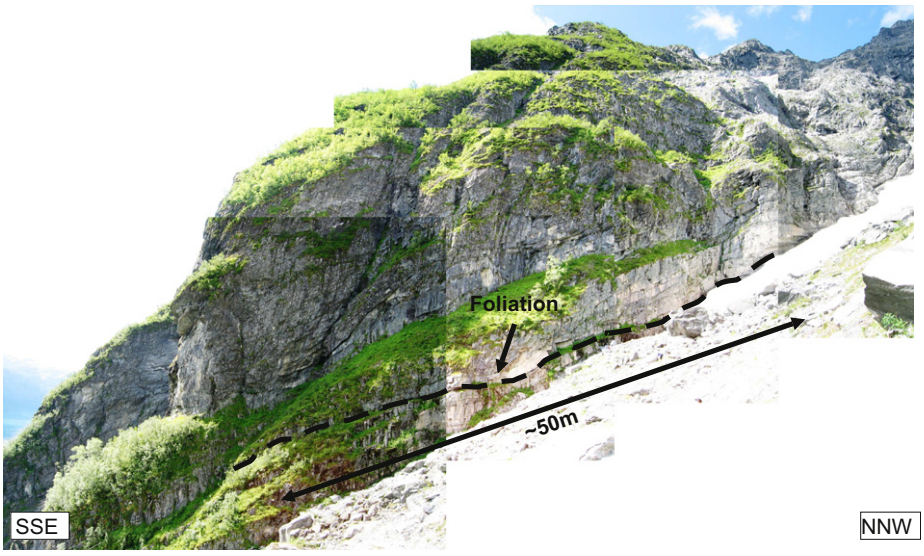

Fig. 5. Foliation in the area, photo of the western wall of the crevasse, photo loc. 1

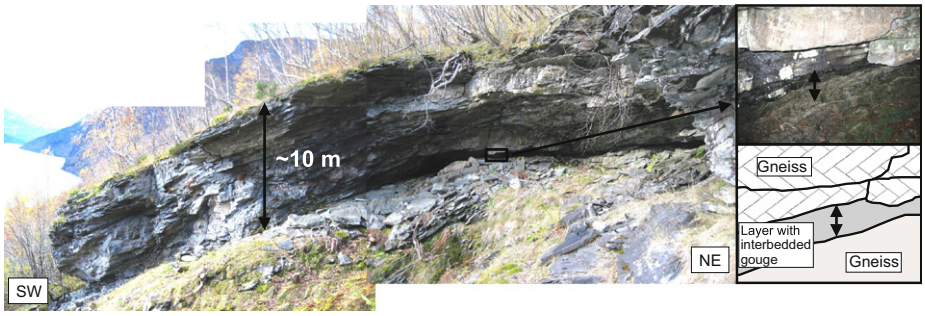

Fig. 6. Possible sliding plane with joint filling daylighting 200 m a.s.l., photo loc. 2.

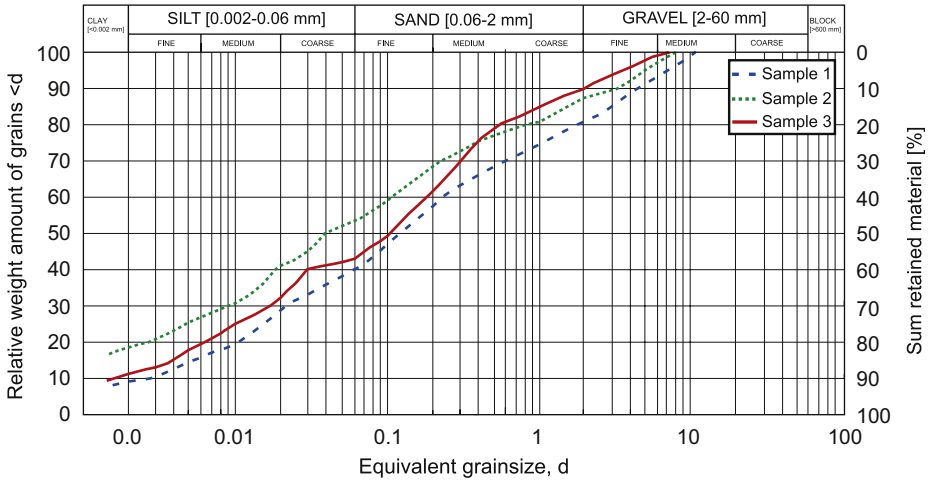

Fig. 7. Grain size distribution of silty sand (sample 1), silty, sandy clay (sample 2) and sandy silt (sample 3).

Table 1
Semi-quantitative mineral distribution of samples taken from the weakness plane.

Mineral	Sample 1 (%)	Sample 2 (%)	Sample 3 (%)
Quartz	9	12	21
Plagioclase	33	42	50
Alkaline feldspar	10	17	12
Micas	44	22	10
Caolinite	2	4	4
Amphiboles	2	3	3

Engineering (ISSMGE). The specimens had cross-sectional area of $A = 23.2\,\text{cm}^2$ and height $h = 10\,\text{cm}$, and were consolidated under confining pressures of 50–300 kPa, based on estimated vertical effective overburden at the sampling site. After consolidation the specimens were loaded at a strain rate of 5% per hour. The shearing phase was terminated after reaching 10% strain, due to practical limitations.

It is not clear whether a drained or undrained stress response is most applicable to the gouge material along the failure plane, undrained shear strength is, however, selected. This is because the rock/gouge interaction is uncertain at this stage, and by testing the material in an undrained triaxial procedure, conservative shear strength parameters for the material are estimated.

4.3. Results

Sampling necessarily results in sample disturbance due to compression of the soil and removal of in situ confining stresses, change in the moisture content due to transportation and storage and desiccation during trimming and placing of the specimen in the triaxial cell. However, in the Åknes-case, a more careful sampling procedure was not possible due to the 1–3 cm thick filled joint at a particular location in the sliding area. Due to the sampling method, the estimation of confining pressures and the choice of an undrained testing procedure, the friction parameters based on this triaxial testing are believed to be conservative.

The results of triaxial testing are presented in terms of a deviator stress path. Due to limited material available for testing, the number of tests was limited to 3 for each of the 3 sample locations (Fig. 8). In this study, the testing is carried out in order to provide a rough estimate of the shear strength of the soil samples as a whole.

Soils located in the sliding plane will be subjected to differential shearing displacements due to the undulating nature of the sliding plane, and therefore represent different shear stress conditions in the soils. The shear stress at a strain of 2–5%, depending on the trend of the individual triaxial curves defines the design condition in this case. Sample 3 shows a slightly dilative response, a common failure mechanism for non-cohesive soils. Samples 1 and 2 show no indication of failure. The curve representing the average design condition for each sample is shown. Effective strength parameters for soil samples are shown in Table 2.

The results indicate that the amounts of biotite and quartz have influence on the strength. Sample 1 contains the lowest percentage of quartz and highest percentage of micas and possesses the lowest shear strength, while the sample with highest content in quartz and lowest in micas (sample 3) possesses the highest shear strength.

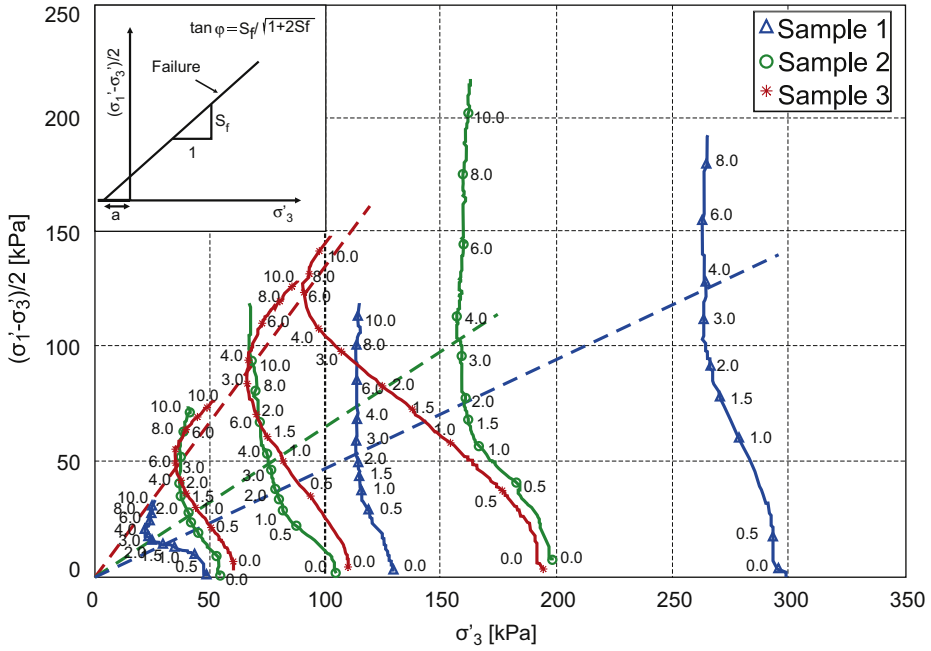

Fig. 8. Results from testing of gouge material in the triaxial cell.

Table 2
Friction angles for gouge material, $c = 0$ kPa.

Gouge	Friction angle ϕ (deg)
Sample 1	18
Sample 2	23
Sample 3	35

Some empirical data based on direct shear testing of fillings/gouges from discontinuities are shown in Fig. 9. The results represent peak friction angle and cohesion. As shown, the results from the triaxial testing of the material from Åknes plot within the empirical data representing "Fault gouge, shear zones, low strength rock" and "Clay infilling" with low or no cohesion.

For Åknes, the mean test value, i.e. $\phi = 25^\circ$ and $c = 0$ kPa, is used in the following.

5. Shear strength of unfilled rock joints

5.1. Basis for estimation

The shear strength of unfilled joints is governed by the joint roughness, the rock strength at the joint surface and the normal stress acting on the discontinuity, as defined by the Barton–Bandis empirical equation [19]:

$$\tau = \sigma_n \tan\left(\phi_r + JRC \log_{10}\frac{JCS}{\sigma_n}\right) \quad (1)$$

where *JCS* is the joint compressive strength, ϕ_r is the residual friction angle and *JRC* is the joint roughness coefficient. This empirical method requires rock joint data obtained by a combination of field work and laboratory testing.

5.2. Measurements and test procedures, results

Main focus concerning shear strength of unfilled rock joints at Åknes has been on foliation joints, since sliding here mainly takes place along the foliation. The character of foliation joints varies from slickensided with low roughness to undulating due to folding. In situ measurements of the *JRC*-parameter have given a mean value of 8.5 for 21 locations when measured over 1 m lengths in three different directions. Block size in the area is close to 1 m and scaling as described by Barton and Bandis [19] has not been required. The other parameters except the basic friction

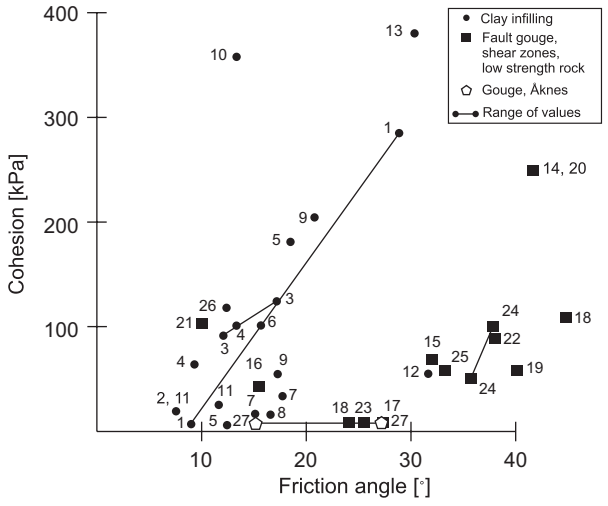

1. Bentonite shale
2. Bentonite seams in chalk
3. Bentonite; thin layers
4. Bentonite; triaxial tests
5. Clay, overconsolidated
6. Limestone, 10-20 mm clay infillings
7. Lignite and underlying clay contact
8. Coal measures; clay mylonite seams
9. Limestone; <1 mm clay innfillings
10. Montmorillonite clay
11. Montmorrilonite; 80 mm clay seam in chalk
12. Schists/quartzites; stratification, thick clay
13. Scists/quartzites; stratification, thick clay
14. Basalt; clayey, basaltic breccia
15. Clay shale; triaxial tests
16. Dolomite, altered shale bed
17. Diorite/granodiorite; clay gouge
18. Granite; clay-filled faults
19. Granite; sandy-loam fault fillings
20. Granite; shear zone, rock and gouge
21. Lignite/marl contact
22. Limestone/marl/lignites; lignite layers
23. Limestone; marlaceous joints
24. Quartz/kaolin/pyrolusite; remoulded triaxial
25. Slates; finely laminated and altered
26. Limestone; 10-20 mm clay infillings
27. Gouge from Åknes; remoulded triaxial

Fig. 9. Relationship between friction angles and cohesive strength obtained from direct shear tests (after Barton [30], modified from Wyllie and Mah [31]). Gouge from Åknes is no. 27.

Table 3
Parameters used in Barton–Bandis empirical equation.

Parameter	Value	Comment
$JRC_{foliation}$	8.5	Measured over 1 m length on 21 locations. Procedure according to Barton and Bandis [32]
$JCS_{foliation}$	111 MPa	Measured on 21 locations. Procedure according to ISRM [23] and chart from Deere and Miller [29]
ϕ_b	28°	Measured on 12 cores, 32 mm in diameter
r/R	45/55	Rebound measured on 21 locations of foliation/unweathered joints
ϕ_r	24°	Calculated using Eq. (2) according to Barton and Choubey [22]

angle, ϕ_b, have been estimated according to procedures described in literature as indicated in Table 3. Measurement results for each individual location are shown in Fig. 2.

Since no general standard or recommendation exists concerning determination of basic friction angle, the NTNU-laboratory has defined its own standard method for this [20] based on a sketch in Barton and Choubey [21], indicating the principle.

Testing for determining the basic friction angle, ϕ_b, is carried out on rock cores with a length/diameter ratio of 2.5. Each core is sawn axially and placed in the apparatus, as if it was an intact core. The apparatus is tilted by a hydraulic pump until the upper part of the core starts to slide, and at this point the angle of tilting is registered by an inclinometer with an accuracy of 0.1°. The test procedure results in 12 measurements for each core. Based on the basic friction angle, the residual friction angle can be calculated as follows [21]:

$$\phi_r = (\phi_b - 20) + 20\frac{r}{R} \quad (2)$$

where the parameter r refers to Schmidt–Hammer rebound value on weathered joint surface and R refers to rebound on unweathered joint surface. In the case of unweathered joints, ϕ_r will be identical to ϕ_b. In accordance with the procedure for estimating the *JCS* [22], the lower 50% of the rebound values were discarded.

6. Shear strength for intact rock

6.1. Sample collection and preparation

Shear strength of intact rock has been determined by triaxial testing in the laboratory. The specimens tested in the triaxial cell were cores recovered at depths of 85–145 m in the vertical boreholes (Figs. 2 and 4). The 54 mm diameter cores from the boreholes needed to be reduced to 38 mm in order to fulfil the NTNU equipment requirements for triaxial laboratory testing (Hoek-cell). Reduction was achieved by using special core drilling equipment. Practical challenges in this procedure limited the triaxial testing to 5 cores of each type of gneiss, i.e. to a total of 15 tests.

6.2. Procedure for triaxial testing

The triaxial rock testing was carried out according to the procedure described by ISRM [23]. All specimens were kept at room temperature and were dry when tested. The axial stress was applied by a hydraulic testing machine and the confining pressure supplied independently by an oil compressor. The SINTEF/NTNU Rock Mechanics Laboratory in Trondheim was used for this testing. For each rock type one specimen was tested at 0 confining pressure, and two specimens were tested under confining pressures of 2 and 4 MPa, respectively.

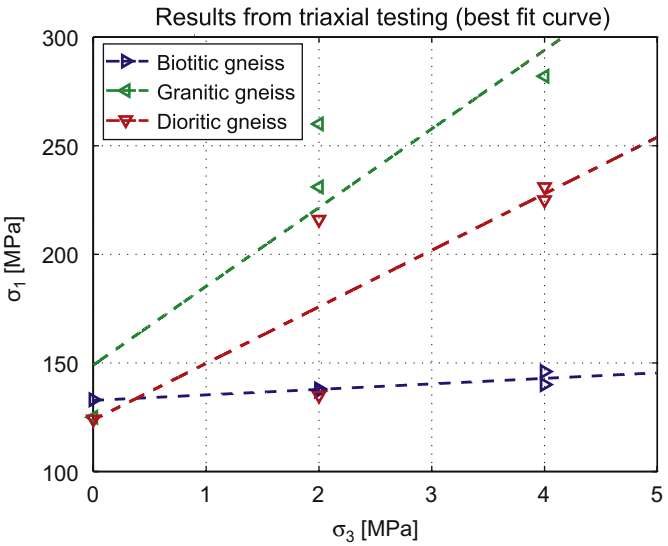

Fig. 10. The results of triaxial testing presented as $\sigma_1 - \sigma_3$-plots.

Table 4
Friction parameters for intact rock specimens.

Rock	c (MPa)	ϕ (deg)
Dioritic gneiss	19	57
Granitic gneiss	25	59

6.3. Results

In Fig. 10 the results of triaxial testing of intact rock samples are shown. As can be seen, the granitic and dioritic gneisses have similar strengths, with the former as the slightly strongest. Based on mapping and site investigation, sliding along foliation joints and in gouge material is believed most likely to take place in the weakest gneiss variety (i.e. mica gneiss), while failure of rock bridges most likely is believed to take place within the gneisses with highest shear strength, representing the "gap" between sliding planes (cf. Fig. 4). For intact rock, friction values for granitic and dioritic gneiss as shown in Table 4 are therefore used in the following. Although the number of triaxial tests was relatively low, the values for intact rock are considered relevant since they correspond well with what has previously been measured for Norwegian gneisses at low confining pressures [24].

Scaling of the intact rock parameters from laboratory to in situ has been carried out by applying the RocLab software [25]. The GSI values for the 21 locations as shown in Fig. 2 vary greatly (between 45 and 80). Most commonly, the GSI values are however within the range of 60–70 in the central part of the area, and the mean value of GSI = 62 was used as a input in RocLab. Based on this, Mohr–Coulomb parameters for the rock bridges were calculated to $c = 12$ MPa, $\phi = 48°$.

7. Discussion

In order to calculate resultant shear strength based on the test results for the three different components, certain assumptions need to be made. The main one is related to the rock stress conditions of the Åknes sliding area. In theory, topography and tectonics may increase the in situ stress considerably (based on rock stress measurements in this part of Norway possibly by a factor of 2–3 and more [24]). The open character of the back scarp and other discontinuities as shown in Figs. 2–5 indicates that this is, however, rather unlikely. It is therefore considered realistic to calculate the normal stress on the sliding plane simply as the weight component of overburden perpendicularly on the plane. For overburden ranging from 25 to 60 m and an average dip angle of 35° for the sliding plane ($\sigma_n = \gamma_{rock} \times h \times \cos \alpha_{slope}$), this gives a range of 0.5–1.3 MPa for the normal stresses. The resultant shear strengths for the respective compositions of the sliding plane are given in Table 5.

As discussed before, it is assumed that sliding along joints will be on foliation joints, while failure in intact rock will be in dioritic and granitic gneiss. The effect of the infilling on shear strength will depend on both the thickness and strength properties of the infilling material. If the thickness of the gouge material is more than about 25–50% of the amplitude of the asperities, there will be little or no rock-to-rock contact, and the shear strength will correspond to the properties of the infilling [26]. The asperity amplitude of foliation planes has been measured at several locations in the area, and found typically to range between 10 and 20 mm. Based on this, it is assumed that the shear strength of filled joints is governed by the shear strength of gouge.

Based on the resulting shear strengths of the various components; analysis of the significance of the composition of the sliding plane for the resultant strength have been made. The results are shown in Figs. Figs. 11 and 12. As can be seen, the resulting shear strength (τ_{res}) increases dramatically with increasing percentage of failure in intact rock. This is as should be expected due to the fact that intact rock by far inherits the highest shear strength. Also as expected, the resultant shear strength is higher for high percentage of failure along unfilled foliation joints than for high percentage of failure in gouge filled joints. Thus, the resultant shear strength of the sliding plane may vary considerably, depending on the composition of the sliding plane.

Although difficult, and connected with a considerable degree of uncertainty, an estimation of most likely composition of the sliding plane at Åknes may now be made. The portion of intact rock in the sliding plane is believed to be limited to local rock bridges. Based on field observations and drill core logging, an assumption of 1–3% of intact rock in the sliding plane is believed to be fairly reasonable. Reliable estimation of the ratio between jointed rock and gouge material in the sliding plane is also difficult. The cores obtained from boreholes indicate that the thickness of gouge in joints is limited to from about 10 to maximum 50 mm. Field observations of the foliation in the area favours the belief that a relatively large percentage of the total sliding surface coincides with unfilled foliation joints. An assumption of 25–35% gouge in the sliding plane is believed to be fairly reasonable, leaving a percentage share of 62–74% of

Table 5
Shear strengths for estimated ranges of σ_n.

Material	τ at $\sigma_n = 0.5$ MPa	τ at $\sigma_n = 1.3$ MPa
Gouge	0.23	0.61
Jointed rock	0.48	1.11
Gneiss	12.5	13.4

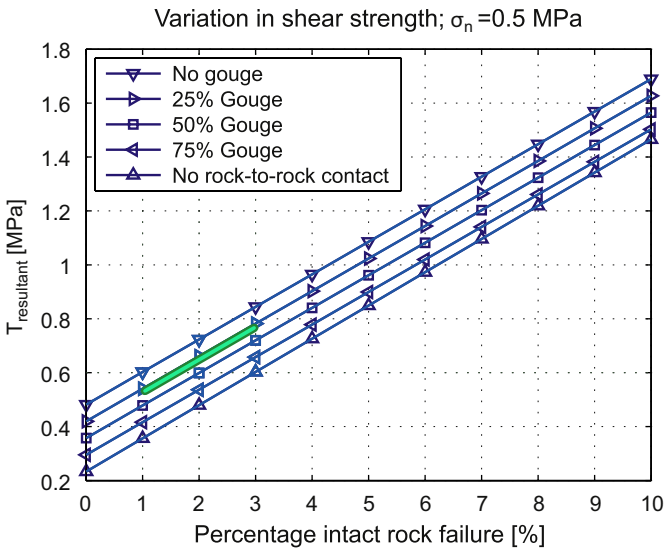

Fig. 11. Resultant shear strength versus percentage intact rock failure for various material compositions of sliding plane located 25 m ($\sigma_n = 0.5$ MPa) below the surface. Green section indicates the assumed range of shear strength.

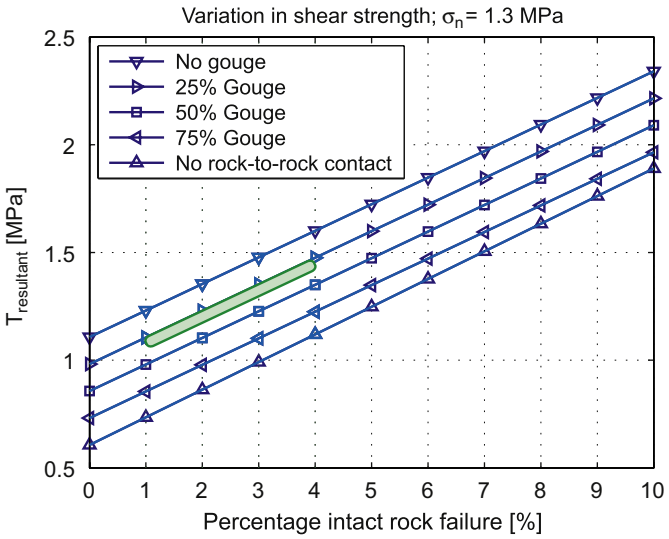

Fig. 12. Resultant shear strength versus percentage intact rock failure for various material compositions of sliding plane located 60 m ($\sigma_n = 1.3$ MPa) below the surface. Green section indicates the assumed range of shear strength.

rock-to-rock contacts. Based on these assumptions, the approximate range of resultant shear strength will be as indicated by the green sections in Figs. 11 and 12.

In rock slope stability analysis, the resultant shear strength may be used directly as input. In limit equilibrium analysis, the frictional parameters c and ϕ are often used, and in some cases the "active" or "total" friction angle (ϕ_a), as described by Barton [27]. By using ϕ_a, frictional resistance is represented by one single shear strength parameter, and for each respective composition of the sliding plane, ϕ_a thus is defined by the following equation:

$$\phi_a = \arctan \frac{\tau_{res}}{\sigma_n} \tag{3}$$

where τ_{res} is the resultant shear strength (as calculated in Figs. 11 and 12) and σ_n is the normal stress range ($\sigma_n = 0.5-1.3$ MPa).

The resulting active friction angle curves for the Åknes case are shown in Figs. 13 and 14. As can be seen, the variation in active friction angle is greater when the sliding plane includes 1% intact

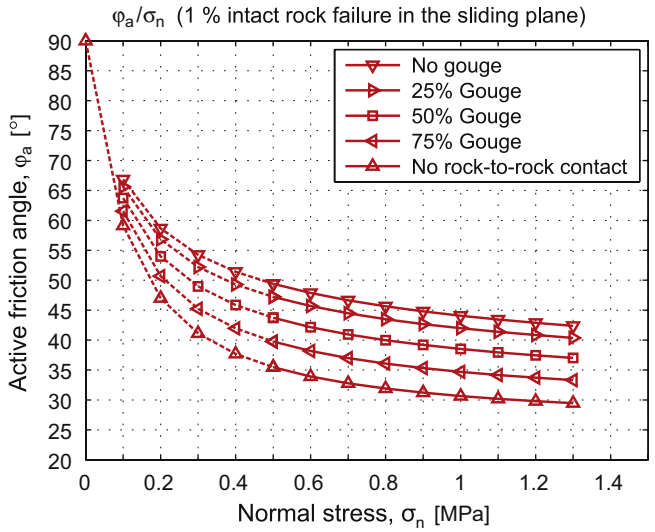

Fig. 13. Active friction angle versus normal stress for 1% intact rock failure in the sliding plane.

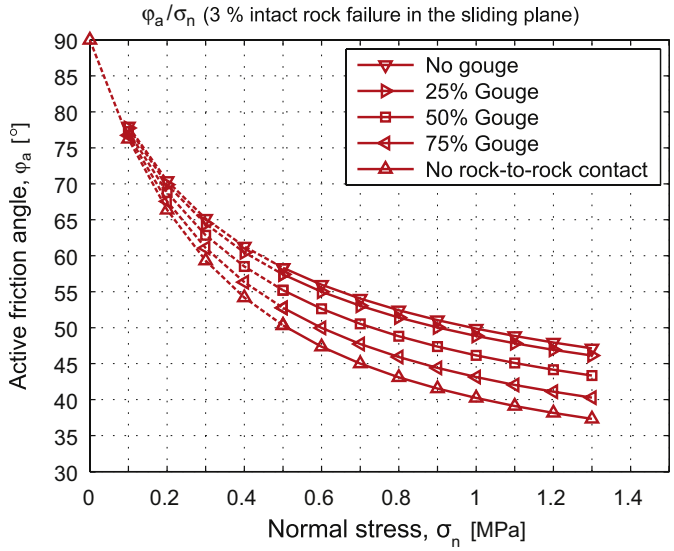

Fig. 14. Active friction angle versus normal stress for 3% intact rock failure in the sliding plane.

rock failure than if it includes 3% intact rock failure. This is due to a more distinct influence of unfilled joints and gouge in the first case. The accelerating increase of ϕ_a with decreasing stress emphasizes the importance of determining the friction parameters in accordance with the normal stress level in question, as described by Nilsen [28].

The shear strength ranges indicated in Figs. 11–14 should be regarded as indicative at this stage. The knowledge concerning sliding plane character and stress conditions at great depth at Åknes is still limited. There is also uncertainty connected to the fact that the materials located in the sliding plane most probably will be progressively weakened as shearing progresses along the plane.

8. Conclusion

Based on field mapping and investigations, logging of cores from boreholes and laboratory investigations of rock and soil, the resulting shear strength for a sliding plane at Åknes located at 25 and 60 m below the surface, respectively, has been estimated to 0.5–0.75 and 1.05–1.3 MPa. This is based on assumption of 1–3% intact rock failure, 25–35% failure along gouge-filled joints and 62–74% failure along unfilled foliation joints. The friction angle is highly dependent upon normal stress level, with the highest value of ϕ_a for the lowest value of σ_n. For the assumed composition of the sliding plane, and depth of sliding plane of 25 and 60 m, respectively, the resultant active friction angles for Åknes are approximately $47-37^\circ$ for 1% intact rock failure and $57-43^\circ$ for 3% intact rock failure.

The main uncertainties associated with the Åknes sliding area are the geometry of the complex sliding plane and the relative distributions of the various material components which form this plane. Site investigations and instrumentation can provide an idea of the location of the sliding plane, but the distribution to a great extent remain unknown.

The analysis and results presented here emphasize the need to perform more thorough investigations of the potential sliding plane at Åknes, particularly aiming at more exact estimation of the composition of the sliding plane and the rock stress conditions. The results illustrate that even very sophisticated stability analysis cannot give reliable results if the material composition and resulting shear strength of the sliding plane are unknown.

Acknowledgements

The work presented in this paper is carried out as part of International Centre for Geohazards (ICG), located at Norwegian Geotechnical Institute (NGI), and the Åknes-Tafjord project at Stranda Municipality. Prof. Lars Harald Blikra, scientific responsible for the latter, is acknowledged for support and cooperation. Special thanks to Prof. Charlie Chunlin Li at the Norwegian University of Science and Technology (NTNU) for having reviewed the manuscript and given useful ideas and comments.

References

[1] Brolili L. New knowledge on the geomorphology of the Vaiont slide slip surface. Felsmechanik und Ingenieurgeologie 1967;5–6:38–88.
[2] Müller L. The rock slide in the Vajont valley. Felsmechanik und Ingenieurgeologie 1964;2:148–212.
[3] Müller L. New considerations on the Vajont slide. Rock Mechanics and Engineering Geology 1968;6:1–91.
[4] Kenney TC. Stability of the Vaiont-valley slope. Felsmechanik und Ingenieurgeologie 1967;5–6:9–16.
[5] Hendron A-J, Patton FD. The Vaiont slide: a geotechnical analysis based on new geologic observations of the failure surface. Technical Report, Department of the Army, US Army Corps of Engineers, GJ-85-5; 1985.
[6] Eidsvig U, Harbitz C. Innledende numeriske analyser av flodbølger som følge av mulige skred fra Åkneset. Technical Report, Norwegian Geotechnical Institute, 20031100-2; 2005.
[7] Bjerrum I, Jørstad FA. Stability of natural rock slopes in Norway. Publication No. 79, Norwegian Geotechnical Institute; 1968.
[8] Blikra LH, Longva O, Anda E, Dehls J, Stalsberg K. Rock-slope failures in Norwegian fjord areas: examples, spatial distribution and temporal pattern. In: Evans SG, Scarawcia Mugnozza G, Strom AL, Hermanns RL, editors. Landslides from massive rock slope failure. NATO science series. Berlin: Springer; 2005. p. 475–96.
[9] Blikra LH, Longva O, Harbitz C, Løvholt F. Quantification of rock-avalanche and tsunami hazard in Storfjorden, western Norway. In: Senneset K, Flaate K, Larsen JO, editors. Proceedings of the 11th international conference and field trip on landslides, Norway. Taylor and Francis Group; 2005. p. 57–63.
[10] Sandersen F, Bakkehøi S, Hestnes E, Lied K. The influence of meteorological factors on the initiation of debris flows, rockfalls, rockslides and rockmass stability. In: Senneset K, editor. Proceedings of the seventh international symposium on landslides, Trondheim, Norway. Rotterdam: Balkema; 1996. p. 114–97.
[11] Derron MH, Blikra LH, Jaboyedoff M. High resolution elevation model analysis for landslide hazard assessment (Åkerneset, Norway). In: Senneset K, Flaate K,

Larsen JO, editors. Proceedings of the 11th international conference and field trip on landslides, Norway. Taylor and Francis Group; 2005. p. 101–13.
[12] Ganerød GV, Grøneng G, Rønning JS, Dalsegg E, Elvebakk H, Tønnesen JF. Geological model of the Åknes rockslide, western Norway. Engineering Geology 2008;102:1–18.
[13] Larsen JO. Tension cracks and landslides in steep hard rock mountains in the Norwegian fjord districts. In: Proceedings of the second international conference on landslides, slope stability & safety of infra-structures, Singapore; 1999. p. 193–200.
[14] Kveldsvik V, Eiken T, Ganerød GV, Grøneng G, Ragvin N. Evaluation of movement data and ground conditions for the Åknes rock slide. In: Proceedings of stability of rock slopes in open pit mining and civil engineering situations. Cape Town: The South African Institute of Mining and Metallurgy; 2005. p. 279–300.
[15] Tveten E, Lutro O, Thorsnes T. Bergrunnskart Ålesund. 1:250 000. Geological Map, Norwegian Geological Survey; 1988.
[16] Braathen A, Blikra LH, Berg SS, Karlsen F. Rock-slope failures in Norway; type geometry and hazard. Norwegian Journal of Geology 2004;84:67–88.
[17] Ganerød GV, Grøneng G, Aardal IB, Kveldsvik V. Core logging of seven boreholes from Åknes, Stranda Municipality, Møre and Romsdal County. Technical Report, Norwegian Geological Survey, 2007.020; 2007.
[18] Håndbok Ingeniørgeologi. Norwegian Group of Rock Mechanics, TAPIR; 1985.
[19] Barton N, Bandis S. Review of predictive capabilities of JRC-JCS model in engineering practice. In: Barton N, Stephansson O, editors. Proceedings of the international conference on rock joints. Balkema; 1990. p. 603–10.
[20] Grøneng G, Nilsen B. Procedure for determining input parameters for Barton–Bandis joint shear strength formulation. Technical Report, Department of Geology and Mineral Resources Engineering, Norwegian University of Science and Technology; 2008.
[21] Barton N, Choubey V. The shear strength of rock joints in theory and practice. Rock Mechanics 1977;10:1–54.
[22] Suggested methods for determining hardness and abrasiveness of rocks. International Society of Rock Mechanics; 1978.
[23] Suggested methods for determining the strength of rock materials in triaxial compression: revised version. International Society of Rock Mechanics; 1983.
[24] Myrvang A. Bergmekanikk. Norwegian University of Science and Technology; 2001.
[25] Rocscience, RocLab. Manual, Rocscience Inc., Toronto, 1.010; 2002.
[26] Goodman RE, Determination of the in situ modulus of deformation of rock; the deformability of joints. Technical Report, American Society for Testing and Materials; 1970. p. 477.
[27] Barton N. Review of a new shear strength criterion for rock joints. Engineering Geology 1973;7:287–332.
[28] Nilsen B. Shear strength of rock joints at low normal stresses—a key parameter for evaluating rock slope stability. In: Stephansson O, editor. Proceedings of the international symposium on fundamentals of rock joints, Bjørkliden, Sweden. CENTEK Publishers; 1985. p. 487–94.
[29] Deere DU, Miller RP, Engineering classification and index properties for intact rock. Technical Report, Air Force Weapons Laboratory, New Mexico, AFNL-TR-65-116; 1966.
[30] Barton N. A review of the shear strength of filled discontinuities in rock. Publication No. 105, Norwegian Geotechnical Institute; 1974.
[31] Wyllie DC, Mah CW. Rock slope engineering, civil and mining. 4th ed. SPON Press Taylor and Francis Group; 2004.
[32] Barton N, Bandis S. Effects of block size on the behaviour on jointed rock. In: Goodman R, Heuze F, editors. Proceedings of the 23rd US symposium on rock mechanics. Society of Mining Engineers of the American Institute of Mining, Metallurgical and Petroleum Engineers, Inc.; 1982. p. 739–60.

Paper II

Geovisualization, geometric modelling and volume estimation of the Åknes rockslide, western Norway

Authors: Trond Nordvik, Guro Grøneng, Guri Venvik Ganerød, Bjørn Nilsen, Chris Harding and Lars H. Blikra

The paper was published in Bulletin of Engineering Geology and the Environment (2009), Vol. 68, pages 245-256, doi:10.1007/s10064-009-0198-x.

Is not included due to copyright

Paper III

Meteorological effects on seasonal displacements of the Åknes rockslide, western Norway

Authors: Guro Grøneng, Hanne H. Christiansen, Bjørn Nilsen and Lars H. Blikra

The paper was submitted to Landslides (May 2009).

Landslides manuscript No.
(will be inserted by the editor)

Meteorological effects on seasonal displacements of the Åknes rockslide, western Norway

Guro Grøneng · Hanne H. Christiansen · Bjørn Nilsen · Lars Harald Blikra

Submitted: May 2009

Abstract In the alpine topography along one of the long fjords with steep and high mountain sides in western Norway the large Åknes rockslide area is defined by a distinct back scarp rising from 800 to 1000 m a.s.l. In 2004, an extensive monitoring program started, including establishment of a meteorological station above the back scarp, 900 m a.s.l. This paper evaluates the significance of meteorological conditions affecting the displacements recorded by five extensometers and two laser sensors in the westernmost part of the back scarp in the period November 2004-August 2008. Meteorological factors of importance for the recorded activity in the back scarp are found to be melt water in spring and large temperature fluctuations around the freezing point in spring, early summer, autumn and early winter. The seasonal activity in the back scarp is decreasing in the second half of the analyzed period even though annual displacements are increasing, indicating that meteorological causes are of decreasing importance for the displacements.

Keywords Rockslide · Meteorology · Displacement · Extensometer monitoring · Åknes

1 Introduction and study area

In the alpine topography of western Norway rockslides occur quite frequently. Especially along the fjords sliding represents a significant threat to the population living there, as evidenced in this century by the sliding catastrophes of Loen (1905 and 1936) and Tafjord

Guro Grøneng
Norwegian University of Science and Technology (NTNU), Dept. of Geology and Mineral Resources Engineering, Trondheim / Norway International Centre for Geohazards (ICG), Oslo, Norway
Tel.: +47-73-594807
Fax: +47-73-594814
E-mail: guro.groneng@ntnu.no

Hanne H. Christiansen
The University Centre in Svalbard (UNIS), Dept. of Geology, Svalbard, Norway

Bjørn Nilsen
Norwegian University of Science and Technology (NTNU), Dept. of Geology and Mineral Resources Engineering, Trondheim / Norway International Centre for Geohazards (ICG), Oslo, Norway

Lars Harald Blikra
Stranda Municipality / International Centre for Geohazards (ICG), Oslo, Norway

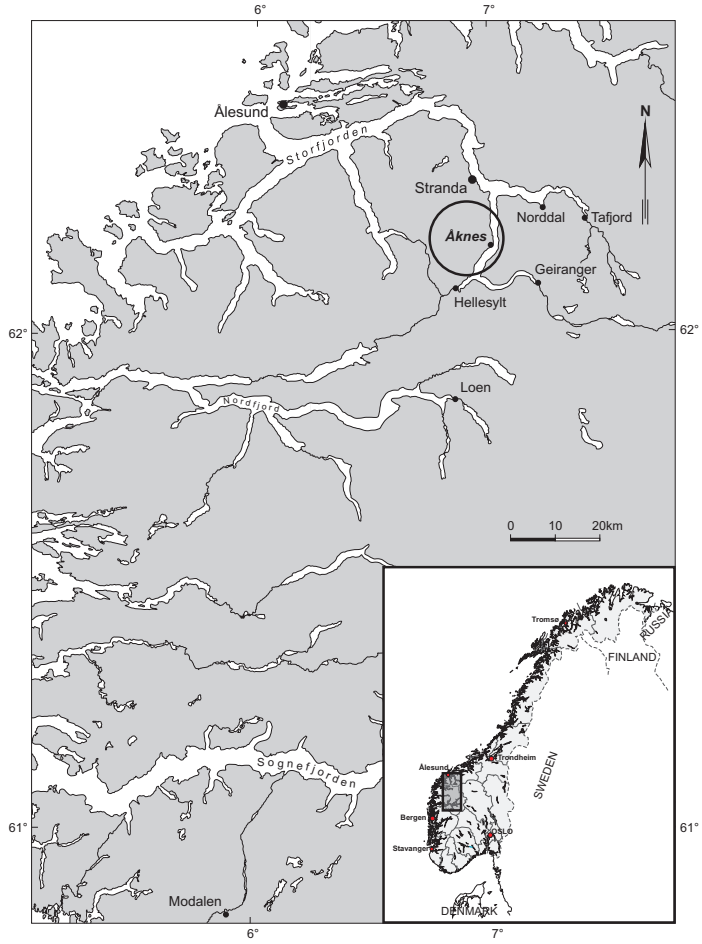

Fig. 1 Locations of the Åknes rock slope, the town of Stranda, settlements and historical rockslides discussed.

(1934), where more than 170 persons lost their lives (Bjerrum and Jørstad (1968)). Rockslides are recurrent hazards in the steep rock slope at Åknes (Kveldsvik et al. (2006)), located up to 1,000 m above sea level at the fjord Storfjorden (Fig. 1). Swath bathymetry from the up to 320 m deep Storfjorden has revealed at least 59 rock slope failures of more than 0.5×10^6 m^3 to have occurred since the last glaciation 10,000 years ago (Blikra et al. (2005)). In addition to the nearly 1,000 people living at the nearby communities Geiranger and Hellesylt located by the fjord, there are 3,500 inhabitants in the town of Stranda, 15 km away from Åknes (Fig. 1). The Åknes rockslide area (Fig. 2) was first brought to the public's attention in 1964, when local people claimed that the back scarp was widening (Sandersen et al. (1996)). This resulted in the installation of bolts on both sides of the back scarp and manual distance measurements across the back scarp began in 1986. A comprehensive monitoring program with several types of movement measurements is in operation in the rock slope area today, funded by the Norwegian Natural Disaster Fund since 2004. At present, the rockslide monitoring project is one of the largest in the world, due to the potential hazard of a tsunami generated as a result of a slope failure. Tsunami modeling indicates that

the communities along the fjord system will be endangered (Eidsvig and Harbitz (2005)), in addition to the tourist industry in the adjacent Geiranger fjord, listed on UNESCO's World heritage list. Current estimates indicate an unstable area of 575,000 m^2, with a volume of about 40×10^6 m^3. The slide is believed to take place along several sliding planes; with the basal sliding plane (the base of the deforming mass) located 105-115 m below the terrain surface (Nordvik et al. (2009)).

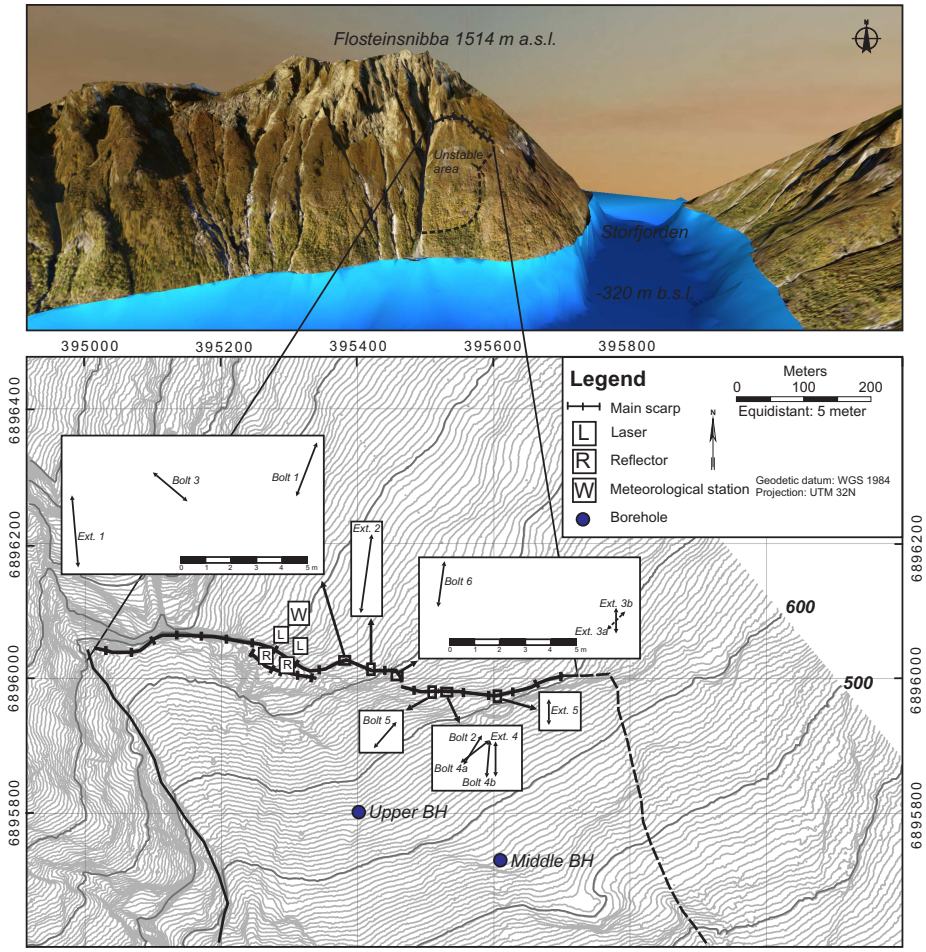

Fig. 2 The Åknes rockslide area with back scarp monitoring.

Meteorological factors with seasonal variations might cause slope deformations, which eventually lead to failure. The relationship between displacement of rockslide areas and seasonal variation has been discussed internationally, e.g. recently by Willenberg et al. (2008), Gunzburger et al. (2005), Crosta and Agliardi (2003) and Bogaard et al. (2000). In Norway, the relationship between historical rockslides and meteorological factors has been analyzed for four large scale historical rockslides (Loen 1905 and 1936, Tafjord 1934 and Modalen 1953), all located within 120 km from Åknes (Fig. 1), to evaluate the significance of me-

teorological factors on initiating the rockslides (Sandersen et al. (1996)). No simple relationship between meteorology and initiation of rockslides was found based on records of precipitation and temperature available from meteorological stations. The intensities of precipitation/snowmelt were found to be normal, with recurrence intervals of only a few years, when these large rockslides occurred. Other processes, not directly dependent on meteorological factors, like disintegration of irregularities along the slip surface due to physical or chemical processes reducing the friction, or steady sliding movement bringing the center of mass closer to its critical position, were mentioned as possible processes.

Establishment of a meteorological station at Åknes in November 2004, as part of the rockslide monitoring program, enabled detailed studies of meteorological seasonal effects on deformation. In this paper we focus on analyzing the various meteorological parameters to investigate their potential influence on rock deformation presented by extensometer- and laser recordings from the back scarp area, from 2004 throughout August 2008.

2 The history of deformation in the Åknes rockslide

Signs of instability at the Åknes rockslide area have been evidenced by occurrence of three smaller rockslides, all along the western boundary of the area, the most recent in 1960, with an estimated volume of approximately 100,000 m^3 (Kveldsvik et al. (2006)). Photogrammetric studies have indicated displacement in the order of 6 cm/year since 1961 (Kveldsvik et al. (2006)). Two sets of bolts for manual reading were installed across the back scarp in August 1986, and supplemented by five sets of bolts in September 1989. On average, the distances between the bolts have been measured manually every 2-3 years. The monitoring of the back scarp deformation was extended by continuous recordings of three extensometers starting in August 1993, and two additional extensometers were installed in October 2004 (Fig. 2).

The early monitoring of distances across the back scarp has been analyzed with respect to seasonal variation by Larsen (2003), Larsen (1999) and Sandersen et al. (1996). Larsen (1999) found that in the period 1986-1995 the bolt distance measurements showed changes every year, assuming movements mostly caused by melt water from snow in the spring or high precipitation during autumn periods. Larsen (2003) analyzed records from three extensometers in the period 1993-1995, and concluded that recording of one of them (Ext. 3) showed seasonal variations, with the most significant extension occurring in spring and autumn/early winter. The extension seemed primarily to be connected to periods around snowmelt in May and to periods with high precipitation in September to December. In winter, January to April, when precipitation as rain in general was small and the joints covered with snow, the recorded extension was negligible.

Sandersen et al. (1996) made a detailed study of the extensometer records also in the period 1993-1995. They concluded that Ext. 1 had the largest displacements during the autumn, Ext. 2 showed a slight increase in displacement rate throughout the period, and Ext. 3 had a specific pattern with no or little movement during the winter and summer months, and marked displacement during springtime. No evident relation between precipitation and displacement was found. This was believed to indicate that water pressure did not play an important role on the movement. The effect of ice was, however, believed to be significant. Especially for Ext. 3, it seemed like the block was fixed when freezing started in autumn/early winter, while displacement accelerated when the ice thawed in spring.

3 Meteorology

In November 2004 the Åknes meteorological station was established at 900 m a.s.l. just above the Åknes rockslide area. The station (Fig. 3) is a part of a large monitoring and communication system with remote data transfer, enabling online access to the data. Standard meteorological parameters such as air temperature, humidity, radiation, wind velocity, wind direction, snow depth and precipitation are measured approx. 2 m above the ground surface, while soil temperature is measured at the boundary between soil and bedrock, with the sensor placed on top of a rock surface covered by a soil layer, 5-10 cm thick. Meteorological data are available from November 11 2004 and have been analyzed in hydrological years (September 1 to August 31) between November 2004 and August 2008.

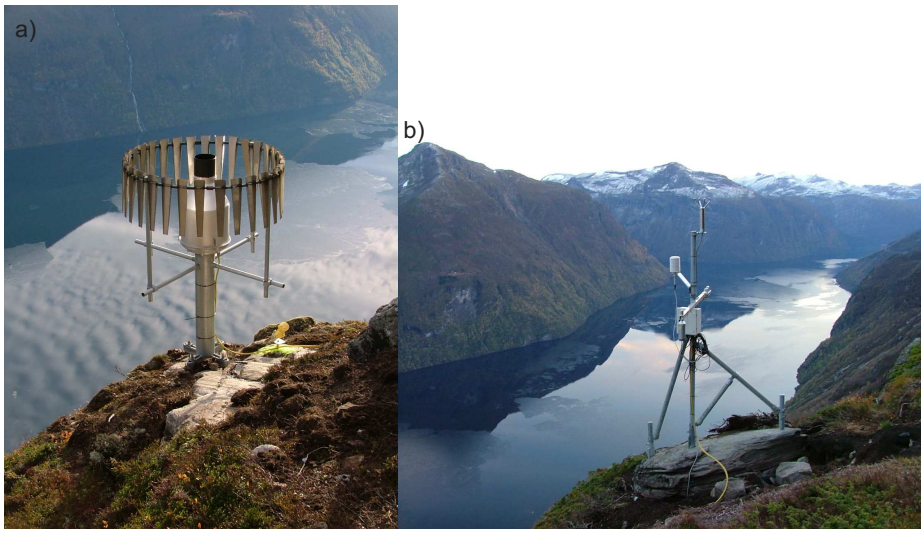

Fig. 3 Meteorological station at Åknes at 900 m a.s.l. operational from 11 November 2004. a) Precipitation gauge (Oscillating string T-200 B from Geonor) b) Meteorological mast monitoring air temp/humidity (Combinationsensor HMP45A from Vaisala), soil temperature (Thermistor 107 from Campbell), wind speed/direction (Windobserver II from GILL), radiation (Combinationsensor CNR1 from Kipp&Zonen), and snow depth (Ultrasoundsensor SR50 from Campbell). The measuring frequency is 5 sec for all instruments except for the snow depth sensor, for which it is 15 min.

3.1 Temperature

Recorded hourly air- and soil temperatures are shown in Fig. 4. Mean annual air temperature (MAAT) varies from $+2.8°C$ to $+3.8°C$. The average daily air temperature is generally negative from November/December to mid/end of April. Large temperature fluctuations around $0°C$ are evident in autumn, winter and spring; temperature fluctuations of 7-11°C within 1-2 days are not unusual, reflecting the marine climate. Soil temperatures vary between $0°C$ and $+15°C$ in the period November 2004-September 2008 (Fig. 4). In winter, from December/January to April/May, when there is a layer of snow on top, the soil temperature is close

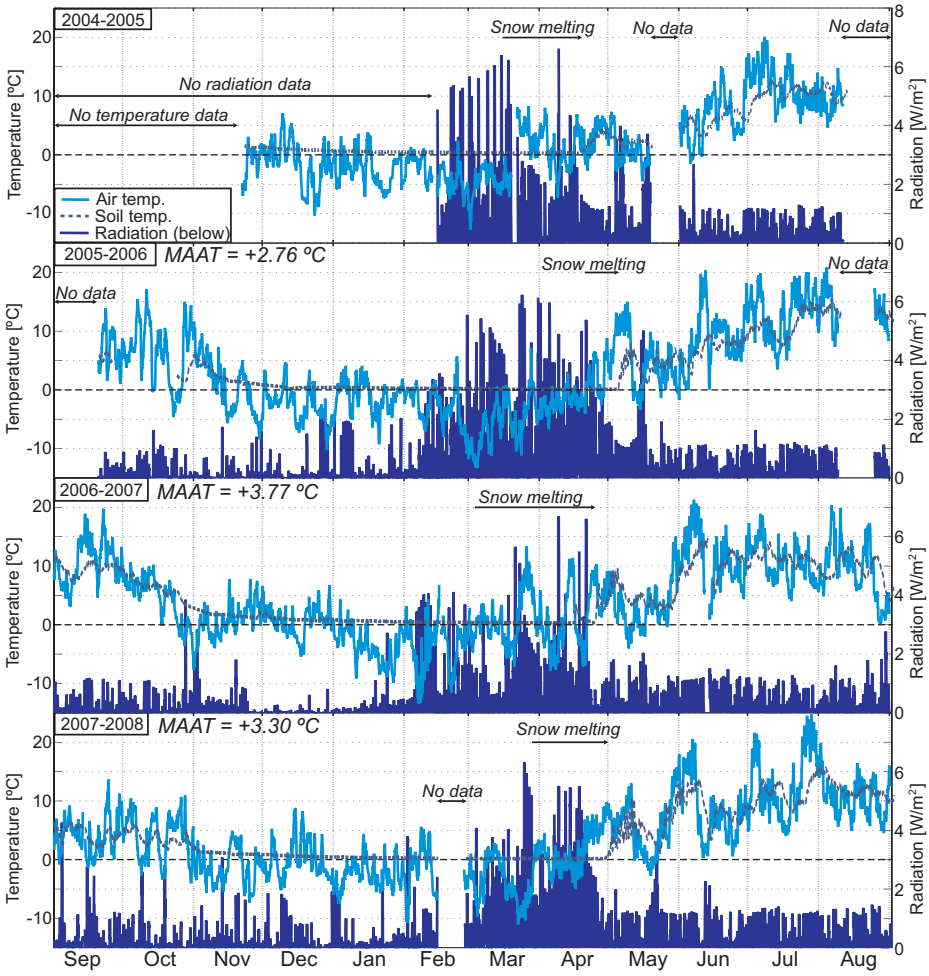

Fig. 4 Hourly air temperature, soil temperature and outgoing longwave radiation recorded at Åknes meteorological station 2004-2008.

to 0°C. The daily variation in soil temperature is largest in springtime (May), with daily variations up to 2.5-3°C.

3.2 Snow duration and radiation

The snow depth is measured for two points at the meteorological station. These measurements, however, can not be used as a basis for detailed analyses of snow depth and duration, because the sensors have been periodically out of order. In addition, the measurements are subjected to a high degree of noise throughout the analyzed period. Generally, the records show that snow accumulates in November and melts completely away by the end of May. The maximum snow depth varies between 1.5 and 2 m in the winter months at the meteoro-

logical station, while it is believed to vary between 0 and more than 4 m locally within the sliding area.

Direct insolation is naturally highest from March to September, and has a significant minimum from November to early February, when the alpine topography prevents direct insolation. Outgoing radiation is highest from March to May, i.e. during the end of the snow covered period, and reaches a low level as soon as all the snow is melted (see Fig. 4).

Estimation of the timing of the snow melting periods can be made by combining air-/soil temperatures and radiation recordings with manual observations. Based on this the snow melting period was from mid March to end April in 2005, from mid April to early May in 2006, from early March to mid April in 2007, and from late March to late April in 2008 (Fig. 4). The length of the snow melting period thus varies from 3 weeks to 1.5 months, controlled largely by the timing of positive air temperatures, the length of freezing periods and the annual snow thickness. This, however, reflects only the snow melting at the location of the meteorological station at 900 m a.s.l., i.e. above the back scarp. Snow stays significantly longer in the back scarp and the graben structure, which are natural topographical lee sites accumulating larger snowdrifts during winter. Snow avalanche threats from higher altitudes generally exist until late June, indicating a prolonged period with water from snow melting in the catchment area.

3.3 Snow- and rain precipitation

Precipitation measurements are carried out with a precipitation gauge (Fig. 3a) containing an anti-freeze solution, i.e. all precipitation is recorded with no distinction between rain and snow. Analysis of monthly precipitation rates at Åknes, from December 2005 to August 2008, show precipitation of 1600-1800 mm/year (Fig. 5). Most precipitation falls in autumn (September-November) with monthly average rates of 190-280 mm. Maximum intensities of 44 mm/hour occur in August. As the temperature is generally below the freezing point from November to end of March/April, precipitation falls mainly as snow in this period. In the spring and summer months from April to August, the precipitation is generally low, with monthly average rates of 60-120 mm and low maximum intensities (8-11 mm/hour).

3.4 Wind speed and direction

Wind speeds generally are highest during winter, and low in summer. Mean annual wind speeds range from 4.8 m/s to 5.8 m/s in the study period. Storms (wind velocities up to 20.8-32.6 m/s) occur mainly during autumn and winter months (mid November to March) (Fig. 6). Storms are also recorded in April 2006 and 2007, June 2006 and August 2007. The maximum wind speed of 29 m/s was recorded in December 2004. The dominating wind direction is approx. 220°, which is also the wind direction during the recorded storms, indicating that the wind travels along the fjord from SW.

3.5 Meteorology of Åknes

The meteorological data demonstrate a Dfc snow climate fully humid with cool summers, according to the Köppen-Geiger climate classification system (Kottak et al. (2006)). Due to the location close to the west coast of Norway, the Åknes site is relatively often exposed to

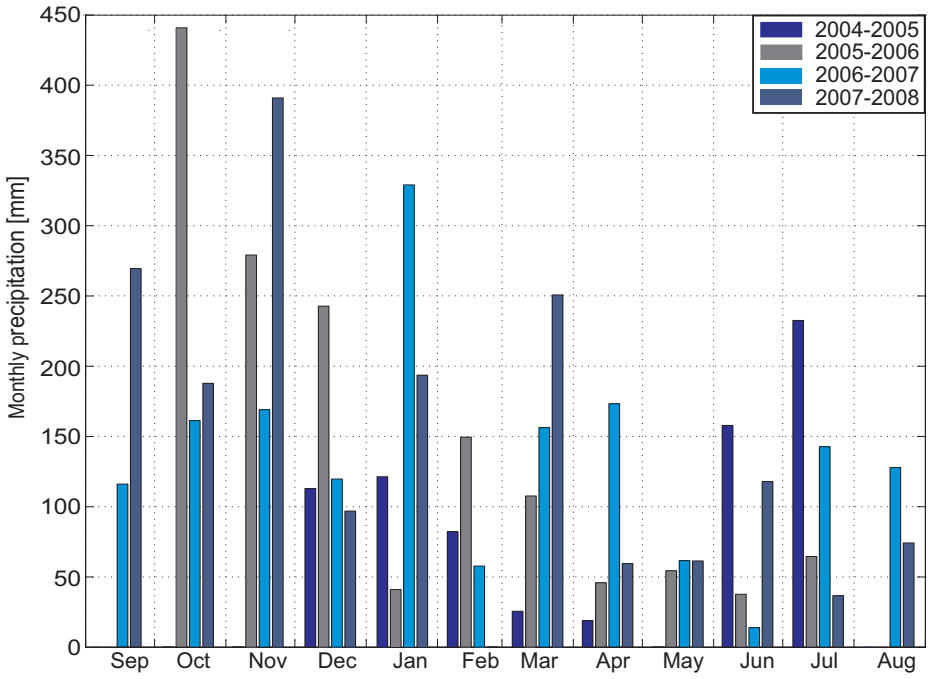

Fig. 5 Monthly precipitation December 2004-August 2008 at Åknes meteorological station.

low pressures approaching from the North Atlantic Sea, bringing intense and large amount of precipitation and southwesterly winds. In summer the rain drains directly into the rock slope, whereas in winter from November to April almost all precipitation accumulates as snow. For the period 2004-2008, the annual precipitation (from September 1 August 31) was in the range of 1600-1800 mm, of which 40-70% fell as snow. Due to the alpine topography the investigated rock slope only received direct insolation from February to October.

4 Groundwater

The groundwater system in the sliding area is believed to be primarily controlled by direct precipitation feeding run-off water in summer and autumn, and in spring supplemented by melt water from the sliding area itself and from snow accumulated in the back scarp, in addition to melt water from the estimated 0.7 km^2 catchment area above. The combination of snow melt water, also from the area above the back scarp, and direct precipitation, potentially can cause increased deformation.

The groundwater level is measured by piezometers in a D.M.S. IU monitoring system (DMS (2009)), which were installed in the upper and middle borehole (Fig. 2) on November 30, 2006. Precipitation rates and daily groundwater levels in the boreholes are shown in Figure 7. The groundwater level fluctuates between -42.5 and -46.5 m below the surface in the middle borehole, and between -51 and -60 m in the upper borehole. Groundwater levels recorded in the boreholes are fluctuating simultaneously, indicating a shared groundwater regime. The fluctuations are however, largest in the upper borehole, reflecting the close

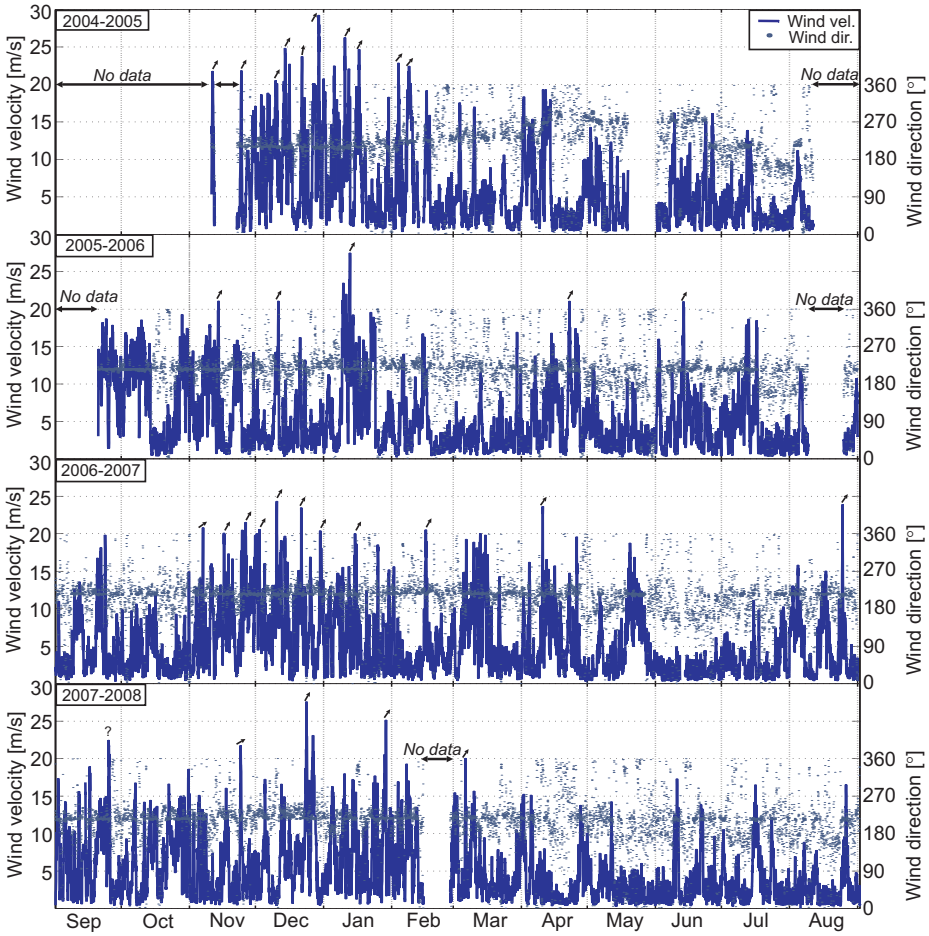

Fig. 6 Hourly wind velocities and directions. Arrows indicate wind directions during recorded storms.

location to the back scarp, which is believed to constitute a major feature for infiltration of water to the sliding area.

In 2007, the snow melting period started in the beginning of March, and this coincides with a sudden rise in the groundwater level in upper and middle borehole 11 days later (from -57 m to -52 m in 5 days in upper borehole). The snow melting period lasted until mid April at the meteorological station, and the large fluctuations in the groundwater level in this period might reflect the temperature fluctuations around 0°C and precipitation causing discontinuous feeding of melting water to the ground. From end April/early May, the water level decreased in the upper and middle borehole, suggesting a decreasing water influx.

In 2008, recorded air temperatures indicate that the snow melting period started in late March. A period with temperatures below the freezing point is however recorded before the temperatures raised and stabilized on temperatures above the freezing point in mid April. This sudden rise in air temperature coincides with the sudden rise in the groundwater level at the upper and middle borehole (from -60 m to -55 m in one week in upper borehole), reflecting that this significant rise in water levels clearly is caused by the annual snowmelt.

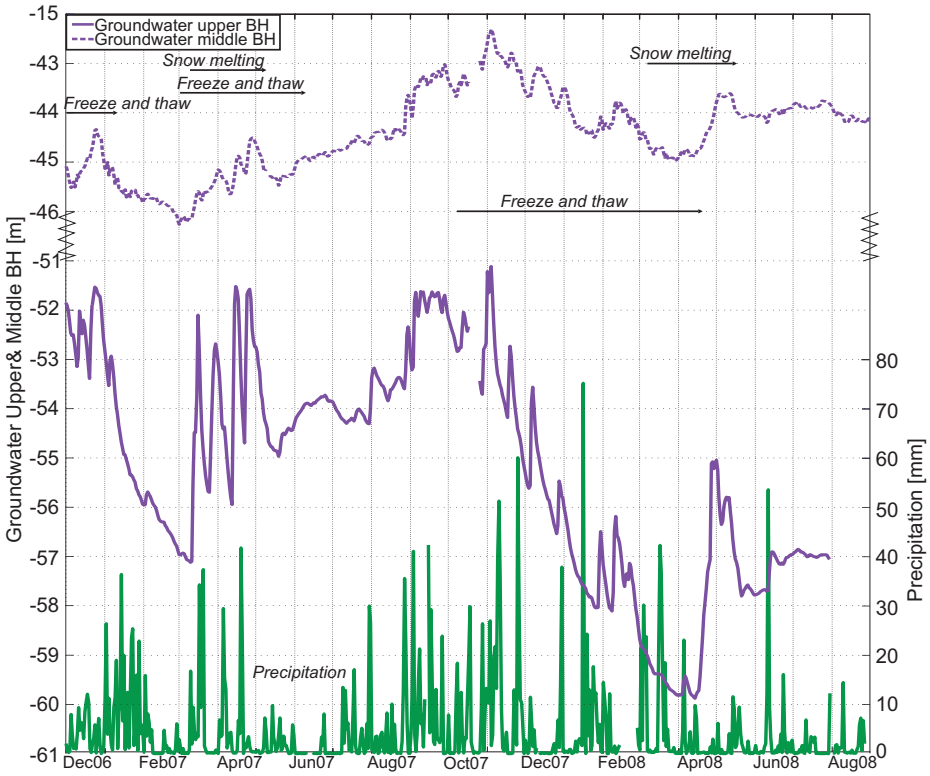

Fig. 7 Groundwater levels in upper and lower borehole in combination with recorded precipitation and air temperatures from Åknes meteorological station, December 2006-August 2008.

Lowering of the ground water level followed by stabilization in the upper and middle borehole is evident from mid May 2008, indicating that the groundwater regime was supplied with melt water from the catchment area above and/or the snow accumulated in the back scarp for additional two weeks after snow melting ended at the meteorological station (end of April).

The autumn groundwater levels from September throughout October 2007 are relatively high due to high precipitation (143 mm, 128 mm, 269 and 188 mm in July, August, September and October, respectively). From the beginning of November, till snow melting starts in April 2008, the groundwater levels gradually drop (from -51 m to -60 m in upper borehole and from -42.5 to -45 in middle borehole), as less water is discharged into the area due to temperatures below 0°C. In the following summer, precipitation is less (37 mm and 74 mm in July and August, respectively), which causes lower groundwater levels in upper borehole this summer, showing that the groundwater levels in the summer and autumn months are a result of the amount of precipitation.

5 Displacement measurements in the back scarp and graben

The back scarp is the most intensively monitored geological structure of the Åknes rock slide, and its expansion clearly shows that the slope is unstable. This structure is an approximately 800 m long tensional fracture, progressively developing toward east, where it currently ends with an opening of approximately 0.5-1 m. To the west, the opening is much larger, with a well-developed 20-30 m wide graben. Manual measurements of the distance between 6 installed sets of bolts, during a 18-year period until June 2004, show a steady widening in the order of 2.8-32.7 mm/year of the back scarp.

The graben is a relieved structure (block) with an estimated volume of 300,000-400,000 m^3, which is believed to be detached from the main sliding mass. The structure is, however, considered to indicate instability and movement of the whole area. The relieved structure moves towards SW, toward a large ravine, which defines the western boundary of the sliding area.

5.1 Extensometers

Five extensometers (Ext. 1-5) (Fig. 8) are placed in telescopic steel pipes, fixed to solid rock on each side of the scarp, and installed across the open back scarp (NGI 1996, 2005). Until March 2006, the data was sampled once a day, stored locally in a datalogger, and then transmitted by a solar powered cellular phone at the site. From March 22, 2006 the reading frequency shifted from daily to every 5 minutes. The extensometers are all orientated in approximately N-S direction, which does not favor measurement of the true displacements in the NW-SE oriented back scarp. The resultant displacement thus is larger. To analyse potential seasonal variations, the measuring period between November 2004 and August 2008 was chosen, for which also meteorological data are available from the Åknes meteorological

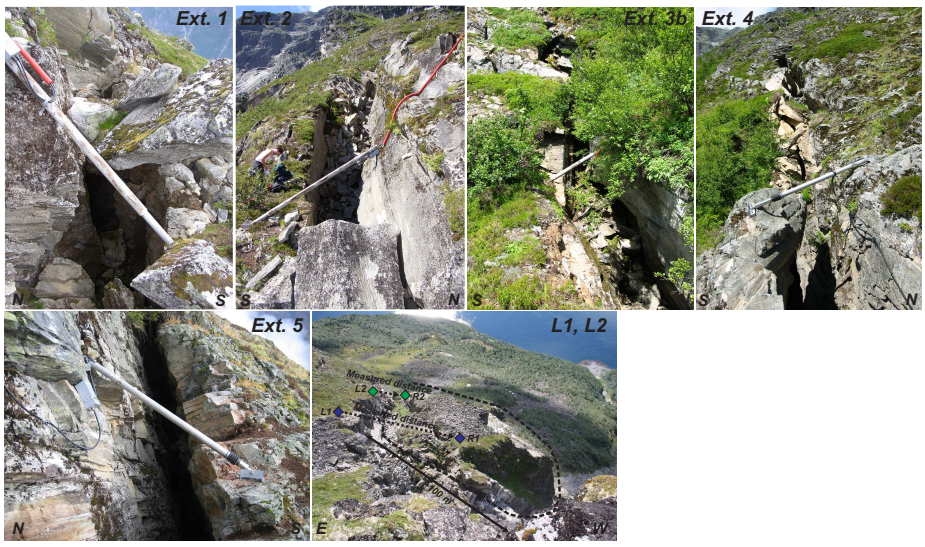

Fig. 8 Extensometers 1-5 located across the back scarp and lasers L1 and L2 located at relieved graben structure at Åknes.

station, as presented above. Due to lightning, which destroyed the data transmission from the extensometers, extensometer data are lacking for the period mid February to July 2008 (Fig. 9). Ext. 3 is termed ”Ext. 3a” until November 2004, when it was reinstalled in a N-S direction and termed ”Ext. 3b”. Ext. 4 and 5 have limited recordings due to damage by snow avalanches; Ext. 4 no recordings after July 2005 and Ext. 5 was operative only for a limited period of about one year (November 2004 - November 2005).

5.2 Lasers

The displacement of the graben structure is monitored by two laser beams as the distance from the two lasers (L1, L2) placed on the stable side of the back scarp to two reflectors (R1, R2), situated in the moving graben structure (Fig. 10). The laser instrument is a DLS-B(H) Distance Laser Sensor from DIMETIX (DIMETIX (2009)) with typical accuracy of 1.5 mm. Meteorological factors such as airborne particles (dust, fog, heavy rainfall and heavy snowfall) as well as bright sunshine on the reflectors reduce the accuracy. Continuous laser data has been recorded since 2005.

The laser distance measurements show quite steady rates when data is filtered for noise, as seen in Fig. 10, although the records due to meteorological factors are not continuous. Between December 2005 and August 2006, the upper and lower lasers recorded displacement in the same order of magnitude (39 mm and 40 mm respectively). From September 2006 to August 2007, the upper laser recorded higher displacement than the lower (65 mm versus 53 mm, respectively), which indicates that the block slightly rotated. In 2007-2008, the recorded displacements were of the same order of magnitude (74 mm was recorded at both upper and lower laser). In addition to the rotation of the graben structure in the year 2006-2007, the recordings show increase of the annual displacements from 2006-2007 to 2007-2008 in the order of 9 mm for the upper laser and 20 mm for the lower laser.

5.3 Possible meteorological influence on extensometer and laser events

To analyse potential meteorological effects on displacements, selected events recorded by the extensometers have been analyzed. In these analyses, an event in the extensometer recordings is defined as a significant increase and/or reduction in movement, recorded at the same time for more than one of the extensometers. Based on this, a total of 12 events were identified, the four major in springtime, and the remaining minor events in autumn (three), in winter (three) and in summer (two) (Fig. 9). In the following, one representative event per season is discussed and analyzed in detail. The other events are summarized in Tables 1-4.

5.3.1 April 2007

Between April 11 and May 1 2007, Ext. 2 and 3b recorded two 0.7-1 mm reductions of the back scarp over 3-5 days and two periods of increased movements of 0.8-1.7 mm over 3-6 days (Fig. 11). Recordings from Ext. 1 show the same pattern (reduction-increase-reduction-increase). A distinct increase of 1 mm is however recorded April 12-13 (prior to the first reduction recorded at Ext. 1, 2 and 3b). The recorded displacements at Ext. 1 are also smaller (reductions of 0.1-0.5 mm and increases of 0.3-0.5 mm). Laser data from monitoring of graben structure are discontinuous in this period, however, the recordings indicate increasing

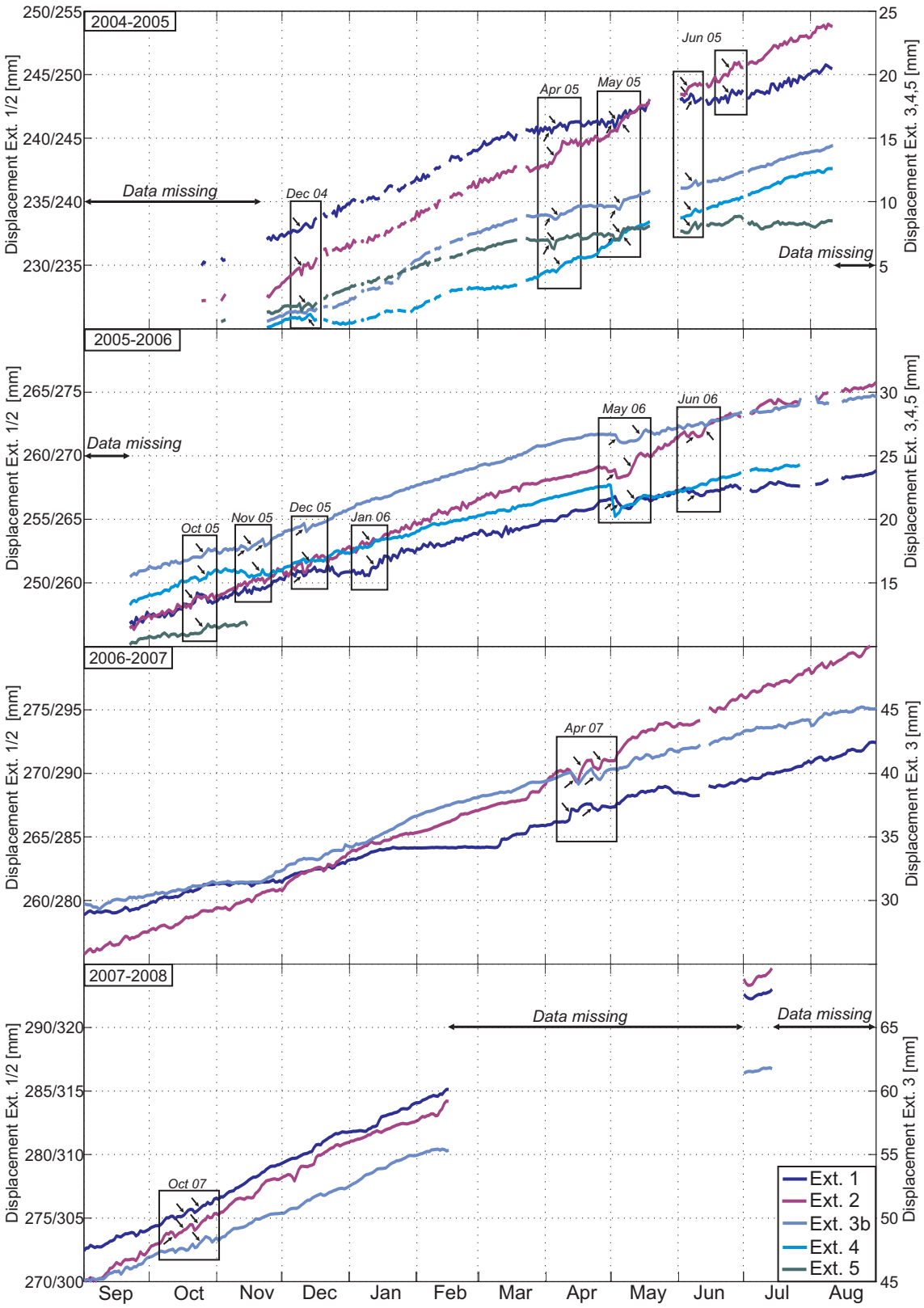

Fig. 9 Movements in the back scarp recorded by Ext. 1-5 December 2004-August 2008. The reading routine for extensometer 1-3b was daily at 12 pm until March 2006, when it shifted to reading every 5 minutes (average daily values are plotted from March 2006).

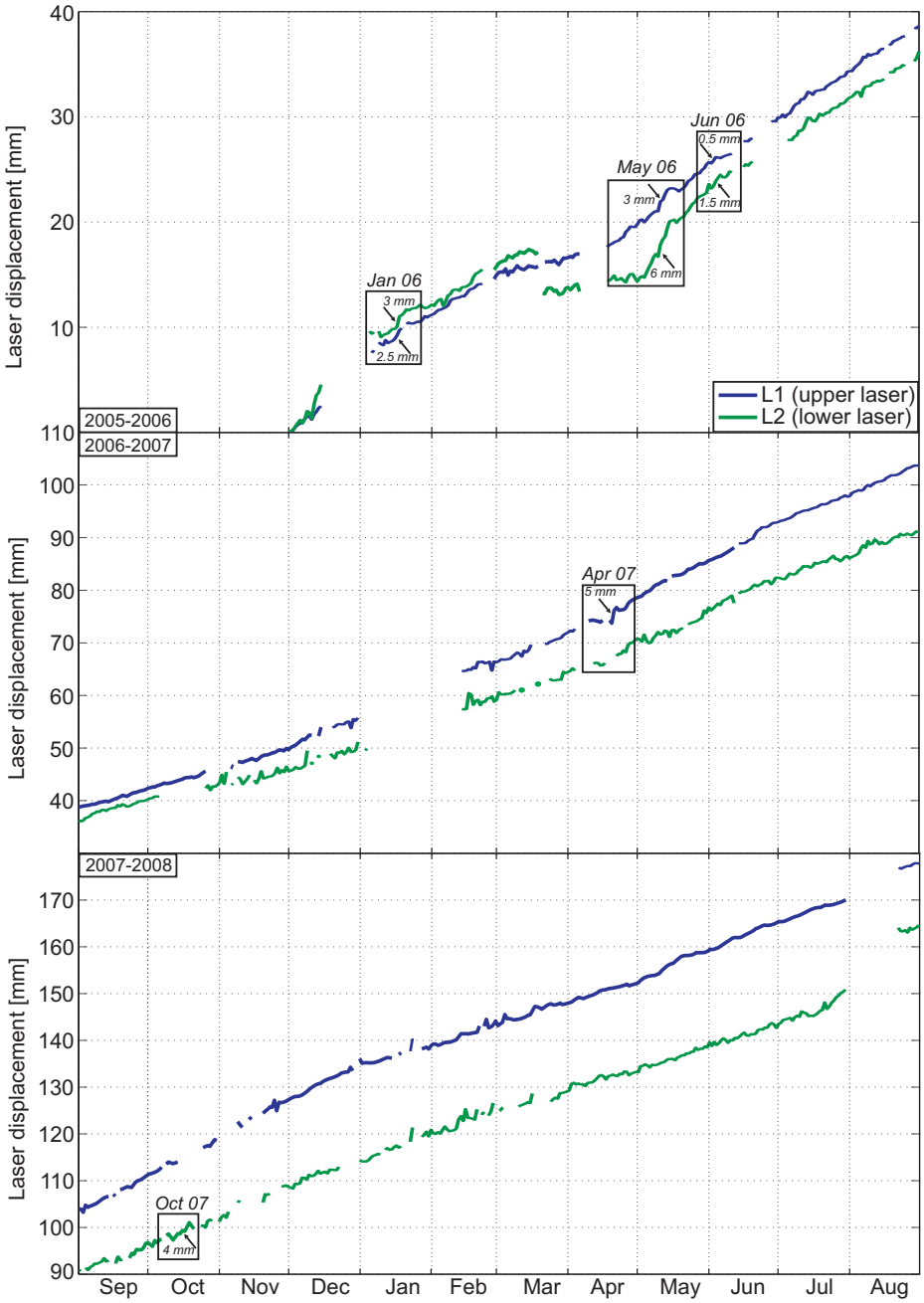

Fig. 10 Laser measurements of distance based on upper- (L1-R1) and lower laser (L2-R2) December 2005-August 2008.

displacements in the order of 4-5 mm for L1 (upper laser) and L2 (lower laser) from April 16 to May 1 (Fig 11).

The air temperature during this period fluctuated between -7.5°C and +11.5°C with two significant cold periods and two relatively warm periods (Fig. 11). The recorded precipitation was 115 mm, of which most fell as snow as the air temperatures was below 0°C during precipitation.

Groundwater levels fluctuated between -56 and -51.5 m in the upper borehole and between -45.7 and -44.5 m in the middle borehole. Increased displacements recorded by Ext. 2 and 3b and lasers seem closely controlled by a raising groundwater level in the upper borehole produced by melt water production as the air temperature increased and became positive in spring.

The air temperature variations seem to directly have affected the groundwater levels in both boreholes in spring. Quickly rising air temperatures from below 0°C to more than +10°C caused significant melting of snow, and thus production of melt water, which infiltrated the back scarp, as well as the rock mass in the area around the back scarp. This lead to large rise of the groundwater level in the upper borehole April 13-17 and April 24-27. When the air temperature again fell below 0°C, the groundwater level relatively quickly dropped back in the upper borehole.

The first increase in deformation recorded by Ext. 1 April 12-13 seems to be caused by a rising air temperature leading to production of melt water in the area where Ext. 1 is located (western part of the back scarp). Although this extensometer shows the same pattern after the first increase in deformation as recorded at Ext. 2 and 3b, the latter show the strongest correlation with measured groundwater level in the upper borehole. Increasing displacements recorded by the lasers also coincides with the air temperature rising above 0°C on April 21 to higher temperatures in the period April 22-26. Decreasing displacements recorded by the extensometers are preceded by periods of 5-7 days with temperatures below 0°C, which cause less melt water discharge and lowering of the groundwater. Importantly, high wind speeds reached several times during the studied period, including a storm on April 10, did not affect the deformation recordings.

For this event it can be concluded that fluctuating temperatures above and below freezing, causing significant snow melting, strongly affected the groundwater level which is believed to have caused increased displacements as recorded by the extensometers and lasers.

5.3.2 June 2006

In early June 2006, Ext. 1 and 2 recorded three periods of extension followed by reductions of the width of the back scarp (Fig. 12). Recordings from Ext. 3b and 4 show a similar reaction with a delay of 1-4 days. The first and second reductions at Ext. 1 and 2 June 4-6 and June 8-11 were in the order of 0.3-0.4 mm. Ext. 3b and 4 show a small increase of the distance across the back scarp in the same periods. Increased displacements of 0.4-0.5 mm were recorded June 1-4, 0.1-0.3 mm was recorded June 6-8 and 0.3-0.9 mm June 12-14 at Ext. 1 and 2. The laser distance recordings show increased displacements of 0.5 mm for L1 June 2-4 and of 1.5 mm for L2 June 2-6.

The air temperature fluctuated daily during this two-week period, with temperatures between -1.5°C and +20.5°C (Fig. 12). The rise in temperature from 0°C June 5 to +14-20°C June 10-12 is typical for the months of May/June, as shown in Fig. 4. Precipitation was relatively small during this period with a total of 20 mm, of which most fell during June 2-4. The precipitation is hence not believed to influence on the recorded event.

The first contraction June 4-6 was recorded shortly after the air temperature dropped to around 0°C June 2-4. The increased displacement June 6-8 was recorded shortly after the rise in temperature from about freezing point to +10.5°C June 5-6, while the second contraction June 8-11, was recorded during continued air temperature increase to +20°C on June 10. Increased displacement on June 12-14 was recorded shortly after a rapid rise in temperature from +8°C to +20°C during the 3 day period June 10-12. Two days with strong winds were recorded, including a storm on June 13, but again with no obvious influence from the strong winds on the deformation recordings (Fig. 12).

For this event, the relatively quick air temperature increase to around +20°C seems to have triggered acceleration of the measured distance across the back scarp. This is believed to be due to melting water from snow melting at higher altitudes, as the sliding area is exposed to snow avalanches until late June, as described earlier.

5.3.3 October 2007

Between 11 and 28 October 2007, two small reductions of the width of the back scarp followed by two larger extensions were recorded at Ext. 1-3b (Fig. 13), the net result being a significant extension of up to 1.2 mm. All three extensometers recorded almost the same during this period, except for a small reduction in distance recorded by Ext. 3b on October 16-18. The reductions were generally 0.2-0.5 mm in one day, and the increases in displacement 0.6-1.1 mm during a period of 2-7 days. Recordings from the lasers L1 and L2 showed increased displacement for both lasers. Due to missing data recordings in the period October 14-25 the degree of acceleration cannot be determined for L1. For L2, an increase in the displacement of 3.5 mm from 11 to 18 October was however recorded.

The precipitation in September 2007 was high (269 mm) compared to September 2006 (116 mm), but for October it was low compared to the other monitored years (Fig 5). The air temperature fluctuated between -3°C and +11°C in the period, with temperatures generally above freezing except in the period October 17-19. The high precipitation the month before is believed to have affected the displacement recordings as this precipitation fell as rain and caused high groundwater levels in September (Fig. 7). Although data from the groundwater levels are missing for October 17-26, the records show that groundwater levels were high until mid October (between -52 and -53 m for the upper borehole and between -43.5 and -43 m for the middle borehole). The period had significant air temperature fluctuations, from around +8-10°C and down to -3°C.

The recorded reductions in distance across the back scarp were preceded by 6-12°C drops in air temperature in 1-3 days (October 11-12 and October 15-18). The first increase in displacement coincided with a significant air temperature rise of up to +10°C October 12-13, and the second increase coincided with the rise in air temperature October 19-21, in combination with the melting of the 63 mm snow that fell the days before. There were significant variations in wind speed during this period (Fig. 13), but as for the other events there is no indication that wind controls the deformation recordings.

For this event, it can be concluded that high groundwater levels due to precipitation and/or snowmelt when the ground was still unfrozen (according to Fig. 4), resulted in net expansion of the back scarp, as well as increased displacement of the graben structure. Reductions in the distance across the back scarp were preceded by 2-3 days with temperatures around or below the freezing point, which lead to lowering of the groundwater level.

5.3.4 January 2006

During the first half of January 2006 a significant net expansion of the back scarp occurred, caused by one large acceleration phase in the order of 0.4-1.5 mm recorded by Ext. 1, 2, and 4 during January 10-17 (Fig. 14). At the same time both lasers recorded increased displacements for the graben structure, L1 in the order of 5 mm January 13-22, and L2 in the order of 6.5 mm January 10-21. An increase in displacement of 0.8 mm at Ext. 2 was also recorded on January 4-7, as well as a minor reduction of 0.2-0.4 mm in distance across the back scarp at Ext. 1 and 2 on January 7-8.

The air temperature fluctuated between -6°C and +4°C on January 1-18, followed by freezing. In total only 19 mm of precipitation fell during this period, and precipitation therefore is believed to have been of minor importance for the recorded event. The stable ground temperature close to 0°C during this period (Fig. 4) indicates that a thick snow cover existed. The increase in displacement recorded January 4-7 might have been caused by the recorded 7°C air temperature increase in 2 days up to 0°C on January 1-3. The second increase recorded January 10-17 coincided with an air temperature increase of 8°C in 1-2 days, from minus to plus temperatures. Minor reductions in the distance across the back scarp coincided with the significant temperature drop to below freezing point on January 7-8. Several storms were recorded during this period (January 10-11, 12 and 13-14), which might have contributed to the recorded expansions.

In this event, increased expansion of the back scarp was recorded when hardly any precipitation occurred, but the ground was already snow covered. Air temperature increased from freezing to around +2-4°C giving periods of 1-4 days with positive air temperatures, which must have caused production of melt water. This seems to be the most likely explanation for the increased displacements recorded by Ext. 1, 2 and 4 as well as at laser L1 and L2. Some potential influence might be represented by the period of 3 storms in 4 days.

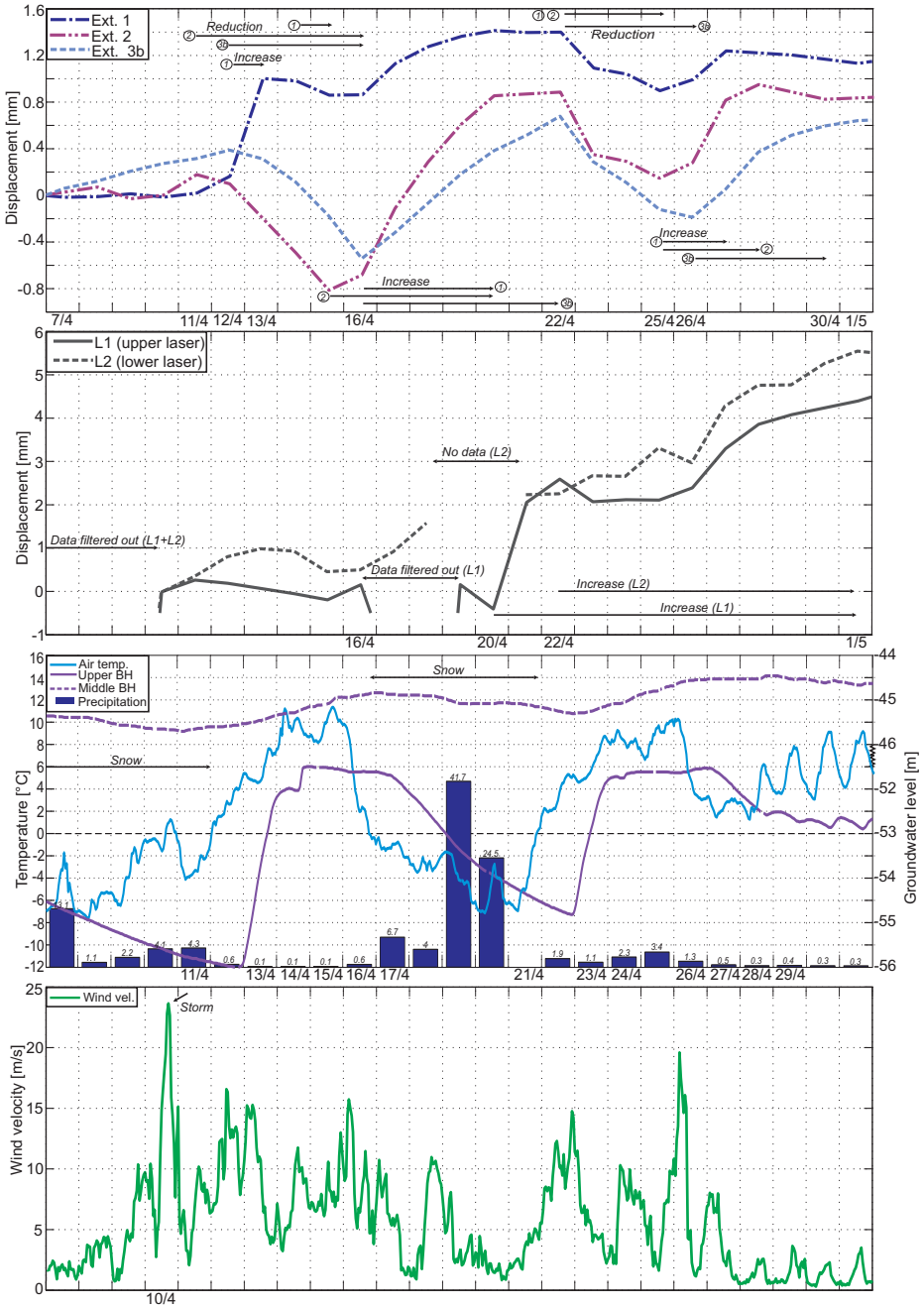

Fig. 11 Event recorded in April 2007 correlated with recorded temperatures, precipitation, groundwater levels and wind speed.

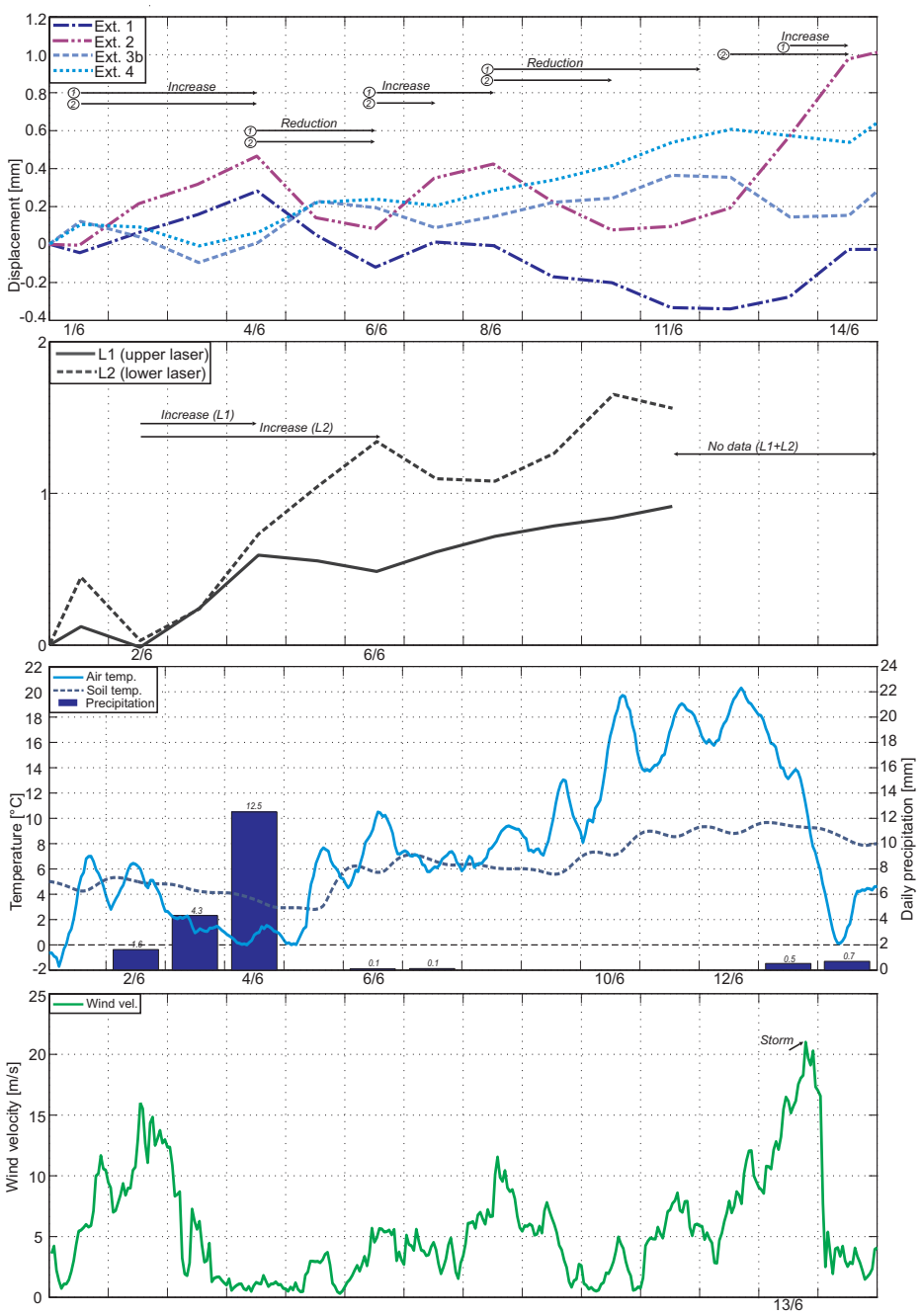

Fig. 12 Event recorded in June 2006 correlated with recorded temperatures, precipitation and wind speed.

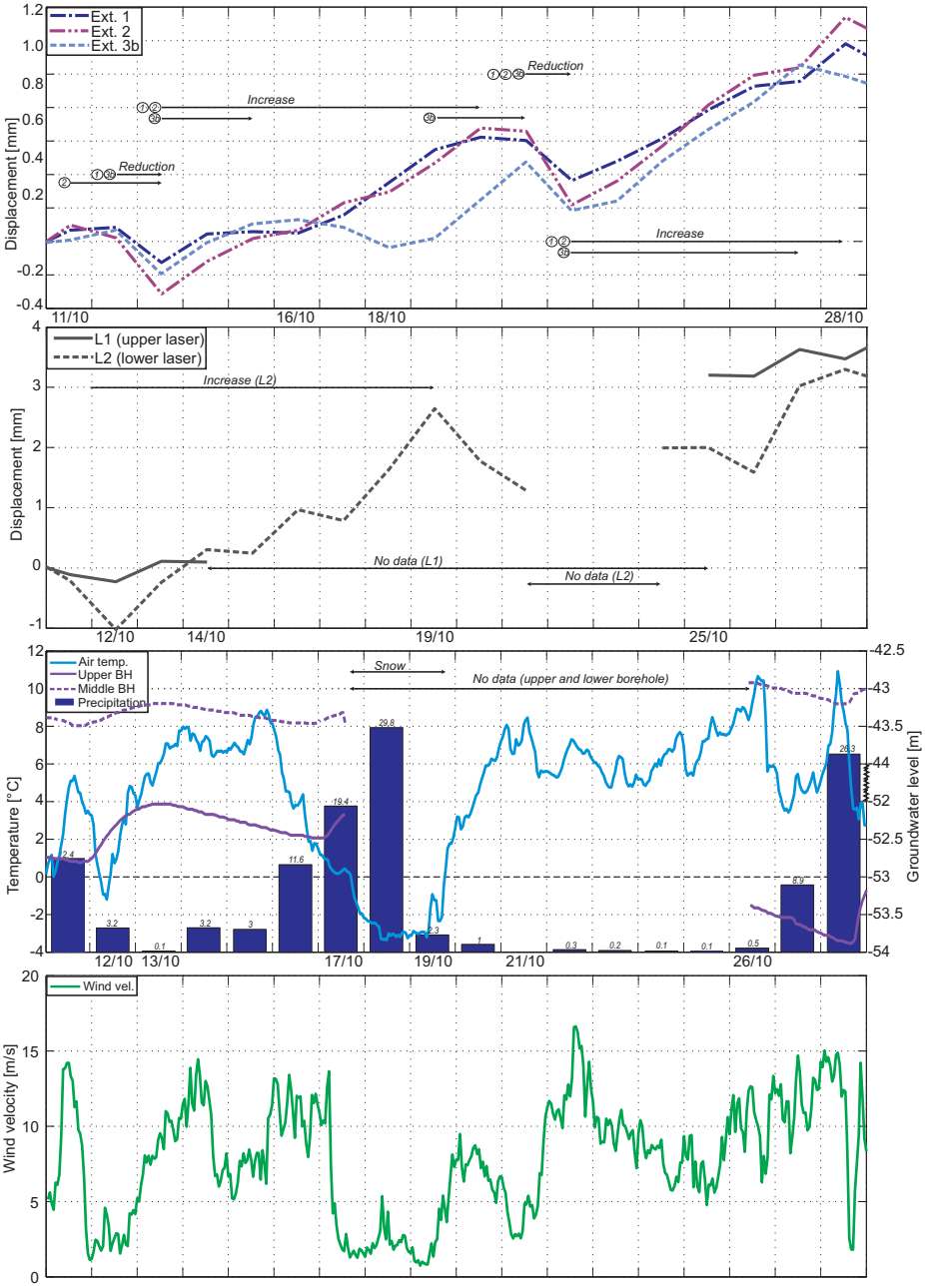

Fig. 13 Event recorded in October 2007 correlated with recorded temperatures, precipitation, groundwater levels and wind speed.

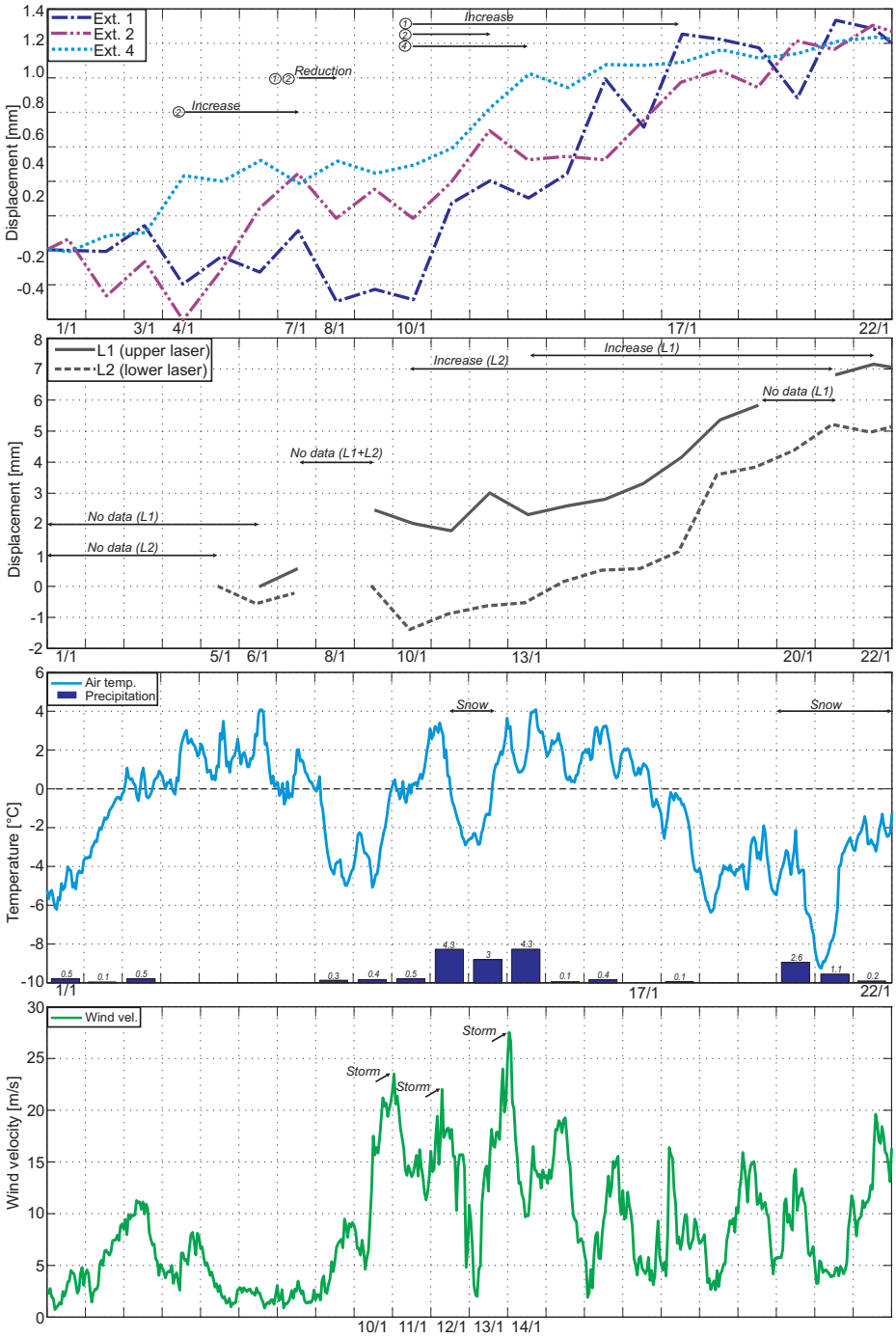

Fig. 14 Event recorded in January 2006 correlated with recorded temperatures, precipitation and wind speed.

6 Discussion

Tables 1-4 summarize the analyzed events and related meteorology. As shown, spring, early summer, autumn and early winter are periods when the back scarp is active. Mid to end of summer (July and August) as well as mid to end of winter (mid January throughout March) generally do not include large displacement events. All events recorded by the extensometers show reduction as well as increase in the distance across the back scarp, but the order is not consistent. In some events, the distance is reduced before increased displacement is recorded (April 05, May 05, December 04 and 05) while in other events, extensions are followed by reduction in the distance across the back scarp (May 06, June 05, October 05 and January 06). Some events have multiple phases where the distance is reduced and increased (April 07, June 06, November 05, and October 07). Most of the events are recorded in 2004-2005 and 2005-2006, indicating less activity in the back scarp in the second half of the analyzed period. This might be due to less precipitation and a generally lower groundwater level in the second half of the period; however, precipitation data presented in Fig. 5 indicate that 2007/2008 recorded the highest annual precipitation.

The annual net expansion of the back scarp is increasing in the analyzed period; i.e. for Ext. 1, 2 and 3b the annual expansion in 2005/2006 is 12.4, 19.6 and 14.1 mm, respectively, while the expansion in 2007/2008 is 20.9, 24.5 and 16.7 mm, respectively. The meteorological effects hence are believed to be of less significance on the displacements in the back scarp in the last half of the period.

Analyses of the laser data show that for the periods where laser recordings are available, all events recorded by extensometers are identified also by the laser recordings (Fig. 10). This indicates that the same meteorological and geological factors which affect the moving graben structure also affect the displacement of the back scarp. The largest recorded event by the extensometers in May 2006 was also the largest event recorded by the lasers, 3 mm and 6 mm increase in displacement May 4-14.

For the four years analyzed, snow melting periods cause the largest annual deformation event. The combination of melt water and large temperature fluctuations around 0°C thus is believed to be primarily responsible for these events. Typically, the air temperature fluctuates considerably during spring (Fig. 4) and periods with relatively high air temperatures causing increased production of melt water are recorded previous to all increased displacements occurring in spring. For the April 2007 event, recorded reductions in the distance across the back scarp coincide with periods of air temperatures below freezing and decreasing groundwater level. This is, however, not the case for every event, three recorded reductions in springtime, of a total of five analyzed reductions, are related to large decreases in air temperature to below or around 0°C.

Events in early summer are recorded in June 2005 and 2006 by extensometers (Table 2), the latter also by lasers. In 2005 and 2006, snow melting at the meteorological station ended in late April and early May (Fig. 4). As the catchment area is located at higher altitudes above the back scarp, melt water is believed to have been fed into the back scarp after the end of snow melting at the meteorological station until all snow was melted in the upper catchment in mid-/late June. Like the events recorded in early spring, periods with high air temperatures precede the recorded increases in displacements, but no consistent explanation is found for the recorded reductions of distance across the back scarp, although two of the three reductions can be related to decreases in the air temperature to below 0°C.

In autumn, periods with heavy precipitation in combination with air temperature fluctuations around 0°C seem to have caused displacement events recorded by the extensometers. In October 2005, a total precipitation of 441 mm was recorded, causing 1-2 mm expansion.

For November 2005, the first increase in displacement most likely was caused by a period of low temperatures, as opposed to the general trend with a period of high temperatures preceding increasing displacement. In October 2007, increased displacements recorded by the extensometers as well as by one of the lasers (L2) were preceded by periods of high temperatures. Recorded reductions in the distance across the back scarp are found to coincide with decreases in air temperatures to below freezing, occasionally followed by a period of 1-5 days with low temperatures.

In early winter, air temperature rise to above 0°C have caused events (December 2004 and 2005, January 2006) registered by extensometer as well as lasers. This is believed to be a result of some production of melt water, when air temperatures occasionally have increased to above 0°C, and the ground has still been frozen. Periods of 1-4 days with positive air temperatures (generally fluctuating between 1°C-7°C) have preceded the recorded increased displacements, and caused some melt water production. Recorded reductions in the distance are found to coincide with decreases in temperatures to below freezing followed by a period of 1-5 days with negative air temperatures.

Air temperature and precipitation thus have been found to be important meteorological parameters governing phases of increasing and decreasing distance across the back scarp as well as increasing displacement of the graben. This is believed to be due to water infiltrating the back scarp area (precipitation and/or melting water), and by this directly increasing the driving force in the back scarp as well as reducing the normal stress on the sliding plane(s). Both these effects will increase displacements. The great impact of groundwater pressure on stability conditions and displacement for the Åknes slope has been confirmed by recent analyses, i.e. Kveldsvik et al. (in press). For the upper borehole, a high groundwater level (between 51 and 52 m below the surface) and/or fluctuating groundwater levels (3-4.5 m change in water level within 1-5 days) seem to be the threshold for deformation events recorded in April 07 and October 07 at extensometer 1, 2 and 3b. For the middle borehole, the relation is less clear. A groundwater level of between 42 and 44 m below the surface and/or a fluctuation of around 1 m in 5 days could be suggested as a threshold for this borehole. Wind speed and recorded storms have been found not to affect the displacements to any large extent. Only in one event there is a slight potential influence.

The reduction of the distance across the back scarp is related to negative air temperatures believed to be caused by a combination of thermal effects and lowering of the groundwater level, especially in the upper borehole. The significance of the former should not be underestimated, for a thermal expansion of 6-9 μm/m$\times$°C for instance (normal range for Precambrian gneiss according to Nilsen and Palmstrøm (2000)) a reduction of temperature of 10°C over a span of a 100 m, in theory will cause a contraction of 6-9 mm.

Table 1 Summary of events and relevant meteorology in spring of the back scarp and graben structure in the Åknes rock slide.

Date	Deformation	Meteorological cause
April 05	0.3-0.7 mm reduction (Ext.1,3b,5)	All events are recorded during snow melting and are believed to be closely related to temperature fluctuating above and below freezing point producing varying amounts of melt water and causing varying groundwater levels (especially in upper borehole). Increasing displacements are preceded by sudden rises in air temperature (generally 5-10°C rise in 1-3 days) and periods of 2-8 days with high temperatures (typically +5-15°C). Recorded reductions in the distance across the back scarp may be a result of decreases in temperature (generally 8-18°C decrease in 2-3 days) followed by 1-4 days with low temperatures (-2 to -7°C). The first decrease recorded at Ext. 1,3b and 5 in April 2005 and the first decrease recorded by Ext. 1, 2 and 3b April 2007 were not preceded by a large drop in the temperature.
(2-11/4)	0.4-1.8 mm increase (Ext.1,2,3b,4,5)	
	0.3-0.5 mm reduction (Ext.1,2)	
May 05	0.3-0.6 mm reduction (Ext.1,3b,5)	
(2-9/5)	0.7-1.2 mm increase (Ext.1,2,3b,4,5)	
May 06	0.9 mm increase (Ext.1)	
(23/4-17/5)	0.6-2.5 mm reduction (Ext.1,2,3b,4)	
	0.9-1.9 mm increase (Ext.1,2,3b,4)	
	3.5-6 mm increase (L1,L2)	
April 07	1.0 mm increase (Ext.1)	
(11-30/4)	0.2-1.0 mm reduction (Ext1,2,3b)	
	0.7-1.6 mm increase (Ext.1,2,3b)	
	0.5-0.8 mm reduction (Ext.1,2,3b)	
	0.3-0.8 mm increase (Ext.1,2,3b)	
	4-5 mm increase (L1,L2)	

Table 2 Summary of events and relevant meteorology in early summer of the back scarp and graben structure in the Åknes rock slide.

Date	Deformation	Meteorological cause
June 05	0.5-1.0 mm increase (Ext.1,2,3b,4,5)	The two events are both recorded in early summer, shortly after the melting period ended at the meteorological station, when temperatures were rising from around freezing point to higher temperatures (+6-8°C in 2005 and +14-20°C in 2006). This warming in combination with melting water from snow at higher altitudes in the area is interpreted to have caused the increasing displacements recorded by the extensometers. Recorded reductions in the distance across the back scarp can be related to drops in the air temperature (4-10°C in 1-2 days) to below 0°C, except the second reduction recorded by Ext. 1 and 2 June 06.
(2-11/4)	0.4-1.8 mm increase (Ext.1,2,3b,4,5)	
(4-11/6)	0.2-0.7 mm reduction (Ext.1,2,3b,4,5)	
June 06	0.3-0.4 mm reduction (Ext.1,2)	
(4-14/6)	0.1-0.3 mm increase (Ext.1,2)	
	0.3-0.4 mm reduction (Ext.1,2)	
	0.3-0.9 mm increase (Ext.1,2)	
	0.5-1.5 mm increase (L1,L2)	

Table 3 Summary of events and relevant meteorology in autumn of the back scarp and graben structure in the Åknes rock slide.

Date	Deformation	Meteorological cause
October 05 (20-28/10)	0.7-1.0 mm increase (Ext.1,2) 0.4-0.8 mm reduction (Ext.1,4) 0.6-0.8 mm increase (Ext.3b,4,5)	The combination of varying air temperature above and below the freezing point and precipitation falling as rain is believed to have caused variation in groundwater levels in autumn. Precipitation falling as snow in periods with temperatures below freezing has contributed to the inflow of water into the back scarp (and surrounding rock mass) only when the air temperature rises again. The recorded increase in displacements was preceded by a period of 2-5 days with high air temperatures (+4-8°C) in combination with precipitation as rain (13-27 mm/day) and/or melting of snow. Recorded reductions in the distance across the back scarp coincide with drops in the temperature (6-15°C) to below freezing point in 2-4 days, occasionally followed by a period of 1-4 days with low temperatures (0 to -5°C).
November 05 (16-29/11)	0.3-0.5 mm reduction (Ext.2,3b,4) 0.4-0.9 mm increase (Ext.2,3b,4) 0.3-0.5 mm reduction (Ext.2,3b,4) 0.3-1.1 mm increase (Ext.2,3b,4)	
October 07 (12-28/10)	0.2-0.4 mm reduction (Ext.1,2,3b) 0.3-1.0 mm increase (Ext.1,2,3b) 0.2-0.5 mm reduction (Ext.1,2,3b) 0.8-1.1 mm increase (Ext.1,2,3b) 4 mm increase (L2)	

Table 4 Summary of events and relevant meteorology in early winter of the back scarp and graben structure in the Åknes rock slide.

Date	Deformation	Meteorological cause
December 04 (9-14/12)	0.2-0.5 mm reduction (Ext.2,4,5) 0.3-0.8 mm increase (Ext.1,2,3b,4,5)	All events are in early winter, before the soil temperature has stabilized at temperatures below freezing when a thicker snow cover has accumulated. Increase in displacements are preceded by increasing air temperatures (7-9°C) from below freezing to temperatures above freezing in 2-3 days, combined with 1-4 days with high temperatures (+1-7°C). Reductions in the distance across the back scarp are preceded by decreases in temperature (3-7°C) in 1-2 days followed by 1-5 days with temperatures below freezing point (typically between 0°C and -6°C).
December 05 (8-17/12)	0.3-0.8 mm reduction (Ext.1,2,3b,4) 0.4-1.3 mm increase (Ext.1,2,3b,4)	
January 06 (4-17/1)	0.2-0.8 mm increase (Ext.2,3b,4) 0.3-0.4 mm reduction (Ext.1,2) 0.4-1.5 mm increase (Ext.1,2,4) 2.5-3 mm increase (L1,L2)	

7 Conclusions

Based on the analyses in this paper, the following main correlations between recorded displacements and meteorological factors have been found for the Åknes slide area:

- In spring (mid March throughout May) and early summer (June), water from snowmelt has large impact on the displacements, causing the largest expansion of the back scarp.
- In summer and early autumn (mid June throughout September), no significant deformation events are recorded in the back scarp.
- In autumn and early winter (October to mid January), decreases in air temperature to below 0°C cause reduction in the distance across the back scarp, but due to the marine climate, this is often interrupted by air temperature increases to above 0°C causing expansion.
- In late winter (mid January to mid March) no significant deformation is recorded, due to stable frozen conditions and the presence of a permanent snow cover.
- 10 out of a total of 12 analyzed events are recorded in the first half of the period (September 2004-August 2006), indicating less significant meteorological effects on the displacements in the back scarp in the last half of the period (September 2006-August 2008).

Acknowledgements The authors would like to thank the Geological Survey of Norway (NGU) and the Åknes/Tafjord project for providing access to data used in this research. The corresponding author has been funded by the International Centre for Geohazards (ICG), located at Norwegian Geotechnical Institute (NGI).

References

Bjerrum, I. and F. A. Jørstad (1968). Stability of natural rock slopes in Norway. Technical Report 79, Norwegian Geotechnical Institute (NGI).

Blikra, L. H., O. Longva, C. Harbitz, and F. Løvholt (2005). Quantification of rock-avalanche and tsunami hazard in Storfjorden, western Norway. In K. Senneset, K. Flaate, and J. Larsen (Eds.), *Landslides and Avalanches: ICFL 2005 Norway*, pp. 57–63. Taylor and Francis Group.

Bogaard, T. A., P. Antoine, P. Desvarreux, A. Giraud, and T. W. J. van Asch (2000). The slope movements within the Mondorès graben (Drôme, France); the interaction between geology, hydrology and typology. *Engineering Geology 55*, 297–312.

Crosta, G. B. and F. Agliardi (2003). Failure forecast for large rock slides by surface displacement measurements. *Canadian Geotechnical Journal 40*, 176–191.

DIMETIX (2009). *DIMETIX Distance laser sensor*. www.dimetix.com. Technical reference manual V1.02.

DMS (2009). *DMS Differential Monitoring of stability*. www.csgsrl.eu. Technical specification for DMS-IU.

Eidsvig, U. and C. Harbitz (2005). Innledende numeriske analyser av flodbølger som følge av mulige skred fra Åkneset. Technical Report 20031100-2, Norwegian Geotechnical Institute (NGI). In Norwegian.

Gunzburger, Y., V. Merrien-Soukatchoff, and Y. Guglielmi (2005). Influence of daily surface temperature fluctuations on rock slope stability: case study of the Rochers de Valabres slope (France). *International Journal of Rock Mechanics and Mining Sciences 42*(3), 331–349.

Kottak, M., J. Grieser, C. Beck, B. Rudolf, and F. Ruber (2006). World map of the kppen-geiger climate classification updated. *Meteorologische Zeitschrift 15*(3), 259–263.

Kveldsvik, V., T. Eiken, G. V. Ganerød, G. Grøneng, and N. Ragvin (2006). Evaluation of movement data and ground conditions for the Åknes rock slide. In *Stability of rock slopes in open pit mining and civil engineering situations, Cape Town*, pp. 279–300. The South African Institute of Mining and Metallurgy.

Larsen, J. O. (1999). Tension cracks and landslides in steep hard rock mountains in the norwegian fjord districts. In *Proceedings of the Second International Conference on Landslides, Slope Stability & Safety of Infra-structures*, pp. 193–200.

Larsen, J. O. (2003). *Some aspects of physical weather related slope processes*. Ph. D. thesis, Norwegian University of Science and Technology (NTNU), Department of Geology and Mineral Resources Engineering.

Nilsen, B. and A. Palmstrøm (2000). *Engineering Geology and Rock Engineering*. Norwegian Group for Rock Mechanics (NBG). Handbook No. 2.

Nordvik, T., G. Grøneng, G. V. Ganerød, B. Nilsen, C. Harding, and L. H. Blikra (2009). Geovisualization, geometric modelling and volume estimation of the Åknes rockslide, western Norway. *Accepted for publication in: Bulletin of Engineering Geology and the Environment, doi:10.1007/s10064-009-0198-x*.

Sandersen, F., S. Bakkehøi, E. Hestnes, and K. Lied (1996). The influence of meteorological factors on the initiation of debris flows, rockfalls, rockslides and rockmass stability. In K. Senneset (Ed.), *Landslides*, pp. 97–114. Balkema.

Willenberg, H., K. F. Evans, E. Eberhardt, T. Spillmann, and S. Loew (2008). Internal structure and deformation of an unstable crystalline rock mass above Randa (Switzerland): Part ii - three-dimensional deformation patterns. *Engineering Geology 101*, 15–32.

Paper IV

Time-dependent behavior of the Åknes rockslide area in western Norway

Authors: Guro Grøneng, Ming Lu, Bjørn Nilsen and Arne K. Jenssen

The paper was submitted to Engineering Geology (September 2009).

Time-Dependent behavior of the Åknes Rockslide Area in Western Norway

Guro Grøneng*,[a], Ming Lu[b], Bjørn Nilsen[a], Arne K. Jenssen[c]

[a] *Norwegian University of Science and Technology (NTNU), Dept. of Geology and Mineral Resources Engineering / International Centre for Geohazards (ICG), Trondheim, Norway.*

[b] *Norwegian University of Science and Technology (NTNU), Dept. of Geology and Mineral Resources Engineering / Sintef Rock and Soil Mechanics, Trondheim, Norway.*

[c] *Norwegian University of Science and Technology (NTNU), Dept. of Electronics and Telecommunications, Trondheim, Norway.*

Abstract

Numerical modelling based on the finite difference programcode $FLAC^{3D}$ and the Burger-Creep Viscoplastic material model has been used for analysing time dependent behavior of the unstable rock slope at Åknes in western Norway. The rockslide has an estimated volume of 43 million m^3, with a basal sliding surface located 105-115 m below the surface. Displacement measurements by GPS- and reflector points, which since 2004 have revealed average annual displacements in the order of 26 mm/year in the central part of the sliding area, have been used to calibrate the model. The results show that a set of parameters which are believed to represent the conditions of the slope at present time result in displacements which stabilise within a 100 year period. However, since the shear strength is reduced for the sliding surface and the unstable mass located above it over time, increased displacement and indications of failure at the toe of the slope are evident within the same time span.

Key words: Rockslide, Numerical modelling, $FLAC^{3D}$, Time dependent behavior, Burger-Creep Viscoplastic material model

1. Introduction

Rockslides are a recurrent hazard for the steep rock slopes in the western part of Norway, as evidenced in this century by the catastrophic rockslides at Loen in 1905 and 1936 and at Tafjord in 1934 (Figure 1), where more than 170 persons perished [1]. In 1964, local people noticed that a back scarp was widening in the S-SE dipping slope located at Åknes [18], 600-900 m above the fjord Storfjorden. Swath bathymetry from the up to 320 m deep fjord has revealed at least 59 rock slope failures of more than 0.5 million m^3 to have occurred since the last glaciation approximately 10,000 years ago, resulting in classification as "high susceptibility zone" for this area based on a spatial distribution and temporal pattern of events (Longva et al. [14], Blikra et al. [3]).

In 2004, an extensive program of monitoring, investigations and research was initiated due to the potential of tsunami hazard as result of a large scale rockslope failure. Tsunami modelling has shown that several villages along the fjord Storfjorden will be affected by a large scale failure [6] as well as thousands of tourists who visit the fjords in the summer months. Stability analyses of the factors controlling the slope stability at Åknes therefore is of great importance. Previous numerical modelling of the Åknes slope includes back-calculation of a historical instability at the western boundary of the slope, termed the "1960-slide" (estimated volume of 100,000 m^3) based on UDEC [13], slope stability analyses based on UDEC and DDA [11] as well as a dynamic analysis of the stability based on UDEC [12]. This paper presents the results of a time-dependent stability analysis of the slope by the use of a creep material model available in $FLAC^{3D}$, the Burger-Creep Viscoplastic material model. Some general conclusions are also drawn on the applicability of such analysis for cases of complex, large-scale rockslides.

2. Åknes sliding area

The Åknes rockslide is located in the Western Gneiss Region of Norway. The bedrock of the area is dominated by gneisses of Proterozoic age, which have been altered and reworked during the Caledonian orogeny [19]. The gneisses have a magmatic origin and are described in the geological map sheet as undifferentiated gneisses that are locally migmatitic in composition, varying from quartz-dioritic to granitic [19]. On the basis of logs from seven boreholes at three drilling sites in the slope (Figure 2), three types of gneiss, quartz-dioritic, granitic and gneisses rich in biotite have been identified [7]. Recent studies estimate the area and volume of the potential unstable mass to be in the order of 575,000 m^2 and 43×10^6 m^3, respectively [15]. The western boundary of the unstable area is defined by a

*Corresponding author

Email addresses: guro.groneng@ntnu.no (Guro Grøneng), ming.lu@sintef.no (Ming Lu), bjorn.nilsen@ntnu.no (Bjørn Nilsen), arne.jenssen@statoil.no (Arne K. Jenssen)

Submitted to: Engineering Geology (September 2009)

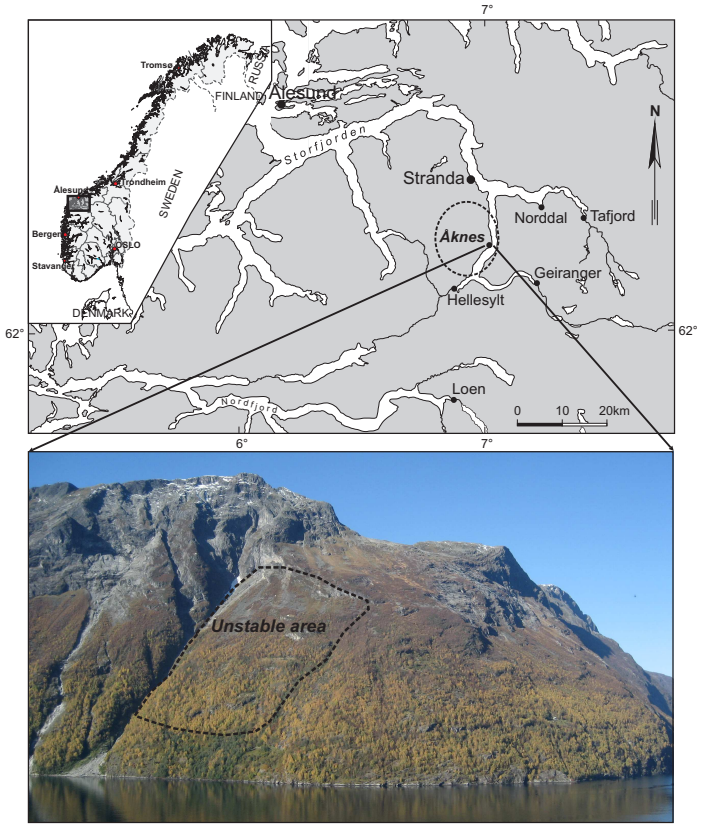

Figure 1: Location of the unstable slope at Åknes.

steeply dipping, NNW-SSE striking strike slip fault while indications of a gently NW dipping, NNE-SSW trending fault might define the eastern boundary [7]. The upper boundary of the unstable area is represented by a distinct, almost continuous tension crack with approximate length of 800 m (Figure 2). Geological conditions believed to control the slope instability and potential failure at Åknes sliding area are believed to be the steep slope angle averaging approximately 30-35° and foliation oriented parallel to the slope (Ganerød et al. [7], Braathen et al. [4]).

Extensive field work in the area in the summers of 2004-2007 including detailed geological mapping, geophysical investigations and drilling of seven boreholes at three locations has generated a vast amount of geological data. Nordvik et al. [15] presented an interactive geovisualization model for analysis of the geometry and volume based on geological mapping, geophysical investigations by 2D resistivity (five slope parallel profiles with E-W strike, and two down-slope profiles with N-S strike, totalling about 10,000 m) and georadar (four slope parallel profiles with E-W strike, one profile with NE-SW strike, and two down-slope profiles with N-S strike, totalling about 5,300 m), data from corelogging and geophysical borehole investigations. The interactive model enabled a refined analysis of the collected data and defined three different scenarios for location of the basal sliding surface at Åknes. A scenario including an undulating basal sliding surface located 105-115 m below the surface was concluded to represent the most likely geometry. The true geometry of the sliding plane is however believed to be an even more complex one, with several sliding planes at different levels, consisting of a combination of unfilled joints, filled joints and bridges of intact rock at different levels [10]. The lower boundary of the unstable slope is not identified. However, a line of springs located at approximately 75-100 m a.s.l. as well as morphological compression features mapped in field around the same elevation [2] may indicate a toe in this area.

3. Numerical model

Generation of a 3D-model in *FLAC* requires reconstruction of the surface topography and the internal structure. As the complex sliding geometry is not yet defined in detail or fully understood, coordinates from the basal sliding surface presented in Nordvik et al. [15] were used as the best estimate to model the sliding layer in the model. A 25 cm thick continuous layer representing the sliding surface has been modeled in order to analyse the time dependency of the sliding plane in this case. Topography has been based on coordinates from airborne laser mapping of the slope.

The numerical 3D model thus consists of three geological units; the base layer termed "solid rock", the sliding surface termed "sliding zone" and the top layer consisting of unstable rockmass termed "fractured rock". The horizontal element size is 25 m by 25 m, resulting in 13,440 elements as shown in Figure 3. The model is fixed at the base while the potential unstable mass above the sliding zone as well as the sliding zone itself are free to move down-slope, except for the toe. As the toe does not daylight in field, the lower boundary of the model is fixed in the horizontal direction.

4. Displacements

Displacements in the slope have been monitored by manually read GPS and reflector points since 2004 (Figure 2). Previous analyses of these datasets have been discussed in Nordvik and Nyrnes [16] and Ganerød et al. [7]. In general, the data show that the slope can be divided into three main areas according to the different velocities and directions measured by the GPS- and reflector points; an *Upper area* which is moving in SW-direction, toward the large ravine forming the boundary to the west, a *Central area* which moves in a SE-S direction, and a *Lower area* which is an indetermined at present due to inconsistent/insignificant measurements. Vegetation and unfavorable satellite conditions in this area have been mentioned as possible explanations [7]. Annual total displacement rate for the points situated within the *Central area* (GPS4, GPS8, R4, R5, R6, R10 and R16) are in the order of 15-42 mm (Figure 4), with an average of 26 mm/year, and

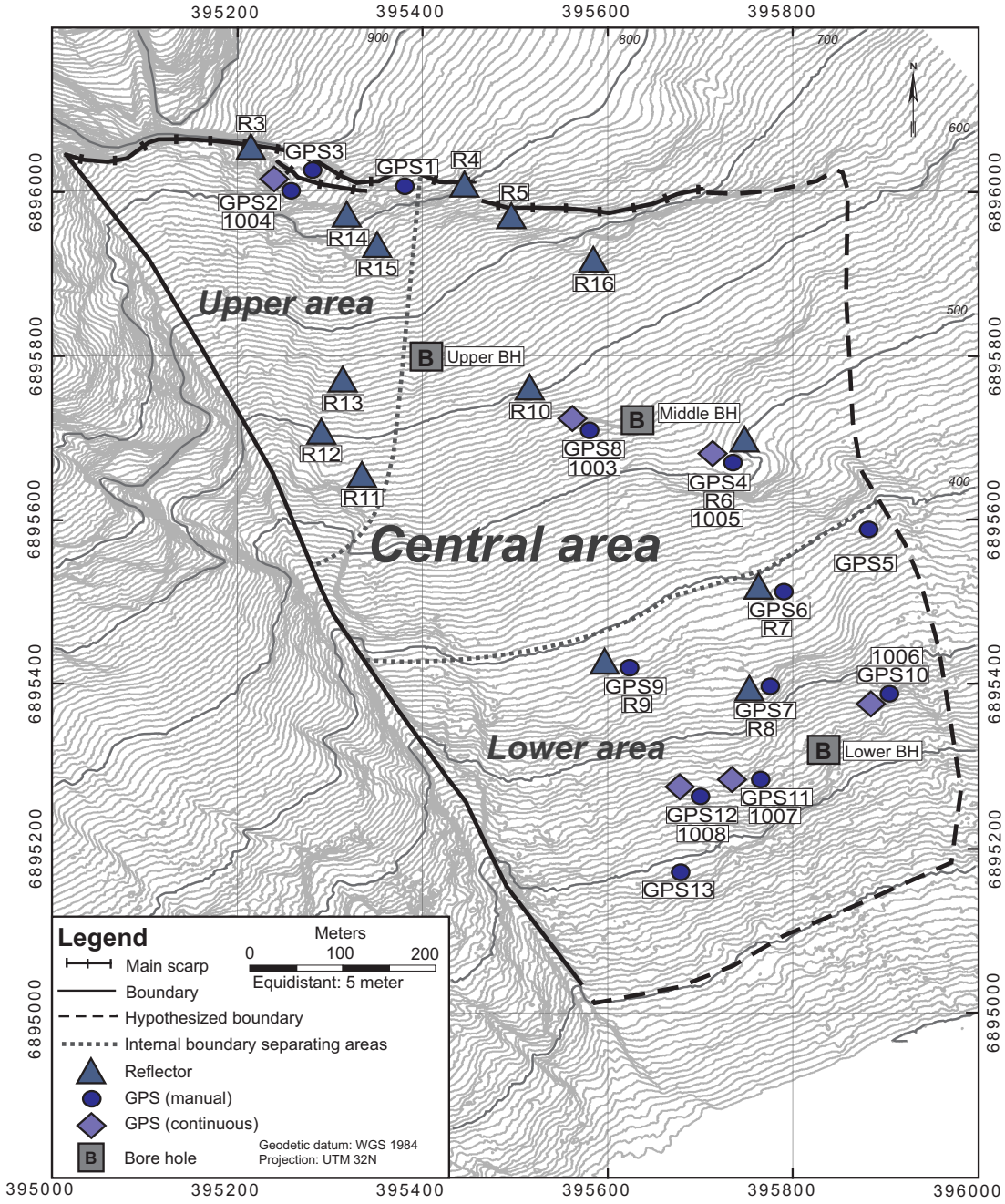

Figure 2: Map of GPS- and reflector points used to analyze the slope deformation. Internal boundaries between areas of different velocities/directions are shown (not defined in field).

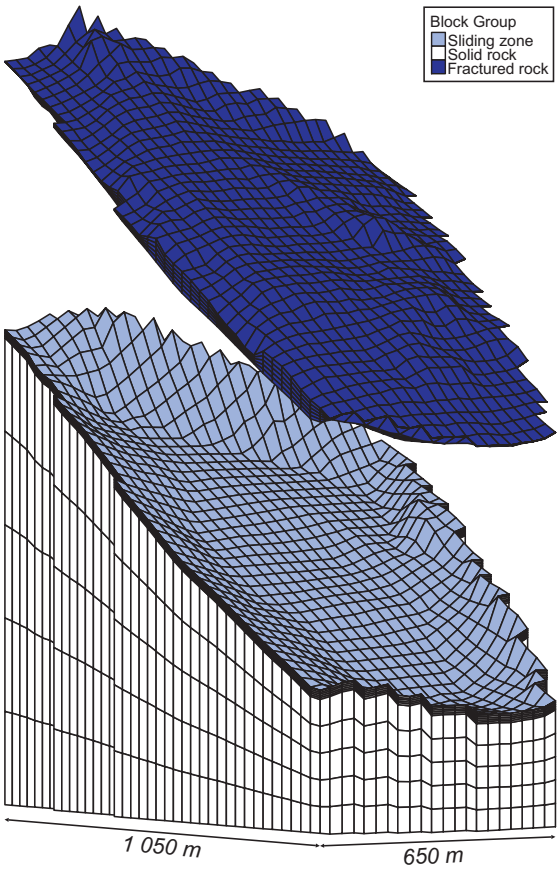

Figure 3: Numerical model of the rockslope at Åknes with 13 440 elements and three geological units.

this has been used as basis for calibration of the numerical model in $FLAC^{3D}$. To use the central area as basis is believed to be most relevant for the modelling carried out here, since the upper area moves individually toward the large ravine and deformation data from the lower area is uncertain at present.

5. Groundwater

The groundwater level is measured by piezometers in a D.M.S. IU monitoring system [5], which was installed in the upper and middle borehole in November 2006. Data from groundwater monitoring shows that the water levels in the two boreholes fluctuate simultaneously, indicating a shared groundwater regime [9]. The fluctuations are however, largest in the upper borehole, reflecting the short distance from the back scarp, which is believed to constitute a major source for infiltration of water to the sliding area. The groundwater level varied by 9 m in the two-year measuring period from December 2006 to December 2008. The groundwater is at its highest levels in spring and autumn, as it is influenced by high precipitation rates (in autumn) and a combination of precipitation and melting of a 1-3 m thick layer of snow which covers the area in the winter (in spring) [9]. The groundwater level is higher

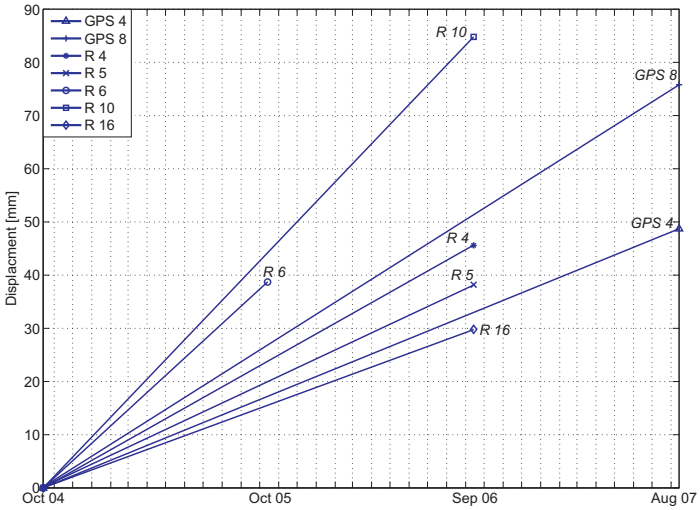

Figure 4: Total displacements in the period 2004-2007 for points located in the central area of the slope.

in middle borehole (between 42 and 46 m below the surface) as than in the upper borehole (between 51 and 60 m below the surface). Average groundwater levels in upper and middle borehole during one year (between August 2007 and August 2008) were -56 m and -44 m, respectively. A groundwater table has been generated in $FLAC^{3D}$ according to this at the top slope, while at the bottom, the groundwater level has been determined to be at the level of the sliding zone, as indicated by the line of springs mapped in field.

6. Input parameters

The sliding layer is modeled with a creep material model available in the $FLAC^{3D}$ program, the Burger-Creep Viscoplastic material model (cvisc) which is a combination of the Burger's model and Mohr-Coulomb model (Figure 5). The unstable mass above the sliding zone termed "fractured rock" is modeled with the Mohr-Coulomb material model while the base layer below the sliding zone termed "solid rock" is modeled as an elastic material in order to force the focus to be on the potential unstable rockmass.

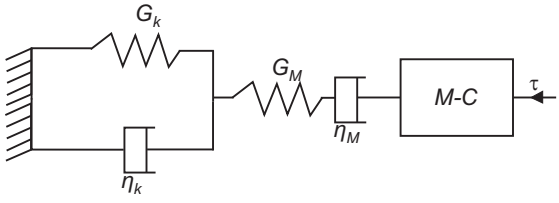

Figure 5: Burger-Creep Viscoplastic material model in $FLAC^{3D}$.

6.1. Mohr-Coulomb parameters

The zone of deformation at Åknes is believed to be highly complex, consisting of a combination of (1) unfilled

joints (rock-to-rock contacts), (2) joints filled with gouge material and (3) bridges of intact rock. Large uncertainties are related to the estimation of input parameters for such a complex sliding surface. However, an attempt was made for the Åknes case by Grøneng et al. [10], who presented a methodology for calculating shear strength parameters of a composite sliding plane. The methodology represents an alternative method for estimation of shear strength parameters by combining shear strength of the various materials in order to obtain a resultant shear strength of the overall sliding zone. The method requires an estimation of probable composition of a sliding plane, which is difficult, and connected with a considerable degree of uncertainty. However, based on field observations and drill core logging, an estimation of most likely composition of the sliding plane at Åknes resulted in 25-35% failure along gouge filled joints, 1-3% intact rock failure and 62-74% failure along unfilled foliation joints. Shear strength estimation of rock and soil was based on triaxial testing and Mohr-Coulomb failure criterion. For unfilled joints, a combination of field investigations and laboratory testing was carried out in order to determine the parameters necessary for the Barton-Bandis joint shear formulation. Figure 6 illustrates the procedure for calculating parameters according to the developed methodology and as indicated, the parameters are calculated according to an estimated normal stress acting on the sliding plane. The normal stress used in this modelling has been calculated as an average normal stress according to the weight component of 110 m overburden acting perpendicularly on the sliding plane with an average dip angle of 35° (σ_n=γ_{rock}×h×cosα_{slope}). This gives a normal stress of 2.4 MPa. The effective normal stress was calculated by subtracting the pore pressure acting on the plane by an average height of the groundwater above the sliding plane of 60 m, resulting in an effective normal stress of σ'_n=1.8 MPa. For the modelling presented here, the methodology has been applied for two alternative compositions of the sliding plane as shown in Table 1.

Alt.	Intact rock bridge [%]	Gouge [%]	Unfilled joints [%]	c_{res} [MPa]	ϕ_{res} [°]
1	3	35	62	0.46	32.8
2	1	35	64	0.23	32.5

Table 1: Two alternative resulting Mohr-Coulomb parameters for the layer termed "sliding zone".

Based on field work and laboratory testing of the various types of gneiss present in the sliding area, Mohr-Coulomb parameters for the layers termed "solid rock" and "fractured rock" were obtained as shown in Table 2. Scaling of values from the laboratory testing and estimation of Mohr-Coulomb parameters were carried out by using *Roclab* [17]. For the layer termed "fractured rock", a GSI of 62 was applied based on outcrop measurements throughout the sliding area, reflecting "good surface conditions" according to the GSI-rating system. Parameters

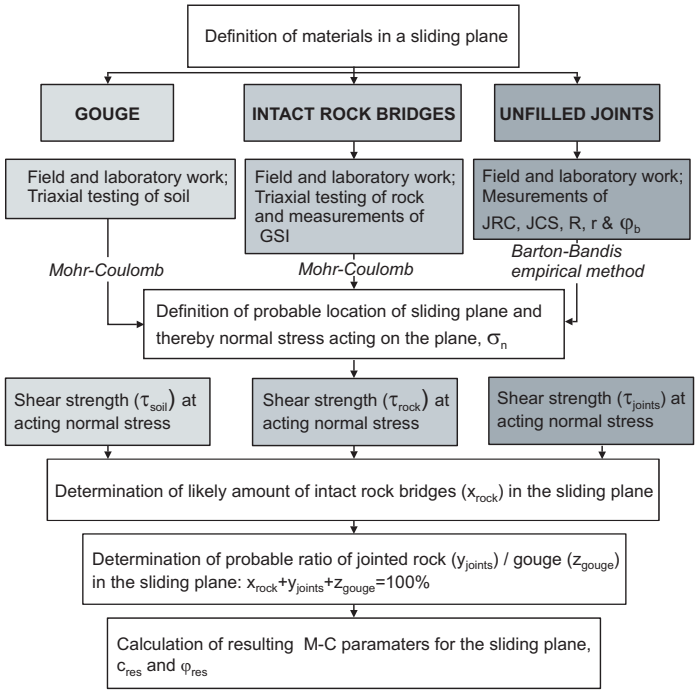

Figure 6: Flowchart illustrating the methodology for estimating shear strength parameters for a sliding plane as presented in Grøneng et al. [10].

according to an alternative GSI of 37 were also calculated, reflecting "fair surface conditions".

Two combinations of parameters were used as a basis for modelling; (1) a scenario where the sliding plane is estimated to consist of 3% intact rock (in addition to 35% gouge and 62% unfilled joints) and a fractured rockmass above the sliding layer according to a GSI of 62 and (2) a scenario where the sliding plane is estimated to consist of 1% intact rock (in addition to 35% gouge and 64% unfilled joints) and a fractured rockmass above the sliding layer according to a GSI of 37. The former scenario is believed to represent the situation today, while the the latter is belived to represent a future scenario, as the shear strength of the sliding layer as well as the fractured rockmass located above it gradually decreases over time. Decrease in shear strength of the sliding layer could be a result of variations in pore water pressure and reduction in the joint roughness due to mechanical or chemical disintegration as discussed in Sandersen et al. [18] while the surface conditions of the rockmass decreases as a result of disintegration caused by sliding movements along the sliding layer.

6.2. Creep parameters

Obtaining creep parameters for the Burger's model (Kelvin and Maxwell rheological model combined in a series) in rock mechanics is normally carried out by creep laboratory tests on rock cores and fitting of the creep curve to the parameters; η_K which determines the rate of delayed elasticity, G_M which is the elastic shear modulus, η_M

Unit	γ	E_i [MPa]	ν	GSI	E_{RM} [MPa]	c [MPa]	ϕ [°]	σ_t [MPa]
Solid rock	2,740	38,700	0.13	80	34,100	-	-	0
Fractured rock (1)	2,740	38,700	0.13	62	21,880	11.5	43	0
Fractured rock (2)	2,740	38,700	0.13	37	5,030	8.17	35.5	0

Table 2: Material parameters for elastic (Solid rock) and Mohr-Coulomb (Fractured rock) material models.

which describes the rate of viscous flow and G_K which controls the amount of delayed elasticity [8]. In this case, the sliding zone is modeled as a continuous layer with Mohr-Coulomb parameters based on the assumption of a composite sliding plane (3 and 1% intact rock bridges, 62 and 64% unfilled joints and 35% joints filled with gouge, respectively). Laboratory testing is hardly possible for this composite material. Therefore, creep parameters for the layer termed "sliding zone" is obtained by calibrating the model according to the annual, average displacement rate of 26 mm/year in the central area. Displacements from several gridpoints in the central area of the model were evaluated after running the model for 1 year and calibration resulted in an alternative set of creep parameters as shown in Table 3.

Unit	G_K	η^K [Pas]	G_M	η^M [Pas]
Sliding layer	0.43e13	0.43e13	0.43e11	0.43e11

Table 3: Creep material parameters for the Burger-Creep Viscoplastic material model.

7. Time dependent deformation

Displacements have been analysed for gridpoints at the surface after simulation of creep for 1, 25, 50, 75 and 100 years. For parameters according to alternative (1) (3% intact rock bridges in the sliding plane and a fractured rockmass with M-C parameters representing a GSI of 62), calibration was chosen to give total displacement of a gridpoint located in the central area of the model of 26 mm after 1 year. Investigation of the displacement curve (Figure 7(a)) indicates a stabilisation of the movement in the central area of the model after about 25 years. However, due to a gradually decrease in shear strength of the sliding surface as well as the unstable rockmass located above it, this is not believed to represent the time dependent behavior at Åknes. Parameters according to alternative (2) (1% intact rock bridges in the sliding plane and a fractured rockmass representing a GSI of 37) shows a steady increase in displacement throughout the 100 year creeping period (Figure 7(b)). An investigation of the surface displacements in the model shows that in case of alternative (1) parameters, the displacements after 100 years of creep are in the range of 0.1-0.2 m in the central area and at the lower boundary (Figure 8(a)). Investigation of the displacement vectors for a longitudinal section in the middle of the model shows a gradual decrease in the displacements towards the lower boundary, indicating that sliding along the creeping layer has not resulted in an unstable toe for alternative (1) parameters (Figure 8(b)). In case of alternative (2) parameters, however, the displacements are in the in the range of 0.4-1.0 m in the central area of the model after 100 years, and at the toe, a zone of displacements in the range of 1-1.8 m has developed (Figure 8(c)). Investigation of the displacement vectors in this plane shows vectors moving out of the slope, a clear indication of failure in this area (Figure 8(d)). Shear strength parameters according to alternative (2) thus are at a critical state.

8. Discussion

The presence of one single continuous sliding plane is unlikely in the Åknes case. The analysis presented here however takes into consideration what is believed to be fairly realistic; a composite sliding layer consisting of intact rock and sliding along unfilled and filled joints. Two different alternatives of shear strength parameters have been analysed, the first with parameters believed to represent the case today, and the second representing reduced parameters believed to represent a realistic future scenario due to gradually decrease of shear strength over time. Alternative (1) parameters with an assumption of 3% intact rock bridges in the sliding surface and surface conditions characterised as "good" according to the GSI-system have been found to result in displacements stabilizing after 25 years, while a reduction of the shear strength parameters to 1% rock in the sliding layer and a more disintegrated rockmass above the creeping layer according to "fair surface conditions" results in increased displacements over time representing a clear indication of model failure. It is hence obvious that displacement along the creeping sliding surface triggers plasticity of the fractured rockmass and when the shear strength of the rockmass becomes below a certain strength, failure will occur. How long this process will take, is impossible to predict based on the modelling that has been carried out. The results presented here are based on a series of simplifications, the most important ones being the simplification of the geometry representing the zone of deformation and the groundwater conditions. In a large scale rockslope such as the Åknes case, the sliding zone is highly complex and seldom fully understood. Hence, the numerical modelling at this stage should be regarded as preliminary analyses of the time-dependent behavior. Analysis of the meteorological effects on seasonal rock displacements at Åknes carried out by Grøneng et al. [9] showed that the groundwater plays an important role in

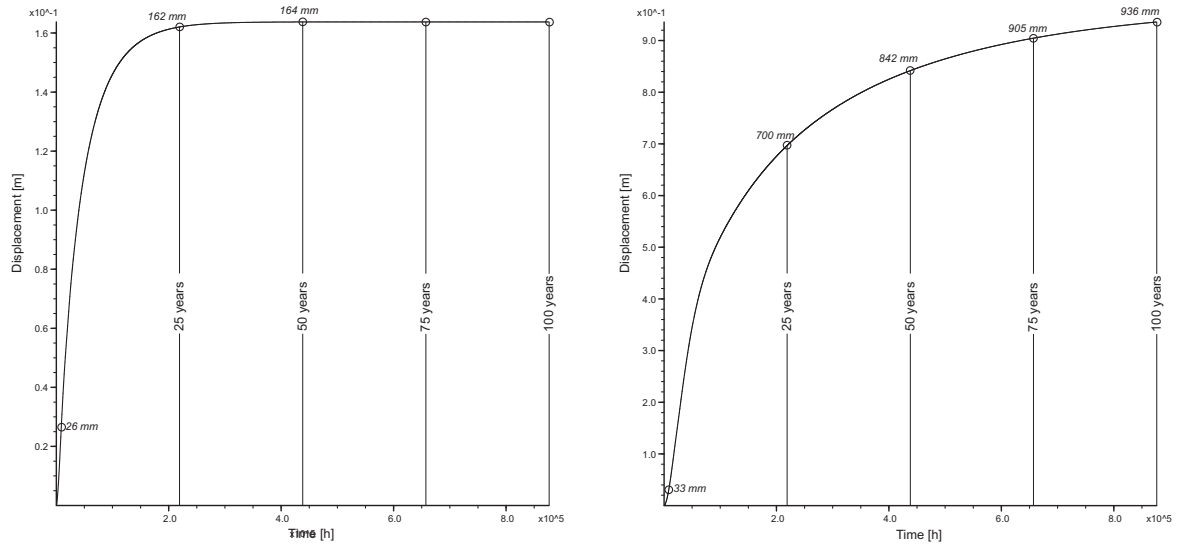

(a) (b)

Figure 7: Displacements from creep modelling in $FLAC^{3D}$ a) Displacement curve after simulation of creep for 100 years, alternative (1) parameters b) Displacement curve after simulation of creep for 100 years, alternative (2) parameters.

the relative stability of the Åknes slope as the largest net expansion of the upper tension crack is closely related to high and fluctuating groundwater levels. A more sophisticated analysis of how the changing groundwater level affects the displacements (hereby also the stability) therefore should be the next step in analysis of the Åknes case. Also, a simplification of the geometry was made in this analysis by modelling three homogeneous layers (solid rock, sliding zone and fractured rock), and in further analysis geometry should be improved as more knowledge becomes available.

Still, increased knowledge regarding the time-dependency of the Åknes slide has been obtained through the analysis presented here, and shear strength parameters resulting in stable and unstable conditions in the model representing the Åknes case have been found.

9. Conclusions

The large-scale Åknes rockslide area has been known since the 1960'ies and extensive monitoring since 2004 has revealed an unstable slope which has the potential to develop into a catastrophic failure in the future. Stability analyses are thus of great importance. Numerical modelling of the slope stability has been carried out by the use of $FLAC^{3D}$ and the Burger-Creep Viscoplastic material model (cvisc). Creep parameters for the cvisc material model which is used to model the sliding layer have been defined based on the average annual slope deformation and Mohr-Coulomb parameters obtained by a combination of field investigations and laboratory experiments. The model is run with two sets of parameters, one believed to represent the present case, and one believed to represent a future scenario. Modelling shows that the Åknes model is stable with a set of parameters representing a composite sliding layer with 3% intact rock, 35% gouge and 62% unfilled joints and a fractured rockmass located above the sliding layer with M-C parameters according to a GSI of 62 (good surface conditions). However, due to gradual reduction in the shear strength parameters, the toe becomes unstable and the surface displacements increase with a set of parameters representing a composite sliding layer with 1% intact rock, 35% gouge and 64% unfilled joints and a fractured rockmass corresponding to a GSI of 37 (fair surface conditions). It should be noted that this is based on several simplifications of the geometry and groundwater conditions in addition to estimation of the composition of the sliding layer. However, as more data is collected and knowledge is gained on the groundwater regime, geometry and the composition of the zone of deformation, the model can act as a basis for further studies of creep deformation in the slope.

Acknowledgements

The work presented in this paper is carried out as part of a project funded by the Research Council of Norway through the International Centre for Geohazards (ICG), which is established by several partners with the Norwegian Geotechnical Institute (NGI) as the host institution. The Åknes-Tafjord project, with Lars Harald Blikra as scientific responsible, is acknowledged for support and cooperation.

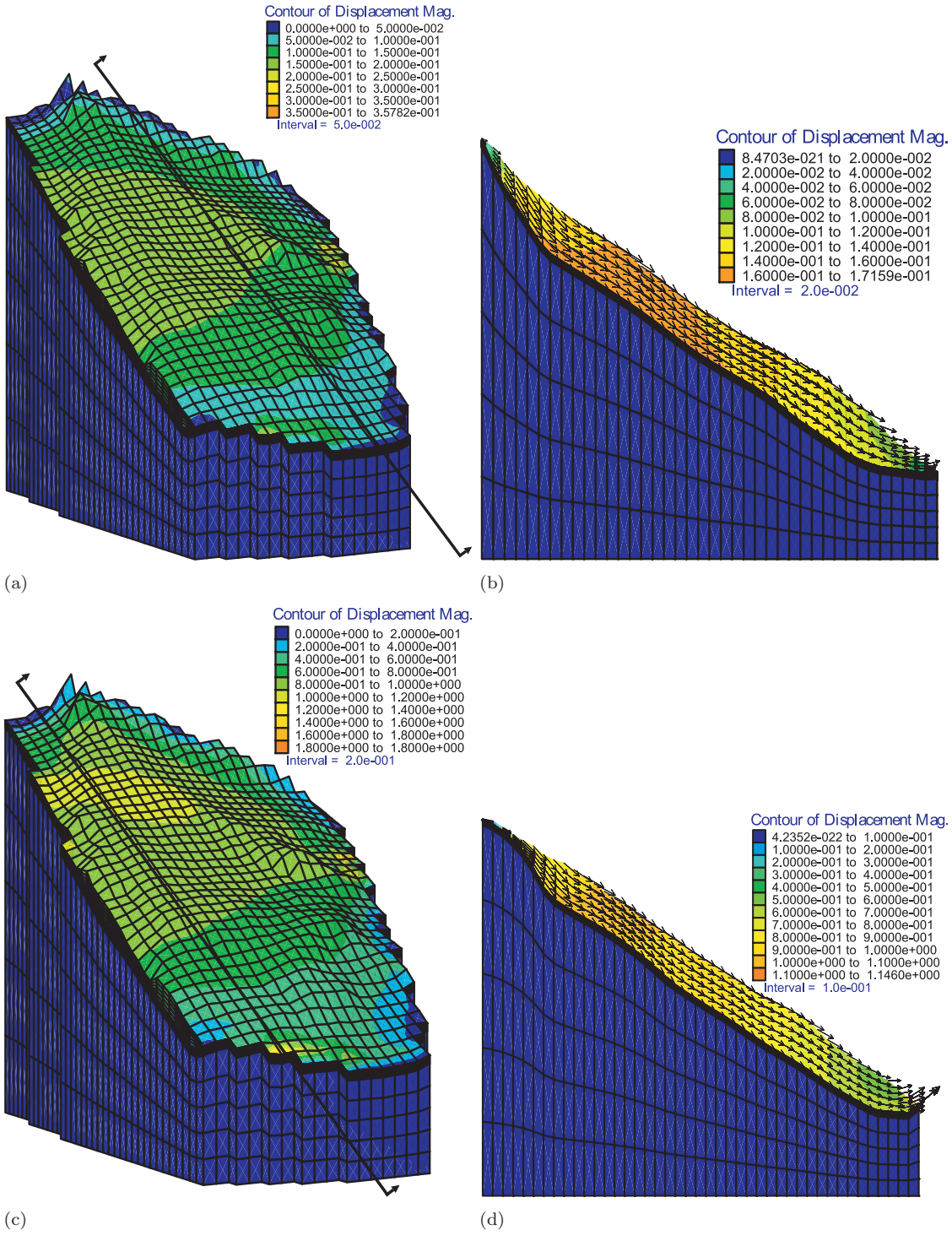

Figure 8: Displacements from creep modelling in $FLAC^{3D}$ a) Displacements at the surface, alternative (1) parameters b) Displacements in a plane located in the middle of the model, alternative (1) parameters c) Displacements on the surface, alternative (2) parameters d) Displacements in a plane located where the deformations are largest at the toe, alternative (2) parameters.

References

[1] Bjerrum, I., Jørstad, F. A., 1968. Stability of natural rock slopes in Norway. Tech. Rep. 79, Norwegian Geotechnical Institute (NGI).

[2] Blikra, L. H., 2008. The Åknes rockslide; monitoring, threshold values and early-warning. In: Chen, Z., Zhang, J., Li, Z., Wu, F., Ho, K. (Eds.), Proceedings of 10^{th} international symposium on landslides and engineered slopes, China. Taylor and Francis Group, pp. 1089–1094.

[3] Blikra, L. H., Longva, O., Harbitz, C., Løvholt, F., 2005. Quantification of rock-avalanche and tsunami hazard in Storfjorden, Western Norway. In: Senneset, K., Flaate, K., Larsen, J. (Eds.), Landslides and Avalanches: ICFL 2005 Norway. Taylor and Francis Group, pp. 57–63.

[4] Braathen, A., Blikra, L. H., Berg, S. S., Karlsen, F., 2004. Rock-slope failures in Norway; type, geometry, deformation mechanisms and stability. Norwegian Journal of Geology 84, 67–88.

[5] DMS, 2009. Differential monitoring of stability. Technical specification for DMS-IU, www.csgsrl.eu.

[6] Eidsvig, U., Harbitz, C., 2005. Innledende numeriske analyser av flodbølger som følge av mulige skred fra Åkneset. Tech. Rep. 20031100-2, Norwegian Geotechnical Institute (NGI).

[7] Ganerød, G. V., Grøneng, G., Rønning, J. S., Dalsegg, E., Elvebakk, H., Tønnesen, J. F., Kveldsvik, V., Eiken, T., Blikra, L. H., Braathen, A., 2008. Geological model of the Åknes rockslide, western Norway. Engineering Geology 102, 1–18.

[8] Goodman, R. E., 1980. Introduction to Rock Mechanics. John Wiley & Sons Inc.

[9] Grøneng, G., Christiansen, H. H., Nilsen, B., Blikra, L. H., 2009. Meteorological effects on seasonal rock displacements of the Åknes rockslide, western Norway. Submitted to Landslides, May 2009.

[10] Grøneng, G., Nilsen, B., Sandven, R., 2009. Shear strength estimation for Åknes sliding area in western Norway. International Journal of Rock Mechanics and Mining Sciences 46, 479–488.

[11] Kveldsvik, V., Einstein, H. H., Nilsen, B., Blikra, L. H., 2008. Numerical analyses of the 650,000 m^2 Åknes rock slope based on measurement displacements and geotechnical data. Accepted for publication in: Rock Mechanics and Rock Engineering.

[12] Kveldsvik, V., Kaynia, A. M., Nadim, F., Bhasin, R., Nilsen, B., Einstein, H. H., 2009. Dynamic analysis of the 800 m high Åknes rock slope using UDEC. International Journal of Rock Mechanics and Mining Sciences 46, 686–698.

[13] Kveldsvik, V., Nilsen, B., Einstein, H. H., Nadim, F., 2008. Alternative approaches for analyses of a 100,000 m^3 rock slide based on Barton-Bandis shear strength criterion. Landslides 5, 161–176.

[14] Longva, O., Blikra, L. H., Dehls, J. F., 2009. Rock avalanches - distribution and frequencies in the inner part of Storfjorden, møre og Romsdal County, Norway. Tech. Rep. 2009:002, Geological Survey of Norway (NGU).

[15] Nordvik, T., Grøneng, G., Ganerød, G. V., Nilsen, B., Harding, C., Blikra, L. H., 2009. Geovisualization, geometric modelling and volume estimation of the Åknes rockslide, western Norway. Accepted for publication in: Bulletin of Engineering Geology and the Environment.

[16] Nordvik, T., Nyrnes, E., 2009. Statistical analysis of surface displacements an example from the Åknes rockslide, western Norway. Natural Hazards and Earth System Sciences 9 (3), 713–724.

[17] Rocscience, 2002. Rocscience, RocLab. Rocscience Inc, Toronto, 1st Edition.

[18] Sandersen, F., Bakkehøi, S., Hestnes, E., Lied, K., 1996. The influence of meteorological factors on the initiation of debris flows, rockfalls, rockslides and rockmass stability. In: Senneset, K. (Ed.), Landslides. Balkema, pp. 97–114.

[19] Tveten, E., Lutro, O., Thorsnes, T., 1988. Bergrunnskart Ålesund. 1:250 000. Geological map.

Appendices

A.1 Additional paper

Geological Model of the Åknes Rockslide, western Norway

Authors: Guri Venvik Ganerød, Guro Grøneng, Jan Steinar Rønning, Einar Dalsegg, Harald Elvebakk, Jan Fredrik Tønnesen, Vidar Kveldsvik, Trond Eiken, Lars H. Blikra and Alvar Braathen

The paper was published in Engineering Geology (2008), Vol. 102, pages 1-18, doi:10.1016/j.enggeo.2008.01.018.

Engineering Geology 102 (2008) 1–18

Contents lists available at ScienceDirect

Engineering Geology

journal homepage: www.elsevier.com/locate/enggeo

Geological model of the Åknes rockslide, western Norway

Guri Venvik Ganerød [a,b,*], Guro Grøneng [c,d], Jan Steinar Rønning [a,c], Einar Dalsegg [a], Harald Elvebakk [a], Jan Fredrik Tønnesen [a], Vidar Kveldsvik [c,d,e], Trond Eiken [f], Lars Harald Blikra [d,g], Alvar Braathen [h]

[a] Geological Survey of Norway (NGU), 7491 Trondheim, Norway
[b] Department of Earth Science, University of Bergen, Norway
[c] Norwegian University of Science and Technology (NTNU), Norway
[d] International Centre for Geohazards (ICG), Norway
[e] Norwegian Geotechnical Institute (NGI), Norway
[f] Department of Geosciences, University of Oslo, Norway
[g] Stranda Municipality, Norway
[h] University Centre in Svalbard, Norway

ARTICLE INFO

Article history:
Received 16 May 2007
Received in revised form 25 January 2008
Accepted 30 January 2008
Available online 4 March 2008

Keywords:
Rockslide
Geological and structural model
Geophysical surveys

ABSTRACT

Åknes is known as the most hazardous rockslide area in Norway at present, and is among the most investigated rockslides in the world, representing an exceptional natural laboratory. This study focuses on structural geology and the usage of geophysical methods to interpret and understand the structural geometry of the rockslide area. The interpretations are further used to build a geological model of the site. This is a large rockslide with an estimated volume of 35–40 million m^3 (Derron et al., 2005) defined by a back scarp, a basal shear zone at about 50 m depth and an interpreted toe zone where the sliding surface daylights the surface. The rockslide is divided into four sub-domains, experiencing extension in the upper part and compression in the lower part. Structural mapping of the area indicates that the foliation of the gneiss plays an important role in the development of this rockslide. The upper boundary zone of the rockslide is seen as a back scarp that is controlled by, and parallel to, the pre-existing, steep foliation planes. Where the foliation is not favourably orientated in regard to the extensional trend, the back scarp follows a pre-existing fracture set or forms a relay structure. The foliation in the lower part, dipping 30° to 35° to S–SSE, seems to control the development of the basal sliding surface with its subordinate low angle trust surfaces, which daylights at different levels. The sliding surfaces are sub-parallel to the topographic slope and are located along mica-rich layers in the foliation.

Geophysical surveys using Ground Penetrating Radar (GPR), refraction seismic and 2D resistivity profiling, give a coherent understanding of undulating basal sliding surface in the subsurface. The geophysical surveys map the subsurface in great detail to a depth ranging from 30–40 m for GPR to approximately 125 m for refraction seismic and 2D resistivity profiling. This gives a good control on the depth and lateral extent of the basal sliding surface, and its subordinate low angle thrusts. Drill cores and borehole logging add important information with regard to geological understanding of the subsurface. Fracture frequency, fault rock occurrences, geophysical properties and groundwater conditions both in outcrops and/or drill cores constrain the geometrical and kinematic model of Åknes rockslide.

1. Introduction

Unstable rock slopes pose a threat to the inhabitants along Norwegian fjords, where prehistoric and historic rock avalanches have created tsunamis, some causing severe casualties (Blikra et al., 2005a). The site presented, Åknes, is located in western Norway (Fig. 1). This is a large rockslide with an estimated volume of 35–40 million m^3 (Derron et al., 2005), defined by a back scarp, a basal shear zone at 50 m depth and a toe zone where the basal sliding surface daylights the surface. Continuous creep of the rock mass and the fact that Åknes is situated above the fjord and in the vicinity of several communities as well as one of Norway's most visited tourist attractions (the Geirangerfjord, listed on the UNESCO's World heritage list), have triggered a comprehensive investigation program. The overall aim of the project is firstly, to assess the likelihood that the rockslide will accelerate into a rock avalanche and secondly, to establish an early warning system with direct monitoring of deformation (translation and rotation), so that the local communities are able to evacuate in time.

* Corresponding author. Geological Survey of Norway (NGU), 7491 Trondheim, Norway. Tel.: +47 73 91 43 13; fax: +47 73 92 16 20.
E-mail address: Guri.Venvik.Ganerod@ngu.no (G.V. Ganerød).

0013-7952/$ – see front matter © 2008 Elsevier B.V. All rights reserved.
doi:10.1016/j.enggeo.2008.01.018

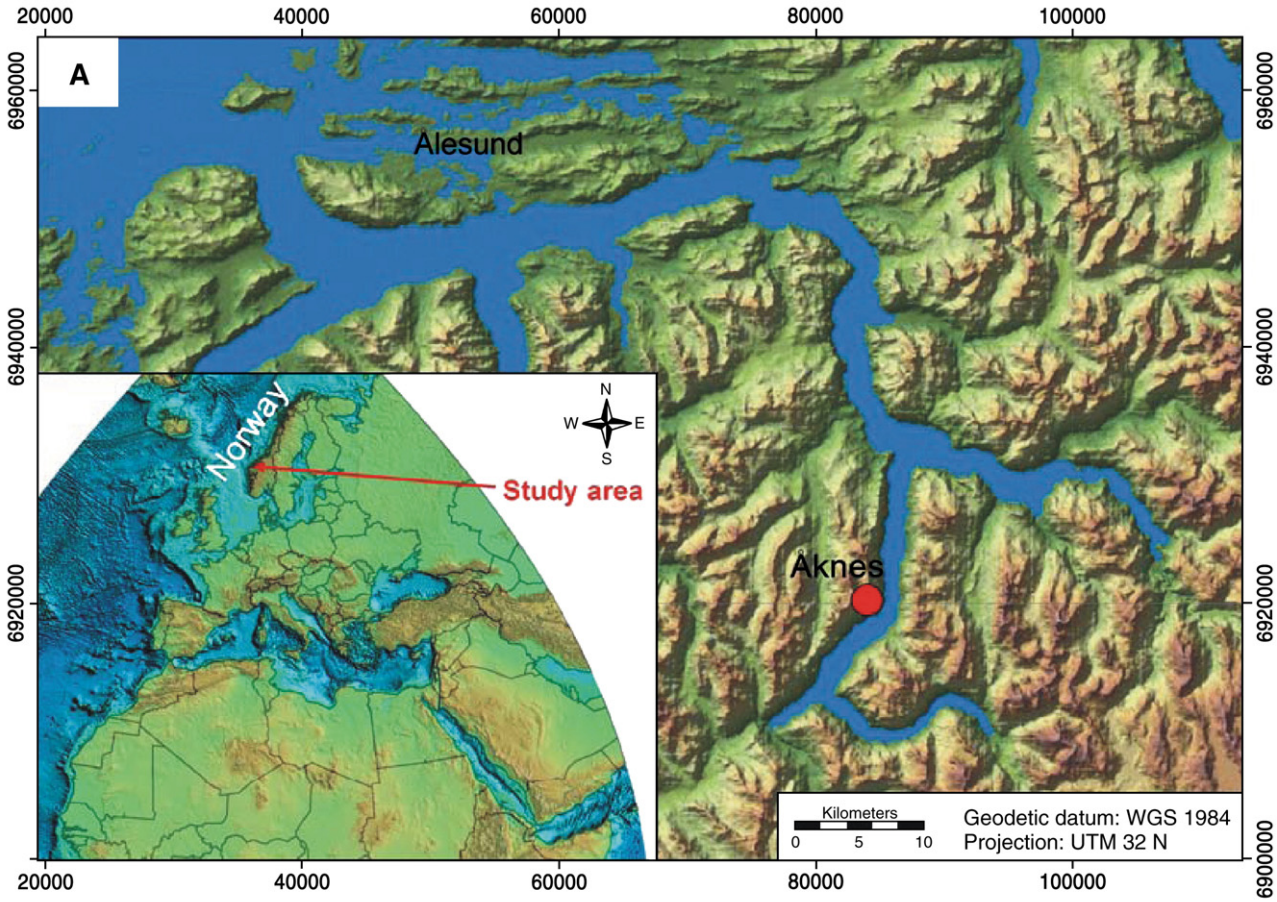

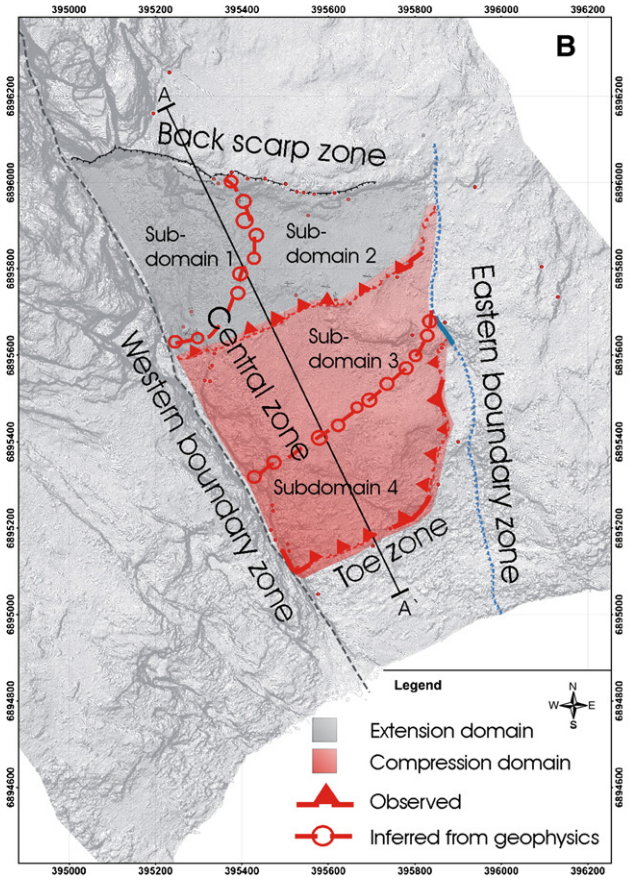

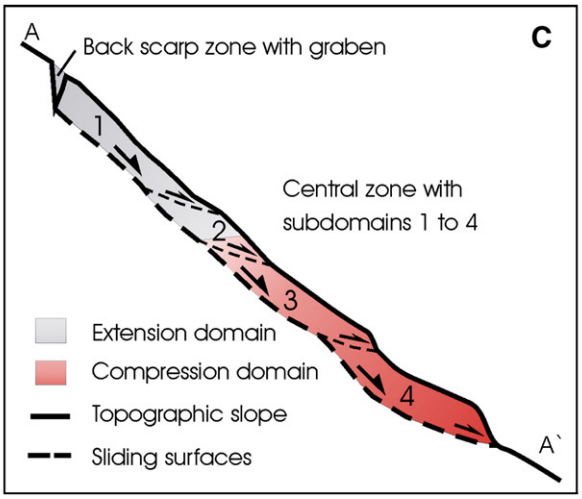

Fig. 1. A) Location of the rockslide site of Åknes in western Norway. This site is found 150–900 m above sea level in a SSE facing steep mountain slope. The main concern for this area is that a rock avalanche will reach the fjord at the foot of the slope, and trigger a tsunami in the fjord system. B) Map that locates domains and sub-domains (1, 2, 3 and 4) and key structures described in the text. C) Schematic profile (located in b) that outline domains, sub-domains and key structures.

Recent regional studies of the area are summarized in Braathen et al. (2004), Blikra et al. (2005a,b), Hermanns et al. (2006), Henderson et al. (2006) and Roth et al. (2006). Henderson et al. (2006) suggest that existing structures in the bedrock, such as foliation, faults and fracture zones, are controlling the development of the rockslides that occur in the fjord system. Where the foliation and slope angle coincide and structural weaknesses are favourably oriented, the rockslide hazard is considered greater (Henderson et al. 2006). Historical data from Åknes reveals three moderately sized rockslide occurrences within a rather short time interval: in the years 1850–1900, 1940 and 1962 (Kveldsvik et al., 2006). Other recent studies from the Åknes area are presented by Derron et al. (2005), who give an estimate of size of the rockslide, and Kveldsvik et al. (2006) who present a brief summary of the investigations and the progress of the project, and analyses of the 100,000 m^3 rockslide that occurred in 1962 (Kveldsvik et al., 2007).

Despite the number of regional and local studies, a detailed structural understanding of the rockslide area is missing. A key issue has been to locate the basal sliding surface of the rockslide, since this is a prerequisite for precise volume estimation. Location of the basal sliding surface will also lead to a better understanding of the sliding mechanism(s) of the unstable area. The ongoing survey of the area is comprehensive and includes borehole logging and monitoring, which will help constrain the location of the basal sliding surface or sliding zone more precisely and yield additional quantitative data regarding spatial and temporal sliding velocities. The aim of this study has been to describe the rockslide area at Åknes by means of detailed structural surface mapping, supported by subsurface data from 2D resistivity, Ground Penetrating Radar (GPR) and refraction seismic profiling, core drilling and geophysical logging of boreholes. Together, these data give a detailed 3D geological understanding of the area, in which the depth to – and the geometry of the basal slide surfaces can be identified and described. A secondary goal of this study has been to propose a geological model of the Åknes rockslide for further numerical modelling, including groundwater and slide dynamics.

Results from the study show that there are structural limits to the rockslide area, consisting of the extensional back scarp zone at the top, a steeply dipping, NNW–SSE trending strike slip fault as the western boundary zone, a gentle dipping NNE–SSW trending pre-existing fault as the eastern boundary zone and a compressional toe zone at the bottom. The rockslide area is divided into four sub-domains (1 to 4), two mapped on the surface (2 and 4) and two mapped in the subsurface by geophysics (1 and 3, Fig. 1). The geophysical surveys indicate that the sub-domains are bound by the basal sliding surface with its four subordinate, low angle thrusts that stack the bedrock lobes upon one another, forming an imbricated thrust fan. The overall geometry is that of extension in the upper part and compression in the lower part of the slope. An outline of the rockslide is given in Fig. 1B and C.

2. Geological setting of Åknes Site

The Åknes site is a southward facing slope, with an average dip angle of 30–35°, with a topography that stretches from sea level to an elevation of 1300 m over a distance of 1500 m (Fig. 2). We propose subdividing the rockslide area into five zones, based upon different structural signatures. The unstable area is estimated to be 800 m across-slope and 1000 m down-slope, with an upper boundary, the *Back Scarp Zone*, located 800–900 m above sea level, and a lower boundary, the *Toe Zone*, at 150 m above sea level. The western margin is a steep NNE–SSE trending strike slip fault, called the *Western Boundary Zone*, forming a narrow, deep crevasse in the mountainside (Fig. 2). On the east side, the rockslide area is bound by a pre-existing fault dipping gently (35–45°) to the west, called the *Eastern Boundary Zone*. The fifth part of the rockslide is named the *Central Zone*.

The Åknes rockslide is located in the Western Gneiss Region. The bedrock of the area is dominated by gneisses of Proterozoic age, which was altered and reworked during the Caledonian orogeny (Tveten et al., 1998). The gneisses have a magmatic origin and are described in the geological map sheet as undifferentiated gneisses that are locally migmatitic in composition, varying from quartz-dioritic to granitic (Tveten et al., 1998). Within certain areas the gneiss has a distinct metamorphic penetrative foliation (S_1, dominantly 080/30) that is folded around gently ESE-plunging axes (Tveten et al., 1998; Braathen et al., 2004). The bedrock at the study sites alters from a white to light pink, medium grained granitic gneiss to a dark grey biotite bearing granodioritic gneiss, and further to a subordinate white to light grey, hornblende to biotite bearing, medium grained dioritic gneiss. There are also laminae, and up to 20 cm thick layers, of biotite schist within the gneiss. All lithologies occur in layers parallel to the metamorphic foliation.

3. Methods

3.1. Structural mapping

Structural mapping is conducted on outcrops in the field, where fracture properties such as orientation, strike and dip with right hand rule (RHR) measurement (Davis and Reynolds, 1996), length/persistence and frequency is collected. The fracture frequency is measured along a ruler in x direction parallel to foliation, y direction perpendicular to foliation, and if possible in a third direction (z) to estimate the block size. The foliation in gneissic rocks commonly represents a weakness in the bedrock and will therefore fracture along it, creating a higher fracture frequency in that direction as demonstrated in Fig. 3. This will give a dominance of fractures parallel to the foliation while other fracture orientations most likely are underrepresented in comparison. The data is later analysed per locality, for example as lower hemisphere stereo plots (Wulff net) of fracture orientation.

3.2. Core logging

A total of seven drill holes were drilled and cored at three sites in the rockslide area. Three holes are vertical to 150 m depth; one is inclined by 60° and goes down 150 m, while the remaining three are vertical and 200 m deep. All cores have been logged (Ganerød et al., 2007) for fractures (discontinuities) per metre giving a fracture frequency per metre by depth (Nilsen and Palmstrøm, 2000). The fractures are classified as foliation parallel or not, and the dip angle between the core axis and the fracture is measured. Since the drill core is not orientated, strike and dip was not measured. The drill hole presented here is from the lowest drilling site and goes down to 150 m depth (Fig. 2).

3.3. Surface geophysical mapping

Geophysical methods such as Ground Penetrating Radar (GPR), refraction seismic and 2D resistivity profiling have been used to map the subsurface. Several lines were measured in the rockslide area, of which parts will be presented here. The 2D resistivity and GPR data were collected along the same profiles, while seismic acquisition was limited to three profiles (Rønning et al., 2006).

3.3.1. GeoRadar

The GPR survey at the rockslide consists of seven profiles of altogether 5300 m. One profile has NE–SW strike, four profiles are slope parallel with E–W strike, and two are oriented down-slope with N–S strike. The GPR profile presented has a total length of 250 m with a NNW–SSE strike.

GeoRadar is an electro magnetic method that is used to detect structures in the subsurface (Reynolds, 1997). With an antenna electro magnetic pulses are sent into the subsurface, which are reflected off surfaces with different dielectric properties and received by a receiver antenna at the surface. The time of the propagating wave is recorded. This measurement is repeated with a fixed interval, giving a

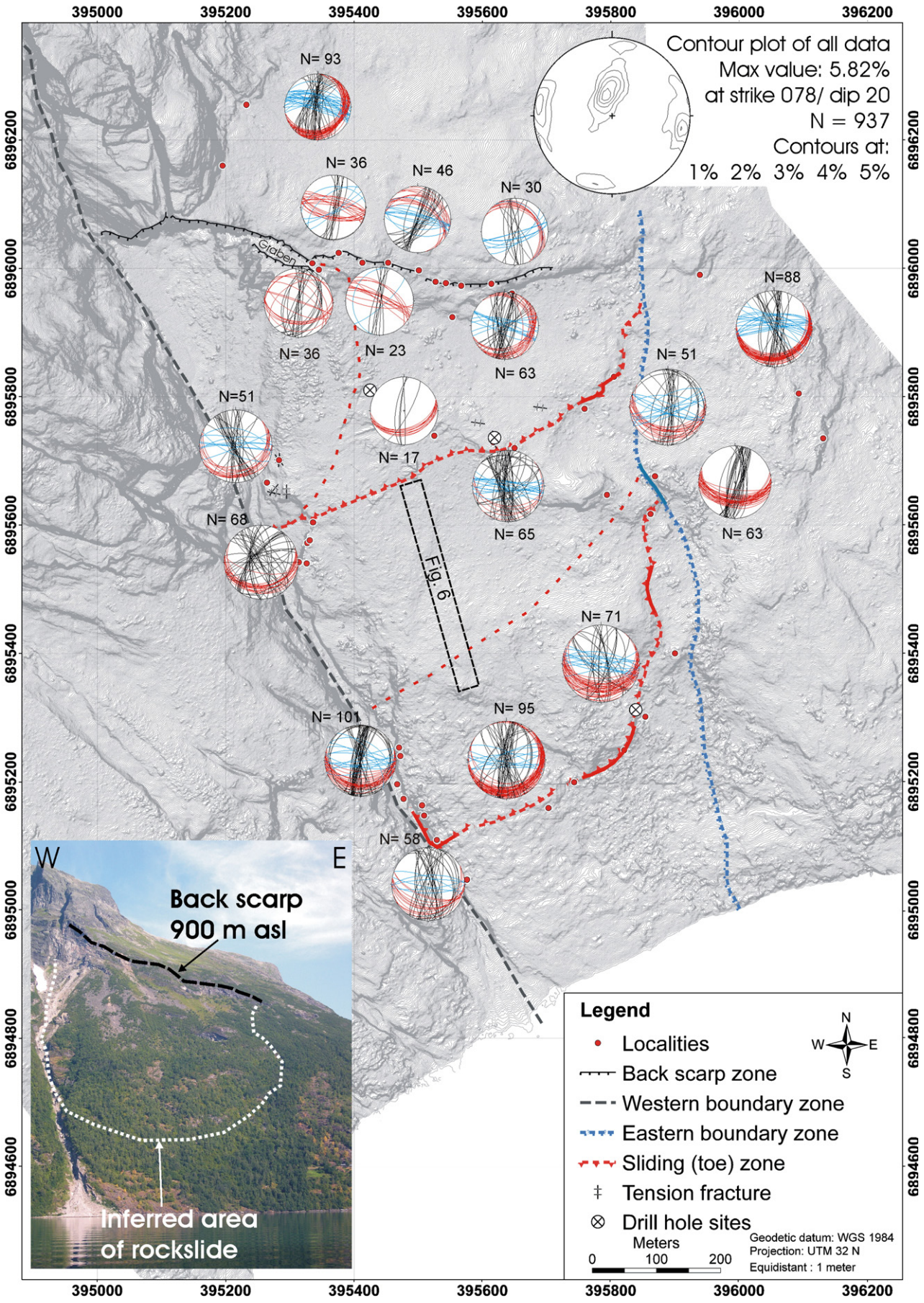

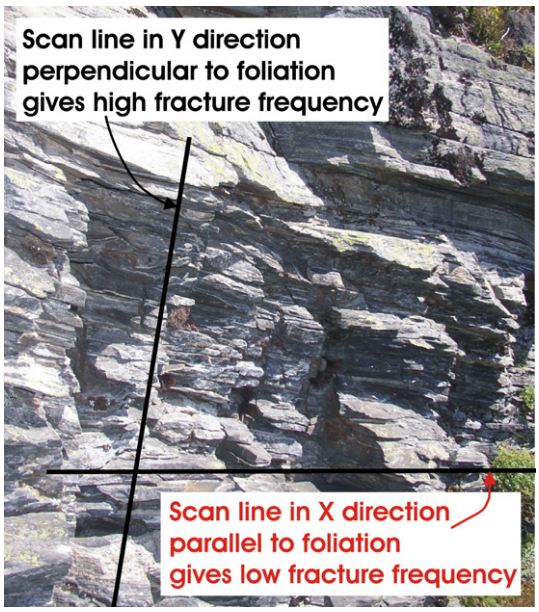

Fig. 3. Example of how structural data such as fracture frequency is collected with the help of scan lines. Fracture frequency is collected in *x* direction parallel to foliation, in *y* direction perpendicular to foliation, and if possible in *z* direction to estimate the block size of the area. Fracture frequency collected in *y* direction gives commonly the highest value.

continuous image of the subsurface structures. The penetration depth and the resolution of the method depend on the signal frequency and the material property, such as electrical conductivity and dielectricity. High antenna frequency (MHz) will give good data resolution but shallow penetration depths and visa versa. The GPR profiles were acquired using a frequency of 50 MHz and a shot point interval of 1 m, with a GPR system called Sensors & Software Pulse EKKO 100. This gives reasonable resolution of the structures in the subsurface, but limits the penetration depths to about 30, and not more than 50 m. The velocity analysis (processed CMP-gathers) performed in the area gave an average velocity to deep structures of 0.11 m per nano-seconds (m/ns), which were used for depth conversion.

3.3.2. Refraction seismics

The seismic survey consists of one slope parallel profile with E–W strike and two down-slope profiles with ~N–S strike, totalling 1440 m. The seismic profile presented has a total length of 420 m with a NNW–SSE strike. For the seismic profiles the geophone spacing was 10 m, with a total of 24 14 Hz vertical geophones depending on operator. Shot point interval was 30 to 300 m with 100 to 600 g of dynamite as energizer for each shot (Rønning et al., 2006).

The seismic method is based on the recording of first arrival times of P-wave travel time of waves in the subsurface. The wave propagates with the elasticity of the material, and the range of the seismic P-wave velocity calculated from the travel time of the wave, commonly range from 200 m/s up to above 6000 m/s. In fractured bedrock the seismic velocity is reduced dependent on fracture frequency, texture and filling (Reynolds, 1997). The refraction seismic is a method that is developed principally for mapping of horizontal layers, and is dependent upon there being an increase in velocity with depth. If a layer has lower velocity than the above laying layer, the seismic wave will not be refracted in the right manner, but continue in depth and gives rise to the phenomenon called a *hidden layer*. This layer is difficult to detect and may be interpreted as part of the above laying layer (Reynolds, 1997).

3.3.3. 2D resistivity

The 2D resistivity survey consists of eight profiles, one oriented NE–SW, five slope parallel with E–W strike, and two down-slope profiles with N–S strike, totalling about 10.000 m. Here, a 420 m long section out of an 1800 m long down-slope profile is presented.

The resistivity method measures apparent resistivity (with unit Ωm) in the subsurface, which is a weighted average of all resistivity values within the measured volume (Dahlin, 1993; Reynolds, 1997). Measured apparent resistivities with different electrode configurations are converted into a true 2D resistivity profile through inversion (Loke, 2001). The 2D resistivity profiles were acquired according to the Lund-system (Dahlin, 1993). Acquisition was collected with both Wenner and Dipol/Dipol configurations, with an electrode spacing of 10 m for the shallow and 20 m for the deeper parts of the profiles. In a few short profiles the electrode interval was reduced to 5 and 10 m (Rønning et al., 2006). The depth penetration of the profile is approximately 130 m, with reliable data coverage to approximately 70 m depth. Slightly resistive material of 3000 to 10.000 Ωm, shown in blue colour in the profile, may indicate material such as fractured and water saturated bedrock (clay filled fractures commonly show resistivity response lower than 1000 Ωm). 10.000 to 35.000 Ωm, shown in green colours in the profile, indicate moderately resistive material, for example fractured and unsaturated bedrock or less fractured but water saturated bedrock. Highly resistive material, 35.000 to 150.000 Ωm indicated with orange to red colours in the profile, may consist of "unfractured" bedrock and dry, unconsolidated material.

3.4. Drill hole logging

All drill holes have been logged by geophysical methods such as water conductivity, water temperature, natural gamma ray, resistivity of the bedrock, and seismic P- and S-wave velocity. Here, only resistivity and P-wave data are shown from the lowest drilling site, which goes down to 150 m depth, are presented since the other logging results concur these logs. All geophysical logging were performed using Robertsson Geologging equipment (http://www.geologging.com).

3.4.1. Resistivity logging in drill holes

Resistivity is the inverse of electrical conductivity, and is thus easily derived from the measured conductivity value. The resistivity probe consists of one electrical current electrode and two potential electrodes; making it possible to measure in two configurations; long and short normal. For the long normal configuration (LN) the distance between the current electrode and the potential electrode is 64 in. (1.60 m), while for the short normal (SN) the distance is 16 in. (0.40 m). The penetration in the drill hole wall is commonly 1/5 of the electrode distance, and the resolution of the data collected depends on the contrast in conductivity. With such short interval in general, the probe can in detail map the apparent resistivity of the surrounding bedrock, often equivalent to the specific resistivity. The resistivity is affected by bedrock porosity, conductivity of the pore water, the shape of the pore and possible conductive minerals in the bedrock. For example, an increase in fracture frequency gives increased porosity, which reduces the resistivity (increased electrical conductivity). During data acquisition the probe is descended down the drill hole to log the electrical conductivity in the drill hole, calculated from the known current and the potential

Fig. 2. Relief map of the Åknes site with stereographic presentation of the fracture distribution compiled from all localities studied. The picture (lower left) outlines the inferred area involved in the rockslide (photo: M.H. Derron). The stereo plots show great circles (lower hemisphere equal area) of fractures mapped at different localities, where c. N–S striking fractures are black, c. E–W striking fractures are blue and fractures parallel to the foliation are red. Structural symbols outline tectonic boundaries along the margin and inside the rockslide area. The western boundary zone is a NNW–SSE striking and sub-vertical, strike-slip fault, whereas the eastern boundary zone is a pre-existing fault with shallow dip to the west. The upper boundary is seen as a pronounced back scarp. Low angle sliding surfaces daylights at two levels in the slope, marked with a red hatched line (sub-domain 2 and 4), while two sliding surfaces are mapped by geophysics, marked with red dashed lines (sub-domain 1 and 3). The foliation is folded and changes within the rockslide, strike 092/dip 44 (RHR) at the western boundary zone, 080/ 30 in sub-domain 2, and the toe zone differs from 066/20 to 093/32 (n=137).

difference between electrodes (Rønning et al., 2006). The maximum measurable resistivity with the logging equipment is 10.000 Ωm. If the true resistivity in the drill hole exceeds 10.000 Ωm, this is seen as constant maximum resistivity on the log. Due to the high conductivity in water the resistivity decreases in saturated fracture zones. It also decreases in clay-rich zones. As water and clay are extensively found in fracture and weakness zones, the aim for the resistivity analysis in drill holes is consequently to detect the low resistivity zones.

3.4.2. Sonic logging of P-wave in drill hole

The purpose of acoustic logging of drill holes is to determine the seismic velocity of the formation (bedrock). Seismic velocity is given in the unit metre per second (m/s). The probe consists of one transmitter and two receivers with an internal distance of 30.4 cm. The probe can automatically calculate the seismic P-wave slowness (inverse of velocity) from picks of first incoming P-waves for each centimetre in the drill hole. For each 20 cm, the full waveform train is transferred to the data logger, and from this, both P- and S-wave velocity can be calculated. Water- or air filled fractures in rock will increase the travel times and thus decrease the velocities, since the P-wave velocity in air and water are 330 m/s and 1450–1530 m/s respectively (Reynolds, 1997). By detecting the low velocity zones in the drill hole, one can discover weaknesses in the bedrock that may be relevant for defining the stability of the rock.

4. Results

4.1. Structural surface mapping

The rockslide reveals gneissic bedrock that is folded. There are significant variations in the orientation of the foliation, from very steep and E–W striking in the upper part, near the back scarp, to E–W striking and sub-horizontal in the lower parts (Fig. 2). This variation in foliation occurs over a few tens of metres. In the boreholes the average dip of the foliation is 31.7°, steepening slightly from top to bottom of the slope (27° to 34°) (Kveldsvik et al., 2006).

Structural bedrock mapping on exposures leaves a large part unmapped due to cover of vegetation and/or scree. Three distinct fracture sets are mapped within the rockslide; steeply dipping fractures with approximately N–S strike and E–W strike, and a third fracture set parallel to the foliation. The dominance and intensity of the different fracture sets vary between localities. The N–S fracture set is present at all localities; its strike varies from NNW to NNE–NE (Fig. 2).

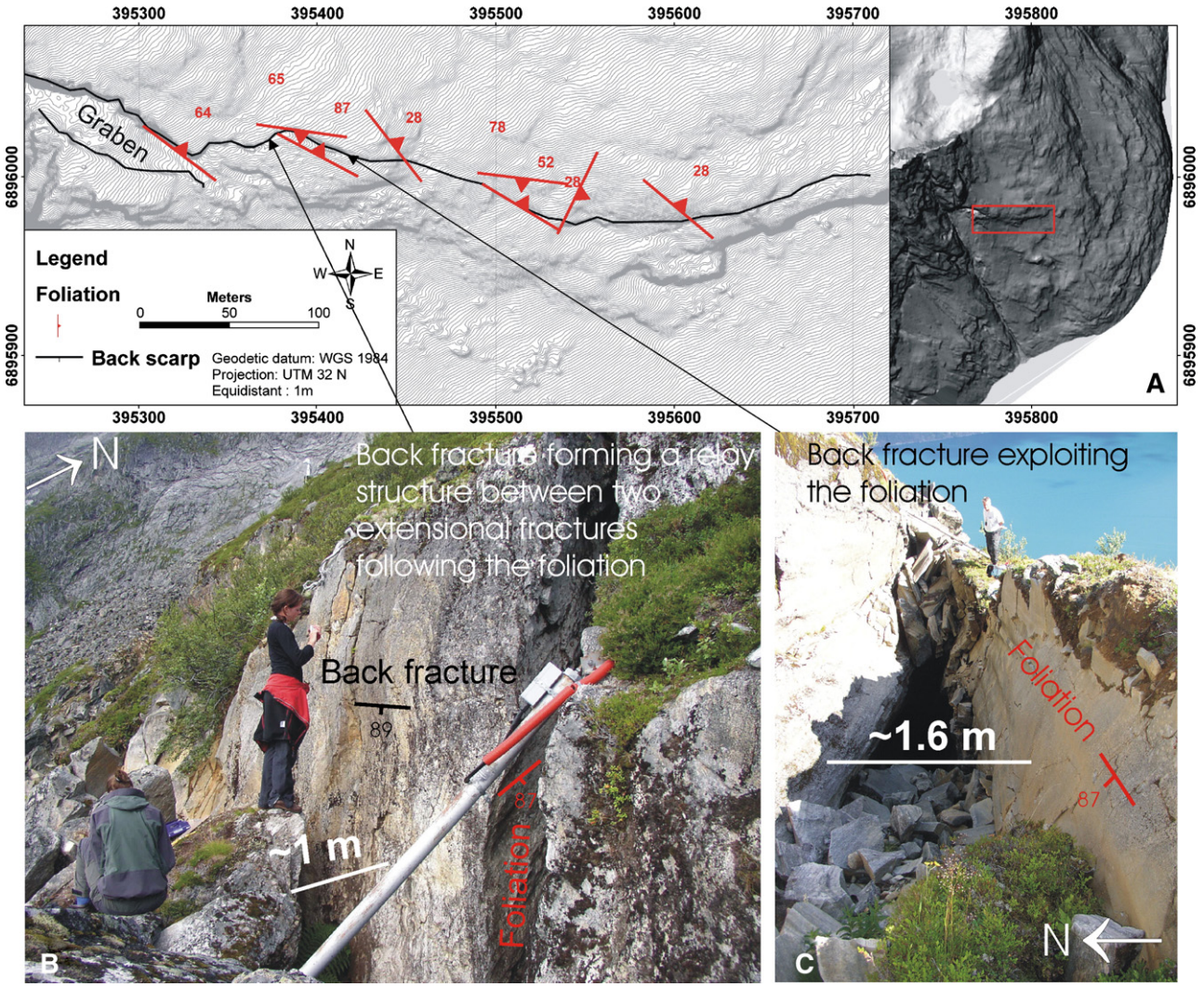

Fig. 4. The foliation of the bedrock controls the development of the back scarp. Where the orientation of the foliation is favourable for extensional fracturing (i.e. when sub-vertical or dipping down slope), the back fracture follows the foliation. In contrast, where the foliation is not favourable for reactivation, the back fracture reuses pre-existing fracture sets that commonly have an E–W strike, and is steeply dipping. Locally, the back scarp zone splits into segments that form relay structures (B). A) Map showing the back scarp zone and the foliation along this zone experiencing extension. B) Example of site where the foliation is not favourable and the back (extensional) fracture has formed a relay structure between two larger extensional fractures, the latter following the foliation. C) Example of back fracture that is controlled by the foliation, which is sub-vertical and undulating due to mesoscopic folding. Both localities are monitored by extensometers, recording the horizontal and vertical movements along the back fracture.

In contrast, the E–W oriented fractures are not present at all localities, but when present, are prominent. An example is the back scarp, which partly follows E–W fracture(s) (Figs. 2 and 4). The trends of these steeply dipping fractures follow the main trends of lineaments in the region (Gabrielsen et al., 2002; Henderson et al., 2006), of which the most pronounced lineaments coincide with major fjords. Chronological data of these structures have not been assessed.

Both outcrop and drill core studies indicate an increase in fracture frequency in and near biotite rich layers of the gneiss, and with the lowest fracture frequency in the fairly homogenous granitic gneiss (Ganerød et al., 2007). The fracture frequency in outcrops varies from 2 to 8 fractures per metre (f/m) in scan lines when measured parallel to the foliation (see Section 4.1 for scan line description). Perpendicular to the foliation, values as high as 23 f/m can be found. However, common values are in the ranges of 8 to 12 f/m. In the drill cores, the fracture frequency varies significantly, from 1 f/m in undisturbed rock to 50 f/m. The latter case is associated with fault rocks, such as breccias and gouge, which appears in discrete zones. In general it is difficult to distinguish between shear and extension fractures due to the lack of markers. However, when there is evidence of separation perpendicular to the fracture surface, the structures are called extension fractures.

Outside the rockslide, the fracture frequency is generally around 5 f/m. The highest fracture frequency occur perpendicular to the foliation, reaching 9 f/m, while the lowest fracture frequency is parallel to the foliation, with 2 f/m (Table 1). Fracture continuity of the different fracture sets has been estimated and varies within the different zones of the rockslide. For fractures outside the rockslide, the continuity parallel to foliation is 5 to 10 m, and for N–S trending fractures, 2 to 5 m. E–W trending fractures, while infrequent, are 1–2 m long (Table 1).

4.1.1. Back scarp zone

The back scarp zone is approximately 800 m long (Figs. 2 and 4). In the west, the first 200 m is a cliff face that has seen one or more rockslides. Thereafter follows a 20–30 m deep, 20–30 m wide and 150 m long graben that shows ongoing extension. The remaining 500 m is an overall open fracture. The extension along the back scarp decreases from the west to the east. The back fracture has a scissor shape, where the maximum width of 20–30 m is found on the western side, while the width decreases towards the east, where the maximum width is 0.5–1 m. The depth of the extensional back fracture is difficult to estimate, since the fracture is partially filled with scree, sediments and ice. The estimated depth in the western part is 60 m, and likely decreases to the east. The back fracture shows both vertical and horizontal separation with a general extension in the N–S direction, directly down-slope (Figs. 2 and 4).

A striking feature of the back scarp zone is the variability in orientation of bedrock foliation. North of this zone the foliation is nearly slope parallel (Fig. 2). In general, the back fracture is steep to sub vertical (Fig. 4), but changes along strike as the foliation is folded. The folds in the back scarp zone are on metre to decimetre scale, are close to tight and normally symmetrical and have short wavelengths. The axial surfaces are sub-horizontal, and the mean vector for the fold axis is 27° towards ESE. This folding makes the foliation change from sub-vertical to sub-horizontal over short distances as shown in Fig. 2 and 4. Where the orientation of the foliation is favourable for extensional fracturing (i.e. when striking ~E–W and dips sub-vertical or down slope), the back fracture follows the foliation (Fig. 4A and C). In contrast, where the foliation is not favourable for reactivation (i.e. when striking ~N–S and dips sub-horizontal), the back fracture reuses pre-existing fracture sets that commonly have an E–W strike, and is steeply dipping. Locally, the back scarp zone splits into segments that form relay structures. Most relays are hard linked in that connecting fractures are cutting across the foliation between segments (Fig. 4A and B). In the vicinity of the back scarp, extension fractures sub-parallel to the back scarp are common, showing a separation of 10 to 12 cm. Riemer et al. (1988) demonstrate that extension preferentially develops along the fold axis, as seen in the back scarp zone at Åknes.

In the back scarp zone all three fracture sets mentioned above are present. However, there is a dominance of N–S oriented fractures. The fracture frequency of the back scarp zone in general is low (Table 1). The length of fractures parallel to foliation is about 10 m. In contrast, N–S trending fractures are shorter (<2 m), as are the E–W trending fractures (2–5 m, Table 1). The combination of long and short connecting fractures and low fracture frequency gives the back scarp zone the largest block size of the site.

4.1.2. Western boundary zone

The western boundary zone is the structural limitation of the rockslide to the west (Fig. 2) and is defined by a steeply dipping, NNW–SSE striking strike slip fault. This fault forms a crevasse that is prone to snow and rock avalanches. The crevasse has cliff sides that are 10 to 40 m in height (Fig. 2). The boundary fault has an extent that exceeds the rockslide area; it can be traced as a lineament for several km. This pre-existing structure is old, probably dating back to the Devonian (Andersen et al., 1997; Braathen, 1999; Osmundsen and Andersen, 2001).

In the western boundary zone, the fracture frequency is generally low (Table 1). Continuity of fracture sets reveals similarities to the back scarp, with lengths of 6 to 10 m for foliation-parallel fractures, 2 to 10 m for N–S trending fractures, and 0.2 to 2 m for E–W trending fractures (Table 1). In addition, there is a NW–SE trending fracture set

Table 1
Fracture frequency (m^{-1}), continuity of fractures sets, and block size of the different zones of the rockslide area

Fracture frequency (m^{-1})	Back-ground data	Back scarp zone	Western boundary zone	Eastern boundary zone	Internal zones	Toe zone
Non-foliation parallel fractures	2	2	2	3	8	4
Foliation parallel fractures	9	5	7	13	17	11
Block size (cm)	10–50	20–50	15–50	~10–30	5–20	10–25
Continuity of fracture sets (along strike, m)						
Foliation parallel fractures	5–10	~10	6–10	10	6–10	10–20
N–S fractures	2–5	0–2	2–10	2	~5	~2
E–W fractures	(1–2)	2–5	0.2–2		1–2	~1
NW–SE fractures			0.5–1			

The value of each zone is an average based on 3 scan lines, perpendicular to and parallel to foliation, for each locality studied within that zone.

with 0.5 to 1 m length. Within the western boundary zone, N–S oriented, steeply dipping fractures dominate. This fracture set is sub-parallel to the strike of the fault, which is defined by a zone of heavily fractured rock (Fig. 2). In the upper part of this zone, there are several extensional fractures (Fig. 5A). Some of these fractures follow the E–W and N–S fracture patterns. Extensional separation along these fractures varies from 10 to 50 cm. Three rockslide events have been recorded along the western boundary zone (Kveldsvik et al., 2006, 2007). All three appear to have occurred as plane failures, with fractures parallel to foliation acting as the basal sliding surface and N–S and E–W oriented fractures acting as release surfaces.

4.1.3. Eastern boundary zone

The eastern boundary zone represents the eastern structural limitation of the rockslide area and is defined by a gently NW dipping, NNE–SSW trending fault. This structure is not well exposed in the

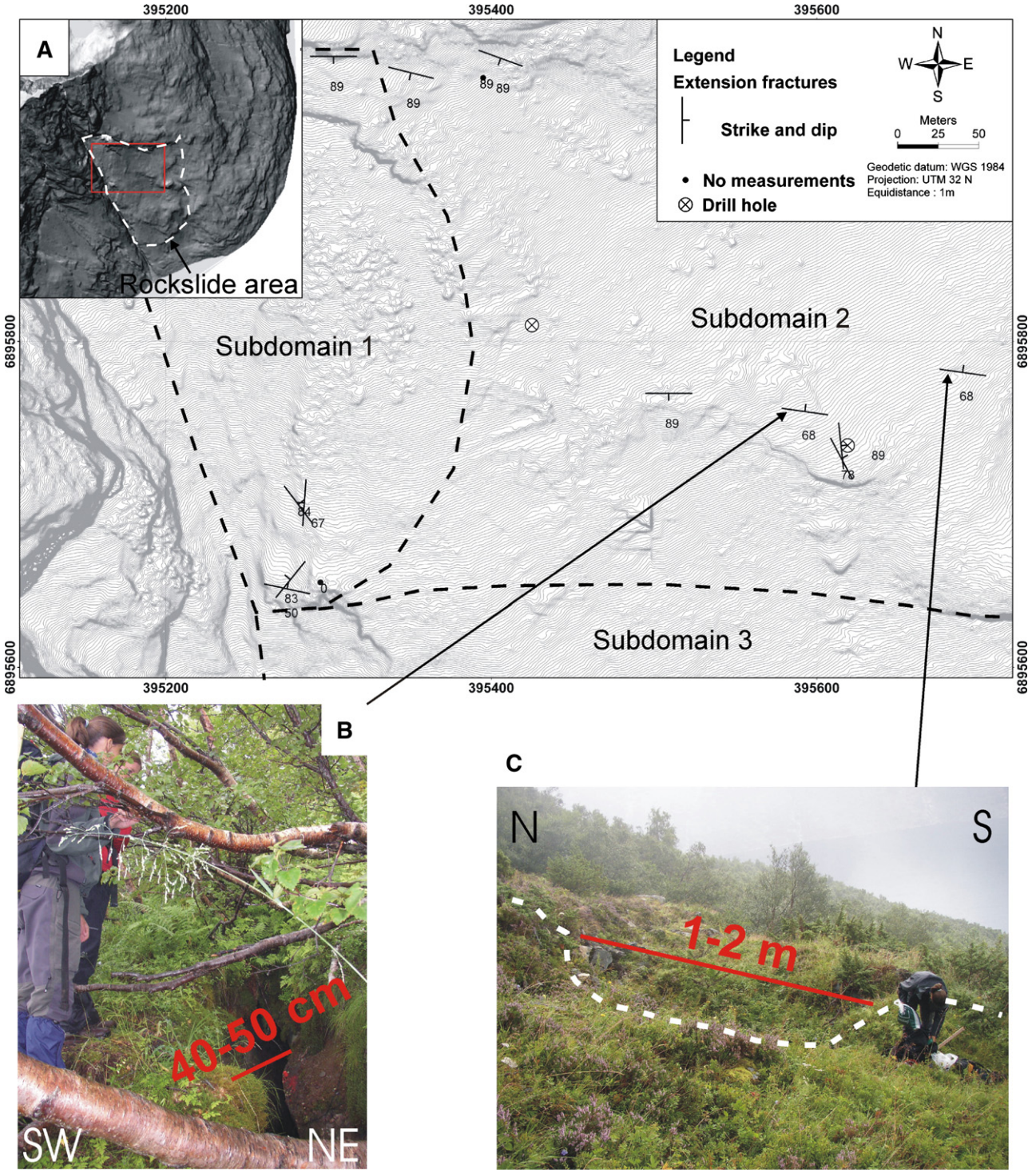

Fig. 5. A) Extensional fractures located in the Åknes slope. In sub-domain 1 are pre-existing fractures oriented c. N–S and c. E–W reactivated by extension, with separation up to 50 cm. In sub-domain 2 are extension fractures that are slope parallel observed as shown by example B) and C). These extension fractures are oriented perpendicular to the movement direction (c. E–W trending and 60–90° dip to N–NNE), and are fractures probably caused by the movement of the rockslide.

topography (Fig. 2). The fault zone is characterized by heavily fractured rock sub-parallel to the well defined fault plane (089/48). No fault rock has been found along the fault zone.

The fracture frequency is higher perpendicular to the foliation (7 to 21 f/m), than parallel to the foliation (1 to 5 f/m) (Table 1). Fractures parallel to foliation are the longest, commonly in the range of 10 m, whereas N–S trending fractures reach 2 m (Table 1). E–W oriented fractures are absent. The foliation is in general dipping 44° to the south, which is steeper than the general trend of the foliation in the rockslide.

4.1.4. Central zone

The central zone of the rockslide area (Fig. 1B), within the boundaries described above and below, reveals a sub horizontal to gently folded foliation that dips moderately towards the fjord. Folding causes an undulating geometry of the foliation. Locally, the foliation reveals more intense folds causing significant variation in the orientation. In areas where the bedrock is more intensely folded, there are hilltops and scarps suggesting that these sites are more resistant to denudation. A sliding surface in biotite rich to biotite-schist layers is mapable in outcrops of the central zone (Fig. 2). This shear zone is heavily fractured with a width of 20 cm, similar to that described below and illustrated in Fig. 6. Gouge can be observed as pockets along fractures, however most fractures have a rock-on-rock contact. This sliding surface forms the lower limit of sub-domain 2.

The fracture frequency of the central zone is the highest recorded in the rockslide area, with the highest frequency perpendicular to the foliation (average of 17 f/m, Table 1). Parallel to the foliation, the fracture frequency is 8 f/m. The length of the fracture sets is comparable to the other zones (Table 1). The high fracture frequency in combination with fracture length gives the smallest block size (Table 1), consistent with the observations that the central zone is heavily fractured and blocky on the surface.

A striking feature in sub domain 2 is the occurrence of large extensional fractures striking approximately E–W, perpendicular to the direction of movement of the rockslide area (Fig. 5). These extensional fractures have an irregular shape and have a dip of 60° to 90°

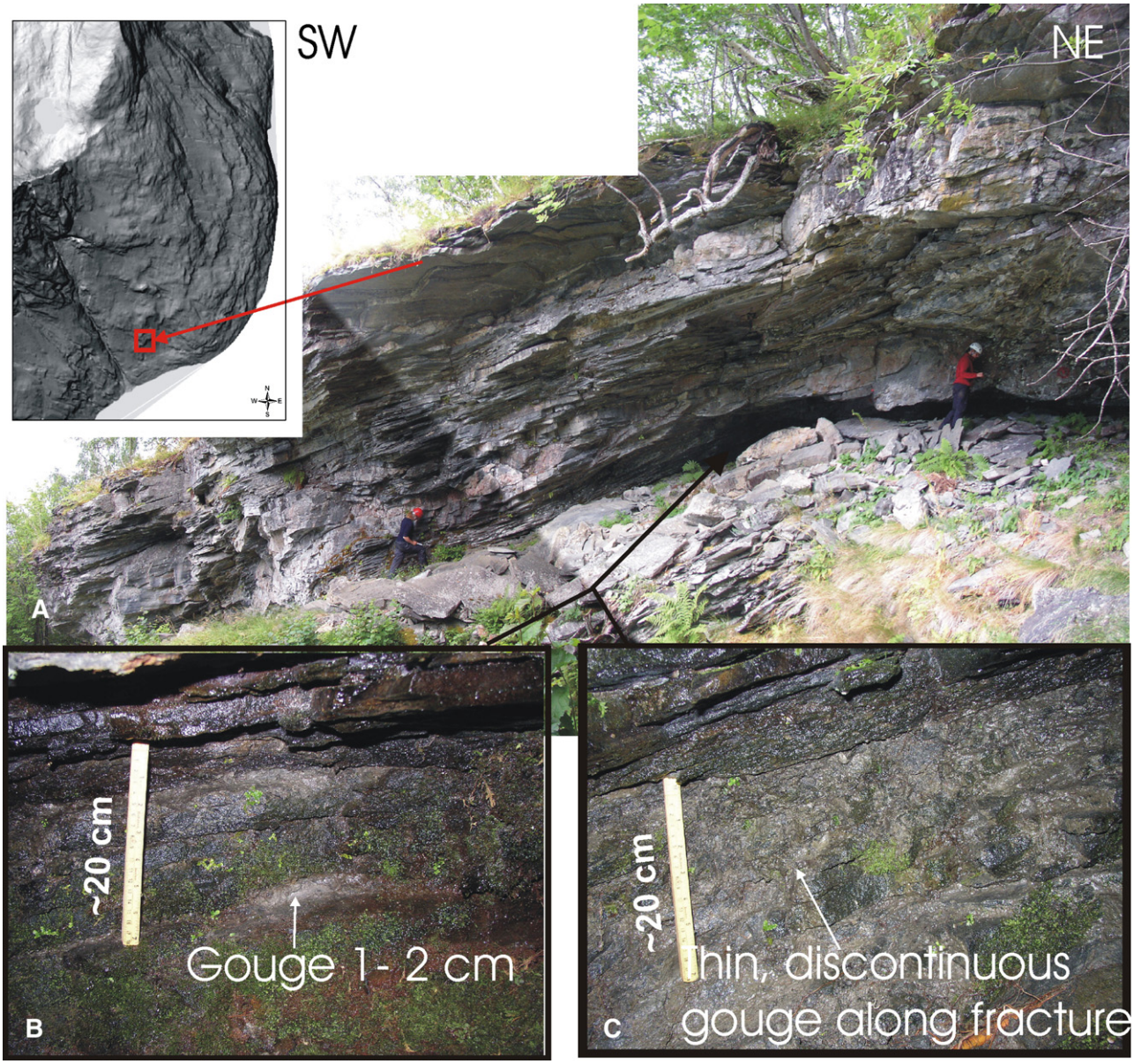

Fig. 6. A) Sliding surface of the toe zone where the basal thrust daylights the rock slope surface. Due to upward and forward separation, the transported block is pushed on top of the vegetated slope, causing the formation of a rock overhang that partly has caved in. B) Fault gouge is located as a thin layer (1–2 cm) with undulating thickness along the shear surface. (C) Example of a network of thin gouge layers that fill fractures within the intensely deformed zone of the sliding surface. This sliding surface is exposed for at least 50 m along strike, and the thickness of the gouge rich zone is approximately 20 cm on average along the exposure. The moss growing on the fractured zone indicates water seepage.

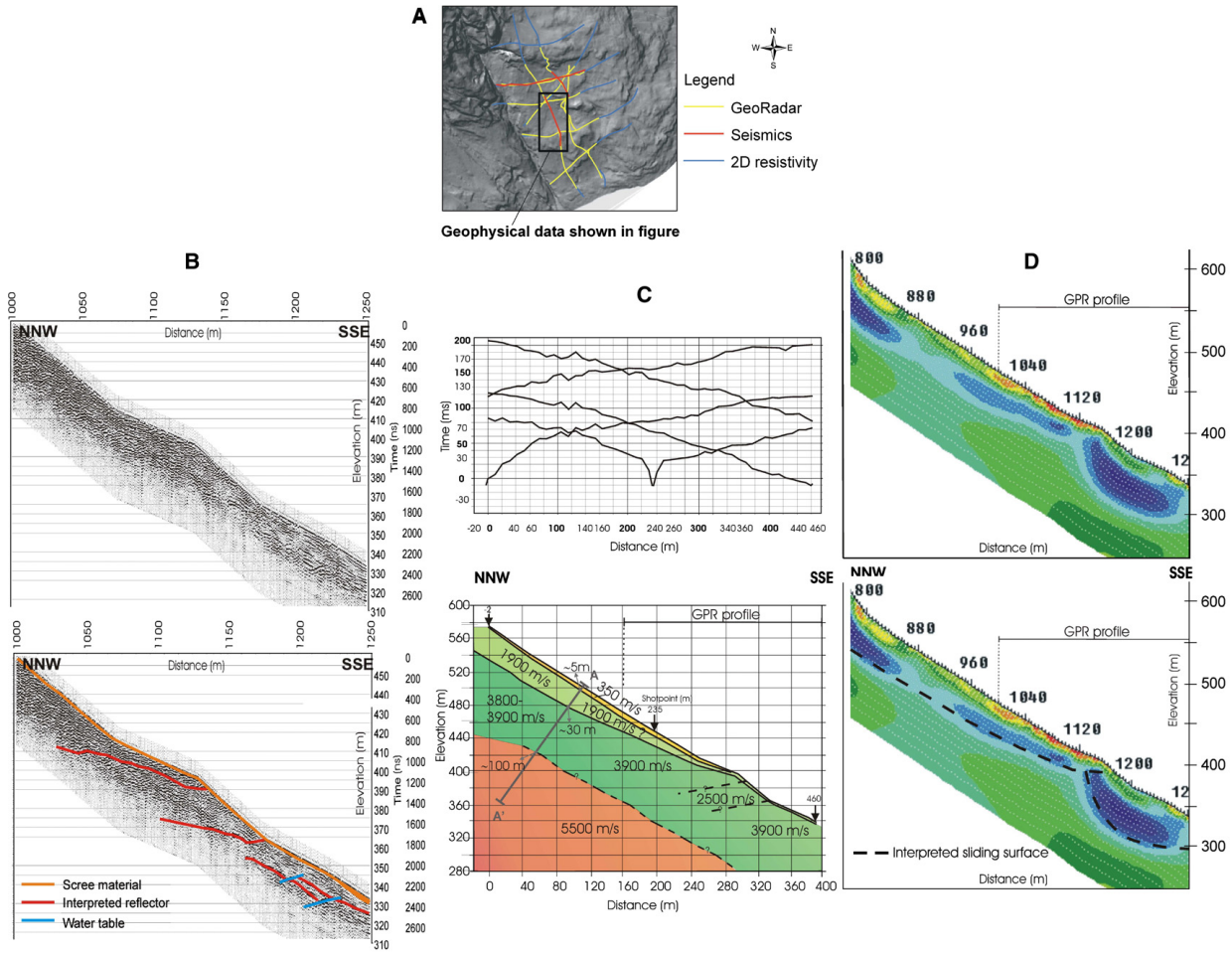

Fig. 7. Geophysical data from Åknes. A) Map showing all the geophysical profiles collected in the rockslide area. The presented profiles b–d are only a selected section of a profile. Profile c and d are the same section, c. 450 m long, while b is 250 m long and its location is marked in profile d. B) GPR profile with NNW–SSE orientation and approximate 35 m depth penetration. Above, profile without interpretations, below; profile showing shallow, undulating structures, interpreted to be foliation-parallel layers that crop out at the slope surface (marked with red lines). C) Refraction seismic; above travel time (ms) vs. distance (m) for first arrival P-wave traces. Below, schematic profile showing four layers with increasing velocities with depth. A–A` is line of cross section for thickness estimates. D) 2D resistivity profile, measured with Wenner configuration, showing layers with different resistivity. Above, profile without interpretation, below; profile showing an undulating resistivity contrast, interpreted as a sliding surface at the bottom of the low resistivity (blue) layer marked with black dashed lines. The profile has the same location as the seismic line (c).

in a northerly direction. The separation on these fractures is slope parallel, and varies from 40 cm to 2 m (Fig. 5). Extensional movement can also be seen on N–S striking fractures, with separations of 10–30 cm, which are mapped throughout sub domain 1 and 2. The latter described fractures are probably rather frequent, but abundant coverage of scree and vegetation makes this a qualitative assessment.

4.1.5. Toe zone

The toe zone is defined by a major sliding surface that daylights the surface (Fig. 6). When observed, this sliding surface is near-parallel but shallower dipping than the topographic slope, with an orientation differing from 066/20 to 093/32. In the hanging wall, rocks are transported both upward and down-slope forming rock overhangs, at places developed into narrow, shallow caves. In these overhangs, slabs of rock have broken off along the foliation, emphasising the position of the sliding surface (Fig. 6A). The sliding surface is defined by fault rock along biotite rich layers of the bedrock, as shown in Fig. 6. Locally, the sliding surface is made up of a narrow (<20 cm) heavily fractured zone. Along the long, nearly continuous exposures of the sliding surface, the fault rock interval is up to 2 cm thick (Fig. 6B). The gouge layers form along-strike, metre-long lenses and/or continuous membranes of variable thickness, commonly in the range of some millimetres to a few centimetres. They are also seen in a network of shear fractures that are filled with gouge (Fig. 6C). The gouge is fine grained and is light grey to dark grey. It contains clay size minerals with some (10–20%) rock fragments. Gouge mineralogy derived from XRD-analysis includes micas, quartz and plagioclase, with micas spanning from smectite, chlorite, and kaolinite to serpentine. Where the sliding surface is defined by a heavily fractured zone, parts of the sliding surface are characterized by rock-on-rock contact. Groundwater springs are common along the sliding surface (Fig. 6), where both seepage and discrete outlets form.

The fracture frequency in the toe zone is in general 11 f/m for foliation parallel fractures and 4 f/m for non-foliation parallel fractures (Table 1), with the foliation-parallel fracture set dominating (Figs. 2 and 6). The length of the foliation-parallel fractures is 10–20 m, whereas the N–S trending fractures are about 2 m and the E–W trending fractures approximately 1 m (Table 1).

4.2. Subsurface mapping

4.2.1. Ground Penetrating Radar (GPR)

The profile shown in Fig. 7B is a 250 m long segment of a profile with a total length of 1150 m. Close to the surface, the reflectors of the GPR profile are parallel to the slope with a thickness of 1 to 3 m. This first layer is interpreted to be scree material or other debris (Fig. 7B). Reflectors at depth that are sub-parallel to the surface are interpreted to reflect the foliation-parallel fractures in the bedrock (Fig. 7B). Two of the interpreted reflectors (marked in red, Fig. 7B) daylight the surface in the same area as mapable features of the seismic and 2D resistivity profiles, indicating that multi-property layers are daylighting (Fig. 7). This is interpreted to be a sliding surface. Due to the limited depth penetration, GPR cannot give any information of the extent or depth of the sliding surface. However, the method gives detailed information of the shallower subsurface. The second layer, about 25 m thick, is interpreted to consist of heavily fractured and drained bedrock, and is comparable to the second zone identified in the seismic and 2D resistivity profiles (Fig. 7C and D) as well as in the drill hole (Fig. 8).

4.2.2. Seismic

The seismic profile can be divided into four zones or intervals (Fig. 7C). The first, near surface zone is up to 5 m thick and has a seismic velocity of 350 m/s. This zone (indicated in yellow colour in Fig. 7C) is interpreted to consist of scree material. The second zone has an approximate thickness of 30 m in the upper part and thins down to 3–5 m down slope; the seismic velocity is about 1900 m/s. This zone is interpreted to consist of heavily fractured rock that is unsaturated (light green colour Fig. 7C). The third zone is approximately 65 m thick, extending down to about 100 m depth (green colour). It has a seismic velocity of 3800–3900 m/s. This interval likely consists of water saturated, fractured bedrock (Fig. 7C). The fourth and deepest zone extends below the seismic resolution, and has a seismic velocity of 5500 m/s. This indicates good rock quality and is consistent with less fractured rock that is water saturated (orange colour, Fig. 7C). A schematic cross section is presented in Fig. 6C to illustrate estimated thickness of the different zones, which also match thicknesses from the drill hole (Fig. 8).

Between 300 and 330 m along the seismic profile, a low angle zone reaching the surface has a seismic velocity of 2500 m/s. This is a lower seismic velocity than the surrounding material at 3900 m/s, consistent with high fracturing or porous rock (fault rock). The mapable, low velocity layer has a length of 30 m at the surface. Due to methodological weakness it is not possible to map the dip of the zone. The low velocity layer might be a rather thin zone lying as a hidden layer between the 1900 m/s (light green) and 3900 m/s (green) layers (Fig. 7C).

4.2.3. 2D resistivity

The 2D resistivity profile in Fig. 6D shows zonation that is interpreted to consist of an approximately 5 m thick layer of scree material at the top (red to orange colour). Below that is a 10–20 m thick layer (light green colour) interpreted to be heavily fractured and drained rock. The next layer has the lowest resistivity (blue colour). This layer is about 20 m thick and is interpreted to consist of heavily fractured rock that is water saturated. This low resistivity layer is undulating and, when followed down-slope, daylights the surface at about 1200 m (blue colour, Fig. 7D). Another segment of the low resistivity layer continues down-slope. The sliding surface is interpreted as being located at the bottom of this low resistivity layer (blue colour). Near the base of the profile is a layer with medium resistivity (green colour), interpreted to consist of less fractured and water saturated bedrock (Fig. 7D).

4.2.4. Drill hole data

The bedrock logged in the drill cores is the same heterogeneous gneiss as mapped in outcrops, altering from medium grained granitic gneiss, through dioritic gneiss to biotite-rich gneiss (Fig. 8). The folded foliation mapped in outcrop scale (metres) is confirmed in centimetre-scale in the cores, where the folds are close to tight with short wavelength (Fig. 8B). The dominating fractures in the drill core are parallel to the foliation, while the other two existing, steep fracture sets mapped in outcrops are under-represented in the vertical drill hole. The fracture frequency of the drill cores decreases with depth, as shown in Fig. 8. In the upper few metres (0–5 m), fracturing is intense and core loss is abundant (Fig. 8A). The following interval (5–42 m) is heavily fractured with a fracture frequency up to 22 f/m. Several zones up to 40 cm thick with crushed rock occur in the interval 18 to 23 m, one with a fracture frequency up to 50 f/m at 22 m depth (Fig. 8A). Fault rocks, such as gouge, occur in narrow zones of up to 5 cm thickness, while a 30 cm thick breccia zone is observed at 21.5 m depth (Fig. 8C). This interval is unsaturated, since the water table is located at 42 m depth (Fig. 8A). However, the groundwater level fluctuates seasonally. The first two intervals have no recording of resistivity or P-wave velocity in bedrock due to the lack of water in the drill hole (Fig. 8A, Rønning et al., 2006). The next interval (42–70 m) consists of heavily fractured rock that is water saturated. This section has a fracture frequency up to 25 f/m, with an average of 7–9 f/m (Fig. 8A). There are large irregularities in both resistivity and P-wave response, giving very low values at several depths in this interval. The suggested location of the sliding surface in the drill core is at 62 m depth, where a zone of heavily fractured rock (25 f/m) and fault rock occurs. The sliding

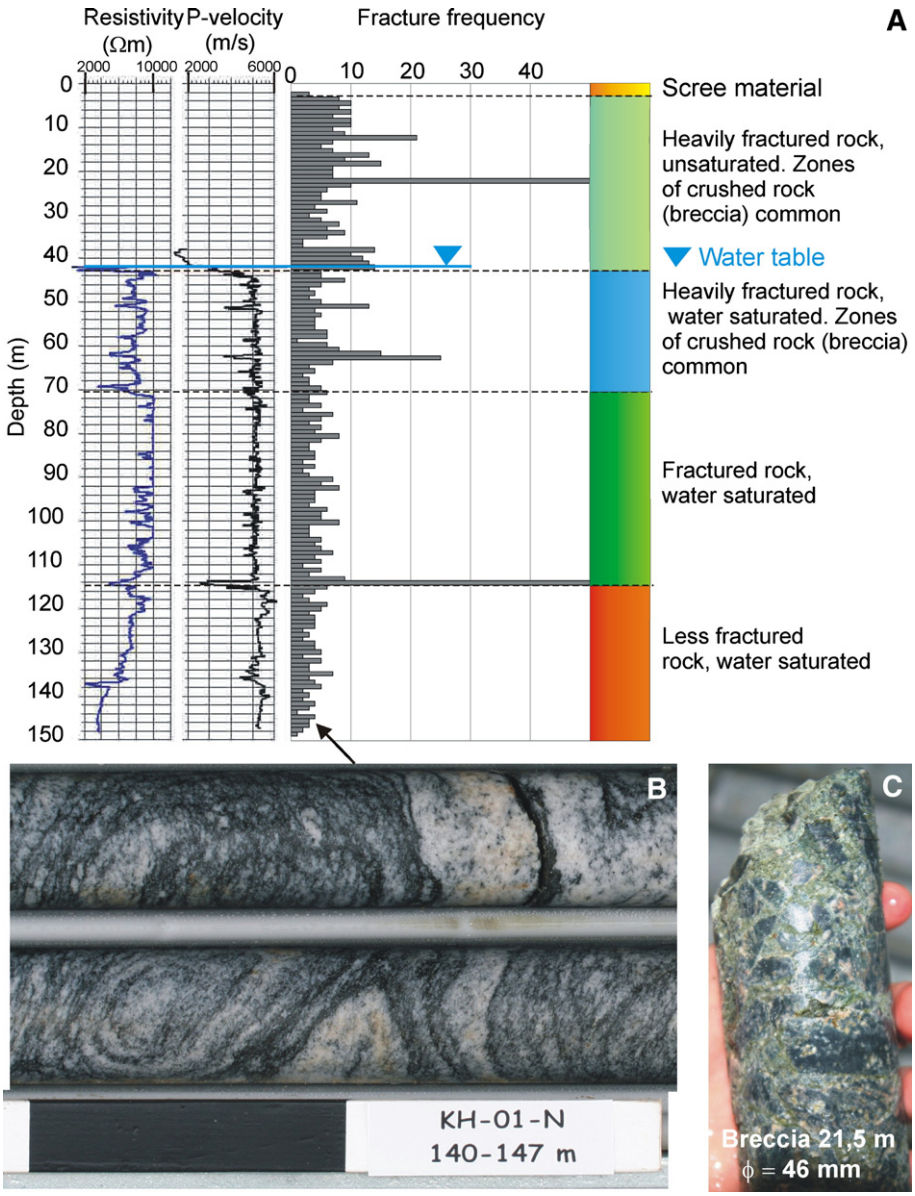

Fig. 8. A) Drill hole and drill core data that show that the fracture frequency decreases with depth. Five zones can be identified on the basis of fracture intervals and responses in the resistivity and P-wave logs of the borehole walls. The colour codes are based on the zonation in the 2D resistivity profile given in Fig. 7D. This colour code is implemented on all subsurface data, to visualise the zonation in the subsurface, with the exception that the blue and green zones in the drill core and 2D resistivity coincide with the green zone in the seismic. B) Drill core showing that the bedrock is a granodioritic gneiss with a folded penetrative foliation on cm-scale. C) An up to 30 cm thick (proto-) breccia that occurs at 21.5 m depth.

surface is thin (max 20 cm) and the occurrence of gouge and ultrabreccia is patchy with a maximum thickness of 1–3 cm (Fig. 8). The following interval (70–115 m) is less fractured, with an average of 5–10 f/m. The interval is water saturated (Fig. 7A). The resistivity and P-wave response for this interval reveal high resistivity levels from 8000 to more than 10,000 Ωm and a seismic velocity of about 5000 m/s (Fig. 8A). There is a local minimum in both resistivity and P-wave at 115 m depth that coincides well with a 50 cm zone of heavily fractured rock in the drill core that has a fracture frequency of 50 f/m (Fig. 8A). The deepest interval (115–150 m) has a low fracture frequency (3–5 f/m), which is regarded as background fracturing. The drill core section is divided into five intervals (Fig. 8A).

5. Recorded movements of the slope

The rockslide area at Åknes was brought to the public's attention in 1964 by local residents claiming that the back scarp was widening (Sandersen et al., 1996). Monitoring of the back scarp started in 1986 with the installation of two pairs of bolts for manual reading. In 1989, an additional five pairs of bolts were installed. A continuous surveillance program started in 1993 with three extensometers, and was extended to five extensometers in 2005 (Fig. 9). Measurements indicate a more or less steady rate of movement in the back scarp from 1986 to the present (Braathen et al., 2004; Kveldsvik et al., 2006); the long-term average velocity varies from 1 to 3 cm/year. The angle

Fig. 9. Average annual slope movements recorded in the period 2004–2006. The vectors represent average total displacement per year. Measurement points no. 1–8 and 14–23 were established in 2004, while point no. 9–13 was established in 2005. Recordings from points no. 6 and 9–13 are not consistent or significant, and thereby not represented by a displacement vector. Maximum movements are recorded on the upper part of the slope, close to the back scarp and along the crevasse to the west (western boundary zone). The extensometers are placed in telescopic steel pipes fixed on each side of the back scarp and are N–S oriented.

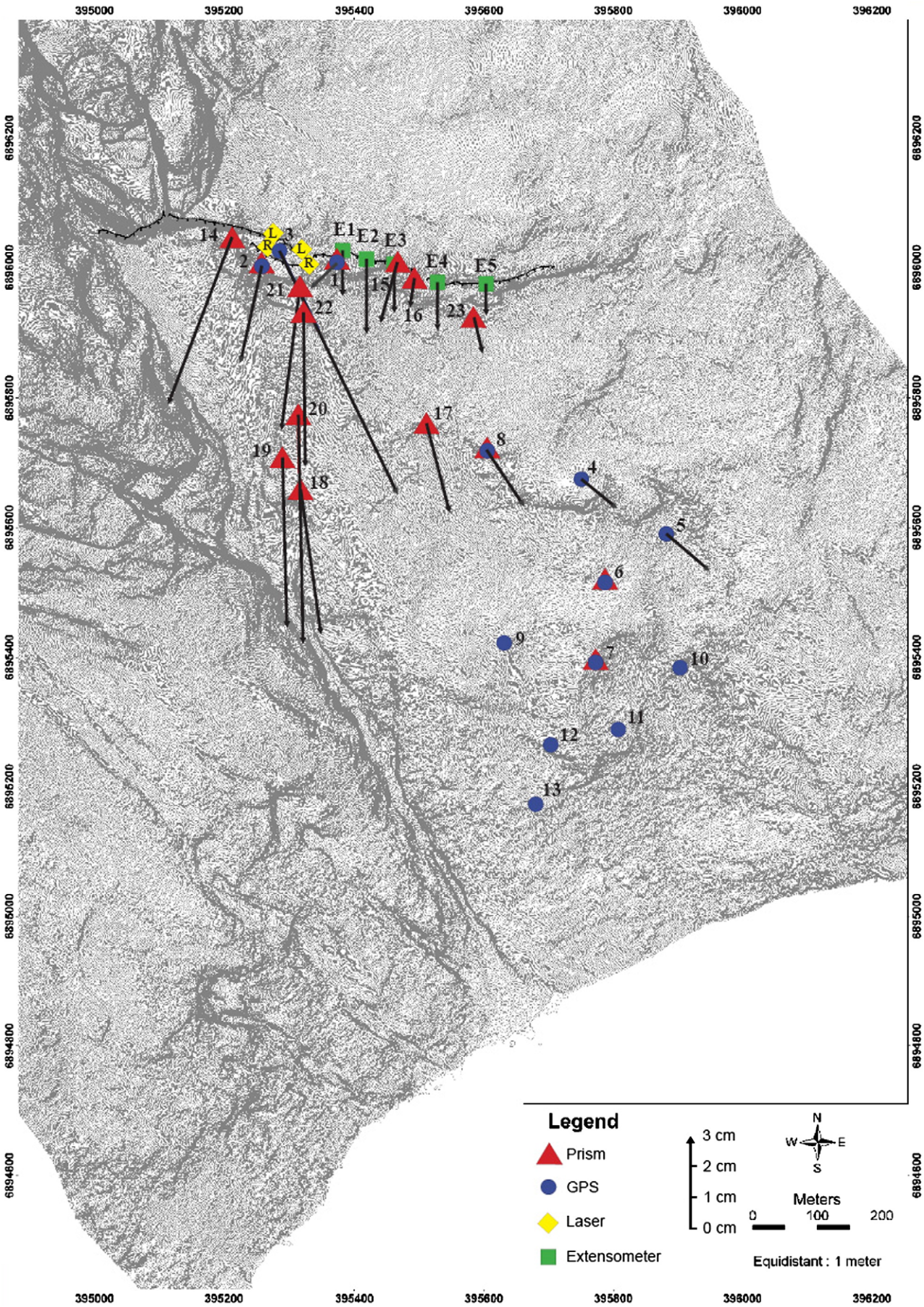

between extensometers 3, 4 and 5 and the strike of the back scarp is not perpendicular, which implies that the true displacements per year exceed the recorded displacements.

A network of GPS-points and reflection prisms for total station geodetic monitoring was established throughout the area in 2004 (point no. 1–8 and 14–23) and 2005 (point no. 9–13, Fig. 9). The analysis of the surface movements is based on recordings from 13 GPS points and 16 prisms, of which 5 of the monitoring points were measured by both GPS and total station. Measurement campaigns have been carried out twice a year, and show consistent movements in the upper part of the area for most points (Eiken, 2006). In the lower part, the area is vegetated and unsuited for reflection points. Furthermore, the GPS measurements are hampered by uncertainty, due to unfavourable conditions for satellite signal reception. The dataset is summarized with displacement vectors in Fig. 9, representing annual displacements, calculated as the average displacement from the two years of recording. The orientation of the vectors is shown as the lateral orientation of the total displacement vector at the last recording in 2006.

Two laser distance metres were installed in 2005 for monitoring of the graben structure along the western part of the back scarp (Fig. 9). The graben structure, with an estimated volume of 10–14 million m^3, is believed to move independently from the rest of the slope failure, with a velocity on the order of 14 cm/year in an S–SE direction (GPS point no. 3).

Surface displacements indicate creep of the whole unstable rock slope, divided into two separate sliding bodies, sub-domain 1+2 and sub-domain 3+4. The maximum movements are recorded on the upper part of the slope, close to the back scarp and the crevasse to the west, which explains the scissor shape of the back fracture with large displacements to SW–SSW at the western side and smaller displacements to S–SE at the eastern side (Fig. 9). Sub-domain 1, includes the graben structure moves differently than the other domains with a larger displacement rate in SW to SSW direction (point 18–20, Fig. 9). This is most likely due to the lack of lateral support on the western flank. Sub-domain 2 shows a lower magnitude of displacement, with the vectors oriented in S to SSE direction (point 8 and 17, Fig. 9). In sub-domain 3, represented by points no. 4, 5 and 8, displacements are recorded toward SE on the order of 1.5 to 2.5 cm/year. In sub-domain 4, measurements are not consistent and some of the points do not show a significant displacement during the period 2005–2006 (Fig. 9). However, all points (points 10–13) in the lower part suggest a positive elevation change on the order of 1 to 3 cm/year (Fig. 9). This indicates a zone of compression and thereby thickening above a sliding surface in the area, supporting existence of the toe zone mentioned earlier.

6. Discussion

6.1. Geological model based on observations

Observations and interpretations of data described above form the basis for the geological model of Åknes rockslide area, as illustrated in Fig. 10. The style of deformation, with bearing on the geometry of the rockslide area, is that of an extensional fault system at the top and an imbricate thrust fan further down-slope. In other words, the rock slope failure can be divided into two; an upper part experiencing extension (Figs. 1 and 4), and a lower part deforming by compression (Figs. 1 and 6). The basal sliding surface split into four subordinate layers that are partially stacked upon each other and bound by sliding surfaces, two that daylight the surface (sub-domain 2 and 4) and two indicated by geophysics (sub-domain 1 and 3, Fig. 10). The depth to the sliding surfaces differs within the four layers. In an east-west cross-section, the depth to the sliding surface shows a general increase to the west and decrease to the east. Down-slope, the sliding surfaces have roughly the same depth, and cut up-section near the toe of the thrust sheet (Fig. 7 and 8). The length and width of the sliding blocks are fairly similar (Fig. 10).

To summarize, the structural mapping of the area shows that the foliation is undulating along and across the slope. It controls the

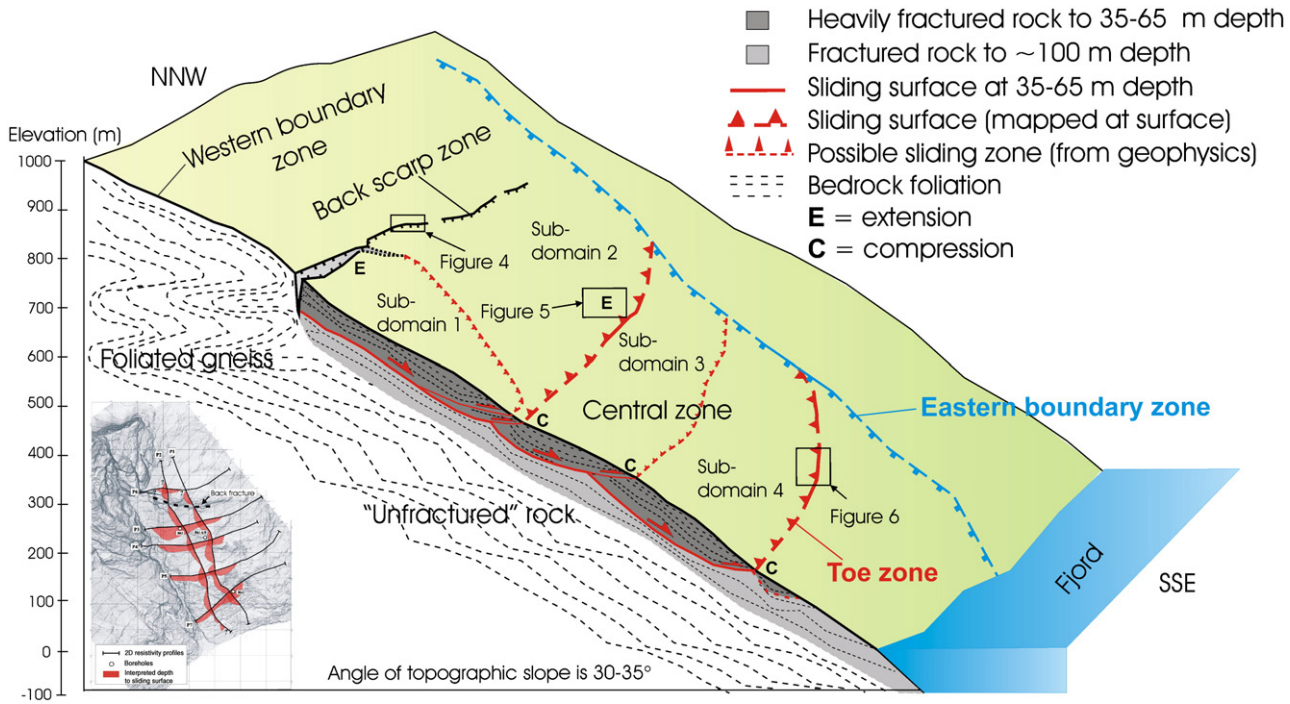

Fig. 10. Geological model of the Åknes rockslide. The block diagram summarizes field observations and geophysical data. Interpretation of structural data correlated well with structural interpretation from the 2D resistivity profiles, suggesting an undulating basal sliding surface with subordinate sliding surfaces that crop out at several levels of the slope. The rockslide can be divided into four sub-domains with different structural characteristics and displacement patterns, where two of the marked sliding surfaces are mapped at the surface and two sliding surfaces are interpreted from geophysical data (2D resistivity). The depth to the basal sliding surface varies, but in general increases towards the west. Structural constraints of the rockslide area to the east and west are pre-existing faults. The top is delineated by an extensional back scarp. The toe zone forms the lower limit of the rockslide are. The foliation is folded, especially in the back scarp zone, but also shows gentle variations down-slope and across-slope, as indicated in the figure by black dashed lines.

development of the back scarp and the basal sliding surface and its subordinate thrust zones. Along the back scarp, extension perpendicular to the fold axis is common when it is favourable, giving open fractures along the sub-veritcal foliation (Fig. 4C). Down-slope the foliation is sub-parallel to the topographic slope, and where the foliation dips shallower than the slope, there are thrusts daylighting the surface as seen at two levels down-slope (Figs. 2 and 6). The rockslide area can be further divided into five zones based on surface characteristics, where the upper structural limitation of the rockslide is the back scarp zone with its scissor like shape (Figs. 2, 4 and 9). The separation along the back scarp zone is gradual and constant on a yearly basis, with a larger movement of the western side than on the eastern (Fig. 9). The western boundary zone is the structural western limit of the rockslide area with a prominent crevasse formed along a NNW–SSE trending strike slip fault. The displacement data show that the upper western part of the rockslide area has the largest movement rates (cm/year), with a SW displacement vector towards the crevasse (Fig. 9). The eastern boundary zone is inferred as the eastern structural limit of the rockslide area (Fig. 2). The displacement along the eastern boundary zone is low or absent, as shown in Fig. 9, most likely due to lack of points of measurement or low satellite signals in the densely vegetated and steep terrain. However, the movement is inferred to be rotational with maximum rotation in the upper part of the zone. The central zone of the rockslide can be divided into four sub-domains separated by subordinate, low angled, sliding surfaces mapped on the surface and interpreted from geophysics (Figs. 2 and 10). In sub-domain 2, several extensional fractures with slope-parallel separation of up to 2 m are located (Fig. 5). These structures have formed perpendicular to the displacement direction (Fig. 9). The total displacement of sub-domain 1 and 2 is larger than that measured for the sub-domain 3 and 4 (Fig. 9). The latter sub-domains has less distinct features, but the occurrence of springs increases down-slope. The toe zone is the lower limit of the rockslide and is defined by a subordinate sliding surface that can be observed at the surface (Fig. 6). The sliding surface is mapped as a low-angle thrust that is more or less continuous. The displacement data for the toe zone is somewhat contradictory, but the general trend seems to be a considerable portion of upward movement (Fig. 9). This fits well with the interpretation of the sliding surface as a thrust ramp that daylight the surface, consistent with compression in the toe zone (Fig. 10).

An interpretation of the eight 2D resistivity profiles in a tied grid, supplemented with drill hole data, GPR and seismic profiles, formed the basis for the mapping of the subsurface with respect to the sliding surfaces (Fig. 7) and, furthermore, the geological model of the rockslide area (Fig. 10). The structures interpreted in the subsurface from geophysical data coincide well with structures mapped on the surface. In addition, the geophysical data indicate the position of the sliding surfaces in the subsurface (Figs. 7 and 8). The two sliding surfaces mapped on the surface (Fig. 2) are also well covered with geophysical data, indicating the extent of the sliding surfaces where they are covered by vegetation and scree. Furthermore, this forms the basis for the extrapolations of the sliding surfaces where they are not exposed (Figs. 2 and 10). The geophysical data indicate two additional sliding surfaces (Fig. 10), with similar signatures to the two observed at the surface. This divides the central zone into four sub-domains as indicated in Fig. 10. All the sliding surfaces interpreted by 2D resistivity have an undulating character, and daylight the surface along the slope. They are shown as low resistivity zones and the sliding surfaces are interpreted to be located at the bottom of these zones (Figs. 7 and 8). The geophysical data also supports the location of the larger structures forming the western boundary, as a sub-vertical structure, and eastern boundary as a gentle, westward dipping structure.

The estimated area and succeeding volume of the four sub-domains are given in Table 2. The preliminary volume estimate of the rockslide is based on a sliding surface at 50 m depth, therefore volumes of the sub-domains with a 50 m deep sliding surface is included in the estimate (Table 2). A basal sliding surface at 65 m depth, as presented here, is more likely and following volume estimates are given (Table 2).

The displacement pattern of the rockslide area is complex (Fig. 9). Extension in an N–S direction characterizes the back scarp zone. A division into four sub-domains fits well with the pattern of movements of the rockslide area. Sub-domain 1, with the graben structure to the west comprises the area with the largest displacement rates, up to 14 cm/year, and has displacement in a S–SW direction (Fig. 9). The displacement rate is less in the other sub-domains and in general decreases down-slope (Fig. 9). Sub-domain 2 shows a more southerly to southeast displacement direction with up to 5 cm/year (Fig. 9). Sub-domain 4 has no displacement direction but shows slight (vertical) upwards movement (Fig. 9), which sustain the indications of compression of the toe zone (Fig. 10).

All observations of the basal sliding surface indicate that it is undulating. Undulations can be caused by three scenarios; 1) growth of the sliding surface as segments, where the undulating composite surface is made up of several connected slip planes and where undulations are found at broken fault segments. 2) heterogeneous biotite schist layer extent and distribution, where layers of biotite schist are linked by fractures, and 3) reactivated folded foliation. Due to the evidence that the foliation is folded, as shown in Figs. 2, 4 and 8, and the fact that the foliation controls the development of the basal sliding surface with its subordinate low angle thrust zones (Fig. 6), the reactivated, folded foliation model is plausible, either as the main controlling factor, or in combination with the other two.

6.2. Geological model in light of other studies

Considering Varnes` (1978) classification of landslide types, Åknes rockslide does not simply fit into one category but forms a complex landslide, which is a combination of two or more principal types of movement. Creep is considered to be continuous in the Åknes rockslide, contributing to the general deformation of the bedrock and displacement of the rockslide. In the upper part of the Åknes rockslide, sub-domain 1 and 2, indications of rotational slide movement is observed in the combination of vertical and horizontal movement of the back scarp as well as backward tilting of blocks (Fig. 9). Translational slide movement is observes along the western flank of the rockslide, especially in sub-domain 1, where also the largest displacement rates are measured. Abundant extensional fractures (tension cracks) in a range of sizes are also observed along the western flank, both with ~N–S and ~E–W strike. However, the toe zone and the eastern flank, primarily sub-domain 3 and 4, of the Åknes rockslide does not fit within Varnes` (1978) classification. This is hereby argued due to control of pre-existing structures such as the fault forming the western boundary zone and the ductile fabric of the bedrock, i.e. the foliation controlling the basal sliding surface with its subordinate thrusts that daylights at several levels, but is most prominent in the toe zone (Figs. 2, 6 and 10). Another argument for the distinctly different appearance is that the Åknes rockslide has not evolved far enough to display the common structures occurring in “the zone of accumulation” according to Varnes` (1978) classification. Anyhow, the basal sliding zone with its subordinate sliding surfaces observed at Åknes

Table 2
Approximate area and volume estimates of the four sub-domains

	Approximate area (m^2)	Min volume (m^3) – 50 m depth	Max volume (m^3) – 65 m depth
Subdomain 1	102,264	5.1 million m^3	6.6 million m^3
Subdomain 2	118,755	5.9 million m^3	7.7 million m^3
Subdomain 3	155,787	7.8 million m^3	10.1 million m^3
Subdomain 4	117,454	5.8 million m^3	7.6 million m^3

rockslide form thrusts, giving compression, and display as an imbricated thrust fan (Fig. 10).

Braathen et al. (2004) define Åknes rockslide as a *rockslide area*, given that the rockslide area has a relative low gradient (<45°), weakness zones sub-parallel to the surface, and movement in the lower parts leading to failures in the upper part of the slope. These weakness zones are, for example, foliation and/or layering or pre-existing fractures oriented sub-parallel to the slope. Results from this study support the view that Åknes is a rockslide area, but with more complex structures (Figs. 1 and 10). Braathen et al. (2004) further address the rockslide kinematics in a down-slope direction. Results from this study imply that Åknes fits with Braathen et al.`s (2004) model of the combined extension–compression scenario, predicting a high frontal friction.

Oppikofer and Jaboyedoff (2007) proposes another type of model of Åknes rockslide based on DEM (digital elevation model) and ground-based Lidar image analyses of Åknes and surrounding occurred and potential rockslides. They use the asperity–amplitude method to estimate the roughness of the foliation which gives the geometry of the basal sliding surface, and analysis of spatial distribution of steep fractures. This provides a model with primarily planar back scarps and a stepped basal sliding surface, where the rockslide is gravitational driven giving mainly translational movement. This is a model similar to that of Eberhardt et al. (2004) described as "sequential failure with internal shearing with yielding of rock bridges" or "multiple step-path failure with intact rock bridges". The sequential failure model is similar to that proposed for the Randa rockslide (Eberhardt et al., 2004). Eberhardt et al. (2004) demonstrate that where sliding surfaces are predefined and controlled by pre-existing structures less internal rock deformation is needed to achieve failure of the rockslide. Tension cracks are commonly an indication of internal rock deformation, and with regards to Åknes rockslide both persistent pre-existing structures and tension cracks are observed, indicating a more complex deformation mechanism with possibly a combination of brittle and ductile behaviour (Eberhardt et al., 2004). This may be the essential difference between the model of Åknes rockslide presented by Oppikofer and Jaboyedoff (2007) and the one proposed in this work. The model by Oppikofer and Jaboyedoff (2007) is not considering the properties of the bedrock as strongly and showing brittle behaviour, while we propose a model based more on ductile behaviour due to the control of pre-existing structures in the bedrock. The most realistic model of Åknes rockslide is probably a combination of that proposed here and that of Oppikofer and Jaboyedoff (2007). However, the morphology of the rockslide models after failure is likely to be similar.

Giraud et al. (1990) gives examples of rockslides controlled by pre-existing structures, such as foliation, where the slope parallel foliation forms potential slip planes, which increase the potential of rockslides progressing into rock avalanches with minor changes in physical or hydrogeological conditions as trigger. These are conditions that are valid for Åknes rockslide, and emphasises the importance of pre-exiting structures as a controlling factor. Giraud et al. (1990) also argue that rockslides with pre-existing structures controlling the slip surface are more likely exposed to translational or rotational types of movement. Another model that has been proposed is the deep-seated slope gravitational deformation model (DSGSD); a model that shows only extension (Agliardi et al., 2001; Crosta and Agliardi, 2003). An example of such DSGSD is the Ruinon rockslide (20 million m^3) of the Italian Alps. This deep-seated slope gravitational deformation indicates one deep, more or less continuous sliding surface, and collapse of the lower part of the slope (Agliardi et al., 2001). At Åknes there is no indication of collapse in the lower part of the slope and there is evidence of several sliding surfaces as well as a combined extension–compression regime, making this model less viable for this site. Seno and Thüring (2006) propose several different landslides models, based on case studies from the Swiss Alps, varying from rotational rockslides to rock slump, sag or deep-seated creep and retrogressive landslide. However, these examples seems to be driven by gravitation, commonly triggered by alteration in groundwater level, and not controlled by pre-existing structures such as faults and ductile deformation of the bedrock, even though two of the case studies have slope parallel schistosity (Seno and Thüring, 2006).

Numeric modelling tools are widely used for kinematic analyses and stability calculation of rock slope (Eberhardt et al., 2004; Stead et al., 2006), however, due to the large uncertainties in input parameters the use of numerical modelling is mainly limited to back analysis (Meric et al., 2005). Therefore, the need for geological data to constrain the models is critical, and this work is an attempt of achieving constraints on geological parameters that will be applied in numeric models (Kveldsvik et al., 2007; Nøttveit et al., submitted for publication).

6.3. Fracture distribution

Two hypotheses are entertained for the existing fracture sets mapped in the rockslide area. Firstly, they are pre-existing fractures, probably of Devonian age, which are reactivated due to movements on the basal sliding surface. Since all recorded fracture sets are present throughout the rockslide area (Fig. 2), this indicates that the fractures are pre-existing. Some of the fractures are reactivated due to shear movement along the basal sliding surface, which coincides with results of Henderson et al. (2006) from regional studies in the vicinity of Åknes. In the second hypothesis, the fracture sets are caused by shear movement along the sliding surface. Slope parallel fractures or fractures that form perpendicular to the displacement direction are indications of fractures caused by movement of the rockslide. Sub-vertical extensional fractures (i.e. tension cracks), which seem to occur randomly, have a strike (~E–W) more or less perpendicular to the direction of movement (SSW) are observed in sub-domain 2 (Figs. 2, 5 and 10). This phenomenon is also observed in other sites in the vicinity (Henderson et al., 2006). At Åknes both types of fractures occur, but the majority of fractures are reactivated older structures. In addition, logging of the drill cores show that the fracture frequency decreases with depth, indicating reactivation of pre-existing fractures and/or foliation rather than initialization of new fractures (Fig. 8).

6.4. Complex groundwater system

The groundwater system of the rockslide area is fed by precipitation both in the rockslide area and in the catchments area. Several seasonal streams flow into the back scarp. Runoff from snowmelt in the springtime brings significant volumes of water into the rockslide area. Several springs are observed at the site and groundwater seepage is common along the observed sliding surfaces. The area beneath the toe zone reveals abundant springs. In the lower part of the rockslide area, towards the fjord, the groundwater table is close to the surface. This is reflected in the shallow penetration depth of the GPR data from the area. Water chemistry, including conductivity, temperature, pH, anion and cation composition from the springs, may reflect the retention time of the groundwater (Derron et al., 2007). The dataset indicates short retention time in sub-domain 2, while springs from sub-domain 3 and 4 seemingly have longer retention times. The lowermost springs, beneath the toe zone, indicate the longest retention time. In total, the groundwater chemistry supports the zonation of the rockslide area, as suggested in the geological model (Fig. 10).

In the boreholes, the groundwater table is between 42 and 52 m depth (Fig. 8). The water table fluctuates seasonally, increasing by as much as 5 m during snowmelt. The drill holes indicate a complex groundwater system, with several inflows and outflows at different depths and possibly perched groundwater aquifers. The latter is seen by different temperatures and water conductivity. The depth to the water table in the drill holes is similar to the top of the low resistivity layer (blue) in the 2D resistivity profiles (Figs. 7 and 8).

Hydraulic factors play an important role as contributing factors to failure of all types of landslides (Giraud et al., 1990). For example, studies of landslide in the Alps show that a large increase in rainfall over a short time period results in an increase in displacements (Giraud et al., 1990; Crosta and Agliardi, 2003; Crosta et al., 2004; Seno and Thüring, 2006). The heavy rainfall and additional runoff from glaciers also worked as a triggering factor for accelerating displacement for the Val Pola landslide in the Italian Alps (Crosta et al., 2004). Seno and Thüring`s (2006) study show that alternations in groundwater level, giving changes in pore pressure, is considered to be the main causes of instability. In this light, melt water runoff and heavy rainfall may also act as a triggering factor for the Åknes rockslide. Grøneng et al. (in preparation) addresses the relation between displacement and precipitation for the Åknes rockslide.

6.5. Uncertainties

The geological model presented is based on all observations described above. However, there are observations that are not included in the geological model, such as mapped layers of low resistivity in the 2D resistivity profiles measured above the back scarp. This may be an indication of an unstable rock mass above the back scarp, in which case the back scarp is not the upper limit of the rockslide area. No field observations indicate movement above the back scarp, other than structures related and close to the back scarp. Several rockslides have occurred in the area to the west and east of Åknes, resulting in rock avalanche deposits as large as 400 million m^3 covering the fjord bottom (Blikra et al., 2005b). This raises the question of how stable the rock mass outside Åknes rockslide is. The supposed lower limit of the rockslide is the toe zone. However, interferometric sonar mapping of the mountainside below sea level reveals indications of a possible sliding surface daylighting at a depth of −20 to −50 m (Longva et al., 2007).

The seismic profile presented here is based on only five shot points (Fig. 6C), which limits both the data resolution and the details mapped in the section. Therefore, the details indicated in the interpretation of the profile are debatable, especially with regards to the sub-vertical structure indicated at ~300 m. However, the layering of the four layers with different seismic velocities is likely, which indicate that the two uppermost layers thins out and truncate at the same area as the 2D resistivity profile indicate a daylighting low resistivity layer (Fig. 7).

There are also indications from the boreholes that there may be deeper sliding surfaces at depths from 115 to 190 m. This is supported by intensely fractured layers encountered in the lower parts of the drill cores (115 m, Fig. 8) and indications of good hydraulic conductivity at even greater depths (150–190 m). The latter was the likely cause of loss of water during drilling. The loss of water can be explained in several ways; i) a perched groundwater level that was punctured by the drill holes, ii) a set of open fractures with good hydraulic communication, and/or (iii) a deep sliding surface in a weaker rock layer that controls the groundwater flow at depth.

As indicated in the geological models presented in Fig. 10, bedrock with higher fracture frequency than the host rock extends down to at least 100 m. This suggests that there may be multiple sliding surfaces, which is very often the case in deep-seated rock slides in crystalline rock (Bonzanigo et al., 2000). This assumption is further confirmed by the presence of heavily fractured rock at 115 m depth (Fig. 8), and is alluded to in the discussion related to Fig. 10 (i.e. that the rockslide may be deeper than the current geological model predicts). However, at this early stage of the investigations no conclusive measurements are given on the movements at deeper levels, hence, not included in the proposed model in Figs. 1 and 10. The intention is to propose a geological model of the rockslide based on existing and documented data, and not infer a model on data that are not documented. Inclinometers are installed in some of the drill holes, at different depth, and further work will elaborate on this issue.

The displacement measurements especially in sub-domain 4 (points 10–13) show divergence in direction and rates. There is inconsistency among the four lower points, making it difficult to draw sound conclusions. The source of error of the measuring instrument is regarded as 4 mm, and according to Demoulin et al. (2007) variation in groundwater level may contribute to mm-scale of local different vertical displacement. However, all points in sub-domain 4 show an (vertical) upward movement that exceeds the level of uncertainty.

7. Conclusions

- The aim of this work was to propose a geological model of the Åknes rockslide based on structural mapping and interpretation of geophysical data from profiling and boreholes.
- The folded foliation controls the development of the back fracture. Where the orientation of the foliation is favourable for extensional fracturing (i.e. when sub-vertical or dipping down slope), the back fracture follows the foliation.
- The folded foliation controls the development of the basal sliding surface with its sub-ordinate sliding surfaces as low angle trusts; i.e. the sliding surface is undulating due to gentle folds in the foliation of the bedrock. The sliding surfaces are mapped where they daylight the surface, and are characterized by the occurrence of fault rocks such as gouge and breccia. In general, the depth to the sliding surfaces varies due to the undulation, generally increasing to the west and decreasing to the east, with a maximum depth of 65–70 m.
- The rockslide area is divided into four sub-domains, confined by sub-ordinate low angle thrusts that daylight the surface. These sub-domains have different displacement patterns and rates, and have the down-slope geometry of an imbricated fan. Extension characterizes the two upper domains of the rockslide whereas compression characterizes the two lower domains.
- The rockslide area is structurally confined with the upper rockslide limit formed by the back scarp zone, whereas a pre-existing NNW–SSE strike slip fault forms the western boundary zone. The eastern boundary zone is a gentle westward dipping pre-existing fault, and the toe zone forms the lower limit, where a sliding surface daylights the surface.

Acknowledgements

Thanks go to Stranda Municipality for finance and management of the Åknes/Tafjord project, and to the International Centre of Geohazards (ICG) for project management and cooperation. Acknowledgement goes to Professor Michel Dietrich and his group at LGIT (Laboratoire de Geophysique et Tectonophysique), Grenoble. Also, thanks to John Dehls, Geological Survey of Norway, for helpful comments. Thanks to Michel Jaboyedoff and two anonymous persons for reviewing and improving the manuscript.

References

Agliardi, F., Crosta, G., Zanchi, A., 2001. Structural constraints on deep-seated slope deformation kinematics. Engineering Geology 59, 83–102.

Andersen, T.B., Osmundsen, P.T., Berry, H.N., Torsvik, T.H., Eide, E.A., 1997. Multi-level detachments and exhumation in the Norwegian Caledonides. Abstracts with Programs – Geological Society of America 29 (6), 317.

Blikra, L.H., Longva, O., Braathen, A., Anda, E., Dehls, J., Stalsberg, K., 2005a. Rock-slope failure in Norwegian fjord areas: examples, spatial distribution and temporal patterns. In: Evans, S.G., Scarascia Mugnozza, G., Strom, A.L., Hermanns, R.L. (Eds.), Massive rock slope failure: new models for hazard assessment. Kluwer, Dodrecht.

Blikra, L.H., Longva, O., Harbitz, C., Løvholt, F., 2005b. Qualification of rock-avalanche and tsunami hazard in Storfjorden, western Norway. In: Senneset, K., Flaate, K., Larsen, J.O. (Eds.), Landslide and Avalanches ICFL 2005 Norway. Taylor & Francis Group, London.

Bonzanigo, L., Eberhardt, E., Loew, S., 2000. Measured response to a drainage adit in a deep creeping slide mass. Proceedings,Eighth International Symposium on Landslides, Cardiff. Thomas Telford, London, pp. 151–156.

Braathen, A., 1999. Kinematics of post-Caledonian polyphase brittle faulting in the Sunnfjord region, western Norway. Tectonophysics 302 (1–2), 99–121.

Braathen, A., Blikra, L.H., Berg, S., Karlsen, F., 2004. Rock-slope failures of Norway; types, geometry, deformation mechanisms and stability. Norwegian Journal of Geology 84 (1), 67–88.
Crosta, G.B., Agliardi, F., 2003. Failure forecast for large rock slides by surface displacement measurements. Canadian Geotechnical Journal 40, 176–191 http://cgj.nrc.ca.
Crosta, G.B., Chen, H., Lee, C.F., 2004. Replay of the 1987 Val Pola Landslide, Italian Alps. Geomorphology 60, 127–146.
Dahlin, T., 1993. On the Automation of 2D Resistivity Surveying for Engineering and Environmental Application. Ph.D. thesis, Lund Technical University, Sweden.
Davis, G.H., Reynolds, S.J., 1996. Structural geology of rock and regions, 2nd ed. Wiley & Sons, p. 776.
Demoulin, A., Ducarme, B., Everaerts, M., 2007. Seasonal height change influence in GPS and gravimetric campaign data. Journal of Geodynamics 43, 308–319.
Derron, M.H., Blikra, L.H., Jaboyedoff, M., 2005. High resolution digital elevation model analysis for landslide hazard assessment (Åkerneset, Norway). In: Senneset, K., Flaate, K., Larsen, J.O. (Eds.), Landslide and avalanches ICFL 2005 Norway. Taylor & Francis Group, London.
Derron, M.-H., Ganerød, G.V., Elvebakk, H., 2007. Hydrochemical characterization of waters on the rockslide site of Åknes (western Norway). Conference proceedings, Geophysical Research Abstracts, Vol. 9.
Eberhardt, E., Stead, D., Coggan, J.S., 2004. Numeric analysis of initiation and progressive failure in natural rock slopes – the 1991 Randa rockslide. Rock Mechanics and Mining Sciences 41, 69–87.
Eiken, T., 2006. Om GPS-målingar av deformasjoner i potensielle fjellskred. Åknes-Tafjord/Storfjorden. Rapport Institutt for Geofag, Universitetet i Oslo, p. 33.
Gabrielsen, R.H., Braathen, A., Dehls, J., Roberts, D., 2002. Tectonic lineaments of Norway. Norwegian Journal of Geology 82, 153–174.
Ganerød, G.V., Grøneng, G., Aardal, I.B., Kveldsvik, V., 2007. Core logging of seven boreholes from Åknes, Stranda municipality, Møre and Romsdal County. NGU report no. 2007.020, pp. 222.
Giraud, A., Rochet, L., Antoine, P., 1990. Processes of slope failure in crystallophyllian formations. Engineering Geology 29, 241–253.
Grøneng, G., Jenssen, A., Christensen, H., Nilsen, B., Blikra, L.H., in preparation. Influence of Meteorology and Seasonal Variation on the Åknes Rockslide in Western Norway.
Henderson, I.H.C., Saintot, A., Derron, M.H., 2006. Structural mapping of potential rockslide sites in the Storfjorden area, western Norway: the influence of bedrock geology on hazard analysis. NGU report no. 2006.052, pp. 1–82.
Hermanns, R.L., Blikra, L.H., Naumann, M., Nilsen, B., Panthi, K.K., Stromeyer, D., Longva, O., 2006. Examples of multiple rock-slope collapses from Köfels (Ötz valley, Austria and western Norway. Engineering Geology 83, 94–108.
Kveldsvik, V., Eiken, T., Ganerød, G.V., Grøneng, G., Ragvin, N., 2006. Evaluation of movement data and ground conditions for the Åknes rock slide. The International Symposium on Stability of rock slopes, at the South African Institute of Mining and Metallurgy, April 2006, pp. 1–24.
Kveldsvik, V., Nilsen, B., Einstein, H.H., Nadim, F., 2007. Alternative approaches for analyses of a 100.000 m^3 rock slide based on Barton-Bandis shear strength criterion. Landslides. doi:10.1007/s10346-007-0096-x.
Loke, M.H. (2001). RES"INV version 3.4. Geoelectrical Imaging 2D & 3D. Instruction manual. (10.15.2004).
Longva, O., Blikra, L.H., Dehls, J.F., 2007. Rock avalanches in the Storfjorden basin; distribution, frequencies and slide inventory. NGU Report no. 2007.038.
Meric, O., Garambois, S., Jongmans, D., Wathelet, M., Chatelain, J.L., Vengeon, J.M., 2005. Application of geophysical methods for the investigation of the large gravitational mass movement of Séchilienne, France. Canadian Geotechnical Journal 42, 1105–1115.
Nilsen, B., Palmstrøm, A., 2000. Enginnering geology and rock engineering. Handbook No. 2, 249.
Nøttveit, H., Ganerød, G.V., Grøneng, G., Braathen, B., submitted for publication. 3D assessment of effects caused by fault rocks and groundwater using petroleum modeling tools; Åknes rockslide, Western Norway. Landslides.
Oppikofer, T., Jaboyedoff, M., 2007. Åknes/Tafjord-Project: DEM analysis of the Rundefjellet/Tårnet area, Report IGAR-TO-005, University of Lausanne, Switzerland.
Osmundsen, P.T., Andersen, T.B., 2001. The middle Devonian basin of western Norway; sedimentary response to large-scale transtensional tectonics? Tectonophysics 332, 51–68.
Reynolds, J.M., 1997. An Introduction to Applied and Environmental Geophysics. John Wiley & Sons, New York, p. 796.
Riemer, U.T., Lecher, T., Nunez, I., 1988. Mechanics of deep seated mass movements in metamorphic rocks of the Ecuadorian Andes. Proceedings of the 5th International Symposium on Landslides, Lausane, 1988. Balkema, 1990.
Robertsson Geologging equipment http://www.geologging.com (12.12.2007).
Roth, M., Dietrich, M., Blikra, L.H., Lacomte, I., 2006. Seismic monitoring of the unstable rock slope site at Åknes, Norway. SAGEEP – Symposium on the Application of Geophysics to Engineering and Environmental Problems, Extended abstract.
Rønning, J.S., Dalsegg, E., Elvebakk, H., Ganerød, G.V., Tønnesen, J.F., 2006. Geofysiske målinger Åknes og Tafjord, Stranda og Nordal kommune, Møre og Romsdal. NGU report no. 2006.002, pp. 1–66.
Sandersen, F., Bakkehøi, S., Hestnes, E., Lied, K., 1996. The influence of meteorological factors on the initiation of debris flows, rockslides and rockmass stability. In: Senneset (Ed.), 7th Int. Symp. on Landslides, Trondheim, Norway. Balkema, Rotterdam, pp. 97–114.
Seno, S., Thüring, M., 2006. Large landslides in Ticino, Southern Switzerland: geometry and kinematics. Engineering Geology 83, 109–119.
Stead, D., Eberhardt, E., Coggan, J.S., 2006. Developments in the characterization of complex rock slope deformation and failure using numerical modeling techniques. Engineering Geology 83, 217–235.
Tveten, E., Lutro, O., Thorsnes, T., 1998. Berggrunnskart Ålesund. 1:250000, (Ålesund, western Norway), NGU Trondheim (bedrock map).
Varnes, D.J., 1978. Slope movement types and processes. In: Schuster, R.L., Krizek, R.J. (Eds.), Landslides – Analysis and Control, U.S. National Acadamy of Science, Special Report, vol. 176, 2, pp. 11–33.

B.1 Report I

Procedure for Determining Input Parameters for Barton-Bandis Joint Shear Strength Formulation

Authors: Guro Grøneng and Bjørn Nilsen

The report was published as an internal report at Norwegian University of Science and Technology (NTNU), Dept. of Geology and Mineral Resources Engineering, No. 38.

ISSN 0803-8171

NTNU
Norges teknisk-naturvitenskapelige universitet

38

August
2009

Guro Grøneng og Bjørn Nilsen

Procedure for determining input parameters for Barton-Bandis joint shear strength formulation.

Ref.: Rep. 38. Institutt for geologi og bergteknikk, NTNU, Trondheim 2009.

RAPPORTER FRA

INSTITUTT FOR GEOLOGI OG BERGTEKNIKK

REPORTS FROM
DEPARTMENT OF GEOLOGY AND
MINERAL RESOURCES ENGINEERING

B.2 Report II

Core logging of seven boreholes from Åknes, Stranda municipality, Møre and Romsdal County

Authors: Guri Venvik Ganerød, Guro Grøneng, Ingrid B. Aardal and Vidar Kveldsvik

The report was published as an internal report at Geological Survey of Norway (NGU), No. 2007.020.

Geological Survey of Norway
NO-7441 Trondheim, Norway
Tel.: 47 73 90 40 00
Telefax 47 73 92 16 20

REPORT

Report no.: 2007.020 | ISSN 0800-3416 | Grading: Open

Title: Logging of drill cores from four boreholes at Åknes, Stranda municipality, Møre and Romsdal County

Authors: Guri Venvik Ganerød, Guro Grøneng, Ingrid Buvarp Aardal and Vidar Kveldsvik

Client:

County: Møre og Romsdal

Commune: Stranda

Map-sheet name (M=1:250.000): Ålesund

Map-sheet no. and -name (M=1:50.000): Geiranger 1219 II

Deposit name and grid-reference: WGS 1984, UTM 32N. E 395800 N6895200

Number of pages: 222 Price (NOK): 250

Map enclosures:

Fieldwork carried out:	Date of report:	Project no.:	Person responsible:
Summer 2005 & 2006	10.03.2007	300601	

Summary:

This report contains data from core logging of seven drill cores from boreholes at Åknes rockslide area, Stranda municipality, western Norway. Four boreholes were drilled in 2005 and the remaining three in 2006. Raw data from the core logging are compiled, without any interpretation. Graphs of fracture frequency (FF) and RQD from the logging are presented and compared from the different drill sites.

Samples are collected from the drill cores and recorded in the logs. Method description for the samples are described in the report. Samples of standard engineering testing, such as UCS, E-Module, Poisson's ratio, Brazil test and sound velocity, are performed after standard ISRM methods, and some results are included in the report.

Keywords:	Core samples	(Borehullslogging)
Core logging	Scientific report	(Fjell)
Bedrock	(Fagrapport)	(Kjerneprøver)

C.1 List of publications

Journal papers

Ganerød G.V., Grøneng G., Rønning J.S., Dalsegg E., Elvebakk H., Tønnesen J.F., Kveldsvik V., Eiken T., Blikra L.H. & Braathen A. (2008): Geological Model of the Åknes Rockslide, western Norway. Engineering Geology, Vol. 102, pages 1-18, doi:10.1016/j.enggeo.2008.01.018.

Grøneng G., Lu M., Nilsen B. & Jenssen A.K. (submitted): Time-dependent behaviour of the Åknes rockslide area in western Norway. Submitted to: Engineering Geology, September 2009.

Grøneng G., Christiansen H.H., Nilsen B. & Blikra L.H. (submitted): Meteorological effects on seasonal displacements of the Åknes rockslide, western Norway. Submitted to: Landslides, May 2009.

Grøneng G., Nilsen B. & Sandven R. (2009): Shear strength estimation for Åknes sliding area in western Norway. International Journal of Rock Mechanics and Mining Sciences, Vol. 46, pages 479-488, doi:10.1016/j.ijrmms.2008.10.006.

Nordvik T., Grøneng G., Ganerød G.V., Nilsen B., Harding C. & Blikra L.H. (2009): Geovisualization, geometric modelling and volume estimation of the Åknes rockslide, western Norway. Bulletin of Engineering Geology and the Environment, Vol. 68, pages 245-256, doi:10.1007/s10064-009-0198-x.

Conference papers

Grøneng G., Nilsen B., Blikra L.H. & Braathen A. (2005): The significance of climate on deformation in a rock-slope failure - the Åkerneset case study from Norway. In: Hungr O., Fell R., Couture R. Eberhardt E. (Eds.), Proceedings of the International Conference on Landslide Risk Management, Vancouver, pages 725-729, Balkema, Rotterdam.

Kveldsvik V., Eiken T., Ganerød G.V., Grøneng G. & Ragvin N. (2006): Evaluation of movement data and ground conditions for the Åknes rock slide. In Proceedings: Stability of rock slopes in open pit mining and civil engineering situations, Cape Town, pages 279-300, The South African Institute of Mining and Metallurgy.

Reports

Grøneng G. & Nilsen B. (2009): Procedure for determining input parameters for Barton-Bandis joint shear strength formulation. Internal report no. 38, Norwegian University of Science and Technology (NTNU), Dept. of Geology and Mineral Resources Engineering, 21 p.

Ganerød G.V., Grøneng G., Aardal I.B. & Kveldsvik V. (2007): Logging of drill cores from seven boreholes at Åknes, Stranda municipality, Møre and Romsdal County. Internal report no. 2007.020, Geological Survey of Norway (NGU), 418 p.

Miscellaneous

Grøneng G. & Moen B. (2008): Kan Åknesskredet temmes? Letter to the editor in: Teknisk Ukeblad 21/08. In Norwegian.